8-14-2020 9:45 AM

Development Of Technologies For High Value Products From Biomass Pyrolysis

Chiara Barbiero, *The University of Western Ontario*

Supervisor: Berruti, Franco, *The University of Western Ontario*
A thesis submitted in partial fulfillment of the requirements for the Doctor of Philosophy degree in Chemical and Biochemical Engineering
© Chiara Barbiero 2020

Abstract

Phragmites australis (Cav.) Trin. ex. Steud. is an invasive perennial grass found in North America, which is rapidly spreading throughout Ontario, damaging the native ecosystem and endangering the wildlife. This infestation has caused a decrease in biodiversity and nutrient availability to the agricultural crops through competition. One of the most effective management practices is spading them, leaving a huge number of dead stalks that need to be disposed of. Pyrolysis was selected as an alternative thermochemical method to convert this feedstock to value-added bioproducts, such as bio-oil and biochar, and to produce valuable renewable chemicals from the pyrolysis oil, such levoglucosan and acetic acid.

This research study objectives are the conversion of *Phragmites australis* through slow pyrolysis with an existing technology developed in ICFAR in previous years and with a new pyrolysis unit designed and built for the scope of this research, to investigate the impact of different operating conditions on the biochar and bio-oil products. Model compounds made of different ratio of the lignocellulosic components were investigated as well to study differences and similarities.

Fast pyrolysis was carried out in the new bench scale pyrolysis unit to study the effect of different pre-treatments on the removal of the alkali and alkaline earth metals (AAEMs) to improve the levoglucosan yield in the bio-oil product.

Finally, the performance of the biochar and activated biochar produced from *Phragmites australis* as sorbent materials was investigated for the removal of ibuprofen, this molecule was chosen as a model compound for the non-steroidal anti-inflammatory drugs (NSAID).

Keywords

Pyrolysis, AAEMs, levoglucosan, biochar, activated carbon, ibuprofen, bio-oil, acetic acid

Summary for Lay Audience

Phragmites australis (Cav.) Trin. ex. Steud. is an invasive perennial grass found in North America, which is rapidly spreading throughout Ontario, damaging the native ecosystem and endangering the wildlife. This infestation has caused a decrease in biodiversity and nutrient availability to the agricultural crops through competition. One of the most effective management practices is spading them, leaving a huge number of dead stalks that need to be disposed of.

This research focused on the exploitation of *Phragmites australis* as a low-value feedstock for the conversion into a liquid product, bio-oil, a solid residue, biochar and gases through a process known as pyrolysis.

Bio-oil is comprised of many interesting compounds, such as sugars and acids that if produced in high yields could have attractive applications as building blocks for the production of biodegradable polymers, solvents and pharmaceuticals.

Biochar is the carbon-rich residue of the lignocellulosic biomass left after the pyrolysis reaction. The use of biochar and activated biochar was investigated as sorbent materials for the removal of ibuprofen commonly used as the first line of medication to relieve pain and reduce inflammation. Ibuprofen belongs to a new class of emerging pollutants, which are biologically active and have strong impacts on the environment even in small concentrations.

Co-Authorship Statement

Chapter 3 and 4
Title: **Slow pyrolysis of *Phragmites australis* and synthetic biomass: Studies on process parameters and product characterization**
Current status: unpublished
Authors: Chiara Barbiero, Sonil Nanda, Tahereh Sarchami, Franco Berruti
Chiara Barbiero performed all the pyrolysis experiments and collected and analyzed the data and wrote this chapter of the thesis. Sonil Nanda and Tahereh Sarchami supervised and helped with the data analysis and experimental work. Franco Berruti supervised the research work.

Chapter 5
Title: **Fast pyrolysis of *Phragmites australis***
Authors: Chiara Barbiero, Steve Horves, Franco Berruti
Current status: unpublished
Chiara Barbiero carried out the design and commissioning and optimization of the pyrolysis unit, designed and executed all the pre-treatments of the biomass and all the pyrolysis experiments. Steve Horves helped with the pyrolysis of the pre-treated biomass. Franco Berruti supervised the research work.

Chapter 6
Title: **High temperature slow pyrolysis for biochar production**
Authors: Chiara Barbiero, Franco Berruti
Current status: unpublished
Chiara Barbiero performed all the pyrolysis experiments, data analysis and writing. Franco Berruti supervised the research work.

Chapter 7
Title: **Adsorption of ibuprofen from biochar and activated biochar from *Phragmites australis***
Current status: unpublished
Authors: Chiara Barbiero, Franco Berruti
Chiara Barbiero performed all the pyrolysis and activation experiments, built the activation unit and performed all the adsorption experiments with ibuprofen and data collection, analysis and writing of the chapter.

Acknowledgments

I would like to thank my supervisor Dr. Franco Berruti for his support and guidance throughout my research program, especially for allowing the construction of the pyrolysis unit I am proud to present in this thesis and for all the learning opportunities I had during conferences and research events.

I would also like to thank the Faculty of Engineering of Western University for the financial support of my doctoral studies and the Natural Sciences and Engineering Research Council of Canada (NSERC) and BioFuelNet Canada for providing the funding for my research, travel awards and the opportunity to attend conferences during my PhD.

Moreover, I would like to express my very great appreciation to Dr. Tahereh Sarchami for her help and assistance in the analytical lab in ICFAR; Thomas Johnston for his in the pilot plant; Chantal Gloor and Christine Ramsden for being always available for assistance.

I am particularly grateful for the assistance given by the University Machine Services (UMS), especially Cody Ruthman for building my pyrolysis unit and all the custom parts I needed for my research, I appreciate every detail.

My special thanks are extended to the staff of Surface Science Western, in particular Ivan Barker for the Micro-CT scans and the macroscope pictures.

I would like to thank all the students, faculty members and staff I had the pleasure to meet and work at ICFAR. In particular, Fang Cao (Flora), the students Ghazaleh Chegini, Afsana Sara Kabir, Xuelian (Cher) Xing, Yulin (Tracy) Hu, Ramon Beims, the international students Roberta Lotito and Steve Horvers who I had the pleasure to share the new pyrolysis unit with, and all the postdocs, in particular Stefano Tacchino, Sonil Nanda and Mohammad Hossain.

A special thanks to my friends, especially Anastasia Colomba, Luana Dessbessel and Marina Morando for their amazing support and being the best motivators I could ever dream of.

Dedication

To my parents and brother.

Table of Contents

List of Tables

List of Figures

List of Appendices

Chapter 1

1   Introduction

1.1   Motivation

The development of sustainable bio-based products and technologies is becoming critical in the world bioeconomy. New product streams, usually from waste or byproduct materials are currently studied and recent advancements pointed out the possibility of targeting value-added chemicals from biomass conversion, which have the potential to substitute compounds derived from fossil fuels.

Biomass is a renewable resource derived from plant material (e.g. trees, grasses and hay) that can be turned into fuels and chemicals [1]. There are currently different technologies and processes that were developed to effectively convert biomass into solid, liquid and gases that can be used for heat and/or electricity or power generation. These technologies include gasification, anaerobic digestion, torrefaction and pyrolysis.

This research investigated the use of *Phragmites australis* as a feedstock for pyrolysis for the production of bio-based products. *Phragmites australis* is a perennial grass, native to Eurasia, which is spreading worldwide, increasing fire hazards, and causing damage to wildlife and its surrounding habitat [2–4]. *Phragmites australis* was classified as Canada's worst invasive plant by Agriculture and Agri-Food Canada [5]. One of the most effective management practices involve cutting the reed above the ground, which leaves a huge number of dead stalks that need to be processed [6].

Phragmites australis was investigated in different studies as an energy crop due to its ability to reproduce fast without any energy or cultivation aids and produce high yield of harvestable biomass [7–14]. In fact, ideally, an energy crop would have high content of cellulose, hemicellulose and lignin [15], low levels of ash and nitrogen [16], and high productivity [17] by minimizing agronomic inputs (e.g. fertilization, irrigation, pest control) [18].

Pyrolysis stands for the thermochemical degradation of an organic molecule in the absence of oxygen into bio-oil, biochar and gases [19]. The advantages of using pyrolysis when processing a biomass waste are that the liquid product, bio-oil, can be stored and transported [20,21]. Moreover, since the bio-oil is a mixture of different chemicals, including sugars, alcohols, acids, aldehydes and phenols, some of these chemicals can be separated and extracted [22–26] allowing the potential production of bio-based chemicals that could substitute fossil fuel-based chemicals.

In this thesis, the main objectives are summarized as follows:

1. Gather more insight in the exploitation of the *Phragmites australis*, which represent a liability for the municipalities and could be used as an inexpensive lignocellulosic biomass for the production of bio-based products while helping to restore biodiversity in the affected areas.

2. Investigate the effect of pre-processing, reactor technology and operation and post-processing:

   a. Determine the impact of different washing pre-treatments on the removal of alkali and alkaline earth metals (AAEMs) and their effect on the composition of fast pyrolysis products, in particular levoglucosan concentrations in bio-oil.

   b. Study slow and fast pyrolysis with two different reactor technologies:

      i. Determine the effect of lignocellulosic components on the slow pyrolysis products by mixing different ratio of cellulose, xylose and lignin and compare the results with the pyrolysis products of the real biomass.

      ii. Investigate the impact of temperature, heating rate, nitrogen flow rate and holding time on the slow pyrolysis of *Phragmites australis* for the production of biochar as a feedstock for activated biochars and for the production of acetic acid in the aqueous phase oil.

      iii. Design and develop a continuous pyrolysis unit to perform fast pyrolysis. Determine the effect of reactor and first condenser (C_1)

temperatures on the levoglucosan yield and selection of the
optimal conditions for the pyrolysis of pre-treated biomass.

c. Study the impact of activation on the biochar products and compare the
performance of slow and fast biochar with activated biochar on the
adsorption of ibuprofen.

1.2   Structure of the thesis

Chapter 2 describes the equipment used in this research and the material and
methodology for the pre-treatments, pyrolysis, activation and adsorption experiments.

Chapter 3 and **Chapter 4** describe the slow pyrolysis experiments in the MFR batch
designed in ICFAR in previous year. The study focuses on the effect of the pyrolysis
operating conditions on the bio-oil and biochar products of *Phragmites australis*
(**Chapter 3**) and model compounds (**Chapter 4**).

Chapter 5 contains the design and description of the new continuous pyrolysis unit and
the fast pyrolysis experiments carried out to find the optimal conditions for levoglucosan
production. Then the pyrolysis of the pre-treated biomass is studied to investigate the
impact of AAEMs on the levoglucosan concentration; the properties of the untreated and
pre-treated biochars are studied as well.

Chapter 6 describes the slow pyrolysis (at temperature above 500°C) of *Phragmites
australis* as a feedstock for the production of activated biochar.

In **Chapter 7**, the biochar produced at 650°C is activated. The biochar from Chapter 5
and Chapter 6 and activated biochar are used as sorbent materials to test the performance
in terms of removal of a solution containing 25 mg/L of ibuprofen.

Chapter 8 contains the final conclusions and recommendations.

1.3   Phragmites australis

The genus Phragmites (Family: Poaceae) is a perennial rhizomatous reed, 2-5 m tall that can grow in close stands [27]. Different species, subspecies and varieties describe the genus Phragmites, including: *Phragmites australis* (Cav.) Trin. ex Steud. [28], *Phragmites karka* (Retz.) Trin. ex Steud., *Phragmites mauritianus* Kunth*, Phragmites japonicus* Steud. [29,30] and *Phragmites frutescens* [31,32]. *Phragmites australis* (Cav.) Trin. ex Steud. (common reed) is a cosmopolitan reed and the most widespread worldwide of the different species [30]. There are three different lineages of *Phragmites australis* (Cav.) Trin. ex Steud. in North America. Among these lineages, one is native and called *Phragmites australis* subsp. *americanus* Saltonstall, P.M. Peterson & Soreng, one lineage is present across the southern U.S., Mexico and Central America (Gulf coast type) [33] called *Phragmites australis var. berlandieri* [29] and, the third is the invasive introduced subsp. *australis*.

Paleontological investigations through peat analysis in North America performed to reconstruct the vegetation of tidal marshes have reported the presence of Phragmites dating 3000-4000 of years ago [34,35]. It is believed that the invasive form was introduced to North America with the contamination of ballast water during the 1800s [33].

In Canada, *Phragmites australis* was introduced in early 1910, and before 1970 it was still scarce in most of the country. In 1950, only few botanical collections had records of *Phragmites australis*, whereas the native species was present in 325 collections. It was assumed that the limited road network at the time could have prevented the spread. Only after 1990 it became documented as an invasive plant, and in 2001 the distinction between native and invasive species was made, separating them into subspecies, subsp. americanus and subsp. australis, respectively. By 2010, subsp. australis was extensively spread in the eastern part of Canada, and it was making its way to western Canada [36]. More recent advanced DNA studies [37,38] investigated which factors can contribute and promote the invasion success of some species, specifically the hypothesis that genome size is related to plant invasion, suggesting that smaller genome size species are more

likely to be invasive than larger genome size. These studies have inferred that many functional traits, such as individual growth, reproductive success and dispersal, are wider in small genomes compare to larger ones, which could be potentially used as a predictor in identifying the factors related to invasion success. In particular, Pyšek et al. [39] found that the monoploid genome size was the significant variable which distinguished the North American native Phragmites from the European species, stating that the European populations that invaded North America had a smaller genome which was associated to functional traits favoring the invasiveness characteristics, including long rhizomes, low C:N ratio in the rhizomes, and earlier shoots growth in spring. However, the authors stated that more investigation is needed to confirm further the relationship between genome size and the traits associated with invasive behavior. Pyšek et al. [38] evaluated the competition between 20 populations of *Phragmites australis* collected both in North America (native and invasive clones) and Europe (native) to gather a better understanding on the role of genome size. Each one was planted in competition with one of the others. Their experiments showed that both European and North American clones were successful at prevailing over the North American native clones. They suggested that a similar competition could have been established between the invasive species and the native one in the first stage of invasion.

The subsp. *australis*, from this point on called *Phragmites australis*, has a fast-growing behavior related to its method of expansion associated with vegetative propagation [27], aerial seeds dispersal and rhizomes spread [33]. The seeds are located at the top of the stem, where each plant can produce annually hundreds to thousands of seeds per year. *Phragmites australis* has a very intricate rhizome network, both horizontal allowing the further spread of the plant and, vertical, for the stem growth [40].

At the early stages of growth, the *Phragmites australis* could show the same morphological characteristics of the native species. The similarities and differences are reported in Table 1.1.

Table 1.1 – Characteristics of native and invasive *Phragmites australis* [6,36]

Plant characteristics	Native	Invasive
Stem Height	Less than 4 meters tall	Over 6 meters tall
Stem Flexibility	Flexible	Rigid
Stem Texture	Smooth and shiny	Rough and dull
Stem Color	Lower stem internodes: yellowish to brown; green stem	Lower stem internodes: reddish-purple; green stem
Seed Heads	Small and sparse	Dense and large
Leaves Color and Orientation	Yellow-green leaves, 30 degrees from stem	Blue-green leaves, 45 degrees from stem
Leaves Characteristics	Leaf easy to remove	Leaf sheath difficult to remove

The invasive species has several impacts on the ecosystem. Since it is taller than most vegetation, it prevents the growth of other plants by blocking the sun and growing in denser stands, thus smothering the native vegetation which result in damage of wildlife habitat especially for Species at Risks [2,6,41,42].

Its aggressive and fast-growing way of spreading has caught the attention of Canadian municipalities to enforce management practices [33,42–45] to assess and control the invasion. There are different control programs, amongst these: herbicide application (glyphosate) and the combination of herbicide and controlled burning [45], mechanical and manual cutting [46], flooding [47], and disposal in landfill [6,42,44]. In Ontario, on the west shoreline of Collingwood, approximately 18 metric tons of *Phragmites australis* were collected and properly disposed at the local waste facility from 2015 to 2017 [48].

Due to the high yield of biomass worldwide, *Phragmites australis* has been investigated as feedstock for bioenergy. In Southern Finland [7] it was estimated that 30,000 hectares of coasts were covered in reed beds with an harvest productivity of 150,000 tons per year

and, it was suggested that the biogas road combined with the use of the sludge waste from digestion should be investigated as a fertilizer to replenish the nutrients in the soil in the summer months. Also, it was suggested that *Phragmites australis* could be a potential local source of additional energy for furnaces and heating plants by processing the reed into pellets or briquettes. However, since grasses have a higher ash content than woody biomass, harvesting the reed in winter is better to avoid ash fusibility on furnace surfaces or heat exchangers, since the nutrients and minerals in winter are stored in the rhizomes and roots [49].

Baute et al. [50] studied the suitability of *Phragmites australis* as a feedstock for anaerobic digestion for biogas production by comparing two commonly used energy crop, *Miscanthus x giganteus* and *Panicum virgatum*, commonly called Switchgrass. They harvested the biomass in July and October 2013 and 2014. The *Phragmites australis* yield in Southwestern Ontario was 1.82 ± 0.9 kg dry matter m^{-2} and it was approximately the same yield of *Miscanthus* and higher than the yield of *Panicum virgatum*. Results showed that the best harvesting time to achieve the highest methane potential per unit biomass was early summer, due to the higher moisture and protein content, which lead to more digestible biomass. To achieve the highest methane yield per area harvested, the best time would be at their peak yield (October). However, since concern existed that the seed and rhizomes of *Phragmites australis* could survive after anaerobic digestion, which could increase the risk of spread, Baute et al. [51] investigated the seed survival rate after digestion. They determined that the viability of the seed is reduced by 95% after 52 hours of digestion, which is lower than typical retention times of anaerobic digesters (240 to 1280 h).

Gao et al. [14] investigated *Phragmites australis* and Switchgrass as alternative low cost feedstocks for acetone-butanol-ethanol (ABE) fermentation. Results indicated that both grasses are suitable for ABE fermentation, with Phragmites yielding an ABE production of 19.75 g/L (10.14 g/L of butanol), whereas switchgrass yielded 22.7 g/L, including 13 g/L butanol. The difference was due to the lower initial glucose concentration in the media for Phragmites (35.69 g/L glucose compared to 40.37 g/L of Switchgrass).

Few studies have investigated pyrolysis for the conversion of *Phragmites australis* [8,52–57], however, compared to Miscanthus and Switchgrass the contribution is still low.

1.4   Lignocellulosic biomass

Plant biomass is a sustainable and renewable resource, formed by the reaction of CO_2 in the atmosphere with sunlight and water into carbohydrates and oxygen. This process is called photosynthesis and it is closely linked with the plant's internal respiration in which carbohydrates are combined with oxygen to release CO_2, water and energy [58].

Extractives, cell walls and inorganic ash represent the main components of plant biomass [59]. The cell walls are made of carbohydrates (cellulose and hemicellulose), lignin and pectin unevenly distributed and linked together with both hydrogen and covalent bonds [60,61]. Cellulose, the main component of the cell wall in plants [62], is a polymer composed of D-glucose units linked via β-1,4 glycosidic bonds forming cellobiose molecules [63]. The monomeric units link together by hydrogen bonds and Van der Waals forces to form chains of 10,000 or more structural units with a high degree of polymerization [64]. These chains form the microfibrils which are surrounded by hemicellulose and lignin, both binding the cellulose fibers together [65]. Hemicellulose is an amorphous polymer consisting of different sugar monomers, such as xylose, mannose, glucose, galactose, arabinose, and glucuronic acid arranged in a branched chain structure with lower degree of polymerization and lower strength compared to cellulose [66]. Lignin is an aromatic macromolecular polymer, amorphous and highly branched, containing guaiacyl, syringyl, and p-coumaric structural units [67], with varying composition amongst different species, for example wood of angiosperm trees comprise only guaiacyl, syringyl units, while grasses contain guaiacyl, syringyl, and p-coumaric units [68]. Lignin cross-links the cellulose fibers with hydrogen bond [68], whereas covalent bonds (mainly ether bonds) have been proposed for coniferous and non-coniferous wood [69]. Hemicellulose and lignin are linked together by hydrogen and covalent bonds [61]. Cellulose and hemicellulose are responsible for the plant strength [59], while lignin has various functions in vascular plants; in cell walls ensures the

impermeability of the vessels that carry the sap, it contributes to the rigidity of the cell walls [70,71], and provide resistance to pest attacks [61,68].

The extractives are non-structural components that comprise fats, phenolics, resin, acids and waxes. They are not-chemically bound to the other compounds and they can be found in the porous structure of the biomass [64,70].

The mineral composition is different between plant species and the ash content can vary from less than 1 wt% d.b. (e.g. woody biomass such as pine wood [72]) to above 20 wt% d.b. (e.g. rice straw [73,74]). The main elements are Silicon (Si), Calcium (Ca), Potassium (K), Sodium (Na) and Magnesium (Mg); Sulphur (S), Phosphorous (P), Iron (Fe), Manganese (Mn) and Aluminum (Al) are typically present in smaller quantities. These elements occur as oxides and salts such as chlorides, carbonates, phosphates and sulphates [73–75].

1.5   Pyrolysis of lignocellulosic biomass

Understanding the reaction mechanisms of cellulose, hemicellulose and lignin during pyrolysis is of fundamental importance. In fact, cellulose, hemicellulose and lignin react at different temperatures and heating rates yielding a wide array of molecules. Early and current work on pyrolysis, which is summarized in the following paragraphs, proposed chemical pathways and, aimed to further improve the understanding of the complex reactions involved to improve the quality of the pyrolysis products.

1.5.1   Primary and secondary cellulose pyrolysis reactions

Different models have been proposed over the years for the decomposition of cellulose. The most cited mechanisms are the the Broido-Shafizadeh model (Bradbury et al. [76]), Waterloo model [77], and Varhegyi-Antal model [78]. The Briodo-Shadizadeh (B-S model) and Waterloo models consider the formation of a controlling intermediate (active cellulose in the B-S model and low degree of polymerization cellulose, in the Waterloo model), before two competing reactions take place to produced char and gases or volatiles. Antal and Varhegyi's investigation [78] confirmed the parallel reaction

mechanism, however they proposed a simple first-order reaction to describe the formation of volatiles and secondary vapor-solid interaction forming char and gases suggesting that the intermediate step at those temperature was either superfluous or it did not take place. Later Shafizadeh [79] updated the mechanism, considering that the volatiles could act as an intermediate for secondary cracking reactions. In recent years, several studies have reported the formation of a liquid intermediate under high heating rate conditions. Boutin et al. [80] investigated the fast pyrolysis of cellulose under radiative heating, reporting that cellulose undergoes a melting to liquid phase in which the sugars (levoglucosan and other oligo-anhydrosugars) become volatiles. In this liquid phase, many of the char forming reactions take place. Fisher et al. [81] studied the pyrolysis behavior of cellulose, hemicellulose and pectin above 400°C. When heating rate above 1000 °C s^{-1} were achieved, all the compounds indicate signs of softening and swelling. Wang et al. [82] investigated the degradation of cellulose by comparing two cellulose samples with different crystallinity. Under slow heating rate conditions at 300°C, the amorphous cellulose was less stable and yielded more levoglucosan. At temperatures between 350°C and 450°C, the more crystalline cellulose yielded levoglucosan and levoglucosenone, whereas the amorphous cellulose degraded forming an intermediate. The intermediate underwent dehydration reactions with the formation of a high yield of 5-(hydroxymethyl) furfural, 5-methylfurfural and furfural followed by the elimination of water. The sample with higher crystallinity didn't show any liquid intermediate.

In general, two reactions are recognized: a reaction favored at low temperature (<300°C) and slow heating rates involving the dehydration of cellulose to form anhydro-cellulose and water, which can further react to form char and gases, and a second reaction at 300–500 °C involving the depolymerization of cellulose to produce a tar phase rich in levoglucosan [83–87]. Levoglucosan is typically formed during fast pyrolysis conditions. If slow pyrolysis is implemented, the dehydration reactions are the predominant mechanism. Scheirs et al. [88] investigated the evolution of water at three temperatures, <220°C, 220–500°C and >500°C. They found that the water had a peak at two temperatures, the first loss with 10% of the total water evolved at 110°C and the second

loss with 90% at around 300°C. This distinction was due to the water that was absorbed and chemically bonded in the material.

Different studies have reported that the yield of levoglucosan is reduced at high temperatures, claiming that the levoglucosan acts as an intermediate for the formation of other products, such as hydroxyacetaldehyde and hydroxymethyl-furfural, that are increased at higher temperatures[89], suggesting a competitive mechanism between levoglucosan and the other products [89,90].

The secondary reactions can take place in solid and intermediate liquid vapor phases, with the production of char accompanied by the formation of CO_2, H_2O and H_2 [88] and acetol, 5-(hydroxymethyl) furfural, furfural and hydroxyacetaldehyde.

Essig et al. [87] proposed that hydrxyacetaldehyde in cellulose forms by a primary ring fragmentation mechanism. It was postulated that a midchain, heterolytic scission of the glycosidic linkage, produced levoglucosan. This was later confirmed experimentally by Piskorz et al. [77]. They proposed that the decomposition of cellulose can follow two major pathways, one leading to levoglucosan with the depolymerization of low degree of polymerization cellulose, and the fragmentation leading to hydroxyacetaldehyde as one of the major products, acetol, acetic and formic acids. The morphology of cellulose, as well as the alkaline cations and temperature determine the probability of the pathways. However, the temperature effect exercises only a mild influence compared to the inorganic salts.

1.5.2   Hemicellulose pyrolysis reactions

Hemicellulose and amorphous cellulose have a similar degradation temperature at 250 – 300°C. Hemicellulose is a branched heteropolymer composed of a C6 and/or C5 sugar backbone linked by β-(1 → 4) glycosidic bonds. Very limited studies are available on the reaction pathways of hemicellulose due to the difficulties of achieving a satisfactory extraction, thus xylan is often used as a model compound. The primary products obtained from the isolated structures of hemicellulose are acetic acid, furfural, formic acid, 5-hydroxymethyl furfural [91].

Shafizadeh et al. [92] compared the pyrolysis products from xylan compounds extracted from cottonwood (4-0-methylglucuronoxylan and 0-acetyl-4-O-methylglucuronoxylan) and D-xylose and methyl β-D-xylopyranoside, selected as model compounds with and without the addition of sodium hydroxide and zinc chloride. They stated that pyrolysis of xylan polysaccharides and related model compounds involves the thermal cleavage of the glycosidic group through a combination of competitive dehydration, fragmentation and disproportionation reactions. The addition of sodium hydroxide favored fragmentation reactions leading to a product with low molecular weight, whereas zinc chloride favored the formation of 2-furaldehyde, water, and char.

Hemicelluloses, arabinoxylan and uronic acids isolated from wheat straw were investigated by TG and pyrolysis gas chromatography and mass spectrometry (py-GC/MS) [93]. The results suggested that the decomposition of hemicelluloses mainly happened between 190 and 315°C and formed a 24 wt% residue at 700 °C. The result of py-GC/MS revealed that the volatile products at lower temperatures were manly acetic acid and other compounds from dehydration, scission of side chain and depolymerization reactions, whereas at higher temperatures the products were more complex including acids, ketones, alcohols and cyclopenten-1-ones.

Patwardhan et al. [94], investigated the primary products of the fast pyrolysis of hemicellulose extracted from Switchgrass by different techniques including micro-pyrolyzer-GC-MS/FID and gas analysis. They identified 16 different products (85% of the total) including CO_2, formic acid, char, xylose, acetol, CO, 2-furaldehyde. The char yield from hemicellulose pyrolysis was about 10.7 wt%, as compared to 5 wt% from cellulose. The effect of minerals (NaCl, KCl, $MgCl_2$, and $CaCl_2$) and ash from Switchgrass were investigated on the pyrolysis product distribution. The inorganics and ash increased the CO_2 and char yield and decreased the formic acid and acetol, whereas the chlorides increased the 2-furaldehyde. They speculated that the decomposition of hemicellulose and the formation of products follow similar reaction pathways as those of cellulose pyrolysis.

The mechanism of hemicellulose fast pyrolysis has been studied recently by Zhou et al. [95]. A hemicellulose structure was extracted from corn stover with a monosaccharide composition of arabinoxylan that had a b-1,4-linked xylopyranose backbone with a-1,3-linked arabinose side groups. Modelling results showed that both the degree of polymerization and the polydispersity index of hemicellulose have an insignificant effect on the pyrolysis product distribution.

1.5.3   Lignin pyrolysis reactions

The mechanism of the thermal degradation of lignin, due to its complex structure, is strongly influenced by nature, reaction temperature and heating rate, which also affect the temperature range of degradation, conversion and product yields [96,97]. Depending on the isolated type of lignin, the pyrolysis products distribution can vary strongly. Evans et al. [98] studied the primary pyrolysis of lignin. Lignins comprise phenylpropane units formed from coniferyl alcohol in softwood, coniferyl and sinapyl alcohol in hardwood, and coniferyl, sinapyl and coumaryl alcohol in grasses. Therefore, the monomeric units in hardwood lignin comprise guaiacyl and syringyl units, whereas lignins from softwood have only guaiacyl units [99]. Results from the pyrolysis of two lignins derived from Japanese wood species, Japanese cedar (softwood) and Japanese beech (hardwood) showed that lignin extracted from hardwood produced volatiles at lower temperature and more coke than softwood, which was consistent with the higher coking reactivity of the syringol compared to guaiacol [100]. Based on results from gas chromatography/mass spectrometry (GC/MS), guaiacol (2-methoxyphenol) and syringol (2,6-dimethoxyphenol) derivatives are formed from hardwood lignin, while vinylphenol is found as a product of the pyrolysis of grasses [101,102].

Lignin decomposes over a wider range of temperatures (200 – 900°C) compared to cellulose and hemicellulose and it is the major contributor to the residue (around 40 wt% [103]). The guaiacyl and syringyl units are linked together though ether (C–O) and C–C bonds. The C–O and C–C bonds in lignin required a higher temperature to open compared to the C–O linkages in cellulose. At higher temperatures, demethylation, demethoxylation, decarboxylation, and alkylation occur, leading to the change of product

distribution toward phenol, catechol, and alkyl phenols such as 2-methylphenol, 4 methylphenol and 2,6-dimethylphenol, whereas the yield of guaiacol and syringol decreased with increasing temperature [104].

Evaluation of the DTA curves at 0.5, 2 and 10 °C/min showed an endothermic peak at 100 –180°C due to the water evaporation, followed by two exothermal peaks at 280°C with the scission of aliphatic groups and some carbonization on the surface, to 380°C with the scission of aromatic parts and complete surface carbonization. The second peak at 460 °C to 500°C suggested that the carbon in the char is condensed into graphite-like rings [97]. TGA analysis were performed [96,105–107] to evaluate the mechanism of lignin degradation. However, a large variation of activation energy was reported in different studies. A single first-order reaction for the thermal decomposition of lignin was assumed for the calculation of the reaction rate constant, and activation energy. The activation energy reported in the different studies varied from 35.5 to 79.42 kJ/mol and increasing to 81.2 – 361 kJ/mol.

1.5.4   Effect of inorganics on the pyrolysis products

It is well known that the AAEMs present in biomass during pyrolysis act as a catalyst of pyranose and furanose ring-fragmentation and dehydration reactions which increase the char, water, gas and light organic yield such as aldehydes and carboxylic acids [79].

One of the many problems created by the AAEMs is the higher water production, which is often responsible of phase separation in the bio-oil increasing its instability during storage [108]. Moreover, the inorganics can cause fouling in the reactor chamber since they have lower melting point, and the combination with other elements can form undesirable slugs and deposits (the reaction between K and Si with Cl leads to the formation of fused glassy deposits and slugs at 800 – 900°C) [109,110].

The main effect of the inorganics on the bio-oil chemical composition is a decrease in levoglucosan content [111–114]. Many researches have attempted to passivate the AAEMs to increase the yield of levoglucosan in the oil. Different pre-treatments have been implemented over the years on woody and grassy feedstocks. Water reduce the

water-soluble minerals (Na and K), nonetheless acid treatment is required to achieve higher removal rates for the water-insoluble minerals (Mg and Ca) [109,110,115–117]. Leaching using water and acidic solutions result in an increased levoglucosan concentration and a decrease in hydroxyacetaldehyde, which is formed in competition with levoglucosan [118]. Radlein et al. [119] used sulfuric acid at different concentration (1, 3 and 5%) at 90°C for 6 and 19 hours to pretreat poplar wood. Results showed that the hemicellulose was hydrolyzed during the treatment. Bio-oil yield was 78 – 80% with a decreased water content and decreased char and gas yield compared to untreated wood. The levoglucosan increased from 3 – 5% to 15% with the mild acid solution and to 30% at higher sulfuric acid concentration. A parallel decrease of hydroxyacetaldehyde was reported from 10 – 12% to 0 – 5%. Similar results were reported by Piskorz et al. [77]. They pre-treated hybrid poplar wood with sulfuric (5%, 100°C and 2 h) and hydrochloric acid (3.7%, 100°C and 2 h; 0.5%, 165°C 6 min) achieving 90% of ash removal. Pyrolysis results showed an increased yield of liquid oil (79.6%) and reduced water, gas and char yield. The levoglucosan yield increased, while low molecular weight aldehydes, ketones and acids were less than 1% on wood basis. However, grassy feedstocks have a higher content of ash compared to woody biomass, which is even more detrimental in terms of bio-oil and levoglucosan yield. Fahmi et al. [120] investigated the effect of water washing on different grass species, confirming that water washing was effective in reducing the metal content to 60 – 80%. Moreover, a similar trend was found for grasses in terms of increased levoglucosan yield and decreased hydroxyacetaldehyde. Kuzhiyil et al. [121] studied herbaceous biomass (Switchgrass and corn stover) using mineral acid infusion (phosphoric and sulfuric acid) to stoichiometrically convert the AAEMs into more thermally stable acid salts (particularly potassium sulfates and phosphates) that not only passivate the fragmentation reactions of the pyranose rings but also promote the glycosidic bond cleavage, thus increasing the levoglucosan yield (from 2% to 10 – 15% for switchgrass). Liu and Bi [117] pretreated pine bark and switchgrass with different acidic solutions and water. Water leached around 40% of the inorganics for switchgrass, and acetic acid was more effective at reducing the ash content compared to HCl and HNO$_3$ at the same pH, however since acetic acid is a weak acid, a higher concentration in

the washing solution is required. Sulfuric acid was the most effective at lowering the ash content in bark. However, they stated that H_2SO_4 and HCl could introduce sulfur and chlorine, which can contribute to increased SO_2 and dioxins and furans emissions. Thus, they suggested acetic and nitric acid as the preferred acidic solutions for biomass pretreatment.

Oudenhoven et al. [122–125] studied the use of the light oil phase from wood pyrolysis which contains acetic acid as a washing solution to reduce the AAEMs content. They found that the AAEMs were significantly reduced in pine wood, and consequently they reported an increased organic oil and levoglucosan yield (3.4 to 17 % on biomass feed basis) and a decreased char yield and water content. However, in order to maximize the levoglucosan, the biomass should be rinsed with water after acid washing [122]. In a another paper [123], they used organic acid leaching for straw, hay and bagasse to evaluate the chemical composition and AAEMs removal efficiency. They found that the treatment was successful at removing 97% of the AAEMs content all the biomass tested with the exception of bagasse, though bagasse was already treated with water in the sugar process. The organic oil was increased for all the feedstocks, and the levoglucosan yield increased from 3% for straw to above 20% in the first condenser. In a recent study [125], the feasibility of the pre-treatment stage using pyrolytic acids was evaluated for a pyrolysis unit of 5 and 50 t h^{-1} to process pinewood, straw and bagasse. The total CAPEX cost increased by 36% considering only acid leaching and 47% if product separation is included in the process. The profit, at the current market state, was obtained only when bagasse was considered as feedstock, due to the high cost of pinewood and straw. They suggested that the feasibility could be further improved when the phenolic fraction is also utilized (for example for phenolic resins) and further process integration with existing waste-water treatment plants.

1.6   Reactor technologies

Typically, the reactors are classified according to their vapor and solid residence time. Fast pyrolysis is carried out at temperature around 500°C, with fast heating of the biomass, particle size distribution less than 2 mm to maximize heat transfer rates, and a

vapor residence time of 1 second. These operating conditions coupled with rapid quenching of the vapors maximize the bio-oil yield. Slow pyrolysis reactors are instead used when the product of interest is biochar [21,126,127]..

1.6.1   Fast pyrolysis

The first types of pyrolysis reactors were entrained downflow reactors. No heat carrier was used to transport and heat the particles and the temperatures were usually between 700-800°C to be able to achieve 1 second of vapor residence time [128]. This type of reactor was later on dismissed due to the insufficient heat transfer during the short particle residence time, which resulted in a char product not properly pyrolyzed and low bio-oil yields [129].

Ablative reactors use high gas flow rates to force the biomass particles towards a heated wall or plate surface, where the biomass is moved rapidly and leaves a film behind which evaporates [130,131]. Since larger particles can be processed with this technology, depending on their size, recirculation is usually implemented to improve the bio-oil yield [59,132]. Although it is more difficult to scale up the reactor since the process limiting step is the rate of heat supply to the reactor it is possible to achieve a higher bio-oil yield, since there is no need for inert gas, also the bio-oil collection equipment can be smaller compared to other systems [133].

Another technology that doesn't require the use of the inert gas is the rotating cone reactor technology. Biomass and hot sand are fed to the rotating cone where the centrifugal force pushes the biomass against the hot wall and the hot sand and char are transported spirally upward. Because of the good mixing, rapid heat transfer rates are achieved. Liquid yields between 60 –70 wt% are reported [134]. This technology is commercialized by the Biomass Technology Group – Biomass to Liquid (BTG–BTL) which also comprises a char combustor to reheat the sand [135].

Bubbling fluidized bed reactors (BFB) use inert gas to keep the bed fluidized. The biomass is fed to the reactor which typically has a hot sand as a heat carrier. The intense contact between the biomass particles and the hot bed provides good heat transfer rates.

Typical bio-oil yields are in range of 70–75 % for woody biomass. The use of cyclones is needed to separate the entrained char particles from the condensate [59].

Circulating fluidized bed reactors are similar to bubbling-bed with the difference that the bed is expanded, and higher superficial gas velocities are achieved. The entrained solids are continuously recycled. High velocities, mixing and internal refluxing result in heating rates around 1000°C/s and residence time in the order of millisecond to a maximum of 5 seconds, which give a bio-oil yield as high as 75%. This reactor configuration has often been used to pyrolyzed woody and herbaceous biomass with bio-oil yields of above 60% at 500°C [20,21,136]. This type of reactor is used by Envergent Technologies (a joint venture between Honeywell's UOP and Ensyn Corp.) for their Rapid Thermal Processing (RTP) technology [137,138]. VTT with a consortium with Metso (Valmet), UPM and Fortum in Finland have developed a fast pyrolysis unit integrated with a fluidized-bed boiler at a commercial scale to convert forestry residues, wood chips and saw dust into bio-oil which is then combusted in a boiler [139].

An integrated process using a twin-screw reactor was developed at Karlsruhe Institute of Technology (KIT) with Air Liquide (Lurgi Technologies) for synthetic fuel production via gasification of wheat straw. The bioliq biomass to liquid (BtL) process involves the production of a slurry consisting of bio-oil with suspended biochar particles that is fed to the gasifier [140]. The energy content of the bio-slurry can be around 90% of the initial biomass energy [141].

1.6.2   Slow pyrolysis reactors

Slow pyrolysis of biomass is the process used when biochar is the main product. The temperature ranges for slow pyrolysis are between 400°C and 800°C, with slow heating rates and long solid residence time [142]. The most common reactors used in slow pyrolysis applications are rotary kilns, drums and screw augers.

Rotary kilns/drums are rotating cylinders, which are typically slightly inclined to ensure the continuous motion of the biochar toward the exit. The angle and speed of the rotary kilns control the residence time of the solid inside the reactor [143]. Rotary kilns are

commonly used for torrefaction. The rotation was found to have a significant effect on the product quality, with high speed leading to a not properly torrefied material and speed too low leading to a carbonized product [144]. The torrefaction of cedarwood was carried out in a pilot-scale rotary kiln where different temperatures (200-290°C) were investigated [145]. Results showed that the grindability and the hydrophobicity of the torrefied product were improved compared to the raw feedstock. Klose and Wiest [146] studied the slow pyrolysis of maize in a bench scale rotary kiln varying pyrolysis temperature, solid residence time and solid space time. Their results showed that temperature and space time had the strongest impact; increasing solid space time (which is related to the gas residence) increased the gas yield, while residence time didn't show a significant effect on the product yields in the range studied.

Screw-type pyrolyzers are reactors in which the solid residence time is controlled by the rotation of the auger. The auger mechanically moves the feedstock from the entrance through the heated reactor chamber to the exit, ensuring good axial dispersion and mixing of the feedstock particles [146]. Tsai and Lin [147] investigated the mixing of granular material for different screw conveyors. They observed that the material flow resembled the plug flow and the degree of mixing could be improved by increasing the screw diameter, flight diameter or thickness or decreasing the pitch. They stated that when a cut-flight conveyor screw with paddles was employed the mixing was increased as well. Also, other operating conditions such as rotational speed of the screw and particle size affected the mixing.

Garcia-Nunez et al. [143] in their review paper, stated that rotary drum and auger reactors are usually easier to operate compared to fluidized bed reactors and the gas produced, being less diluted with the sweeping gas, could be used for combustion in boilers or engines. Both type of reactors can be externally heated by a furnace or gas burners, or internally by heat carriers such as sand, steel balls. Moreover, the rotary drums can operate on a wide varieties of scales [148].

1.6.3   Condensation trains

There are many aspects to keep in mind when designing a condensation unit. Fast
pyrolysis aims to produce high yield of bio-oil. The condensable fraction of the pyrolysis
vapors needs to be cooled down rapidly to avoid secondary reactions that promote char
and gases [21]. Moreover, to improve the stability and tailor the production of specific
chemicals, fractional condensation is usually carried out, which aims to recover the oils
in different stages (condensers) at different temperatures.

Many studies have focused on condensation trains [149–152] including spray towers,
cyclonic condensers and electrostatic precipitators that use an induced electrostatic
charge to condense the vapors that are in aerosol phase.

Typically, the condensation unit comprises stages in series at different temperatures
selected according to the condensation temperatures of the molecules of interest. Pollard
et al. [152] developed a bio-oil fractionation system to target the condensation of
different compounds at different stages according to their dew points. Their condensation
system comprised five stages at reducing temperature; the first stage was a shell-and-tube
heat exchanger designed to operate in laminar flow to capture levoglucosan and
compounds with high dew points, stage 2 and 4 comprise electrostatic precipitators to
condense the aerosol, stage 3 and 5 were again shell-and-tube heat exchangers designed
to condense compounds with dew points similar to phenol and light oxygenated
compounds, respectively. Results from the pyrolysis of red oak at 500°C showed that the
water insoluble compounds (pyrolytic lignin) were highest in the first two stages, with 45
wt% collected in the ESP (oligomers derived from lignin occur as aerosol), and 44.2 wt%
in stage 1, likely due to the fact that water insoluble compounds existed as volatile,
relatively low molecular weight compounds before polymerizing to phenolic oligomers.
Levoglucosan was collected in stage 1 at concentration of 4.9 wt% and stage 2 at
concentration of 3.2 wt%. The condensation of levoglucosan in the ESP indicated that it
existed as an aerosol as well. The acetic acid was successfully condensed in stage 5,
although a small fraction (< 2.4 wt%) was collected in the first 2 stages and in relatively
high concentration in stage 3 and 4 (7 and 10.5 wt%).

Rover et al. [153] investigated the effect of the pyrolysis temperature (300-550°C) on the bio-oil yield and composition with the same pyrolysis unit described by Pollard. Although the yield of the products was strongly impacted by the pyrolysis temperature, the composition of single compounds in the oil fractions and their distribution weren't significantly changed. The highest sugar yield was found to be 13.5 wt% at 450°C. The phenols were highest (29.4 wt%) when the reactor temperature was at 400 °C. The majority of anhydrosugars and phenols were collected in the first 2 stages. The highest water content was observed in stage 5, when the reactor temperature was 550°C.

Westerhof et al. [149] investigated the effect of reaction and condensation conditions on the bio-oil composition. They studied the fast pyrolysis of pine wood in a fluidized-bed reactor at 330°C and 480°C, with two counter-current spray towers in series. The first condenser temperature was varied between 20 and 115°C, while the second condenser was kept at 20°C. Results showed that decreasing the reactor temperature to 330°C, reduced the amount of mid-boilers (phenols and furans) and heavy compounds being released from the feed, whereas when the reactor temperature was increased to 480°C, the sugar content increase of 1.7 times, mid-boilers 1.9 times (because of their low vapor pressure) and water-insoluble lignin-derived oligomers 4.4 times than at 330 °C. No significant changes in the yields of light organics where observed. When the temperature of the first condenser was maintained around 70−90 °C, the bio-oil collected had less water content and less acetic acid (3-2 wt%), and above 90% of light fractions were collected in the second condenser with a 10% acetic acid content.

1.6.4   Market and value-added products

Motivated by environmental concerns, considerable efforts have been made around the world to move towards a bio-based economy built on renewable resources. According to the IEA Bioenergy Task 42 [154] bio-based chemicals are expected to double in next years due to different drivers including increasing oil prices, the need to reduce greenhouse gases emissions and the need to diversify energy resources.

However, challenges still exist due to the high cost associated with the process, and the need to improve separation techniques and recovery. Moreover, the final product might not exhibit the same performance of the fossil-derived one (less reactive phenols in bio-oil compared to pure phenol [155–157] for phenol-formaldehyde resins). Nonetheless, research efforts continue. The feasibility could also be improved by selecting low-cost available materials.

Different pyrolysis processes have been proposed to produce chemicals. A list of the main chemical of interest specific for this research has been reported as follows.

Levoglucosan is an organic compound with five chiral centers which has the potential to be used as a raw material for the synthesis of biodegradable polymers, solvents [158,159] and pharmaceuticals, for the synthesis of aminoglycoside mimetics [160] that are known for their bactericidal properties, and more recently for the development of new antiviral agents. High yield of levoglucosan can be obtained with fast and vacuum pyrolysis of cellulose and starch though one of the challenges is separating the levoglucosan from the other pyrolytic compounds [161]. Rover et al. [25] extracted crystallized levoglucosan from organic phase bio-oil produced from red oak. They studied a combination of bio-oil fractionation, liquid–liquid extraction, and resin filtration which produced a mother liquor with 81.2 wt% total sugars of which 44.7 wt% was levoglucosan. The filtration step successfully removed phenolic compounds and other contaminants, followed by solvent washing of the crystal mass allowed to recover 24.7% levoglucosan from the mother liquor as crystals. Techno-economic analysis showed that their process to obtain levoglucosan crystals had a cost of $1333 per MT, which is ten times lower than the current market price range ($10 000–50 000 per MT). This is a promising results since the low cost recovery and purification are what hinder levoglucosan extensive use [161].

Another chemical present in bio-oil is acetic acid, which is the main organic acid in the oil. It is formed by the thermal decomposition of all three main components of the biomass [16]. Acetic acid is widely used as an intermediate for vinyl acetate monomer which is the precursor to polyvinyl acetate used in paints, adhesives, textiles, paper, films

and chewing gum [162]. Global acetic acid market size is set to reach USD 17.9 billion by 2024 [22].

Phenolic compounds in the bio-oil could have the potential replace phenols from fossil fuels. It was estimated that the phenolic fraction in the oil (around 30%) could yield around 12% by weight of phenolic resin [163].

This study includes the use of water and acid washing pretreatment for the biomass, therefore, the potential exploitations of the leachate is of interest. Wastewater management is an important variable to consider for the development of lignocellulosic biorefineries. Tobin et al. [164] investigated different treatment options for the waste water, stating that the process design should attempt to minimize the downstream treatment, maximizing the product recovery such as fresh water and natural gas.

The leachate from washing pre-treatments was subjected to reverse osmosis (RO) to recover nutrients from biomass washed with water [165,166]. Studies show that RO could recover over 80% of calcium, magnesium, phosphorus, and silica, although high permeate flux were reported at the beginning of the filtration, due to the initial total solid concentration of leachate. It was suggested that a spiral-wound membrane for future studies to improve the RO performance [166]. Jenkins et al. [165] studied reverse osmosis as a treatment option for the leachate obtained by washing rice straw with water. They evaluated the ion and chemical oxygen demand (COD) rejection by the membrane as a function of feed concentration. Recovery above 90% was achieved with rejection of COD and ions also above 90%, when processing a leachate rich in K and Cl. They suggested that land application of both leachate and concentrate could take advantage of nutrients extracted from the biomass.

Oudenhoven et al. [125] investigated the characteristics of the leachate collected after washing straw from herbaceous and agricultural waste with water and an acetic solution. They found that the chemical oxygen demand (COD) of the wastewater streams varied between 13 and 70 g/kg. Then, they considered the biological oxygen demand (BOD) as 70% of COD in order to check the potential to produce methane via anaerobic digestion.

Since their values were higher than 1 g/kg, implementing the anaerobic digestion step could help to reduce the treatment costs of the waste water.

Lastly, the biochar, considered a by-product of the pyrolysis reaction, gained more interest in the past decade due to its properties that could enhance soil carbon sequestration and other soil characteristics including water holding capacity, nutrients availability, microbial activity and alkalinity. Moreover, different biochar and activated carbon uses have been investigated in the literature, including use as a feed additive and its effect on the ruminant methane emissions and microbiota [167–169], adsorption of toxic contaminat from drinking and waste water [170–175], charcoal fibers in the textile industry [176,177].

Chapter 2

2   Materials and Methodology

This chapter contains the description of the equipment used for the pyrolysis and activation experiments, the materials and methodologies and all the analytical techniques used in the thesis.

2.1   Equipment

2.1.1   Batch pyrolysis reactor

The slow pyrolysis experiments in Chapter 3 and 4 were carried out in the Mechanically Fluidized Reactor (MFR) developed in previous years in ICFAR. The reactor is a cylinder made of 316 stainless-steel with a diameter of 15 cm and height of 25.4 cm (Figure 2.1). The lid comprises an internal vertical blade stirrer to keep the biomass/biochar in motion (8 rpm) during the pyrolysis reaction. The shape is displayed in Figure 2.2. After loading the biomass, the lid is placed on the reactor body's top flange with a graphite gasket in between to ensure proper sealing. The reactor body includes a hollow shaft where the mixer is engaged. An opening at the top of the shaft ensures the exit of the vapors released during the pyrolysis experiments into the condensation train (Figure 2.3).

The pressure inside the reactor is monitored with a pressure gauge with a 15-psi fast-acting pressure relief valve (McMaster-Carr, Cleveland, OH, USA). The inert gas (nitrogen) is introduced at the top of the reactor with a ¼ inch port. The reactor is heated by two mineral-insulated band heaters independently controlled using Watlow PID digital controllers (EZ-ZONE® PM, Watlow, Minnesota, USA) set to a constant temperature profile.

The temperature is provided using a type K thermocouple (Omega, St-Eustache, Quebec, Canada) placed within the bed of char. Other thermocouples are placed at the bottom, at the top of the reactor and at the entrance and at the exit of the first condenser. All the temperatures are recorded with an HH309A four-channel data logger (Omega, Quebec,

Canada). The temperature of the char bed is plotted versus the desired heating rate to check that the operating conditions are met during the pyrolysis experiment (Figure 2.1). When the vapors reach the condenser, a 90-degree elbow directs them towards the wall of the condenser which allows good heat transfer and agitation [150].

The bio-oil is collected using one condenser maintained at 0°C. A second condenser and a cotton filter are placed in series after the first condenser to ensure proper condensation of the pyrolysis vapors and accurate mass balance. The condensers are made of 304/304L-stainess steel, 2-inch pipe size, 24 inch long. The condenser was developed and optimized in a previous study [150]. The first condenser is placed overnight in a water bath inside a freezer. In this way, the ice bath is kept for the entire length of the experiment (Figure 2.2). The condensers and cotton filter are weighed before and after each experiment with the bio-oil still inside. The bio-oil is collected and centrifuged at 7000 rpm for 10 minutes in order to separate the heavy phase from the aqueous phase for the GC-MS analysis.

The biochar is removed from the reactor chamber and weighed the day after the experiment. The yields are calculated according to equation 2.1.

$$Yield\ (wt\%) = \frac{kg\ product\ formed}{kg\ of\ biomass\ loaded} \cdot 100\% \tag{2.1}$$
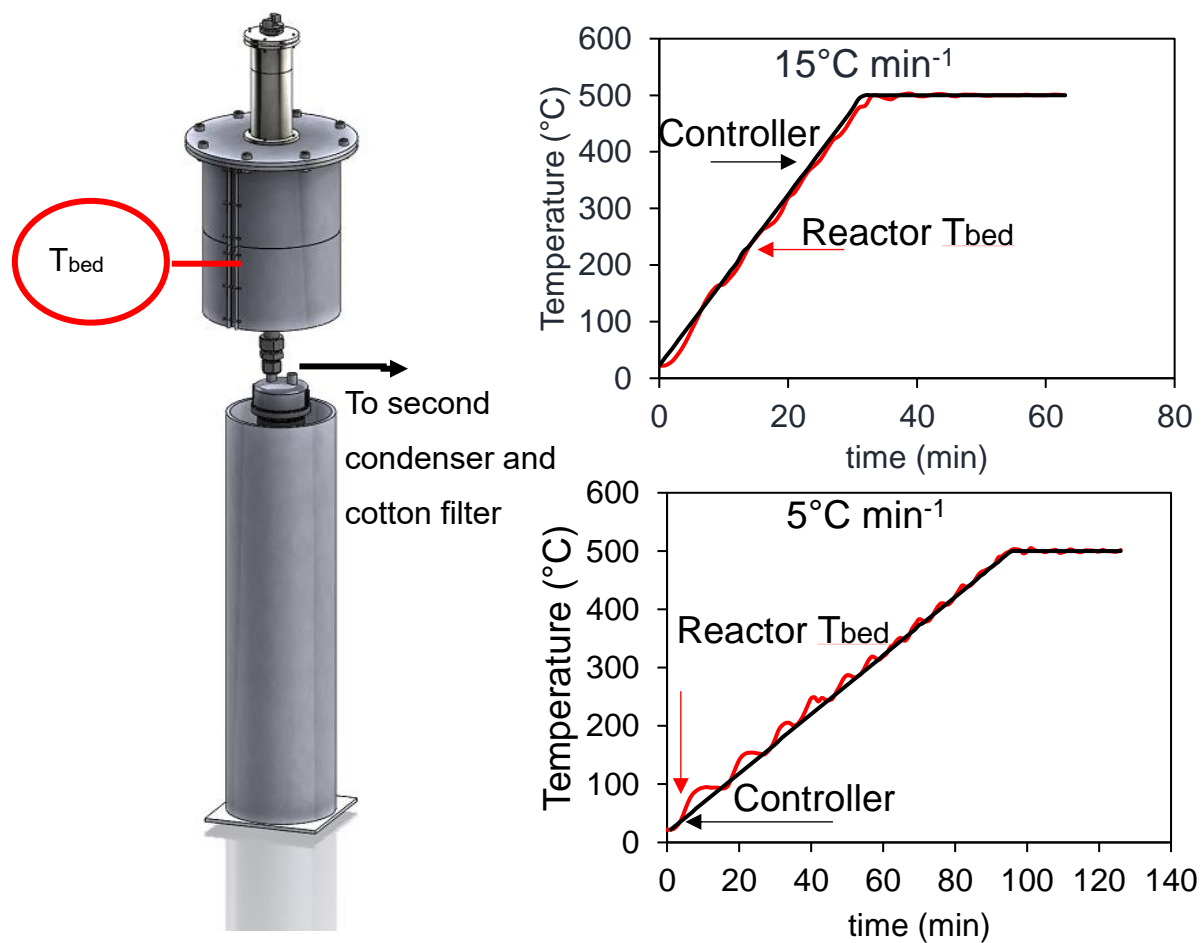
Figure 2.1 – Pyrolysis unit configuration and temperature control

Figure 2.2 – Unit components; a) stirrer; b) condenser after pyrolysis; c) reactor;
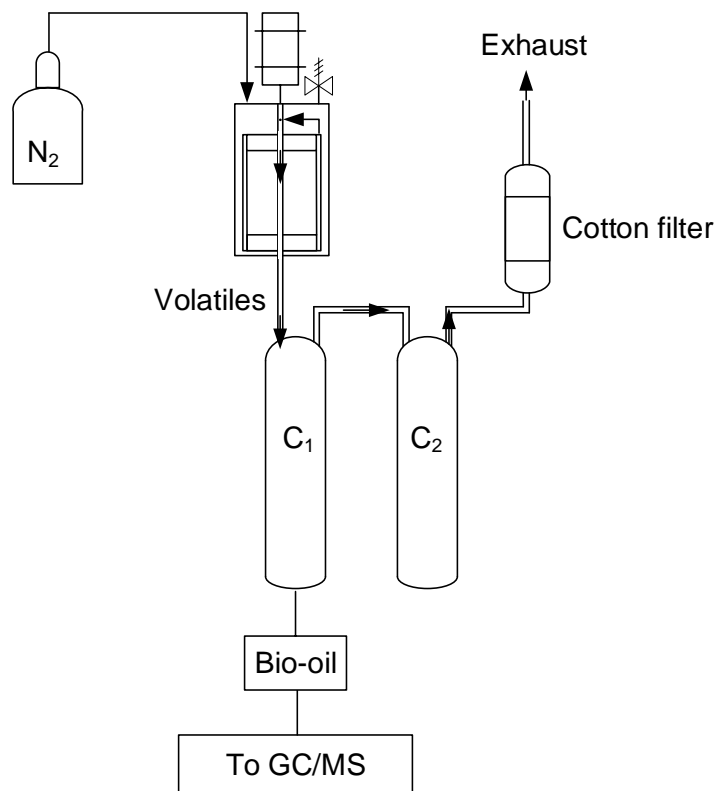
Figure 2.3 – Slow (batch) pyrolysis unit flow diagram

2.1.2   Design of a novel continuous pyrolysis reactor

The pyrolysis experiments described in Chapter 5 and Chapter 6 were carried out in a bench scale pyrolysis unit made of 316 stainless-steel designed and built for the purpose of this research (Figure 2.4 and Figure 2.5).
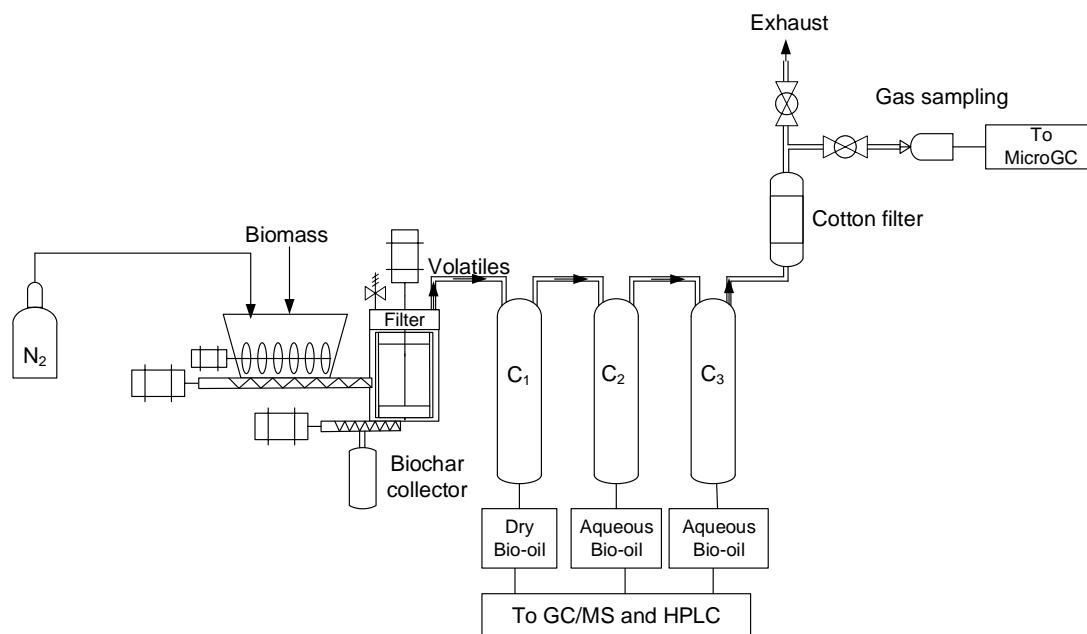
Figure 2.4 – Flow diagram of the fast pyrolysis process
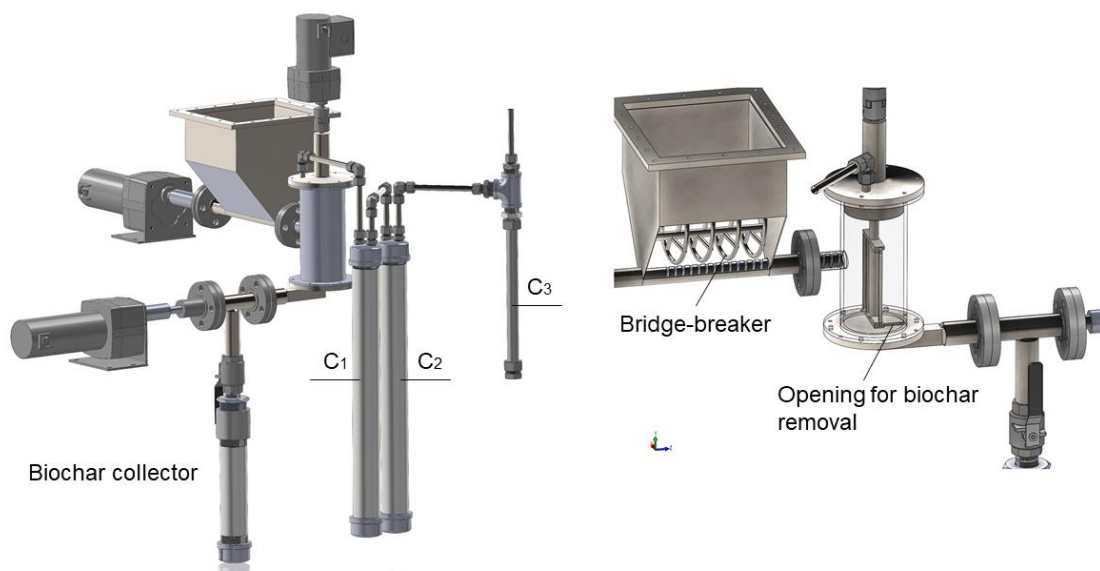
Figure 2.5 – Slow and fast pyrolysis unit with continuous extraction of biochar

The unit consists of a biomass screw-conveyor feeder, a 1.4-liter reactor vessel, one biochar collector for the removal of biochar during the pyrolysis experiments and a three-stage bio-oil fractionation system. The feeder comprises a bridge-breaker to avoid the bridging of biomass and have a constant feeding rate to the reactor.

Nitrogen is fed from the feeder to the reactor. To ensure proper mass balance, the condensation train including connecting lines and cotton filters were weighed before and after each experiment. The reactor was opened daily to collect any remaining biochar and the filter was changed before performing the experiment. All the parts of the unit were properly cleaned before each run to eliminate all chances of cross-contaminations between runs. Duplicates of pyrolysis experiments were performed to test the reproducibility of the pyrolysis set-up. However, due to the time consuming process for the preparation of the pre-treated biomass only one pyrolysis experiment could be carried out per treatment. The unit is described in detail in Chapter 5.

2.1.3   Biochar activation unit

The biochar produced at 650°C with 1 L min^{-1} of nitrogen and 60 minutes holding time in the new pyrolysis unit was physically activated with CO_2.

The activation was carried out in a horizontal 316 stainless-steel fixed bed tube, with a diameter of ¾ inch, wall thickness of 0.035 inch and 3 ft long. The biochar was placed in between two stainless-steel woven mesh and the activation was carried out in a furnace (Thermo Scientific Lindberg STF55666C Blue M Three-Zone Tube Furnace) at either 850°C or 900°C with a constant CO_2 flow rate of 200 mL/min. The impact of two holding times of 60 and 90 minutes were investigated on the activated char properties. Mass balance was carried out by weighing the biochar before placing it in the tube reactor and by weighing the activated carbon after removal.

2.2   Methodology

2.2.1   Sample preparation

The *Phragmites australis* used in the experiments were harvested in Ilderton, Ontario from a site near the ICFAR facility (University of Western Ontario) from 2015 to 2019. All the parts of the reed were used except for the rhizomes. After collection the biomass was air-dried and then grinded with a hammer mill (Valmetal 1215, Fritsch Equipment Corp., Wisconsin, USA) with a 1 mm mesh. The biomass was sieved with a USA standard sieve (ASTM E-11, Number 18 and Number 120) to have a particle size between 125 μm and 1 mm and different batches were characterized also with ICP-OES, thus ensuring consistency between experiments.

Before each pyrolysis experiment, the biomass was dried overnight at 105°C, to remove the moisture. Removing the moisture is necessary since it will require more heat to vaporize water during the pyrolysis process, and moisture will also reduce the organic yield in the bio-oil phase since the water can recondense with the bio-oil lowering its calorific value and stability [66].

2.2.2   Pretreatments

The biomass was pre-treated with different solutions to investigate the decrease of AAEMs responsible for secondary cracking reactions of the volatiles during fast pyrolysis and to improve the selectivity of target compounds, in particular levoglucosan. Different techniques have been studied and tested, comprising cold and hot water and dilute acetic acid solutions.

2.2.2.1   Water leaching in a water oven

The biomass was weighed (60 g) and placed in a Pyrex container with 1 liter of deionized water. The Pyrex container was sealed and placed in a water oven (SousVide, CO, US). The temperatures and holding times chosen for the experiments are reported in Table 2.1.

Table 2.1 – Water bath operating conditions

Washing conditions				
Water temperature (°C)	30		90	
Holding time (h)	1	24	1	24

After the selected holding time, the pH of the leachate was measured (Table 2.2), and the biomass rinsed with deionized water until the pH was in the range of 6-7.

Table 2.2 – pH of the water leachate before and after rinsing

Biomass pre-treatment	pH leachate after treatment	pH after rinsing
30°C 1h	4.50	6.02
90°C 1h	4.40	6.14
30°C 24h	5.13	6.38
90°C 24h	5.20	6.36

2.2.2.2   Water leaching with Soxhlet extractor

The Soxhlet extractor is an apparatus commonly used for the extraction of soluble components from a solid. The Soxhlet comprises three main parts, the boiling flask with

the extraction solvent, the extraction chamber where the biomass is placed inside a cellulose thimble to be washed and the condenser.

The boiling flask was placed in a heating mantle to boil the water (Figure 2.6). The vapors then passed through an arm at the top of the extraction chamber where condensation occurred. The condensate flooded the thimble until it reached the siphon, and then, the water was flushed back in the flask.

30 g of biomass were loaded in a cellulose thimble. The Soxhlet was operated for 48 hours for each batch until the desired quantity of biomass was obtained (300g).

The temperature of the biomass inside the thimble was monitored throughout the experiments (50-54°C).
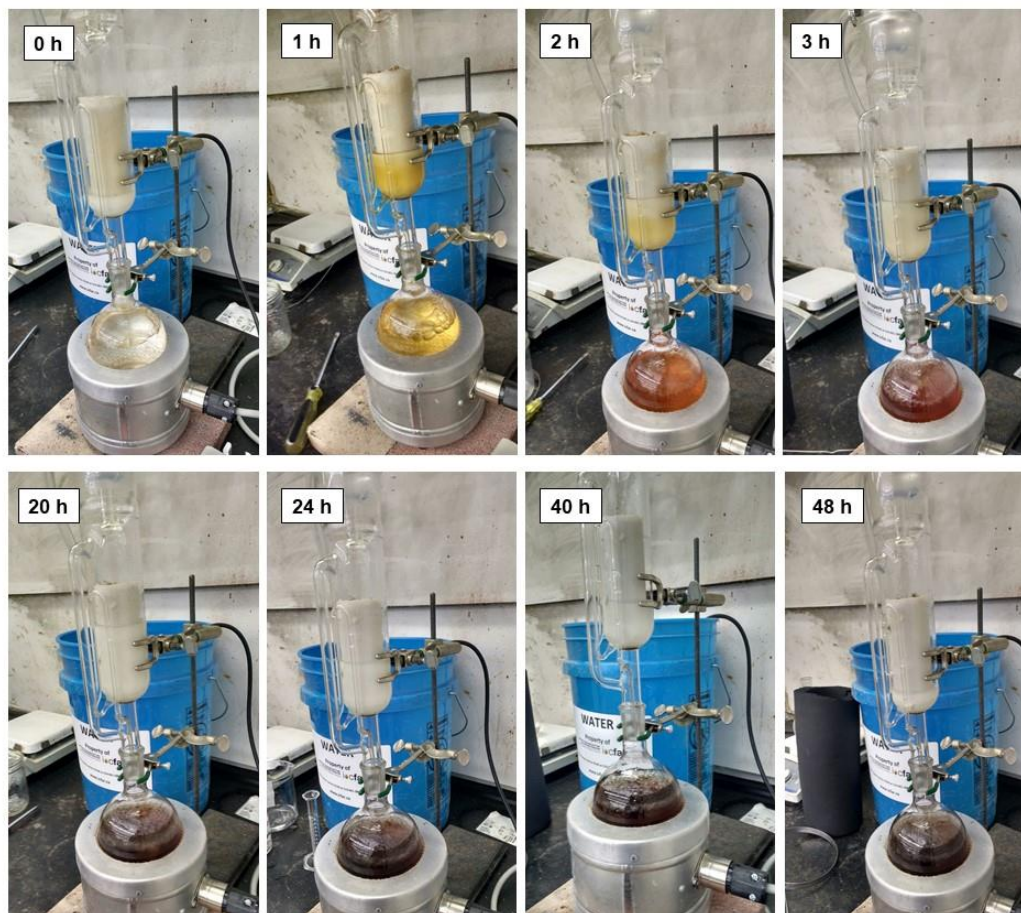
Figure 2.6 – Soxhlet extraction process

2.2.2.3   Acid leaching in a water oven

Acid washing is a common pretreatment used to remove the inorganic components in the biomass that are not water soluble [178–181].

The biomass (60 g) was soaked in 1 liter of 10 wt% acetic acid at 30 and 90°C for 24 hours. After the holding time, the pH was recorded (Table 2.3). The biomass was then filtered and rinsed with deionized water to reach a pH value ranging from 5–6. The biomass was then dried in the oven at 105 °C overnight before the pyrolysis treatment.

Table 2.3 – pH of the acidic water bath leachate before and after rinsing

Biomass pre-treatment	pH leachate after treatment	pH after rinsing
30°C 24h	2.74	5.74
90°C 24h	2.19	5.01

2.3 Sample characterization

2.3.1 Biomass composition

Determination of carbohydrates and lignin in biomass was performed following the standard NREL protocol [182]. The extractives were not quantified.

2.3.2 Proximate analysis

Proximate analysis was carried out to determine moisture, volatile content, ash of the biomass and biochar using ASTM procedures [183–185]. The volatile matter of a biomass is a measure of the condensable and non-condensable volatiles released when the biomass is heated at a certain temperature. The ash content gives a measure of the mineral and inorganic matter of the biomass and biochar after the sample is burned [59]. The moisture content in the biomass is an important characteristic to consider when pyrolysing, since it requires additional energy to vaporize water. Fixed carbon was calculated according to equation 2.2 on a weight percentage basis.

$$Fixed\ carbon = 1 - moisture - volatile\ matter - ash \tag{2.2}$$

The fixed carbon is a measure of the solid carbon left after devolatilization [59]. The carbon in biomass comes from the fixation of the CO_2 during photosynthesis, where carbon is converted to organic molecules [186].

2.3.3 Elemental analysis

The C, H, N, S, and O content of the biomass, biochar and bio-oil samples were determined using Thermo Flash EA 1112 series analyzer. The system was calibrated with 0.5, 1, 2 and 2.5 mg of BBOT (2,5-Bis (5-tert-butyl-benzoxazol-2-yl) thiophene) (CE

Elantech, NJ, US). 1-2 mg of biomass and biochar was weighed and placed in tin capsules with 8-10 mg of vanadium pentoxide required to achieve complete conversion of sulphur. 1-2 mg of bio-oil was placed with 8-10 mg of vanadium pentoxide and Chromosorb (CE Elantech, NJ, US). The analysis was performed in triplicates. Samples were combusted at 900°C in a stream of helium with a measured amount of oxygen. This produced N_2, CO_2, H_2O, and SO_2, which were then separated and quantified by gas chromatography using a 5 mm diameter steel packed column with a length of 2 m, helium carrier gas with a flow rate of 140 mL min^{-1} detected with a Propack model thermal conductivity detector (TCD). The oxygen content was determined as shown in equation 2.3, where the C, H, N, S, O and ash are mass percentages. The biomass and biochar samples were dried before each analysis, thus the hydrogen and oxygen in the ultimate analysis doesn't contain the moisture.

$$Oxygen\ \% = 1 - C - H - N - S - Ash \qquad (2.3)$$

The molar ratios (H/C) and (O/C) were derived from the ultimate analysis.

2.3.4 Higher heating value (HHV)

Higher heating values of the biomass, biochar and bio-oil were performed in a IKA C200 Oxygen Bomb Calorimeter (Wilmington, USA), following the standard method [187]. Benzoic acid was used as standard to ensure the proper performance of the equipment. 0.3–0.4 mg of the samples were placed in a plastic bag inside a quartz crucible placed in the decomposition vessel that was closed and pressurized with oxygen at 30 bar. The higher heating value is the heat released by the unit mass of the sample after combustion [59].

2.3.5 Biomass and biochar pH

Biomass and biochar pH values were determined according to the method reported by Rajkovich et al. [188]. A ratio of 1 g of the sample and 20 mL of deionized water was prepared in duplicates with 1.5 hours equilibration time using the BNIS-100 Bionexus Thermo Incubator Shaker (Oakland, CA, USA). After that, the slurry was filtered (Filter

paper P8-creped) and the pH determined with an Orion 2 STAR pH meter (Thermo Fisher Scientific, Massachusetts, United States).

2.3.6   Thermogravimetric analysis

TGA tests were performed using the Pyris 1 TGA Thermogravimetric Analyzer (PerkinElmer, Massachusetts, United States). In each experiment, about 8–10 mg of the sample was heated from 30°C to 800°C with a heating rate of 10°C min^{-1}, and a nitrogen flow rate of 20 mL min^{-1}, under atmospheric pressure.
Biomass was also tested with the combination of TGA–FTIR using the TL8000 Balanced Flow FTIR EGA system (PerkinElmer, Massachusetts, United States).

2.3.7   FT–IR

The analysis of biomass, biochar and bio-oil was performed with Frontier FTIR Spectrometer (PerkinElmer, Massachusetts, United States) to determine the organic functional groups. The wavelength range used is from 500 to 4000 cm^{-1}.

2.3.8   Surface area and pore volume

Biochar and activated carbon samples were tested for Brunauer-Emmett-Teller B.E.T. with Nova 1200e Surface Area & Pore Size Analyzer (Quantachrome Instrument, Florida, US). The tests were performing using 0.3 g of samples by nitrogen gas sorption at 77.35 K. Samples were degassed at 105°C for 1 hour to remove moisture, then the temperature was increased to 300°C and manteined for at least for 3 hours before analysis.

2.3.9   Micro-CT scan and Optical macroscope

Micro Computed Tomography (Micro-CT) is a non-destructive 3D imaging technique which employs a highly energetic X-ray beam to capture slices of 2D planar X-ray images where the internal density and atomic number variations can be seen through different grayscales. The X-rays beams, generated within an X-ray source, are transmitted through the sample, magnified and recorded by the X-ray detector as a 2D projection image. The sample is then rotated by a fraction of a degree and another X-ray projection

is recorded and repeated up to 360 degrees. These projections are computed and reconstructed to create a virtual 3D model [189]. The 3D images and videos were aquired by an X-ray micro CT instrument (Xradia 410 Versa; Carl Zeiss AG, Oberkochen, Germany) with the following specifications (X-ray voltage = 40 kV, X-ray power = and 4 W, objectives = 0.4x, 5 seconds exposure, air (no) filter.)

The efficiency of transmission is dependent on density and atomic number variations within the sample volume, such that higher atomic number materials will transmit less X-rays than low atomic number materials [186]. The stem 'density' was estimated as the pixel intensities of a region. The slices were computed by the Dragonfly pro software. The blue, green red module was applied displaying the different colors, representing different densities. Heavier, more dense particles appear as a bright red.

2.3.10   SEM-EDX

The biomass and biochar samples were analyzed by SEM-EDX using a Hitachi SU3500 Scanning Electron Microscope (SEM) combined with an Oxford AZtec X-Max50 SDD energy dispersive X-ray (EDX) detector. Backscatter Electron (BSE) imaging was selected to better analyze the particles, with variations in greyscale based on the average atomic number of the material. EDX is a semi-quantitative technique that can detect all elements with a minimum detection limit of approximately 0.5 wt%. A 10 kV accelerating voltage was used for these analyses. The samples were coated with a thin layer of gold to minimize charging effects.

2.3.11   Optical Microscope

Pictures of the stem of *Phragmites australis* were taken with the aid of Keyence VHX-6000 Digital Microscope (Mississauga, ON, Canada).

2.3.12   XRD

The sample was analyzed using a Rigaku SmartLab automated multipurpose X-ray diffractometer (XRD) system equipped with Cross Beam Optics (CBO) system and a high-precision theta-theta goniometer featuring a horizontal sample mount, and a 2D

HyPix-3000 detector. HyPix-3000 is a hybrid multi-dimensional detector with a large active area of approximately 3000 mm² with a small pixel size of 100 μm², resulting in a detector with high spatial resolution. In addition, the HyPix-3000 is a single photon counting X-ray detector with a high-count rate of greater than 10^6 cps/pixel and fast readout speed. Measurements were performed in Bragg-Brentano geometry using a Ni-filtered CuKα radiation (λ= 1.54059 Å). Diffraction data were originally acquired over a 2θ range from 10° to 90° with a step width of 0.02°. SmartLab Studio II software was used to acquire XRD data. The ICDD PDF-4+ 2019 inorganic database was used to search for phase identification.

2.3.13   GC-MS

Bio-oil samples (50 mg) were dissolved in 1 ml of 2-Propanol to obtain a concentration of 50 mg/mL, then each sample was filtered through a 0.2-micrometer filter. The GC–MS system consists of a gas chromatograph coupled to a quadrupole mass spectrometer (GC–MS QP 2010, Shimadzu) using a capillary column (DB5MS, 30 m × 0.25 mm i.d.; film thickness, 0.25 μm). Electron ionization (EI) was used with an ion source temperature of 200°C and the interface temperature of 250°C. In EI, the instrument was used in SCAN mode initially to confirm the identity of the compounds. The GC system was equipped with a split/splitless inlet. The injector temperature was 200 °C. AOC-20S autosampler with a 10 μL syringe was used for injections of 1 μL at a rate of 10 μL s^{-1}. The carrier gas was helium (UHP) at a constant flow of 1.5 mL min^{-1}. The oven temperature program had an initial temperature of 40°C held for 10.0 min, rising by 10°C/min to 200°C held for 10.0 min and rising by 10 °C min^{-1} to 300°C, which was held for 30 min, with a total run time of 75.0 min. This temperature program was selected to provide adequate separation of the compounds of interest.

2.3.14   HPLC

Sugars, organic acids, furfural, 5-(hydroxymethyl)furfural, catechol and acetol concentrations were determined by Shimadzu high performance liquid chromatography (HPLC) with a CBM-20A system controller, using external standards for identification and quantification of peak areas. These components were quantified using an Agilent Hi-

plex H (7.7 × 300 mm) column (Agilent USA, Santa Clara) at 50°C in a column oven
(CTO-10A) using 10 µL of injection volume. 0.005 M H_2SO_4 was used as the isocratic
mobile phase at a constant flow rate of 0.5 ml/min. A refractive index detector (RID-
10A) at 50°C was used for compound detection. Before injection, samples were diluted to
appropriate concentration with 0.005 M H_2SO_4 and filtered through a 0.2 µm membrane
filter twice and loaded into the SIL-20AC auto-injector.

2.3.15   Karl Fischer

The moisture content of the bio-oil was measured by Karl Fischer titration following the
ASTM E203-16 [190] using a Mettler Toledo V20 equipment. The bio-oil samples were
analyzed in triplicates.

2.3.16   Micro-GC

A Varian mobile Micro-GC (CP-4900) equipped with M5Å (Molecular Sieve 5 Å, 10 m),
PPU (PolarPlot U, 10 m), and 5 CB (CP-Sil 5 CB, 8 meter) column modules was used to
analyze the H_2, CH_4, CO, CO_2, C_2H_4, C_2H_6, C_3H_6, C_3H_8, and C_4H_{10} concentrations.
Helium and Argon (99.999%) were used as carrier gases for the thermal conductivity
detector (TCD) at a pressure of 80 psi. Further details of the Micro-GC are shown in
Table 2.4. Before entering the Micro-GC, the carrier gas was passed through an external
gas clean moisture and oxygen filter to remove the suspended moisture and oxygen
associated with the carrier gas.

Table 2.4 – Micro-GC parameters for gas determination

Gas chromatography	Varian Micro-GC CP49000
Column	M5Å, 10 m
Column	PPU, 10 m
Column	5 CB, 8 m
Detector	TCD
Oven temperature (°C)	50
M5Å Column head pressure (kPa)	150
PPU Column head pressure (kPa)	145
5 CB Column head Pressure (kPa)	70
Carrier and reference gas	Helium and Argon

The gas components from each sample were detected in a typical 3.0 min and automatically integrated using the Galaxie software. Due to the high utilization frequency, the Micro-GC was conditioned every week. The conditioning time was extended overnight to remove any water present inside the column as a result of the gas samples or the carrier gas. The conditioning was conducted by increasing the oven temperature of the columns to maximum column oven temperature. Each gas sample was analyzed a minimum of three times, and the average was calculated to estimate the gas concentration.

2.3.17 ICP-OES

Metals leached from the char and biomass sample were determined by Optical Emission Spectrometry technique (ICP-OES). A 54704 Sigma-Aldrich Multielement Standard solution 5 for ICP that follows the ISOMEC 17025 and ISO Guide 34 was used.

2.4 Biochar and activated carbon adsorption

Adsorption is one of the most common techniques used for the removal of pollutants [191]. There are two stages that can be identified during the adsorption process, a first dynamic stage where the concentrations of the pollutant to remediate are changing and a second stage where the equilibrium is reached, and the concentrations remain constant. The process parameters affecting the adsorption are temperature, pH, initial concentration of the contaminant, adsorbent dose, and the surface chemistry of the adsorbent.

2.4.1 Equipment

The adsorption experiments were carried out in 22 mL glass vials at different conditions as described in section 2.4.2.

2.4.2 Procedure for the adsorption study

The adsorption studies were carried out with 80–160 mg of biochar at different pH and holding times (30 min, 1h, 2h, 18h, 48h, 65h). The initial concentration of ibuprofen selected was 25 mg/L. The experiments were performed with 20 ml of the ibuprofen solution and either 80 or 160 mg of biochar in 22 mL vials placed in the shaker at 22 °C

and 1000 rpm. After the selected holding time, the biochar was filtered from the solution with a filter paper (Whatman® Grade 1 filter paper) and the latter was analyzed by UV-vis spectrophotometer (Thermo Scientific Evolution 220). The solution was placed in quartz cuvettes and spectra from 190–350 nm was recorded. The amount of ibuprofen compounds adsorbed was calculated according to the equation 2.4:

$$q_e = \frac{(c_i - c_f)V}{m} \qquad (2.4)$$

Where c_i and c_f represent the initial and final concentration of ibuprofen in mg/L, V is the volume of ibuprofen solution in contact with the biochar and m is the mass of the biochar in grams.

The percentage removal of ibuprofen at a time t_i was calculated with equation 2.5:

$$\% \ Removal = \frac{(c_i - c_f)}{c_i} \cdot 100\% \qquad (2.5)$$

where c_i and c_f represent the initial and final concentration of ibuprofen in mg/L.

2.4.2.1   Point of zero charge determination

The point of zero charge is defined as a measure of surface charge distribution of porous carbons representing the total net surface charge [192]. To determine the point of zero charge, 0.1 g of biochar was mixed with 10 ml of 0.01 M NaCl at pH ranging from 2 to 12. Then, the samples were placed in the shaker BNIS-100 Bionexus Thermo Incubator Shaker (Oakland, CA, USA) at 22°C and 1000 rpm for 48 h. After that, the biochar was filtered, and the solution pH was measured with the pH meter. The point of zero charge was determined by plotting the difference between the initial pH and final pH versus the initial pH.

2.4.2.2   UV-Vis spectrophotometer

The initial and final concentrations of the ibuprofen solutions were measured by UV-Vis Thermo Scientific Evolution 220. 3 ml deionized water was used as a blank for each

experiment. Quartz cuvettes were used to measure the absorbance of all the solutions. Spectra were obtained from 350 nm to 190 nm to detect the maximum peak of ibuprofen. Calibration curves were prepared before the experiments.

2.4.2.3   Boehm titration

The surface chemistry of the biochars from slow and fast pyrolysis, as well as the activated biochars was determined using the Boehm titration method [193]. A mass of 0.1–1 g of either biochar or activated char was added to 50 mL of a 0.05 M NaOH (Anachemia). The samples were placed in the shaker 420 Thermo Scientific and agitated at 120 rpm for 24 hours and then filtered. 10 mL aliquots were taken and acidified with 20 mL of 0.05 M HCl (ACS reagent, Sigma Aldrich) and back-titrated with NaOH. NaOH reacts with all functional groups, therefore it will provide the moles of acidic groups [194]. To calculate the basic functional groups, 0.1–1 g of either biochar or activated chars was placed in 50 mL 0.05 M HCl solution. The samples were shaken for 24 hours and then titrated with NaOH. NaOH and HCl solutions were standardized before each experiment. To ensure the reproducibility of the experiments, each sample was prepared in triplicates and the titrations were repeated three different times for each sample.

Chapter 3

3   Slow pyrolysis of *Phragmites australis*: studies on process parameters and product characterizations

3.1   Introduction

Phragmites australis has been investigated for the production of biofuels and biochemicals through torrefaction and pyrolysis [54–56]. Pyrolysis is the thermochemical degradation of biomass in the absence of oxygen, yielding three products: bio-oil, biochar and incondensable gases. Depending on the operating conditions, pyrolysis can be classified into two main classes: slow pyrolysis, with slow heating rates and high vapor and solid residence time [195], and fast pyrolysis, with high heating rates, vapor residence time less than 2 s and rapid quenching of the volatiles to condense a liquid intermediate called bio-oil [21].

A few studies are available in the literature on the exploitation of Phragmites as a feedstock for pyrolysis. Sutcu [52] studied the slow pyrolysis of *Phragmites australis* under different operating conditions, and the results showed that the char yield decreased from 45.28% to 33.71% from 350 °C to 650 °C at 5 °C min^{-1}, and 42.85% to 31.02% at 25 °C min^{-1}. The maximum oil yield (23.07%) was achieved at 550 °C at 25 °C min^{-1} and with 100 ml min^{-1} of carrier gas. Garrido et al. [56] studied the effect of acid hydrolysis and torrefaction pretreatment before pyrolyzing *Phragmites australis*. They aimed to reduce the high inorganic content while creating a biomass rich in cellulose. They found that a combination of 4% H_3PO_4 and 220°C torrefaction prior the fast pyrolysis at 500°C increased the carbohydrates concentration in bio-oil of 10 folds (from 2.8% to 32.1%) while reducing the ketones (due to a reduction of hemicellulose content), phenols and furans. They also stated that the biochar product had a lower volatile content and high fixed carbon and phosphorous, which could be potentially used as a soil amendment. Zhao et al. [53] investigated the pyrolysis kinetics using a non-isothermal TG method, under different temperatures (50 to 800 °C) and heating rates (5,10, 25, 30 and 50 °C min^{-1}) in order to determine the degradation mechanism of *Phragmites australis*. They found

three degradation stages of *Phragmites australis*, the first stage happening at around 50-200°C due to the moisture loss and the devolatilization of lower molecular weight compounds, the second stage at 200–400°C, due to the main pyrolysis degradation of hemicellulose and cellulose, and the third region above 400°C due to the devolatilization of residual components. The apparent activation energy was deduced as 291.8 kJ mol^{-1}. Park et al. [9] investigated the pyrolysis of *Phragmites australis* at different temperatures (400–560°C), nitrogen flow rates (30, 50 and 100 ml min^{-1}), and particle sizes. Results showed that the carrier gas flow rate didn't have a significant effect. The maximum bio-oil yield (52%) was achieved at 520°C. Increasing the particle size from 0.85 to 7.5 mm, incresed the bio-oil yield and decreased the char yield, which was attribuited to the improved heat transfer when the particles were larger and packed more loosely than the smaller ones.

Biochar has attracted wide attention for its unique properties, first as a soil amendment and later on adopted for environmental management [196]. Biochar produced from *Phragmites australis* at 600°C with 10°C min^{-1} used for phytoremediation and modified with $MgCl_2$ showed high surface area (26.31 to 170.20 m^2 g^{-1}) and pore structure. The functionalized biochar demonstrated high adsorption of ammonium and phosphate, indicating that it could be used in the treatment of eutrophic water [197].

This work aims to characterize the biochar produced with slow pyrolysis to gather a better understanding of the effects of the pyrolysis conditions on the products, which can be a useful exploitation of this destructive invasive reed. Moreover, the bio-oil organic and aqueous phase is characterized to study the chemical composition.

3.2 Materials and methods

The pyrolysis reactor used for this chapter is the batch MFR described in the Equipment section of Chapter 2, Section 2.1.1 (Figure 2.1, Figure 2.2 and Figure 2.3). Experiments were planned to study the effect of temperature, heating rate and nitrogen flow rate on the pyrolysis product yields and characteristics.

The first set of experiments was carried out at 5 and 15°C min^{-1} and final temperatures of 350, 400, 450, 500 and 550°C. In the second set of experiments the temperature and heating rates were kept constant at 450°C and 15°C min^{-1}, while the N_2 flow rate was varied from 0 to 5 L min^{-1}.

Phragmites australis samples of about 150 g were heated to the set point temperature with the selected heating rate and N_2 flow rate and then kept for 30 minutes to complete the pyrolysis reaction.

3.3 Results and discussion

3.3.1 Feedstock characterization

The higher heating value, proximate, ultimate analysis and composition of the biomass are presented in Tables 3.1 and 3.2. Determination of carbohydrates and lignin in biomass was performed following the standard NREL protocol [182]. The extractives were not quantified. The biomass composition (Table 3.1) is similar to other studies on *Phragmites australis* [36–38].

Table 3.1 – Cellulose, hemicellulose and lignin content of *Phragmites australis*

Lignocellulosic component	wt% d.b.
Cellulose	37.2
Hemicellulose	24.8
Lignin	21.0

The *Phragmites australis* biomass was analyzed by TGA (Figure 3.1) and TGA-FTIR (Figure 3.2). The TGA is one of the most common techniques used to analyze the thermal decomposition of biomass. The TGA-FTIR was performed according to the methodology described in Chapter 2, section 2.3.6. As seen in thermogravimetric studies, there are two overlapping peaks, a single peak with a shoulder peak. The shoulder peak, which starts after a first stage between 80 to 125°C due to the release of water from the biomass, corresponds to the degradation of hemicellulose occurring at around 260 to 290°C with maximum weight loss point at 270°C. The single peak is due to the degradation of cellulose which occurs at around 300 to 360°C with a maximum weight loss at 325°C. By 400°C, all cellulose is converted to condensable and non-condensable gases. The

devolatilization of lignin happens on a wider range of temperatures (200–700°C) compared to cellulose and hemicellulose because it is more difficult to decompose [103,198]. These findings are also confirmed by other researchers, showing the same trend [9,13,53,54].
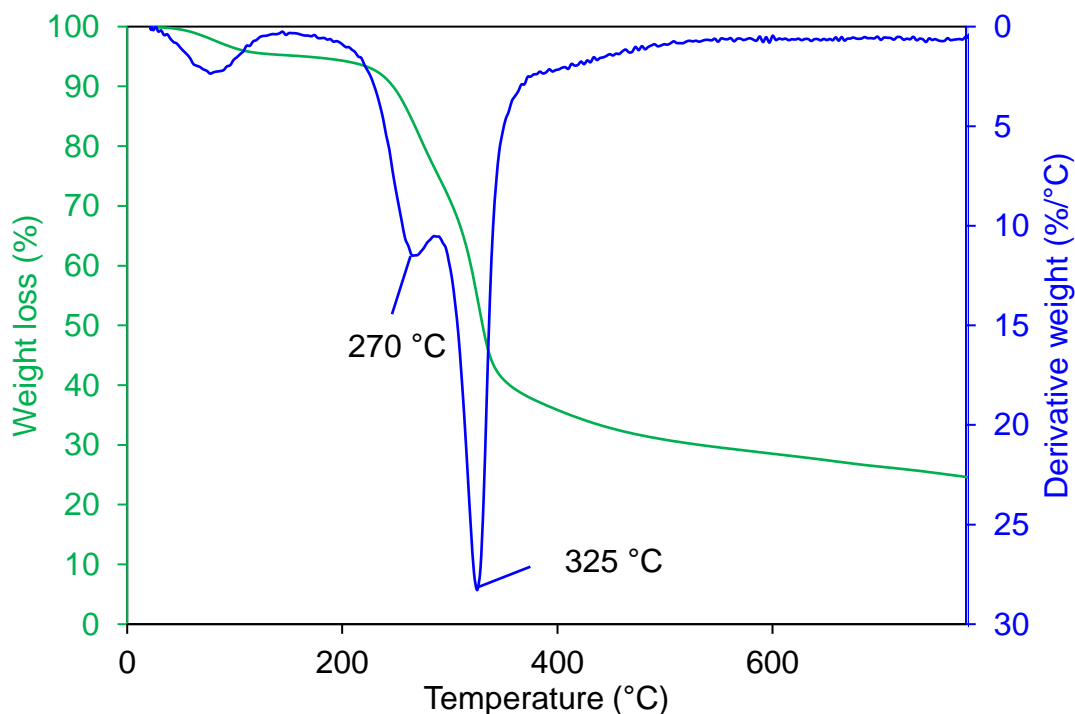
Figure 3.1 – TGA and DTG of *Phragmites australis*

The devolatilization of *Phragmites australis* has been recorded with the TG coupled to a FTIR spectrophotometer (Figure 3.2) every 100°C at different temperatures (150–550°C). Many absorption peaks were detected at the decomposition temperatures between 350–550°C. At 150°C only the release of water was detected. When the pyrolysis process starts, more gases are produced. CO_2 started to be released at 350°C at 2239–2222 cm^{-1} and 734–568 cm^{-1}. According to the literature, formation of carbon dioxide at temperatures below 350°C is likely due to the cleavage of xylan chain of hemicellulose via decarboxylation reaction [92,199] with only a small contribution from cellulose and lignin [103]. The release of carbon dioxide at high temperature (>500°C) was attribuited to lignin degradation [103]. The characteristic peak of CO (2216–2134 cm^{-1}) was seen

only at 350°C. CO production was found to be mostly from cracking of carbonyl (C–O–C) and carboxyl (C=O) of hemicellulose in the whole pyrolysis temperature range (<600°C) and mostly from lignin at higher temperature, due to secondary cracking reactions of the tar residue in the char [103].

At 350°C new volatiles were produced including aldehydes, ketones and acids (1838–1600 cm^{-1}), alkanes, alcohols, phenols, ethers, lipids (1442–924 cm^{-1}) and aromatics (1562–1446 cm^{-1}). In particular, the peak at 1184 cm^{-1} might be associated to the phenols or alcohol structure. Above 350°C a small peak at 3000 cm^{-1} can be seen and it was likely associated with the release of CH_4 [200,201], which started at higher temperature due to the higher energy required to break the –O–CH_3 bond to form CH_4 [103].

Phragmites australis
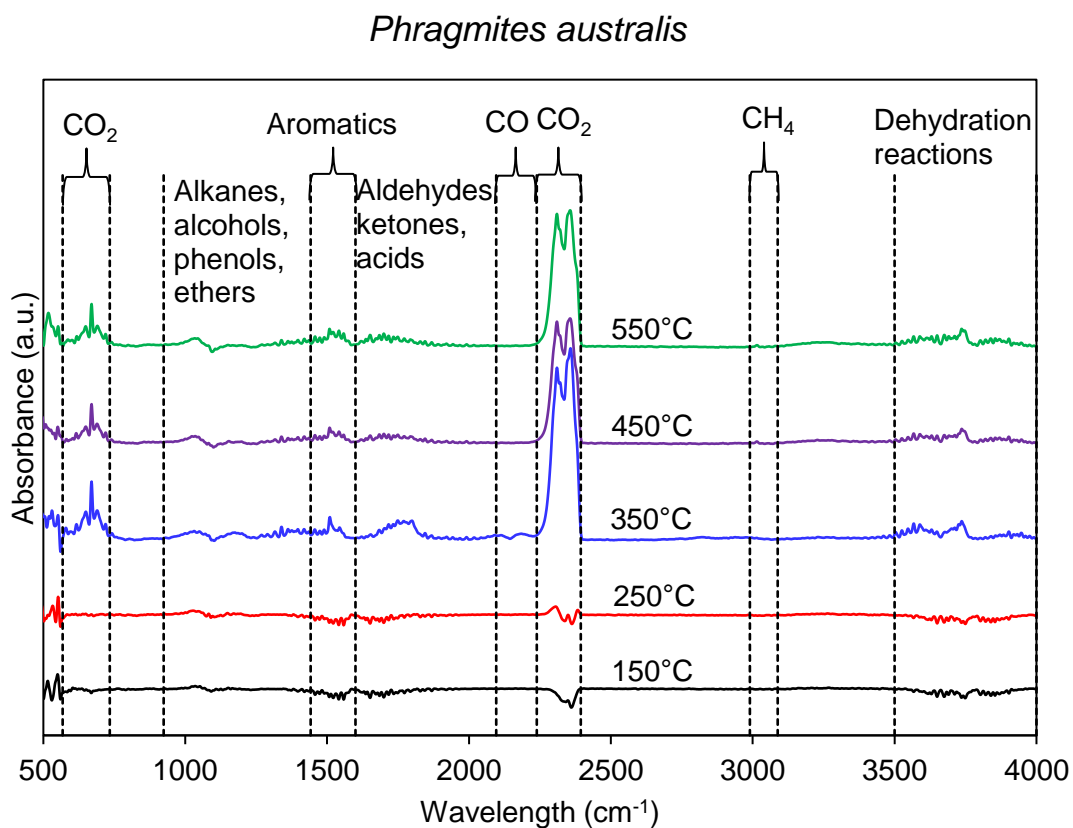
Figure 3.2 – FT-IR spectra of volatiles evolution at different pyrolysis temperatures

3.3.2 Product yields

The first set of experiments were performed at 5 and 15°C min^{-1} and final temperatures of 350, 400, 450, 500 and 550°C, holding time 30 minutes without any inert gas. At 5°C min^{-1} the char yield decreased from 45 wt% at 350°C to 34 wt% at 550°C (Figure 3.3), while at 15°C min^{-1} decreased from 42 wt% at 350°C to 34 wt% at 550°C (Figure 3.4). The decrease in char yield with increasing temperature could be explained by the greater primary decomposition of *Phragmites australis* at high temperature or by the secondary decomposition of char, which also might contribute to the increase in non-condensable gases [202–204].

The bio-oil yield produced at 5°C min^{-1} increased from 38 wt% to 43 wt% at 450°C and then it remained stable at 43 wt% when the temperature was further increased to 550°C. Increasing the heating rate to 15°C min^{-1}, the bio-oil yield increased from 38 wt% to 40 wt% and then decreased to 38 wt% at 550°C. The lower yield at higher temperature could be due to secondary cracking of the pyrolysis vapors. This is caused by the combined effect of high temperature and the char inside the reactor catalyzing the reaction, which also contributes to the increased gas yield [126,203,205]. The highest oil yield (43 wt% d.b.) was obtained at 450°C at 5°C min^{-1}. Increasing the heating rate to 15°C min^{-1}, slightly decreased the bio-oil yield from 40% to 38%. Similar behaviour was observed in other studies [206].
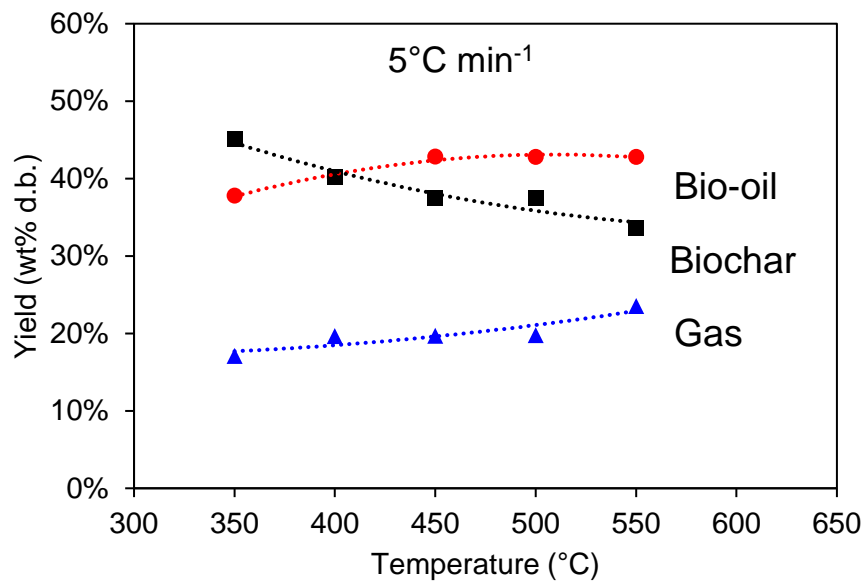
Figure 3.3 – Slow pyrolysis, effect of temperature (5 °C min⁻¹)
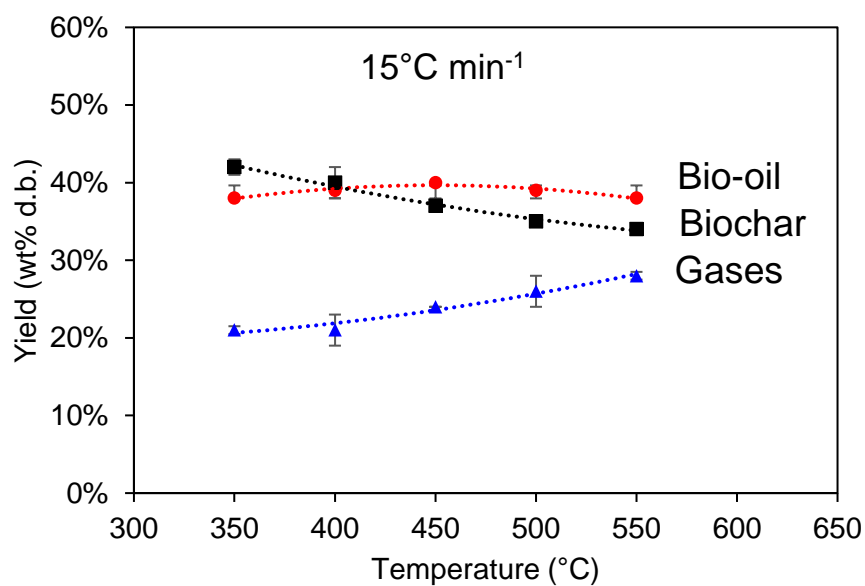
Figure 3.4 – Slow pyrolysis, effect of temperature (15 °C min⁻¹)
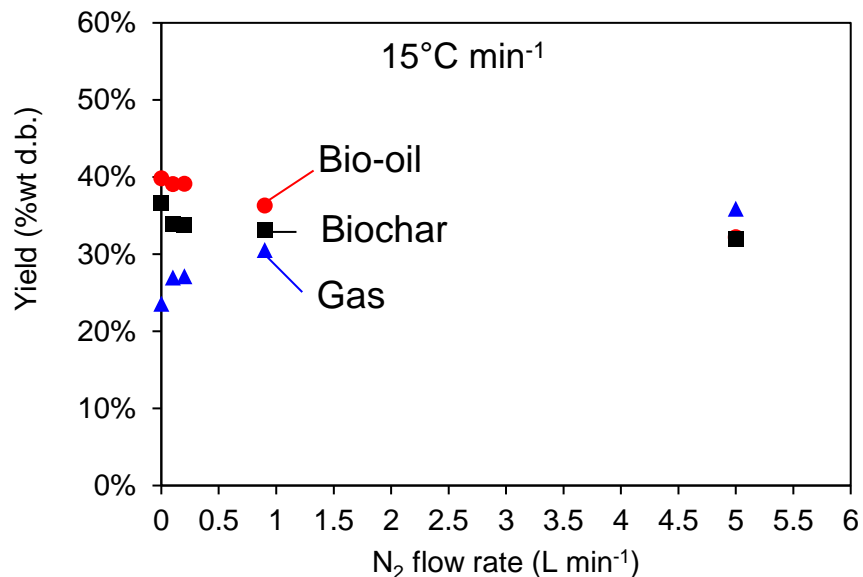
Figure 3.5 – Slow pyrolysis, effect of nitrogen flow rate

The effect of sweeping gas (Figure 3.5) on the pyrolysis products was investigated by changing the flow rate to 0.1, 0.2, 0.9 and 5 L min^{-1}. During these experiments, the temperature setpoint was maintained at 450°C with a constant heating rate of 15°C min^{-1}. Over this range of nitrogen flow rates, even the lowest flow rate (100 mL min^{-1}) decreased the average bio-oil yield (Figure 3.5). It is well known that the use of the sweeping gas decreases the residence time of the pyrolysis vapors in the reactor, thus avoiding unwanted cracking reactions such repolymerization and recondensations [21]. However, a decrease in the bio-oil and biochar yield was observed, while the gas yield rised with increasing nitrogen flow rate. This could be explained by the fact that high sweep gas flow rates tend to decrease bio-oil yields and increase the gaseous product yields due to either insufficient cooling or lower residence time of the pyrolysis vapors in the quenching zone [207].

3.3.3   Biomass and biochar characterizations

The characterization of both biomass and biochar is reported in Tables 3.2 and 3.3. At the slowest heating rate (5°C min^{-1}), the fixed carbon was 52 wt% at 350°C, whereas increasing the heating rate to 15°C min^{-1} led to a lower fixed carbon content of 47 wt%. It

can be observed that the highest volatile content for the char samples was at 350°C and 15°C min^{-1}, which indicates that at this pyrolysis operating condition the temperature was probably not high enough to achieve a fully pyrolyzed char.

In general, increasing the pyrolysis temperature from 350°C to 550°C decreased the volatile content of the char, while increasing slightly the amount of ash from 15-17 wt% at 350–400°C to 21–22 wt% at higher temperatures, and consequently increased the fixed carbon. As noted by Ronsse et al. [208], slow pyrolysis comprises a series of devolatilization reactions that lead to an more condensed carbon structure. The high volatile matter at 350 and 400°C could be explained by the recalcintrance of lignin, which is not still thermally decomposed at these low temperatures [209]

The higher heating values (HHV) of the produced biochars increased with increasing pyrolysis temperature for both heating rates.

Table 3.2 – Biomass and biochar proximate analysis and HHV content

Pyrolysis temperature (°C) - Heating rate (°C/min)	Proximate analysis (wt% d.b.)				HHV (MJ/kg)
	Fixed Carbon	Volatile matter	Ash content	Moisture (wt%)	
Raw Phragmites	19.05±0.12	69.11±0.16	5.54±0.80	6.29±0.15	17.02±0.05
350 – 5	52.23±0.38	27.45±0.18	15.41±0.20	4.90±0.50	24.66±0.11
400 – 5	52.93±1.12	26.62±0.90	16.71±0.14	3.73±0.08	24.16±0.06
450 – 5	63.80±0.03	14.86±0.13	18.23±0.21	3.11±0.02	25.26±0.00
500 – 5	66.03±0.82	10.11±0.16	21.15±0.22	2.58±0.06	25.84±0.08
550 – 5	67.20±0.62	8.53±0.94	21.75±0.32	2.79±0.13	25.55±0.07
350 – 15	47.00±0.62	34.79±0.49	14.91±0.08	3.29±0.05	24.42±0.12
400 – 15	55.63±0.11	23.56±0.33	17.90±0.21	2.65±0.18	24.52±0.05
450 – 15	63.71±0.13	12.84±0.15	20.44±0.13	2.73±0.15	25.36±0.16
500 – 15	62.85±0.05	13.46±0.18	20.95±0.23	2.73±0.01	25.43±0.08
550 – 15	67.87±0.34	8.22±0.05	21.67±0.30	2.23±0.30	25.19±0.15

The pH values and ultimate analysis of biomass and biochar are reported in Table 3.3. Interestingly, the carbon (C) content for both heating rates is similar, increasing with the pyrolysis temperature. Hydrogen (H), sulfur (S) and oxygen (O) content decreased with increasing pyrolysis temperature. As stated by Della Rocca et al. [210], the decrease of O and H is due to the scission of weaker bonds associated with the release of volatile matter. The increase in N content was attributed to the heterocyclic ring structures of N in the biomass/biochar samples, and C-N bonds are less easy to break [211]. The molar composition of O/C and H/C was calculated; both ratios decreased with increasing temperature. It is possible to relate the O/C and H/C ratios with the stability of the biochar. According to Spokas [212], O/C ratio higher than 0.6 indicates a biochar's half-life likely below 100 years, O/C ratio between 0.2 and 0.6 corresponds to a half-life of 100–1000 years and at O/C ratio lower than 0.2 (soot and graphite) the half-life is most likely higher than 1000 years. According to this stability criteria, all the biochars meet the half-life expectation of 100–1000 years with the biochars produced at 500-550°C meeting the highest requirement (O/C lower than 0.2). However, based on the protocol developed by IBI [213], the H/C ratio is a better estimate since it doesn't include the oxygen content which is typically calculated by difference. According to this protocol, a range of H/C between 0.4 and 0.7 was determined as the percentage of organic carbon in the biochar that is predicted to remain in soil after 100 years. Based on these criteria, the biochar samples produced at 350°C with both heating rates don't meet the requirements to be classified as biochar. The rest of the samples meet both IBI Guidelines and Euro Guidelines [214].

Different studies [208,215] indicated that the pH of the char is likely correlated to oxygen functionalities, where at higher process intensity the number of carboxyl groups is reduced leading to a more alkaline char in solution. Moreover, it was reported [215] that at high temperature there is an increase of alkaline minerals in the ash that could further contribute to higher pH. The biochar pH in solution increased with the temperature and heating rates. In particular, between 350°C and 450°C the pH of biochars produced at 5°C min^{-1} were 1 unit lower than the biochars produced at 15°C min^{-1}. Zhao et al. [215] reported a similar trend for the pH of rapeseed stem biochar, where pH increased with

increasing heating rates (higher than 5°C min^{-1}), although a direct comparison is difficult due to the different biomass and pyrolysis temperature used.

Table 3.3 – Biomass and biochar pH and ultimate analysis (Oxygen calculated by difference)

T (°C) – HR (°C min^{-1})	pH (H$_2$O)	Ultimate analysis (wt% d.b.)				
		C	H	N	S	O
Raw Phragmites		45.13±0.31	5.49±0.39	1.20±0.14	0.24±0.02	42.39±0.62
350 – 5	6.03±0.02	60.80±0.94	4.05±0.09	2.43±0.16	0.00±0.00	17.31±0.75
400 – 5	7.15±0.03	63.22±0.45	3.49±0.08	2.31±0.1	0.00±0.00	11.37±0.29
450 – 5	8.67±0.03	62.98±0.76	2.98±0.06	2.24±0.12	0.00±0.00	13.57±0.88
500 – 5	9.49±0.02	66.44±2.45	2.43±0.09	2.35±0.04	0.00±0.00	7.62±2.56
550 – 5	9.97±0.02	67.22±1.02	2.15±0.09	2.20±0.16	0.00±0.00	6.68±0.78
350 – 15	7.68±0.53	59.45±1.73	3.88±0.03	2.42±0.06	0.00±0.00	16.36±1.72
400 – 15	8.76±0.05	62.80±0.14	3.46±0.03	2.35±0.05	0.00±0.00	13.49±0.07
450 – 15	9.82±0.03	67.18±0.39	2.78±0.06	2.22±0.07	0.00±0.00	7.38±0.36
500 – 15	9.77±0.03	67.94±1.25	2.54±0.1	2.31±0.08	0.64±0.03	5.77±1.10
550 – 15	10.03±0.02	67.76±0.70	1.89±0.02	2.18±0.13	0.7±0.01	5.80±0.09

The effect of the sweeping gas on the biochar properties can be observed in Table 3.4 and Table 3.5. The carbon content increased slightly at all gas flow rates, whereas hydrogen decreased. Sulfur was detected in the biochar samples when nitrogen was employed.

Table 3.4 – Effect of N$_2$ flow rate on the biomass and biochar characteristics (450°C 15°C min^{-1})

N$_2$ (L min^{-1})	Proximate analysis (wt%, d.b.)			Moisture (wt%)	pH (H$_2$O)	HHV (MJ/kg, d.b.)
	Fixed C	Volatiles	Ash			
0	63.71±0.13	12.84±0.15	20.44±0.13	2.73±0.15	25.36±0.16	63.71±0.13
0.1	62.75±0.94	16.00±0.07	17.87±0.30	3.38±1.17	10.12±0.03	25.73±0.02
0.2	64.19±0.17	15.78±0.10	17.95±0.07	2.08±0.01	10.04±0.01	26.33±0.02

0.94	63.72±0.19	16.16±0.46	17.64±0.29	2.47±0.01	9.96±0.03	26.00±0.02
4.72	63.68±0.05	16.36±0.29	17.06±0.28	2.90±0.05	9.78±0.07	25.57±0.12

Table 3.5 – Effect of the N_2 flow rate on the C, H, N, O, S analysis of the biochar samples pyrolyzed at 450°C and 15°C min^{-1} (Oxygen calculated by difference)

N_2 (L min^{-1})	Ultimate analysis (wt%)						
	C	H	N	S	O	O/C	H/C
0	67.18±0.39	2.78±0.06	2.22±0.07	0.00±0.00	7.38±0.36	0.2	0.5
0.1	68.24±1.00	2.67±0.05	2.19±0.16	0.55±0.03	8.48±1.00	0.19	0.47
0.2	69.81±0.20	2.65±0.07	2.02±0.02	0.44±0.01	7.14±0.24	0.15	0.46
0.94	67.81±3.28	2.41±0.27	1.95±0.13	0.46±0.10	9.73±3.26	0.22	0.43
4.72	69.68±0.38	2.62±0.01	1.94±0.16	0.42±0.05	8.28±0.32	0.18	0.45

The surface area and total pore volume of the chars produced at the lowest (350°C) and highest temperature (550°C) with both heating rates are presented in Table 3.6. The surface area increased with temperature and heating rate. In fact, at high temperature the removal of volatiles is more intense, creating more pores, which contribute to the higher surface area [216]. At 350°C there is no surface area detected, probably because the pyrolysis is not yet completed, which is confirmed also by the high volatile content. The total pore volume increased with the temperature, with the highest value at 0.0455 cm^3 g^{-1} for the char sample at 550°C and 15°C min^{-1}. According to the classification adopted by the International Union of Pure and Applied Chemistry (IUPAC) [217], the char produced at 550°C–15°C min^{-1} has an average pore size diameter of 1.8 nm, which is considered as micropores, while the char produced at the same temperature but at 5°C min^{-1} is mesoporous.

Table 3.6 – BET analysis of the biochars

Sample name	BET surface area (m² g⁻¹)	Total pore volume (cm³ g⁻¹)	Average pore size diameter (nm)
350°C-5°C min⁻¹	0	0.0002	8.88
550°C-5°C min⁻¹	23.327	0.0347	3.66
350°C-15°C min⁻¹	0	0	27.51
550°C-15°C min⁻¹	32.125	0.0455	1.80

The FTIR of the *Phragmites australis* and biochars pyrolyzed at 5°C min⁻¹ and different temperatures (350, 400, 500 and 550 °C) were studied to determine the vibration frequencies of the functional groups (Figure 3.6). The bands in the spectra correspond to different functional groups indicated in Table 3.7. In the biomass, several bands are associated with the presence of cellulose, hemicellulose and lignin. In the fingerprint region, the peaks associated to the cellulose are 901 cm⁻¹ (C–H stretch) and 1034 cm⁻¹ (C–O and C–C stretch of >CH–OH and –CH₂OH groups) [218]. The band at 1161 cm⁻¹ is associated to the asymmetric –C–O–C– ring for cellulose and hemicellulose, while 1237 cm⁻¹ is assigned to the guaiacyl ring breathing with C–O stretching [219] in lignin and xylan [220]. The peak at 1733 cm⁻¹ is assigned to C=O stretching of acetyl and carbonyl groups (hemicelluloses). Outside this range, there are two peaks at 2852 cm⁻¹, 2919 cm⁻¹ and at 1347 cm⁻¹ and 1440 cm⁻¹ assigned to aliphatic functional group (CH₂ stretch) [221]. According to Chen et al. [221], these peaks correspond to cutin and cutan polymers in plants, which are lipid components of cuticles. Analysis of *Phragmites australis* plants indicate the presence of a layer of cuticular wax in the epidermis [222,223], which could be responsible for these peaks. The broad peak at 3346 cm⁻¹ originated from bonded –OH indicating the presence of alcohols and phenols [219].

The FTIRs of the biochars present clear variations from the biomass spectra. Several functional groups disappeared. The –OH stretching vibration at 3346 cm⁻¹ vanished, probably because of dehydration reactions [224] and the peaks associated with the CH₂ stretching bands disappear in all biochars, although still slightly present in the biochar treated at 350°C, suggesting the removal of aliphatic components with increasing temperature [225]. The peak of hemicellulose at 1735 cm⁻¹ disappears at 350°C,

confirmed by the range of degradation temperature of hemicellulose [103]. The peak at 1600 cm^{-1}, corresponding to aromatic C=C and C=O components of conjugated ketones and quinones increased in intensity to 400°C and then decreased with further increase of temperature. Previous studies have reported a similar trend [223,226] stating that this behaviour might be consistent with the presence of both acidic and basic groups. The decrease of the intensity of the peak at 1161 cm^{-1} associated to the –C–O–C– or C–O groups in cellulose and hemicellulose, is in good agreement with the TGA/DTG results that show the increase of CO and CO_2 at 350 °C. The appearance of a peak at 870 cm^{-1} indicates the presence of aromatic C (out of plane deformation) .

Table 3.7 – FT-IR assignments

Band position (cm^{-1})	Component
Biomass	
901	C–H alkenes bend
1034	C–O stretching vibration (cellulose, hemicellulose and lignin) [220,227]
1161	–C–O–C– asymmetric stretching in cellulose and hemicellulose [220]
1237	Syringyl ring breathing and C–O stretching in lignin and xylan [220]
1733	C=O stretching of acetyl and carbonyl groups (hemicelluloses) [218]
2852, 2919	>CH_2 stretch [221]
3346	O–H stretching (broad)
Biochars	
750, 798, 870, 901	out-of-plane deformations of aromatic C–H or C–C
1074, 1112	–C–O–C– symmetric stretching
1440	aliphatic CH_3 and CH_2 stretching and deformation vibrations [228]
1600	Aromatic C–C ring stretching
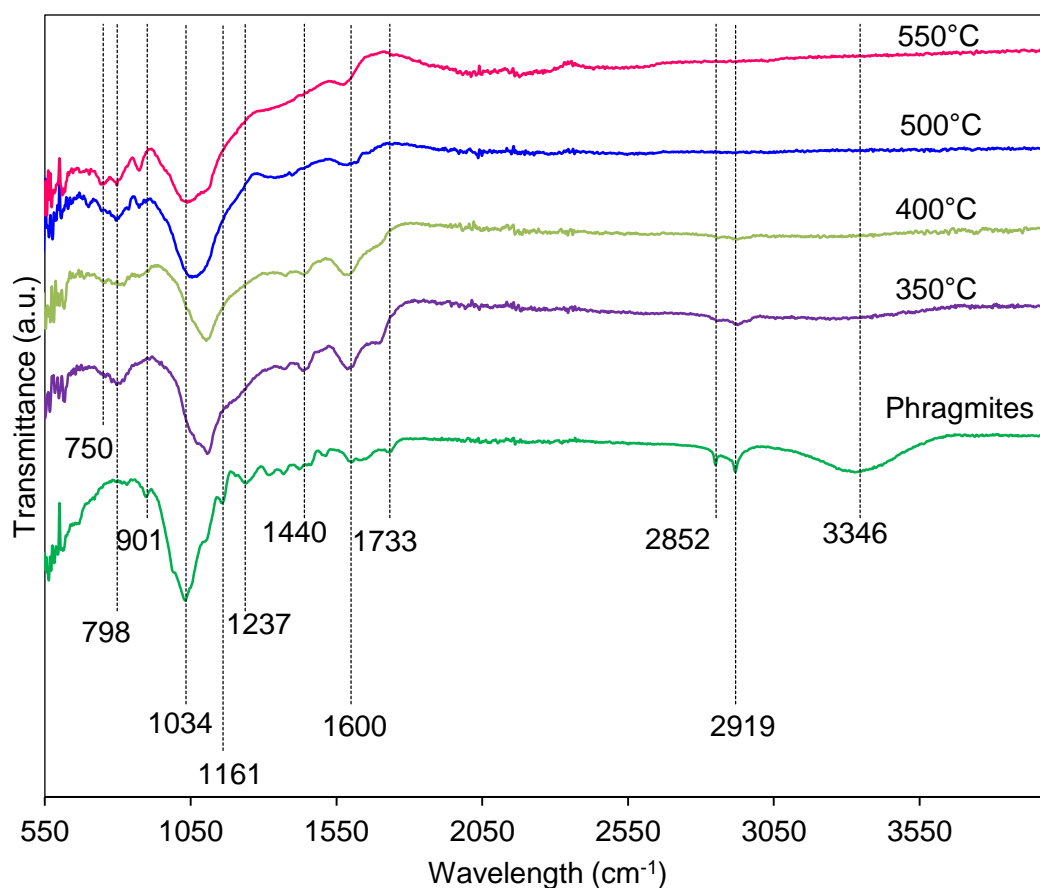
Figure 3.6 – FTIR spectra of biomass and biochar samples (5°C min^{-1})

The surface morphology of the biomass and biochars obtained at different temperatures and pyrolyzed at 5°C min^{-1} was investigated by SEM-EDX analysis. SEM of the raw biomass presents a smooth surface with some pores in the background, but without any ridges Figure 3.7 a). The pyrolysis process with temperature increasing from 350°C to 550°C showed a morphological change in the structure of the biochar, with more pores on the surface, from 350°C to 450°C. At 550°C the matrix structure seems to be significantly decomposed.
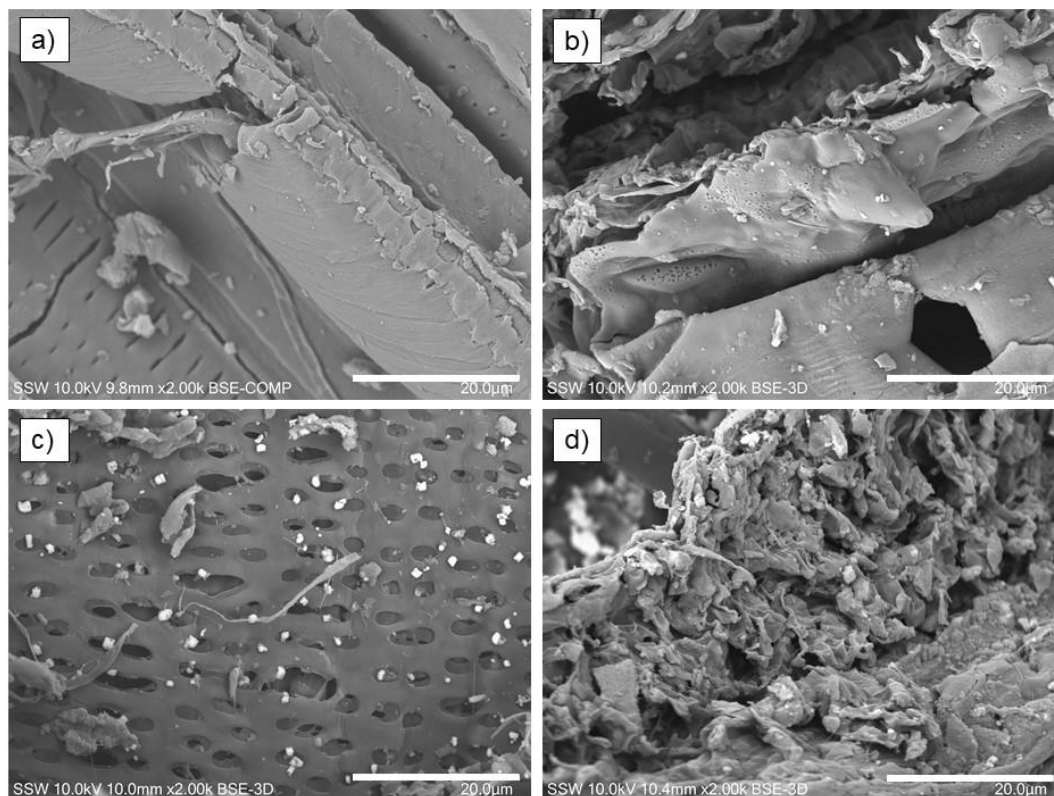
Figure 3.7 – SEM magnitude 20 µm; a) *Phragmites australis***, b) Biochar 350°C, c) 450°C, d) 550°C**

The SEM-EDX of the raw biomass and biochars detected elements such as potassium, sodium, calcium and magnesium (Figure 3.8), which are the most abundant alkali and alkaline earth metallic species (AAEMs) especially in herbaceous materials [117,229]. The presence of chlorine in the sample was also found in another study on *Phragmites australis* [54]. It was noted in the pyrolyzed samples the presence of high amount of silicon. Silicon enhances plant grow and development and it is present in significant concentrations in plants, similar to other elements such as P, S and Ca [230].
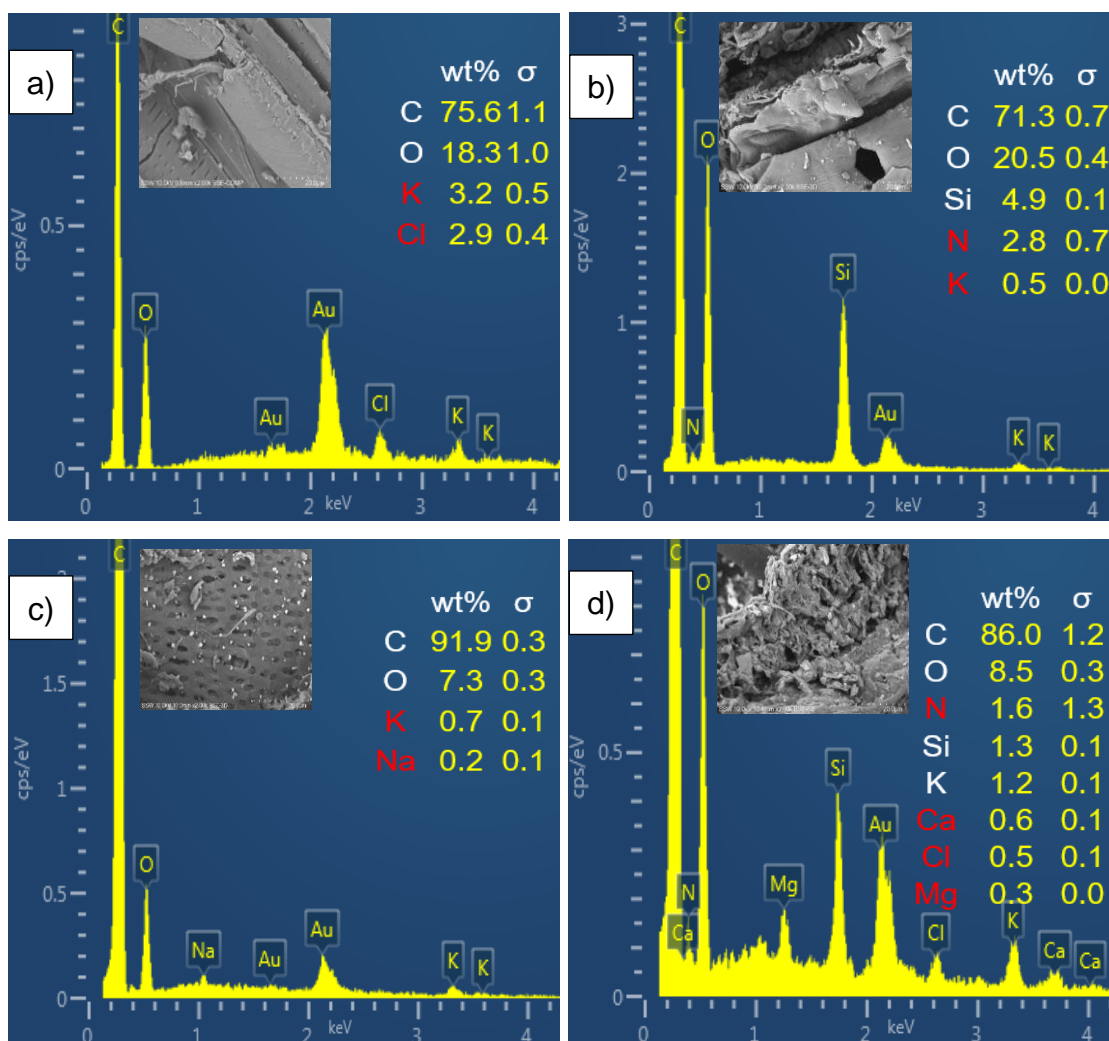
Figure 3.8 – SEM-EDX; a) *Phragmites australis*, **b) Biochar 350°C, c) 450°C, d) 550°C**

3.3.4   Bio-oil characterizations

The composition of the organic phase bio-oils produced at 5°C min^{-1} at different temperatures was investigated by FTIR. The spectra for different bio-oils are similar (Figure 3.9). The broad peak ranging from 3300 to 3600 cm^{-1} can be assigned to the –OH stretching, indicating the presence of phenols and alcohols. The peaks at 1611 and 1706 cm^{-1} are assigned to the C=O (carbonyl) stretching vibrations due to the presence of ketones, quinones and aldehyde groups [231]. As reported in previous literature [232], the occurrence of both O–H and C=O stretches indicate the presence of carboxylic acids

and their derivatives. The bands between 2850–2963 cm^{-1} indicate the symmetrical and asymmetrical C–H stretches of aliphatic CH$_3$ and CH$_2$ groups, while the C–H bending vibrations between 1370–1463 cm^{-1} are due to the presence of alkanes derived from the biomass [231]. The region between 950–1300 cm^{-1} could be assigned to the C–O stretching O–H bending of the primary, secondary and tertiary alcohols, phenol, esters, ethers [232,233]. The peaks from 650–900 cm^{-1} indicate the possible presence of mono, polycyclic and substituted aromatic groups as well as in the region between 1460–1611 cm^{-1} [202,232,234].
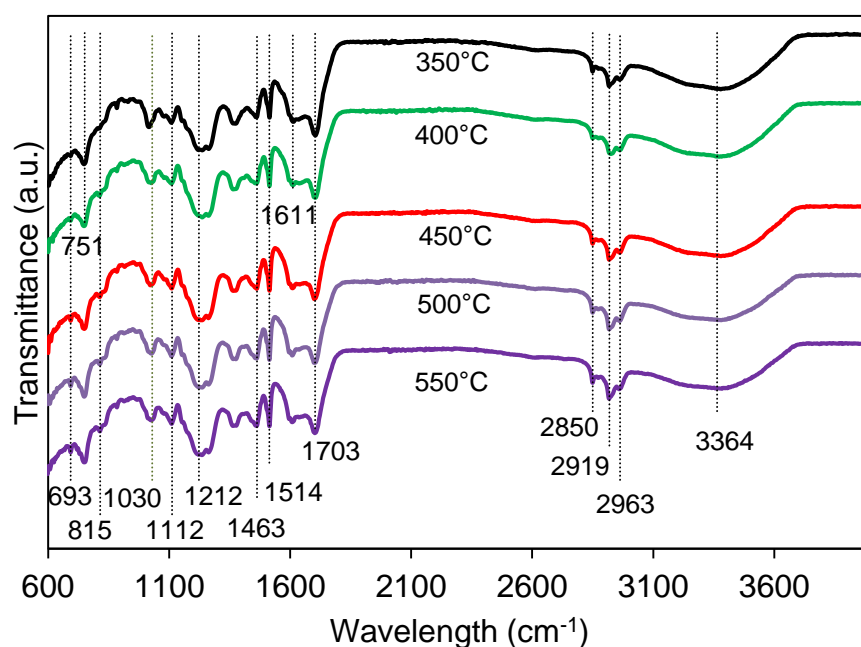
Figure 3.9 – FTIR bio-oil (organic fraction)

All the bio-oil fractions were tested using GC-MS (Figure 3.10). Bio-oil is a complex mixture of oxygenated organic compounds, and the distribution of the bio-oil products can be divided into different groups, including acids, ketones, phenols, aldehydes, sugars and others. The anhydrosugars consisted mostly of levoglucosan, which is the main product from the degradation of cellulose [79,83]. Furans comprised mostly of 2-furan methanol, 2,3-dihydrobenzofuran, tetrahydro-2-furan methanol and furfural. Furans are dehydration products of levoglucosan [235]. The phenolic compounds, derived from lignin, included phenol, 2-methylphenol, 3-methylphenol, 4-methylphenol, 4-

ethylphenol; methoxyphenols such as 2-methoxyphenol, 2-methoxy-4-vinylphenol, isoeugenol, benzenediols such as catechol (1,2-benzendiol). Ketones were mostly 1-hydroxy-2-propanone, 3-hydroxy-2-butanone and -methyl-2-cyclopenten-1-one. Methoxy phenol and alkyl phenol are from primary pyrolysis of lignin and phenols and phenol derivatives are from secondary pyrolysis of lignin [236].

The GC-MS chromatograms reported 180 compounds in the organic phase, while 92 in the aqueous phase although only around 26 compounds had a % peak area above 1%. The components with the peak area above 1 % are reported in Figure 3.10.

By comparing the peak areas and the relative abundance in terms of area percentage within each sample, it was found that for the organic phase at both heating rates, the most abundant groups were phenolics compounds (confirmed by FTIR analysis) which accounted for around 30–37% of the total peak area, followed by carboxylic acid and furans which accounted for 6–7%. Instead, the aqueous phase exhibited a higher relative content of carboxylic acids, around 39 to 47%, followed by all the other groups which were below 10%, with the exception of phenolic groups in samples collected at 5°C min^{-1} which reached almost 17% of the peak area. Pentanal, a product from cellulose degradation [237] was only detected in the aqueous fractions for all the pyrolysis temperatures. Levoglucosan was detected mostly in the aqueous fraction for both heating rates. The presence of syringyl phenols (2,6-Dimethoxy-phenol) and h-phenols (Phenol, 2-Methyl-phenol, 3-Methyl-phenol, 4-Methyl-phenol, 2,6-Dimethyl-phenol and4-Ethyl-phenol) is due to the syringyl and p-hydroxyphenyl structural units present in grass feedstocks [237].
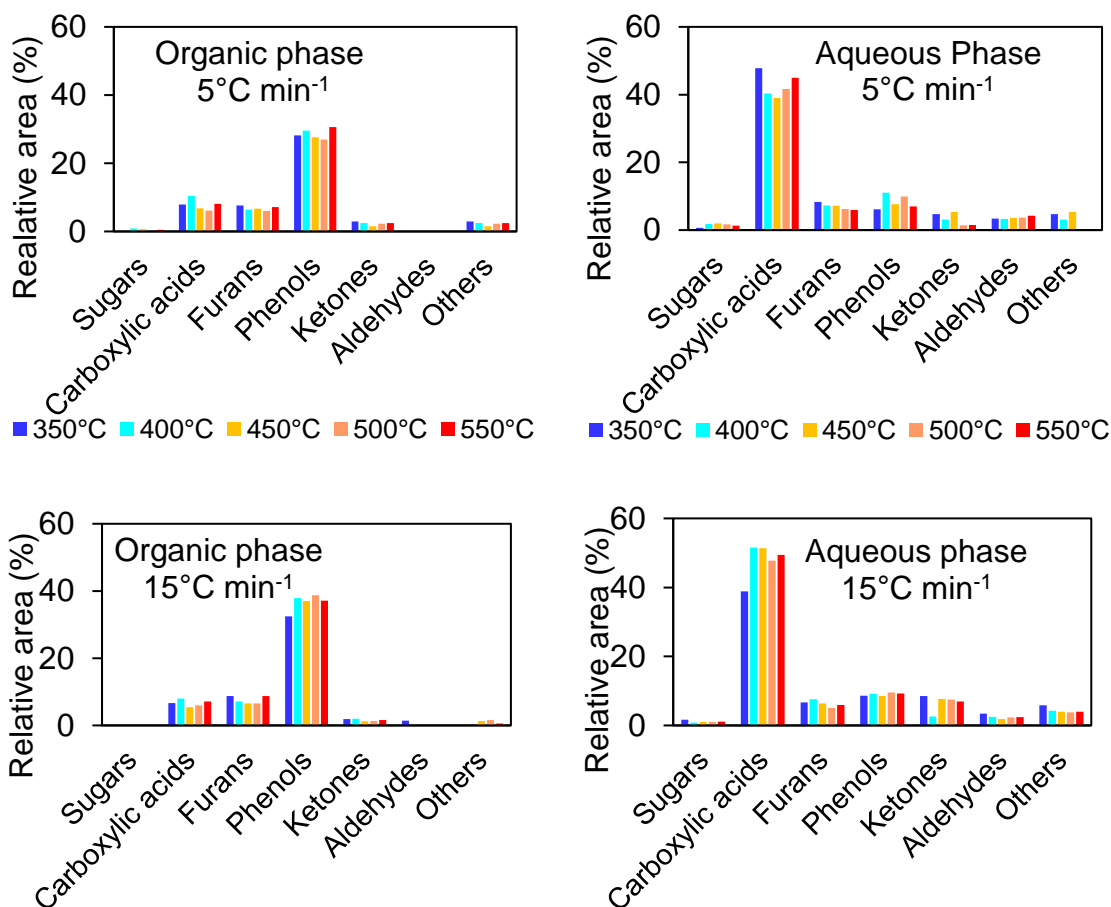
Figure 3.10 – Relative % peak area of all the bio-oil fractions from GC-MS analysis

3.4   Conclusions

In this study, *Phragmites australis* was used as feedstock for the pyrolysis experiments performed under slow pyrolysis conditions to investigate the effects of the operating parameters on the product yields. The results show that there is a marginal effect on bio-oil and biochar yields at the heating rates investigated in this study. The highest oil yield (43 wt% d.b.) was obtained at 450°C at 5°C min^{-1} although a similar yield (40 wt% d.b.) was observed when the bio-oil was pyrolyzed at 15°C min^{-1}. The biochar yield decreased from 42–45 wt% at 350°C to 34 wt% at 550°C.

Moreover, the sweeping gas flow rate did not have a consistent effect on the biochar products, although some minor differences were noted, such as the lower ash content and higher carbon content compared to the biochar produced without any nitrogen.

The results from bio-oil tested with GC-MS show a prevalence of phenolic compounds in the organic fraction while acetic acid was the predominant component in the aqueous phase.

The results of this study show the possibility to transform negative-value invasive common reed species into high-value energy and chemical products, such as acetic acid and phenols in bio-oil and a biochar residue with increased aromaticity and polarity.

Chapter 4

4 Slow pyrolysis of model compounds: Studies on process parameters and product characterizations

4.1 Introduction

Thermochemical conversion technologies such as pyrolysis and gasification are becoming more popular for the production of bio-based products from more sustainable energy resources. During pyrolysis, temperature, heating rates and holding times are the main operating conditions that affect the pyrolysis products. However, the effect of the biomass components plays a fundamental role in the pyrolysis process by modifying the characteristics of the products during the reaction. Several studies investigated the interaction between cellulose, xylan and lignin [199,238–241] during pyrolysis.

Hosoya et al. [241] investigated the interactions of the lignocellulosic components at 800°C. Their results showed that lignin decreased the thermal polymerization of levoglucosan formed from cellulose and enhanced the formation of low molecular weight products from cellulose with reduced yield of char fraction; secondary char formation was decreased from lignin, because the cellulose inhibited the vapour phase carbonization and enhanced the formation of lignin-derived products such as guaiacol, 4-methyl-guaiacol and 4-vinyl-guaiacol. No significant effect was reported for cellulose and hemicellulose interactions. Zhang et al. [240] investigated the effect of native mixture of the components. Their findings showed that the only significant effect was observed for herbaceous native cellulose-lignin mixes, where levoglucosan yield was decreased and the yield of low molecular weight compounds and furans increased. No interaction was found for the native cellulose-lignin from woody biomass. They speculated that the higher degree of covalent bonding between cellulose and lignin in herbaceous biomass could decrease the levoglucosan yield. Wu et al. [199] investigated cellulose and hemicellulose during fast pyrolysis observing that this interaction favours the formation of hemicellulose-derived products including acetol, acetone, acetic acid, 1-hydroxy-2-butanone and CO_2, while slightly inhibiting cellulose-derived products, especially levoglucosan.

In this study, the effect of the major biomass components, cellulose, hemicellulose and lignin, was investigated to gather a better understanding on the characteristics of the pyrolysis products.

The model compounds were also mixed with the same weight percentage of the real biomass, to address similarities and differences of the pyrolysis products.

4.2   Materials and methods

The pyrolysis reactor used for this chapter is the batch MFR described in the Equipment section of Chapter 2, section 2.1.1.

Experiments were planned to study the effect of heating rate and model compound ratios on the pyrolysis product yields and characteristics.

The temperature 450°C was chosen as the ideal temperature for the pyrolysis experiments based on the results of Chapter 3. The experiments were carried out at 5 and 15 °C min^{-1} with different ratios of model compound.

The chemical composition of the real biomass is reported in Table 4.1.

Table 4.1 – Model compounds

Model compounds wt%	Model compound ratios
60% cellulose - 20% xylose - 20% lignin	3:1:1
20% cellulose - 20% xylose - 60% lignin	1:1:3
33% cellulose - 33% xylose - 33% lignin	1:1:1
45% cellulose - 30% xylose - 25% lignin	9:6:5 (real biomass)

Mass of about 150 g was mixed and heated to the set point temperature with the selected heating rate and and then maintained for 30 minutes to complete the pyrolysis reaction. No nitrogen purge was used in these experiments.

Microcrystalline cellulose Avicel ® PH-101 (Sigma-Aldrich), D-(+)-Xylose (Fisher Scientific) and dealkaline lignin (Fisher Scientific) were used in this work. D-(+)-Xylose was chosen to represent hemicellulose [242]. Different ratios of the components were pyrolyzed to study their effects on the pyrolysis products (Table 4.1). The composition of *Phragmites australis* has been determined according to the NREL procedure described

in Chapter 2 and the last row of Table 4.1 represents the composition of the real biomass. Feedstock and biochar characterizations were carried out with TGA-FTIR (biomass only), higher heating value, proximate, ultimate analysis SEM-EDX, FTIR and BET surface area (biochar only). The bio-oil was anaylzed by GC-MS.

4.3   Results and discussion

4.3.1   Feedstock characterization

The weight-loss trend of different ratios of model compound with increasing temperature is reported in Figure 4.1. When the temperature is lower than 340°C the xylose was the major contributor to the mass loss rate. At temperatures above 340°C cellulose was dominant for mass loss. For the sample with 60% of cellulose, the first peak in the DTG graph occurred at 214°C and the second peak at 349°C; for the sample with the highest lignin content (60% lignin), the first peak was at 205°C and the second at 343°C, and finally for the sample with the same ratio of the three model compounds, the first peak occurred at 213°C and the second at 343°C. Increasing the cellulose content increased the value of the second peak, whereas, an increase in the lignin content decreased the temperature of the first peak. Comparing the TGA-DTG results of the real biomass, it was noted that the cellulose and hemicellulose in the model compounds had individual peaks, whereas the real biomass exhibited one peak and a shoulder.

The sample with the highest lignin content (red line in Figure 4.1) had the lowest weight loss. This is confirmed by other studies [238] where hemicellulose was found to be the highest contributor to the mass loss at temperature below 327°C, cellulose at temperatures above 327°C and lignin contributed the most to the residues. Moreover, lignin continued to decompose above 700°C, confirmed by other studies [243,244].
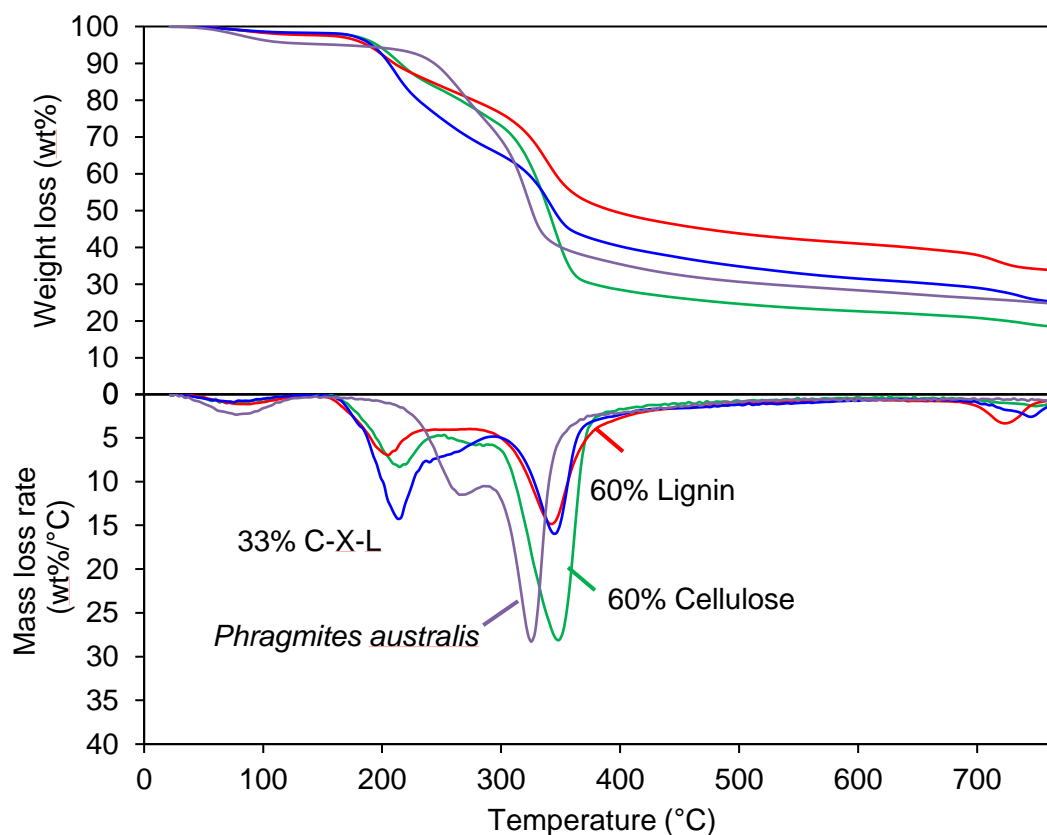
Figure 4.1 – TGA and DTG curves of model compounds and real *Phragmites australis*

The influence of the model compounds on the gas evolution is reported in Figure 4.2. The gas evolution was recorded every 100°C from 150°C to 550°C. The main gas release started at 250°C and continued until 450–550 °C, depending on the sample. The main similarity between model compounds and real biomass was the release of CO_2 at the characteristic wavelengths of 2294–2239 cm^{-1} and 794–568 cm^{-1} and at temperatures starting at 250°C and 350°C, respectively. The CO_2 is usually attributed to the primary pyrolysis [103]. The main difference was the prominent adsorption peaks in the wavelengths 1442–1600 cm^{-1} attributed to the aromatics and 1600–1932 cm^{-1} representing the aldehydes, ketones and acids for the sample with 60% cellulose recurring at all the temperatures. These peaks were recorded only for the sample with the same ratio of model compounds at 250°C. Same trend was observed for the sample with the highest amount of lignin, however less pronounced. The sample with 60% cellulose

also had the most prominent peaks at 4000–3500 cm^{-1} due to O–H stretching vibration related to dehydration reactions [245]. A small peak of CH_4 in the range of 3088–2990 cm^{-1} was observed for all samples starting at 450°C, most pronounced for 60% lignin and 33%, and very small for the rest. This peak is associated with the secondary cracking of volatiles and aromatic char [246] due to the fact that lignin had the highest amount of aromatic rings and methoxy groups (O–CH$_3$) [103,247,248]. The formation of CO was weak for all samples, generated only at 350°C.
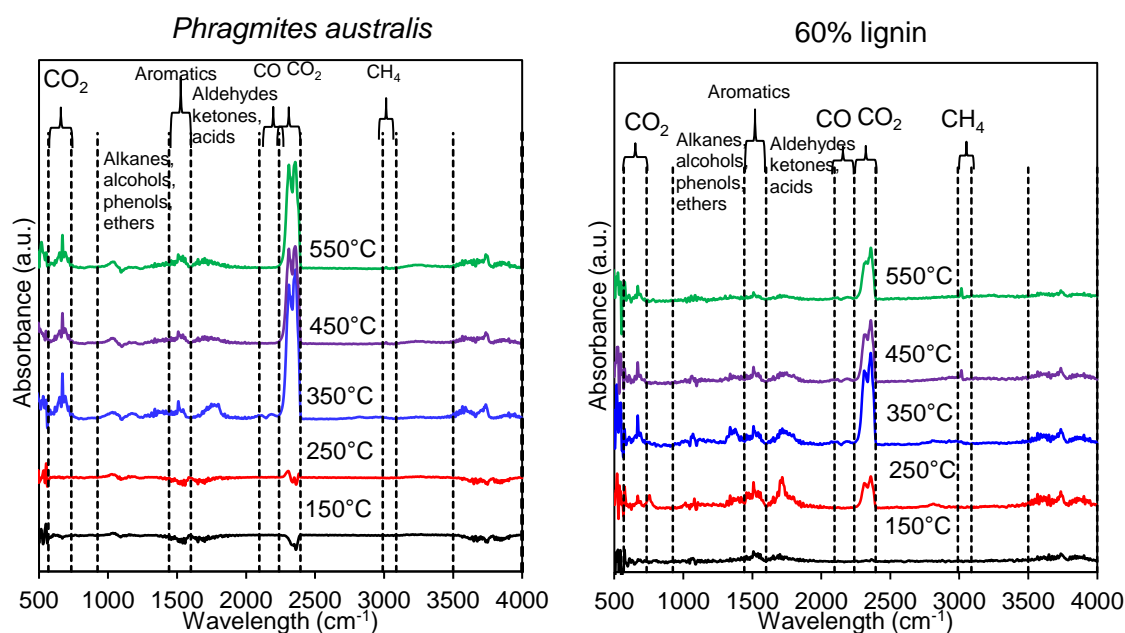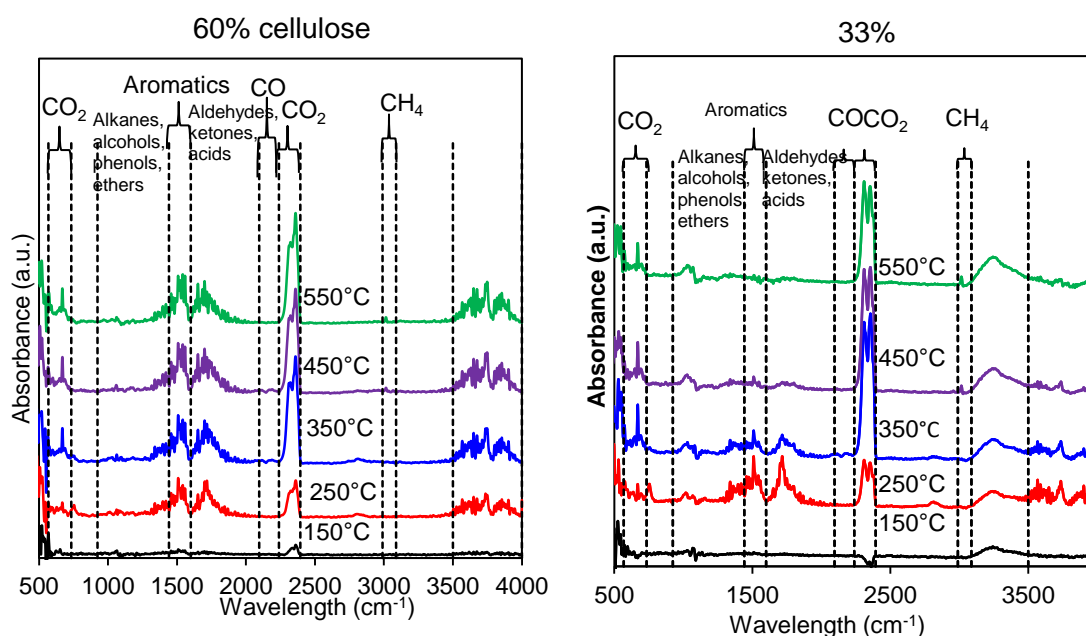
Figure 4.2 – FTIR gas evolution, *Phragmites australis* and model compounds

The characteristics of the model compounds before pyrolysis (individual and mixed) are reported in Table 4.2 and Table 4.3. Proximate analysis was carried out to measure moisture, volatile matter, fixed carbon and ash content. The ash content was the highest for the lignin sample and the mixture with 60% lignin content. The proximate and ultimate analysis of the dealkaline lignin are confirmed by another study [249].

Table 4.2 – Model compounds proximate, moisture and HHV analysis

Samples	Proximate analysis (wt%, d.b.)			Moisture (wt%)	HHV (MJ/kg)
	Fixed C	Volatiles	Ash		
Avicel P-101	6.83±0.34	89.66±0.32	0.00±0.00	3.53±0.03	16.35±0.04
Xylose	5.54±0.04	94.12±0.09	0.20±0.061	0.59±0.12	15.35±0.01
Dealkaline Lignin	27.17±1.05	47.80±0.97	15.2±0.11	9.85±0.04	20.11±0.13
60% C - 20% X - 20% L	15.93±0.96	78.77±0.28	2.81±0.02	3.19±0.70	16.89±0.06
20% C - 20% X - 60% L	23.26±1.71	63.75±0.27	8.71±0.01	5.62±1.43	18.52±0.06
33% C - 33% X - 33% L	19.39±0.80	72.91±0.07	4.20±0.29	3.56±0.70	17.45±0.03

45% C - 30% X - 25% L	11.42±0.08	82.190.14	2.58±0.03	3.79±0.03	16.99±0.02

Table 4.3 – Ultimate analysis of the model compounds (Oxygen calculated by difference)

Samples	Ultimate analysis (wt%)				
	C	**H**	**O**	**N**	**S**
Avicel P-101	42.67±1.55	6.07±0.12	49.91±0.65	1.33±0.06	0.02±0.00
Xylose	40.87±0.95	5.67±0.08	52.84±0.36	0.42±0.03	0.00±0.00
Dealkaline Lignin	61.15±2.54	5.53±0.06	17.20±1.00	0.89±0.04	0.03±0.00
60% C - 20% X - 20% L	45.79±2.98	5.86±0.09	44.33±1.17	1.21±0.07	0.00±0.00
20% C - 20% X - 60% L	53.45±2.78	5.59±0.12	31.41±1.09	0.89±0.04	0.01±0.00
33% C - 33% X - 33% L	47.70±1.48	5.73±0.11	41.28±0.55	1.08±0.08	0.01±0.00
45% C - 30% X - 25% L	46.69±1.21	5.80±0.06	44.00±0.47	0.93±0.06	0.00±0.00

4.3.2   Product yields

Figure 4.3 and Figure 4.4 report the product yields at 450°C and 5 and 15°C min^{-1} heating rates. The bio-oil yield was higher (52% at 5°C min^{-1} and 49.5% at 15°C min^{-1}) for the sample with the highest content of cellulose and it decreased with decreasing cellulose content and increasing lignin content. The biochar yield had the opposite trend; it is the highest with the highest content of lignin (44.5% at 5°C min^{-1} and 42.5% at 15°C min^{-1}). The highest char yield at the lower heating rate can be explained by the progression of cross-linking reactions resulting in char formation, since the samples have more time in the region of "optimal char formation" [250]. Other researches also report this trend with different biomass [251–253]. Instead, the non-condensable gas yield increased from 5 to 15°C min^{-1}. This behavior could be explained by the longer residence time of the volatiles in the reactor which favors the second cracking leading to more gas production [252].
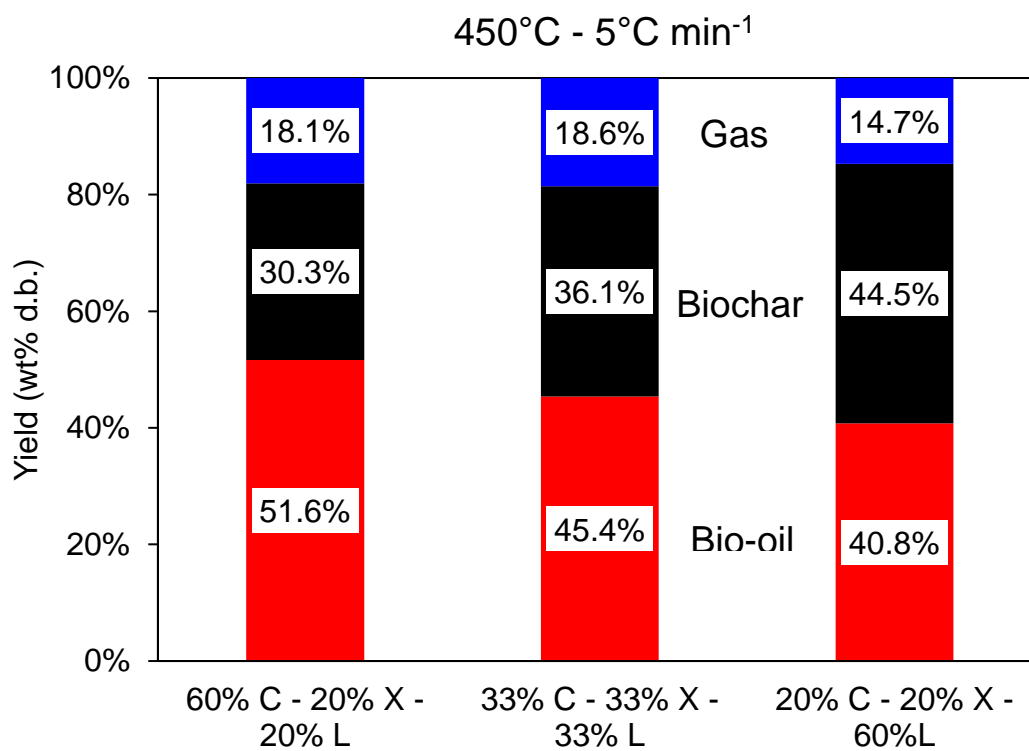
Figure 4.3 – Product yields at 5°C min⁻¹
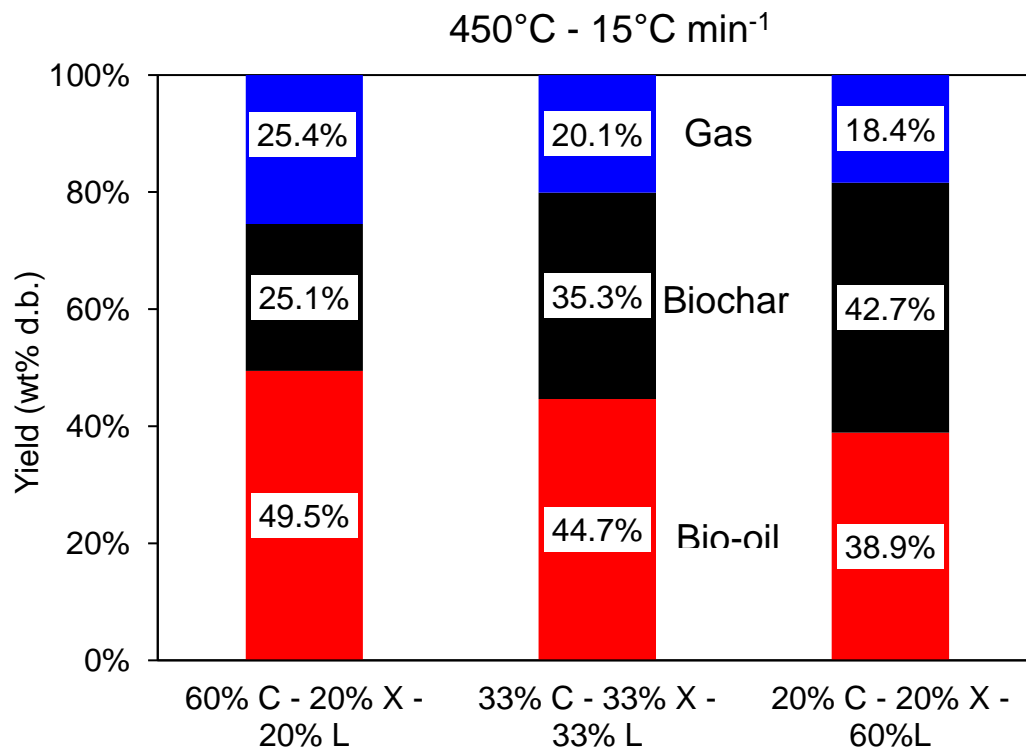
Figure 4.4 – Product yields at 15°C min⁻¹

Comparison between the yield of the products obtained from the real biomass and the model compounds with the same composition of the *Phragmites australis* (Figure 4.5 and Figure 4.6) showed that the bio-oil yield was higher for the model compound mixture for both heating rates. One possible explanation to this behavior could be that the real biomass had a higher ash content (5.5 wt%) compared to the model compound (2.6 wt%). As stated in the literature review, the ash acts as a catalyst for cracking reactions that lead to less bio-oil and more production of gases. The biochar yield was higher for the *Phragmites australis*.
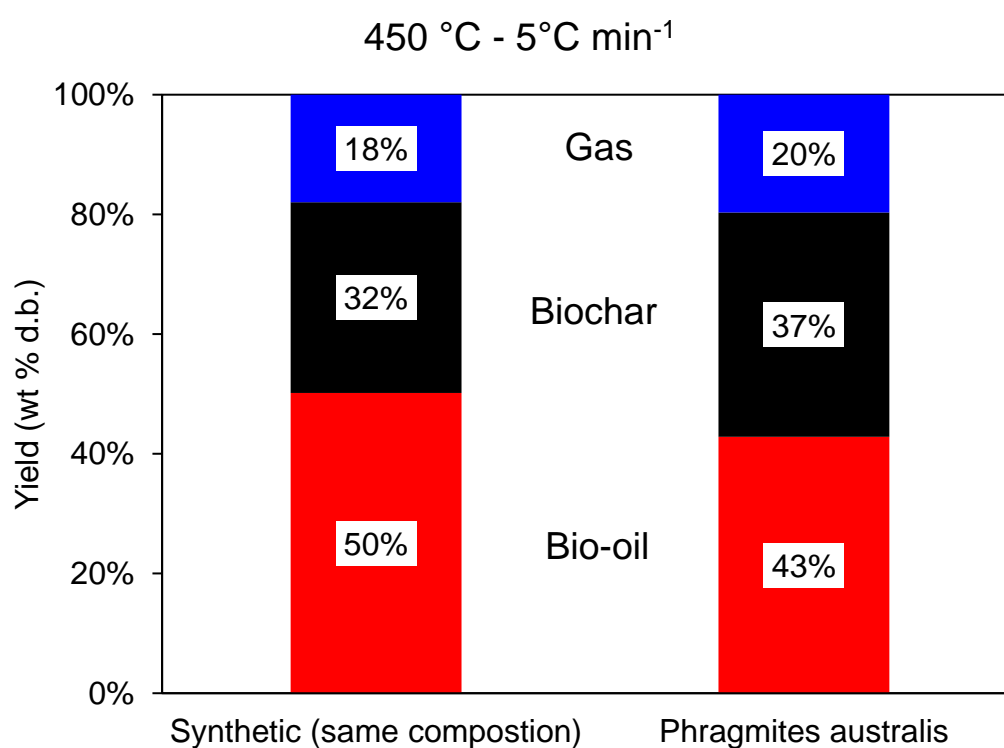
Figure 4.5 – Product yields at 5°C min^{-1} (synthetic vs real biomass)
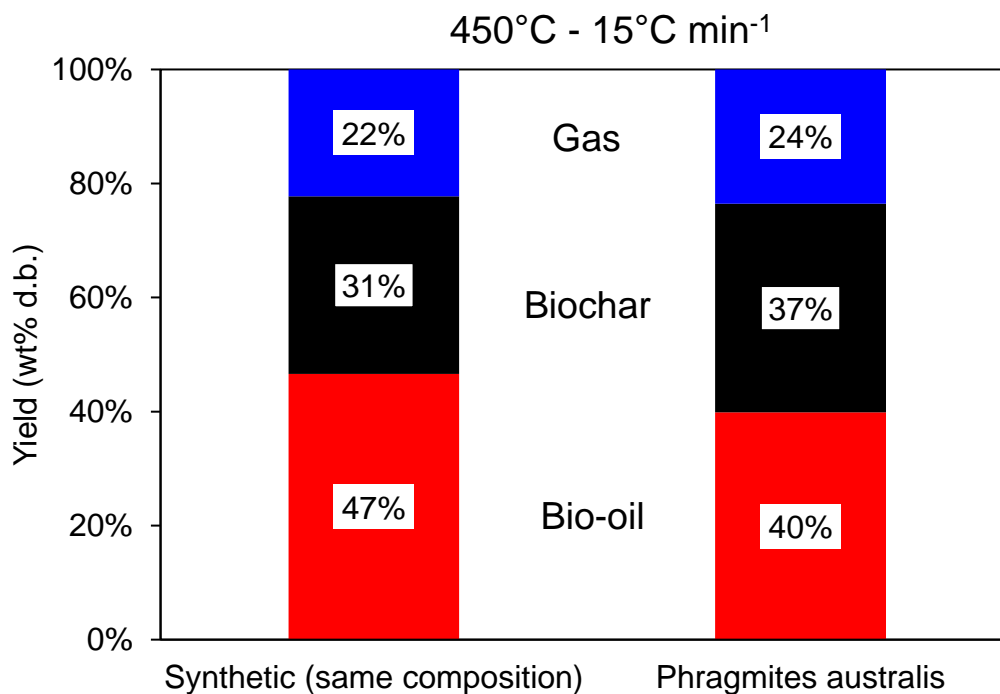
Figure 4.6 – Product yields at 15°C min⁻¹ (synthetic vs real)

4.3.3   Synthetic biochar characteristics

Following the same trend of the model compounds before the pyrolysis treatment, the ash content increased with increasing lignin content for both heating rates (Table 4.4 and Table 4.5). The higher heating values increased with the increasing cellulose content in the sample. The ultimate analysis showed similarity with the elemental content of the biochar mixtures for both heating rates. The ash content of the char produced from the real biomass was double compared to the synthetic biochar. The carbon content was higher for the synthetic biochar, 77.8% of carbon versus 63% of the real biochar at 5°C min⁻¹ and 77.9% of carbon versus 67.2% of the real biochar at 15°C min⁻¹ (Table 4.6).

Table 4.4 – Synthetic biochar characteristics at 5°C min^{-1}

Synthetic biomass	Proximate analysis (wt%, d.b.)			Moisture (wt%)	HHV (MJ/kg)
	Fixed C	**Volatiles**	**Ash**		
60% C - 20% X - 20% L	70.67±0.39	17.50±0.45	9.54±0.85	2.3±0.01	30.12±0.11
20% C - 20% X - 60% L	62.45±0.51	18.66±0.25	16.91±0.08	1.97±0.20	27.30±0.10
33% C - 33% X - 33% L	69.49±0.15	17.34±0.06	11.18±0.12	1.98±0.09	28.92±0.02
45% C - 30% X - 25% L	72.68±0.01	15.97±0.21	9.39±0.34	1.95±0.13	28.82±0.60

Table 4.5 – Synthetic biochar characteristics at 15°C min^{-1}

Synthetic biomass	Proximate analysis (wt%, d.b.)			Moisture (wt%)	HHV (MJ/kg)
	Fixed C	**Volatiles**	**Ash**		
60% C - 20% X - 20% L	67.31±0.78	21.40±0.62	8.31±0.02	2.98±0.16	29.40±0.27
20% C - 20% X - 60% L	55.55±0.22	25.06±0.36	16.13±0.02	3.25±0.11	26.53±0.01
33% C - 33% X - 33% L	67.79±0.60	18.34±0.51	12.04±0.1	2.00±0.18	28.18±0.01
45% C - 30% X - 25% L	73.98±1.98	16.15±0.25	7.48±2.03	2.38±0.20	28.60±0.58

Table 4.6 – Ultimate analysis synthetic biochar (Oxygen calculated by difference) (Oxygen calculated by difference)

Synthetic biochar 5°C min^{-1}	Ultimate analysis (wt%)				
	C	**H**	**O**	**N**	**S**
60% C - 20% X - 20% L	79.48±0.30	2.93±0.02	5.80±0.31	0.51±0.02	1.74±0.05
20% C - 20% X - 60% L	71.45±0.33	2.50±0.41	6.08±0.15	0.46±0.07	2.6±0.41
33% C - 33% X - 33% L	73.72±1.66	2.93±0.02	9.58±0.65	0.49±0.04	2.10±0.09
45% C - 30% X - 25% L	77.81±2.37	3.01±0.06	7.48±0.91	0.46±0.04	1.84±0.04
Synthetic biochar 15°C min^{-1}					
60% C - 20% X - 20% L	77.80±0.65	3.08±0.03	8.60±0.24	0.48±0.13	1.73±0.05
20% C - 20% X - 60% L	71.47±3.44	2.70±0.03	6.06±1.34	0.52±0.09	3.12±0.22
33% C - 33% X - 33% L	74.79±0.30	3.12±0.04	8.32±0.11	0.57±0.06	1.15±0.05
45% C - 30% X - 25% L	77.93±0.47	3.05±0.04	9.06±0.76	0.54±0.09	1.99±0.05

The BET values are reported in Table 4.7. The values of BET surface area were smaller compared to the values of the biochar from *Phragmites australis*.

Table 4.7 – BET area of synthetic biochars produced at 5°C min^{-1}

Model compounds	BET surface area (m^2/g)	Total pore volume (cm^3/g)	Average pore size diameter (nm)
60% C - 20% X - 20% L	9.98	0	1.79
20% C - 20% X - 60% L	5.387	0.00724	2.29
33% C - 33% X - 33% L	2.215	4.45E-05	116.57
45% C - 30% X - 25% L	1.288	0	1.79

The SEM analysis of the synthetic biomass is shown in Figure 4.8 and Figure 4.9. The particles were spherical with an irregular surface and some cracks. The pyrolysis treatment increased the porosity on the surface. Different researches have studied the pyrolysis of lignin in its different phases. Different studies [254–257] reported that at temperatures starting from around 150°C, a liquid intermediate is formed from the lignin particles and continued until 182°C when the lignin completely liquefied. As the temperature increased to 218–241°C, all the particles were liquified and some foaming occurred. The formation of foam and bubbles is due to the release of volatiles [255,256,258], which continues as temperature increases. Above 350°C, Dufour et al. [258] reported a fast solidification with the formation of a solid matrix by cross-linking reactions.

Large agglomerations of biochar were noted in the sample with 60% lignin content and not in the biochar produced when the lignin content was lower (Figure 4.7). Several studies [257,259] investigated the pyrolysis of lignin, indicating that due to its complex polymeric structure, different degradation stages occur at different temperatures. When the temperature is around 400°C and higher, cross-linking reactions (solidification stage) lead to broadly agglomerated particles which could explain the large agglomerates found after pyrolysis.

Figure 4.7 – Biochar produced at 500°C, 5°C min^{-1} from the sample with 60% lignin content
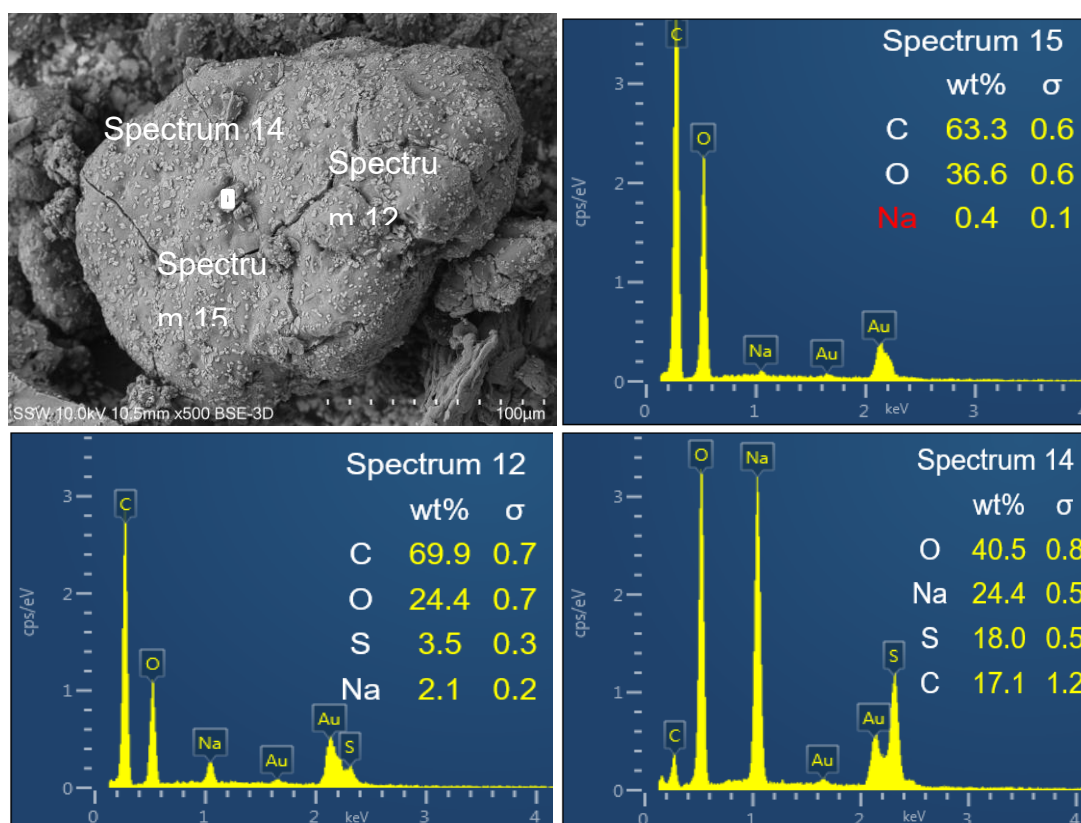
Figure 4.8 – SEM/EDX synthetic biomass sample (60% lignin)
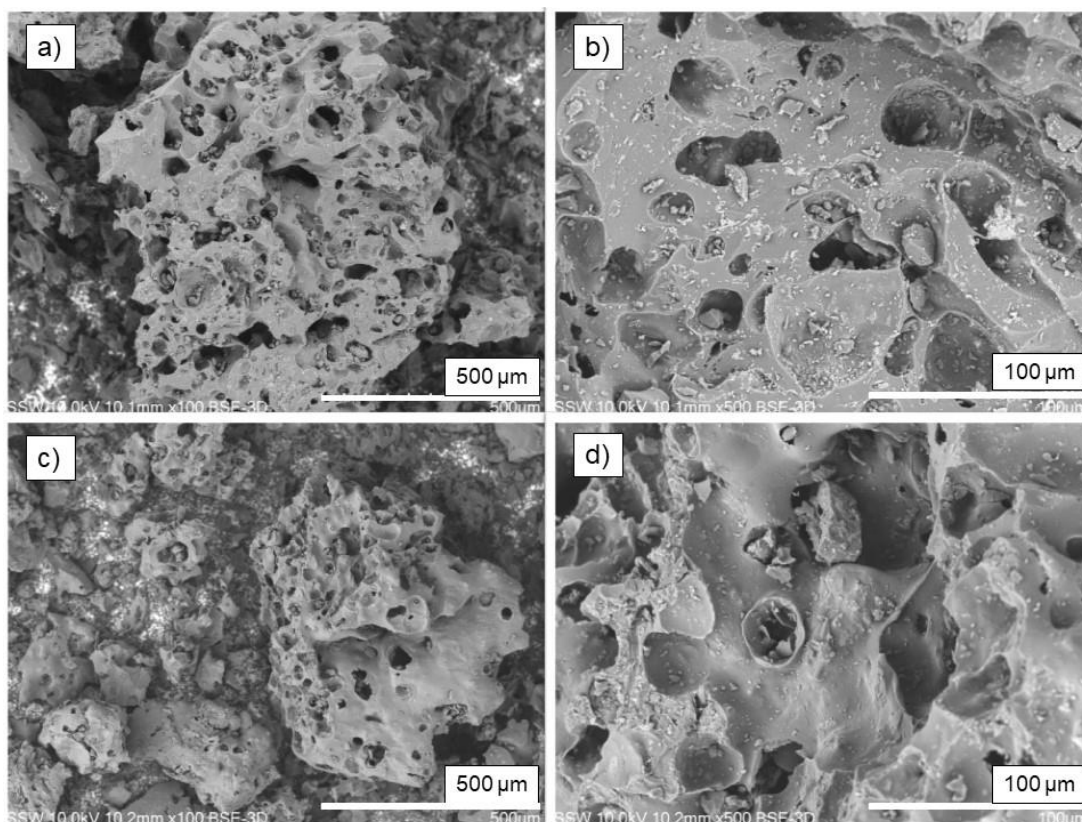
Figure 4.9 – SEM synthetic biochar samples (60% lignin); a) and b) produced at 5°C/min and c) and d) produced at 15°C/min

The FTIR analysis was performed on the individual model compounds and the mixture with the same ratio to detect the changes in functional groups on the surface before and after pyrolysis at 450°C and 5°C min^{-1} (Figure 4.10).

The IR spectra of the raw materials comprised different peaks similar to the actual biomass. The peak around 3300 cm^{-1} associated with the –OH stretching, hydrogen bonds consisting mostly of acids, alcohols and phenols is present in cellulose and D-xylose but not in the dealkaline lignin. In cellulose indicated the –OH in the glucose units [260]. The peak at 2909 cm^{-1} is assigned to C–H$_n$ stretching due to alkyl, aliphatic and aromatic compounds and it is present in cellulose and D-xylose [103,248]. Peak associated to the asymmetric –C–O–C– stretch of the β-1,4- glycosidic linkage in cellulose was observed at 1156 cm^{-1} and the C–O stretching at 1050 cm^{-1}. Lignin had some characteristic peaks: at 1505 and 1600 cm^{-1} associated with C=C stretching due to aromatic skeletal vibrations

(aromatic ring) plus C=O stretch [261]; at 1268 cm^{-1} related to the C–O stretching of guaiacyl unit; at 1127 cm^{-1} due to the syringyl C–H in-plane deformation, and 1036 cm^{-1} due to the guaiacyl C–H deformation with C–O deformation in primary alcohol [219,262]. The spectra of the mixed sample (1:1:1) had a combination of the different peaks found in the individual compounds.

The spectra of the biochars resembles mostly the lignin, in fact they retained the peaks at 1600 (aromatic C=C stretching and C=O associated with ketones or quinones) and 1127 cm^{-1} (aromatic C–H in-plane deformation). The peak at 1160 cm^{-1} assigned to the –C–O–C– vibrations of cellulose disappeared in the biochar samples, indicating that structural changes occurred during the pyrolysis treatment, as well as the peaks at 1515 cm^{-1}. There is no peak at 1735 due to cellulose and hemicellulose in the synthetic compounds. There are two new peaks in the biochar samples related to aromatic C, one at 1440 cm^{-1} assigned to C–H bending vibration and at 878 cm^{-1} out-of-plane deformations of aromatic C–H [225,227,261].

Table 4.8 – FTIR band assignments

Band position (cm^{-1})	Component
Synthetic biomass	
760	C–H out of plane bending vibration aromatic ring (cellulose and d-xylose) [263]
902	C–H alkenes bends out of plane in position ring stretching in cellulose due to β-linkage
1036	C–O stretching vibration (cellulose, xylose and lignin)
1156	–C–O–C– asymmetric stretching in cellulose of the β-1,4-glycosidic linkage [264], and –C–O–C– stretching in xylose [263]
1267	Syringyl ring breathing and C–O stretching in lignin and xylan

1450	C–H bending vibration [265]
1512, 1600	C=C stretching vibration in benzene ring [265]
1735	C=O stretching of acetyl and carbonyl groups (hemicelluloses)
2851, 2918	$>CH_n$ stretching
3336	–OH stretching (broad)

Synthetic biochars

752, 797, 876	C–H, aromatic hydrogen
1074, 1112	–C–O–C– symmetric stretching
1448	Alkanes C–H
1591	Aromatic C–C ring stretching
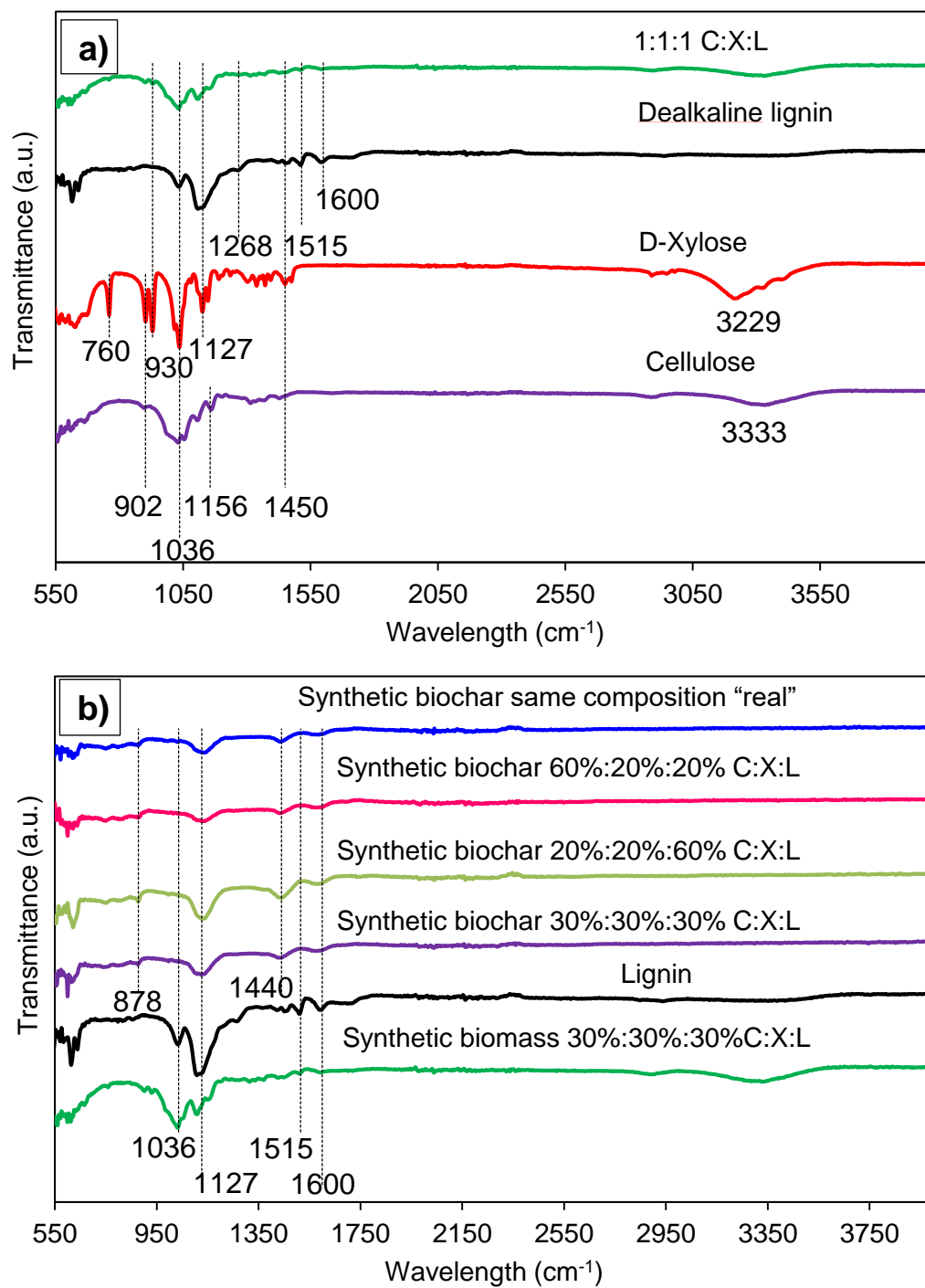
Figure 4.10 – FTIR spectra of model compounds before pyrolysis a) and after pyrolysis b)

4.3.4   Bio-oil characterizations

The composition of the bio-oils produced at 450°C and 5°C min^{-1} was investigated by FTIR. The spectra for the different bio-oils are similar (Figure 4.11). The broad peak ranging from 3300 to 3600 cm^{-1} can be assigned to the -OH stretching, indicating the presence of phenols, alcohols and water [52,234,266]. The peaks in the range of 3000-2800 cm^{-1} represents C–H stretching vibration typically assigned to alkanes. The peaks at 1611 and 1706 cm^{-1} was assigned to the C=O (carbonyl) stretching vibrations due to the presence of ketones, quinones and aldehyde groups [231]. As reported in previous literature [232] the occurrence of both O–H and C=O stretches indicate the presence of carboxylic acids and their derivatives. The bands between 2850–2963 cm^{-1} indicate the symmetrical and asymmetrical C–H stretches of aliphatic CH_3 and CH_2 groups, while the C–H bending vibrations between 1370–1463 cm^{-1} are due to the presence of alkanes derived from the biomass [231]. CH_3 groups bending vibration can be located at 1390 cm^{-1}, which can be assigned to methyl groups [234]. The aromatic C=C stretching vibration of alkenes was observed at 1645 cm^{-1}. The region between 690–900 cm^{-1} and 1450–1611 cm^{-1} indicates the possible presence of mono and polycyclic and substituted aromatic groups [202,232,234]. Moreover, the region between 900–1300 cm^{-1} could be assigned to the C–O stretching O–H bending of the primary, secondary and tertiary alcohols, phenol, esters, ethers [232,233].
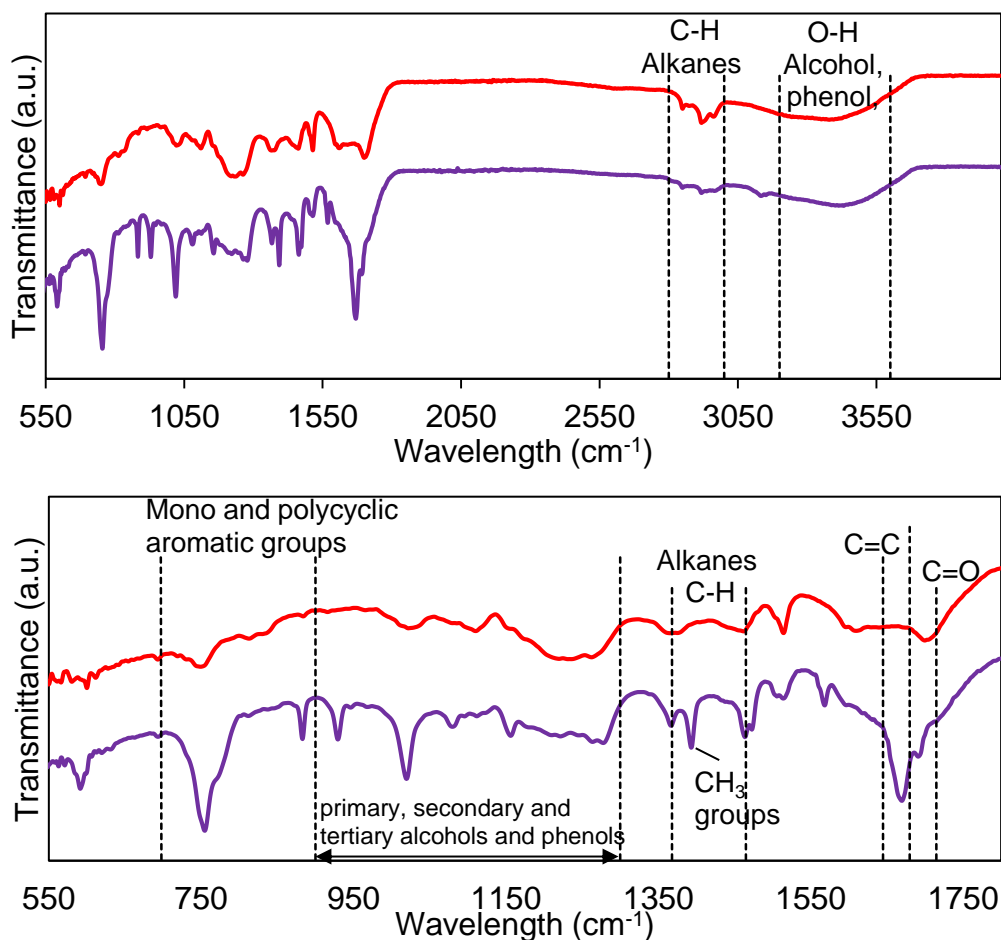
Figure 4.11 – Comparison between bio-oil from model compounds (purple) and bio-oil from *Phragmites australis* (red) at 450°C 5°C min⁻¹

Many differences were observed in the bio-oil produced from *Phragmites australis* and the model compounds with the same composition as the real biomass. The bio-oil collected from the model compounds didn't have the characteristic tarry organic phase, typical of the bio-oil produced from biomass. Only one fraction had been thoroughly mixed and analyzed for the model compounds. Table B.1 in Appendix B lists the compounds with highest peak area % and compounds that were common between the fractions in GC-MS. The organic phase of the actual biomass had 180 compounds identified, but only 23 were with a % area above 1. The aqueous fraction of the actual biomass had 80 compounds identified and 21 above 1% peak area. The bio-oil from the

synthetic biomass had 50 compounds at both heating rates, and only 20 compounds (% area > 1) at 5°C min^{-1} and 15 at 15°C min^{-1}.

Carboxylic acids, furans and phenolics were the main compounds in the bio-oils, the heating rate didn't affect the chemicals, but it changed the relative contents. The organic phase had the highest relative peak area compared to the other components present within the fraction at both heating rates. The aqueous phase of the actual biomass had the highest relative content in acetic acid (carboxylic acid), followed by phenols and furans. The bio-oil obtained from the synthetic model compounds presented acetic acid and furfural with the same relative content at both heating rates. The levoglucosan had the highest % area in the sample pyrolyzed at 15°C min^{-1} (Figure 4.12).
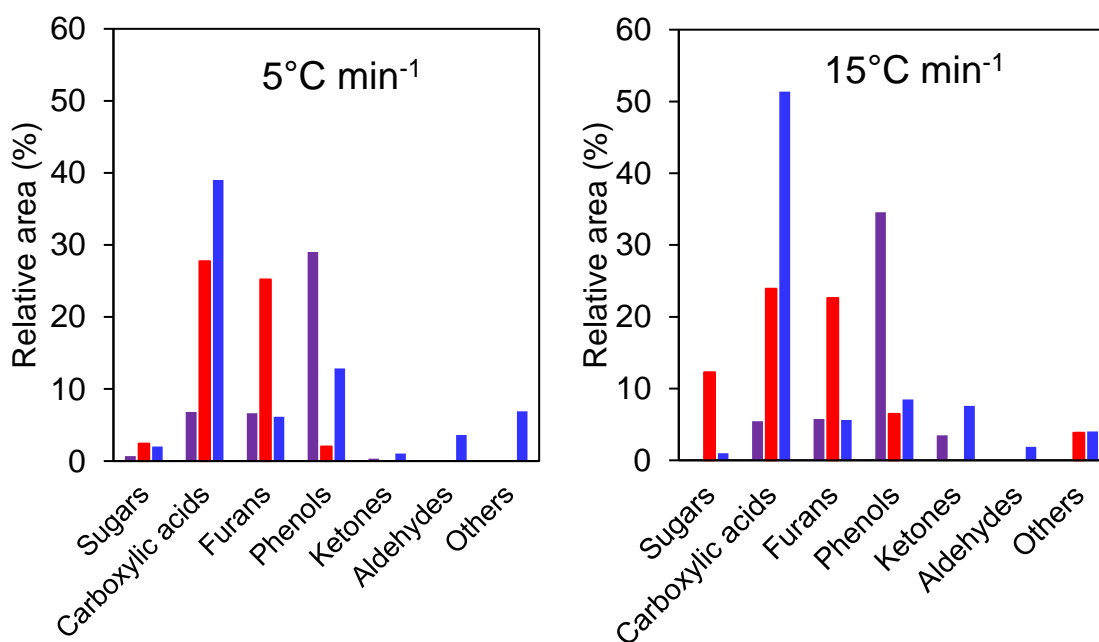
Figure 4.12 – GC-MS Relative area % (purple: organic phase real biomass, blue: aqueous phase real biomass, red: bio-oil synthetic biomass)

4.4   Conclusions

The slow pyrolysis of cellulose, xylose and lignin in different ratios was carried out to investigate the similarities and differences compared to the actual biomass. The main findings are summarized as follows.

The comparison between the product yields at 450°C and 5 and 15°C min^{-1} showed that the bio-oil yield was higher for the synthetic biomass (47-50% yield for synthetic biomass versus 40-43% for *Phragmites australis*) while the char yield was higher from Phragmites biomass (37% compared to 31-32% yield for the synthetic biomass). The highest bio-oil yield was observed for the sample containing the highest cellulose content, while the char yield was the highest for the sample prepared with 60% of lignin. It was also noted that the biochar sample from the pyrolysis of 60% lignin formed as large agglomerates, compared to the powder form of the biochars where the amount of lignin was lower.

GC-MS analysis showed a different distribution of the bio-oil chemical compounds, with an increased furfural in the bio-oil from the synthetic biomass.

The different trends and products obtained from the real biomass and the model compounds highlight that the structure of the lignocellulosic components in the biomass plays a significant role in the pyrolysis product distribution.

Chapter 5

5 Design of a bench scale pyrolysis unit for the production of bio-oil and biochar

A continuous, bench scale pyrolysis unit was designed for slow and fast pyrolysis to conduct the next experimental part of the thesis. The unit was built at the Western University Machine Shop (UMS).

The most common reactor configurations, specifically for fast pyrolysis, are fluidizing bed reactors, due to the well-known technology and excellent heat transfer rates and temperature control which allow to achieve high bio-oil yields. However, they required sand as a heat carrier, and char separation.

The main objective of this chapter was the design of a bench-scale unit easy to operate, that gives reliable and consistent results without the use of sand as a heat carrier. Moreover, the main idea was to remove the char inside the reactor vessel as fast as possible (given the maximum rpm of the motor of the extractor auger), to avoid the accumulation of a bed of char, thus reducing and avoiding the catalytic effect of the char on the vapor cracking reaction [139].

5.1 Pyrolysis unit overview

The pyrolysis experiments were carried out in a bench scale pyrolysis unit made of 316 stainless-steel designed and built for the purpose of this research (Figure 5.1).
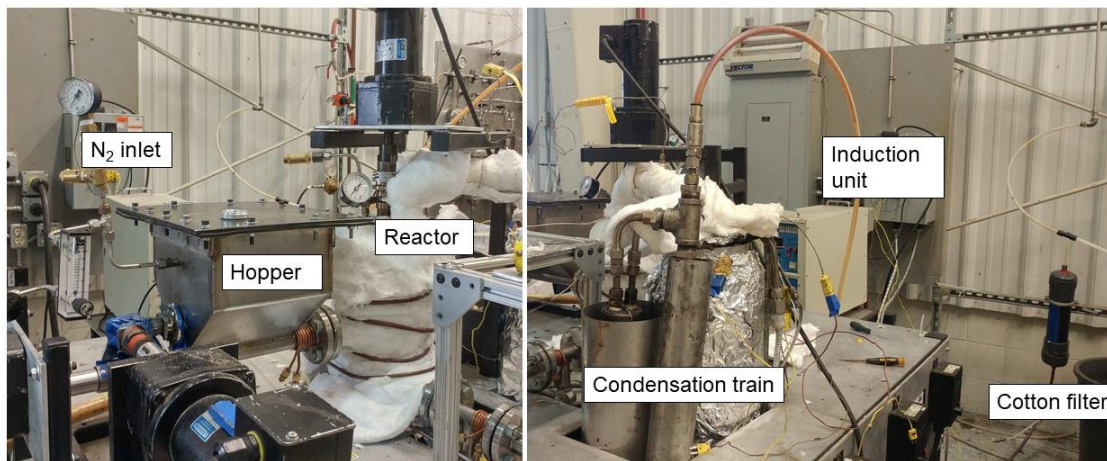
Figure 5.1 – New bench-scale pyrolysis unit

The unit consists of a biomass screw-conveyor feeder, a 1.4-liter reactor vessel, one biochar collector for the removal of biochar during the pyrolysis experiments and a three-stage bio-oil fractionation system. The feeder comprises a bridge-breaker to avoid the bridging of biomass and have a constant feeding rate to the reactor. The main components are described in Section 5.1.1.

5.1.1   Pyrolysis unit components

5.1.1.1   Feeder

One of the challenges to consider when designing a feeding system is how to feed the biomass into the reactor chamber with a continuous and uniform flow. Although different feeding system are commercially available the biomass particles can vary in size distribution, density and moisture, which make it difficult to have a single system suitable for different biomass fuels. Woody biomasses have a higher bulk density compared to herbaceous feedstocks. *Phragmites australis* with 1 mm average particle size has a bulk density of 297 kg/m^3, which increases the tendency to bridge (Figure 5.2 a)). To avoid this problem, the feeder was equipped with a magnetic bridge breaker (Figure 5.2 b) and c)). The bridge breaker was made of a copper coil helix that rotates and agitates the biomass. Two neodymium magnets where placed at both side of the wall of the feeder and a ¼ hp motor was coupled to allow rotation. The use of the magnets was chosen to

allow easy removal of the bridge breaker and cleaning of the feeder. The lid was equipped with a light and a 1 inch through-wall sight, rated for 25 psi, to check the biomass flow during the experiments.

Figure 5.2 – Feeder internals

The feeder has a capacity of around 6 liters and a screw auger 0.5-inch OD to feed the biomass to the reactor. The nitrogen is injected through the feeder to avoid the back flow of pyrolysis vapors through the hopper, thus allowing to have a positive pressure into the reactor. The feeding system feeds the biomass on the side of the reactor at approximately 8 cm from the bottom with a feeding rate between 0.9-1.5 kg/h. This range was selected as the optimal feeding rate versus extraction rate that ensured a well pyrolyzed biochar. The calibration of the feeder is reported in Table C.1 in Appendix C. The calibration was performed at cold with N_2 to simulate the actual condition during the pyrolysis experiments.

The speed of the feeding auger, extraction auger and bridge breaker are controlled with variable DC motor controls Vari-Drive™ (KB Electronics, Inc, FL, US), while the stirrer controller uses a variable DC motor control SPEEDMASTER™ (Leeson Electric Corporation, WI, US).

5.1.1.2   Reactor vessel

The reactor is made of 316 stainless-steel. It comprises three part: the reactor vessel, the bottom and the lid. The bottom of the reactor comprises a trench with a screw extractor to remove the char from the reactor chamber to the char collector. Two thermocouples are placed at the bottom for temperature control. The reactor chamber is equipped with an agitator which sweeps the biochar from the reactor chamber to the screw auger and into the char collection pot. The agitator comprises a filtering basket equipped with different layers of a Super-Small-Particle-Filtering Stainless Steel Wire Cloth (McMaster-Carr, OH, US) for high-flow applications to separate the particulates from the vapors. The wire cloth is made of 304 stainless-steel and it was rated to remove particle size down to 10 microns, with the following specifications: wire diameter 0.003 inch horizontal and 0.006 inch vertical (Figure 5.3).

Figure 5.3 – Reactor filtering basket

The reactor is heated by a 12-kW induction system (Superior Induction Company, California, US). The induction system comprises the induction, a PID controller and the induction coil. The induction coil consists of a five-loop copper coil with tube size of 7.04 mm. Induction heating is preferred to heat the ferromagnetic vessel by a magnetic field that induces currents flow (eddy currents) causing the material to be heated by Joule effect [267]. In this way the heating takes place directly in the wall of the reactor and agitator instead of heat conduction, thus the object can be heated homogeneously.

The temperature inside the reactor was monitored and recorded with a temperature data logger HH309A (Omega, QC, Canada). Since the induction can cause interference between the readings, only one thermocouple was plugged in per data logger. The maximum temperature reached with this set-up was 730 °C. In order to keep the temperature of the reactor as close as possible to the temperature set point, the PID controller was set to start heating when the temperature was 3°C below the set point.

The vapor residence time was maintained < 2 seconds as indicated in numerous publications on fast pyrolysis [21,112,268] by regulating the nitrogen flow rate.

5.1.1.3 Condensation train for fast pyrolysis experiments

The condensation train comprised three condensers and a cotton filter. The bio-oil collection system is designed to condense vapors according to dew point temperatures [152]. The first two condensers (C_1 and C_2) were built with a 2-inch pipe and a single ½ inch pipe bent at 90° for the inlet vapors and a 50 cm ½ inch tube size for the outlet. The inlet temperature of the vapor coming from the reactor was controlled and maintained at 350°C. The first condenser was placed in a water bath with a cartridge heater and an air bubbler to keep the temperature constant and avoid hot spots. The first condenser was designed to catch the higher molecular weight components, in particular levoglucosan. The second condenser was placed in a water bath at 25°C. The last condenser size was 1-inch diameter and 60 cm long and it was placed in a water bath and kept in the freezer before each pyrolysis experiments. The last two condensers were designed to condense the lighter organic fraction of the bio-oil. At the end of the line a filter packed with fiberglass, was used to condense any remaining volatiles to allow for an accurate mass balance. The gases were collected in gas bags every 5 minutes and analyzed by a Varian Micro-GC.

5.1.1.4 Biochar collection system

The biochar inside the reactor was swept away into the trench and inside the char collection pot with the highest rpm allowed by the motor (Table C.1. Appendix C). This was done to prevent the catalytic cracking of the vapors to secondary char [21] since most of the AAEMs are retained in the biochar [133] and to maximize the production of levoglucosan.

5.1.1.5 Condensation train for slow pyrolysis experiments

The condensation train for the slow pyrolysis runs consisted of a single condenser (same size as the third condenser of the fast pyrolysis condensation train) placed in water and kept in the freezer until the start of the experiment. The main products of the slow pyrolysis experiments were the biochar and the water fraction bio-oil. The organic fraction of bio-oil deposited at the bottom of the condenser and was easily separated by

the water phase. At the end of the line a cotton filter was placed before the gas bag sampling system.

5.1.1.6   Mass balance

The condensers, cotton filter, connecting lines and the char pot were weighed before and after each experiment. After the fast pyrolysis experiments, a small amount (typically 2-4%) of the biochar remained in the reactor at the end of the run, therefore the reactor was opened daily to retrieve biochar and weighed for mass balance calculations. The char collected in the reactor was kept separated from the char collected from the pot for characterization purposes. If the biochar inside the reactor was more than 4%, than the run was discarded and repeated to keep the extraction rate as constant as possible for the set of experiments.

5.2   Fast pyrolysis for the production of bio-oil and biochar

5.2.1   Introduction

Fast pyrolysis is commonly used to maximize the liquid products, at temperatures in the range of 400-550°C and reaction time on the order of seconds [21]. Due to the complexity of the pyrolysis reactions, the effect of the process variables and feedstock properties on the product distribution should be considered as key parameters for the optimization of the chemicals of interest. Herbaceous biomasses have a higher mineral content compared to woody feedstocks, that is known to decrease the sugar yield by catalyzing secondary cracking reactions of the vapor phase [79,83,119]. When levoglucosan is the product of interest, the passivation of AAEM is required to ensure high sugar yields.

The main objective of the study described in this chapter was to determine the effect of the removal of AAEMs on the bio-oil composition, in particular levoglucosan, to gather a better understanding on the impact of the pre-treatments described in Chapter 2. The second objective was to evaluate the characteristics of biochars obtained from the

untreated and pre-treated *Phragmites australis* to gather more insight on the possible biochar applications.

5.2.2   Materials and methods

The biomass was pretreated with the methodology described in Chapter 2 Section 2.2.2.

5.2.3   Results and discussion

The biomass characteristics are reported in Tables 5.1 and 5.2. There are few studies that investigated the mineral distribution in the *Phragmites australis* organs. Ho studied the mineral composition through different months in the Scottish Lochs [269]. Leaves were observed to have higher ash content, N, Ca and Mg than the below ground organs. Roots and rhizomes had instead higher level of Na and Fe. Seasonal changes affected the mineral content in the stem for N, P, K and Ca, where high concentrations were found in spring and then decreased for the rest of the season. The leaves had a similar trend for N, P and K however the decrease was more gradual [269]. Silicon (Si) is another element found in plants [270]. The concentration can vary widely but in some cases there is an excess of 10% [271]. Silicon is usually found as SiO_2 called Silica [270]. Schaller et al. [272] studied the effect of different Si concentration supplied to the reed in pot experiments. They found that high Si supplies promoted the deposition in the epidermis of the leaves altering N and P ratios. They also noted how high Si supply decreased the plant growth. For this study all above ground parts of the reed were used for the pre-treatments and pyrolysis experiments. As pointed out by Vassilev et al. [273,274], since the moisture in plants contains mineral cations and ions during harvesting and drying, part of the moisture evaporates causing the minerals to precipitate in the form of phosphates, carbonates, sulfates, chlorides, and nitrates which have different level of solubility. The ash content decreased for all the pretreated biomass; increasing leaching temperature and time resulted in an increased ash removal, with the best result achieved when the biomass was treated with water at 90°C for 24 hours (29% removal). As a result, the volatiles increased slightly compared to the untreated biomass, this trend is also seen in other studies [110,275]. The pH of the biomass increased, with one exception (30°C 24h).

Table 5.1 – Proximate analysis, pH and HHV of untreated and pretreated biomass

Biomass pre-treatment	Proximate analysis (wt%)			Moisture (wt%)	HHV (MJ/kg, d.b.)
	Fixed C	Volatiles	Ash		
Untreated	11.32±0.64	79.3±0.47	5.68±0.17	4.25±0.07	18.03±0.24
30°C 1h H_2O	8.79±0.25	82.66±0.2	5.30±0.07	3.33±0.04	18.08±0.15
90°C 1h H_2O	8.89±0.54	83.4±0.59	4.61±0.17	3.10±0.38	18.48±0.11
30°C 24h H_2O	8.31±0.06	82.8±0.19	5.41±0.06	3.46±0.06	18.23±0.01
90°C 24h H_2O	7.95±0.49	84.6±0.26	4.04±0.06	3.05±0.1	18.63±0.12
30°C 24h ac. acid	8.89±0.13	82.7±0.27	5.46±0.32	2.96±0.1	18.22±0.13
90°C 24h ac. acid	7.98±0.22	83.9±0.25	4.88±0.07	3.20±0.05	18.19±0.09
Sox H_2O 48h	8.41±0.34	83.7±0.04	4.68±0.16	3.23±0.07	18.9±0.04

The washing treatment didn't have a noticeable effect on the C, H, O content, but it decreased the N and S content (Table 5.2). Similar results were found in other studies [276].

Table 5.2 – Ultimate analysis of untreated and pretreated biomass (Oxygen calculated by difference)

Biomass pre-treatment	Ultimate analysis wt%					pH H_2O
	C	H	O	N	S	
Untreated	47.2±0.51	5.56±0.04	41.21±0.63	0.23±0.06	0.09±0.02	4.52±0.02
30°C 1h H_2O	47.02±0.42	5.49±0.06	41.98±0.44	0.24±0.04	0.05±0.01	5.33±0.02
90°C 1h H_2O	47.59±0.97	5.57±0.07	42.12±1.04	0.11±0.01	0.01±0.01	5.54±0.07
30°C 24h H_2O	47.41±0.39	5.54±0.02	41.53±0.39	0.09±0.02	0.01±0.01	5.01±0.00
90°C 24h H_2O	47.41±0.22	5.63±0.09	42.87±0.50	0.04±0.01	0.00±0.01	5.32±0.03
30°C 24h ac. acid	46.13±0.43	5.39±0.06	42.82±0.50	0.20±0.02	0±0	4.37±0.06
90°C 24h ac. acid	47.74±0.21	5.57±0.03	41.79±0.20	0.02±0.01	0±0	4.89±0.10
Sox H_2O 48h	47.60±0.16	5.48±0.07	42.23±0.21	0.01±0.01	0.0±0.01	4.96±0.04

The quantification of inorganic species in biomass was performed by ICP-OES. The analysis has been carried out on some individual pre-treatment batches (Table C.2 and Table C.3 Appendix C) and the final mix (reported in Table 5.3). Amongst the elements, Ca had the highest variability. The pre-treatment performed at 30°C for 1 h in water had a 4% removal of Ca, however looking at the single batches repeated 3 times (Table C.2 Appendix C) the values for Ca ranged from 1059 to 2051 mg/kg, which indicate the variability of calcium in the samples considered. Variability confirmed also by the results obtained from the pre-treatment at 90°C 24h with water (Figure 5.4).
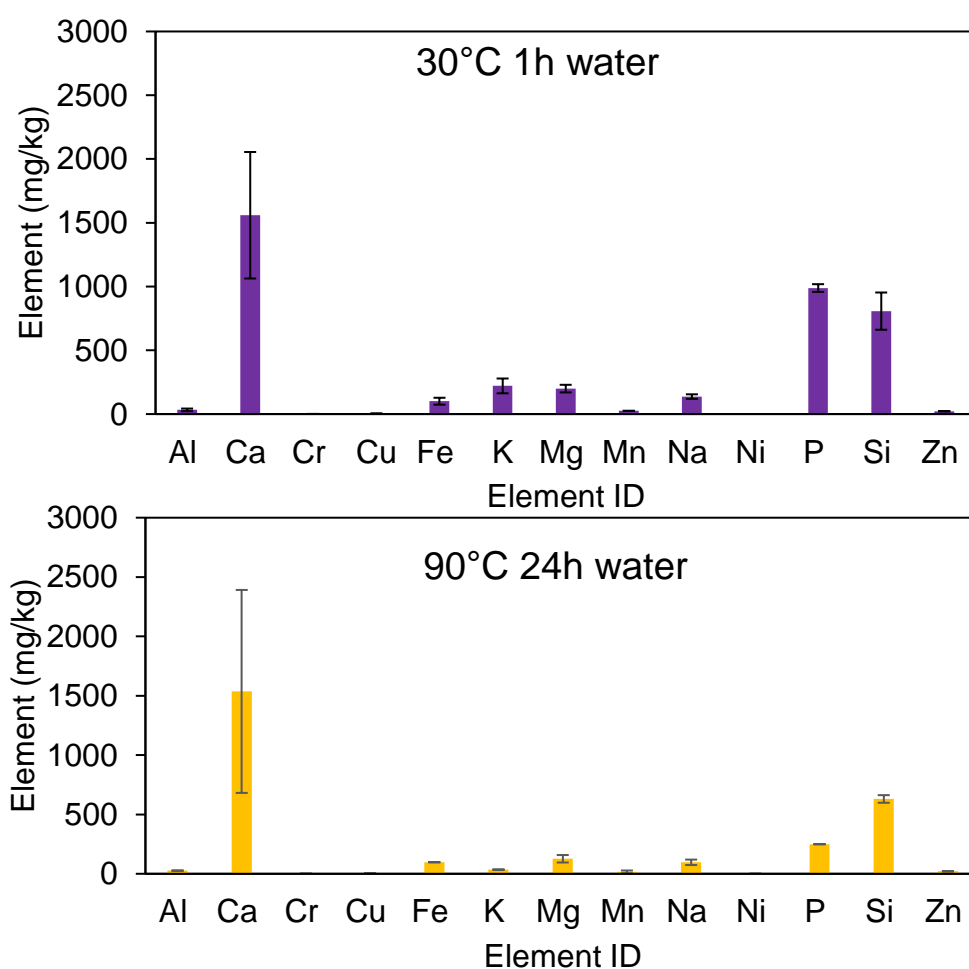
Figure 5.4 – Average values and standard deviations of individual pre-treatment batches (ICP-OES)

The biomass washed with water heated at 90°C had the lowest AAEMs content (Table 5.3), K was almost all removed. On the other hand, when the water was replaced by the acetic acid solution, the AAEMs removal reached above 90% efficiency. Regarding other elements in the biomass (Table C.2 Appendix C), Si was left unaffected by the washing, P had removal between 75% (30°C 1h in water) to 90% (90°C 24h in water).

Many researches in the field have attempted to decrease the AAEM content by pre-treating the biomass with water [36,45–47] or acid leaching [31,48–50]. Water leaching removes most of the Na and K, but Mg and Ca are still in high amounts because their carbonate salts dissolve only partially in water [123]. Fahmi et al. [51] washed Switchgrass and *Festuca arundinacea* with deionized water at 25°C for 2 hours. Results showed that K and Na were almost completely removed (>80% removal), whereas Mg and Ca removal were only between 12 and 30%. Liu and Bi [52] washed Switchgrass with deionized water at 20°C for 48 h, achieving similar removal for Na and K (above 80% removal), although they achieved a higher removal of Mg (74% removal). Pre-treatment of Banagrass [109] with mechanical dewatering and water leaching decreased the ash content by 45%. Results showed a decrease of all the elements such as, K (90%), Cl (98%), S (55%), Na (68%), P (72%) and Mg (68%). Si and Ca were the two most difficult elements to leach out, in fact these elements were either left unaffected by leaching or their concentration would increase. They suggested that probably these two elements are not quantitatively removed, due to their structural roles in the plants.

Table 5.3 – ICP-OES of the biomass (in bold the % removal)

| | **Raw** | **Water bath** | | | | **Acetic acid bath** | | **Sox 48 h** |
		30°C 1h	**30°C 24h**	**90°C 1h**	**90°C 24h**	**30°C 24h**	**90°C 24h**	
Ash %	5.68	5.26	5.42	4.61	4.04	5.46	4.9	4.684
		-7.4%	*-4.6%*	*-18.8%*	*-28.9%*	*-3.9%*	*-14%*	*-18%*
HHV (MJ/kg)	18.04	18.08	18.23	18.47	18.63	18.223	18.193	18.48
		+0.2%	*+1.1%*	*+2.3%*	*+3.3%*	*+1%*	*+0.9%*	*2%*
Na^+ (mg/kg)	537	149.00	122.00	118.00	126.00	128	92	68.9
		-72%	*-77%*	*-78%*	*-77%*	*-76%*	*-83%*	*-87%*

K$^+$	1803	220.00	99.80	97.20	33.60	9	8.6	17.4
		-88%	*-94%*	*-95%*	*-98%*	*-99%*	*-100%*	*-99%*
Mg^{2+}	447	247.00	167.00	138.00	119.00	9.4	19	185
		-45%	*-63%*	*-69%*	*-73%*	*-98%*	*-96%*	*-59%*
Ca^{2+}	2786	2679.00	1923.00	1215.00	1405.00	64	200	2175
		-4%	*-31%*	*-56%*	*-50%*	*-98%*	*-93%*	*-22%*
Sum AAEMs	5575	3295	2311.8	1568.2	1683.6	210.4	319.6	2446.3
		-41%	*-59%*	*-72%*	*-70%*	*-96%*	*-94%*	*-56%*

The water from different pre-treatments was collected (Figure 5.5), however it was not possible to analyze it for carbohydrate content. By looking at the water collected after the washing treatments, the Soxhlet seemed to be the most severe treatment compared to the other treatments. The pH of the leachates (Table 2.3) collected after the water treatment were around 5. Liaw and We [277] reported that some organic acids were leached from the biomass samples, thus producing an acidic leachate.
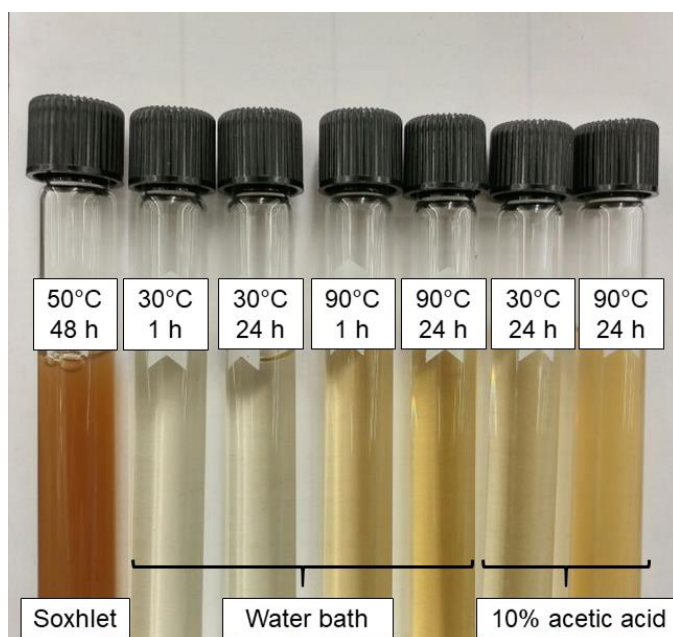
Figure 5.5 – Water collected from the pre-treatments

Another interesting characteristic already mentioned by Jenkins et al. [110] was the different colors of the ash of untreated and pre-treated biomass (Figure 5.6). They pre-treated rice straw with either flushing or soaking in distilled and tap water. The untreated ash contained dark and light particles and they suggested the possibility of carbon in the form of carbonates or iron compounds. Instead pre-treated rice straw resulted in a pure white ash.
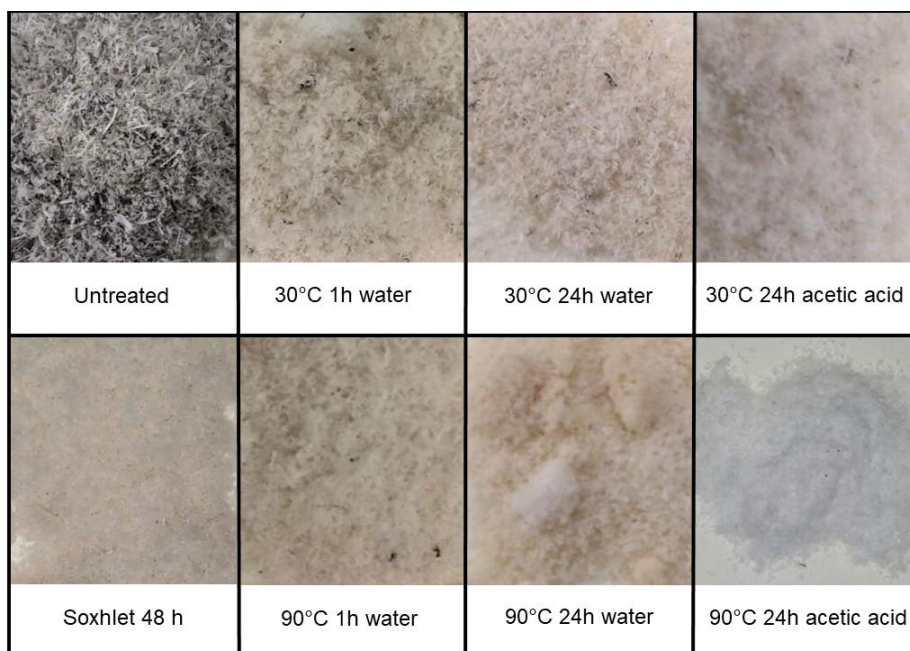
Figure 5.6 – Ash color untreated and pre-treated biomass

The effect of the demineralization pretreatment on the thermal degradation behavior of the biomass was investigated by TGA analysis (Figure 5.7). The DTG curves reported the characteristic shoulder (first peak) attributed to hemicellulose degradation and the second peak attributed to the degradation of cellulose [278]. It can be observed a shift at higher temperatures for both peaks, in particular the first peak shifted from 264°C for the untreated biomass to 324°C and 321°C for 90°C 24h H_2O and 90°C 24h acetic acid, respectively. This likely indicates that the thermal degradation of hemicellulose and cellulose happened at higher temperatures likely due to the reduction of the catalytic effect of AAEMs. This trend is seen in other studies involving the leaching of AAEMs [120,279], in which the char and AAEMs have the ability to decrease the degradation

temperatures of biomass and decrease the yields. The intensity of the peaks is also higher in both washed samples.
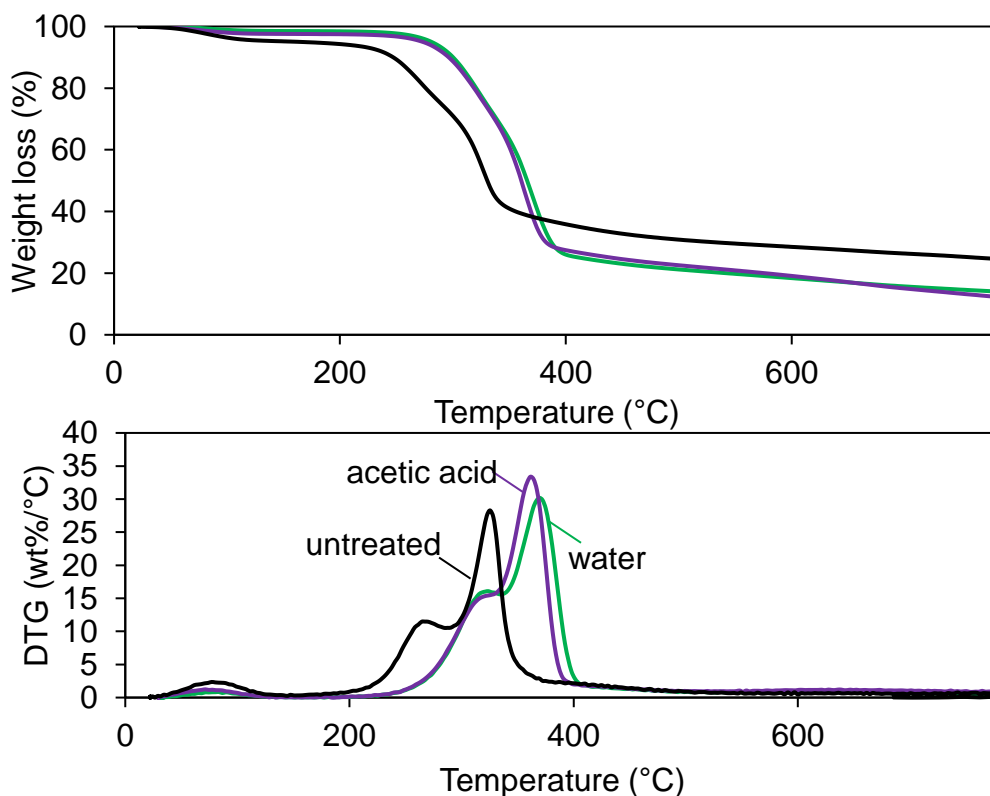
Figure 5.7 – TGA/DTG graph untreated and pretreated biomass(90°C 24h H$_2$O and 90°C 24h 10% acetic acid)

5.2.4　Product yields

5.2.4.1　Product yields untreated *Phragmites australis*

The yield of the products from the pyrolysis of untreated *Phragmites australis* is reported in Table 5.4. The total bio-oil yield increased from 450 to 500°C and decreased again at 550°C for both 40°C and 80°C (temperature of the first condenser C$_1$). It should be noted that when the pyrolysis temperature was increased to 550°C with C$_1$ = 80°C, the bio-oil collected in C$_1$ was completely solid and difficult to retrieved.

These results were compared with other studies on fast pyrolysis of grasses with similar ash content. Most of the studies considered for comparison utilized a fluidized bed reactor with 1 kg/h feed rate with various herbaceous feedstocks including Miscanthus, Straw, Reed canary grass, Switchgrass. Although a proper conclusion with results from different feedstock is difficult due to the variation in AAEM and ash content as well as the lignocellulose composition and reactor and condensers configuration it is still useful to compare the results to understand possible ways to improve yields and increase the content of some chemicals of interest such as levoglucosan.

Mos et al. [280] studied the fast pyrolysis of Miscanthus in a 1 kg/h continuous bubbling fluidized bed reactor at 525°C with a vapor residence time of 1.5 seconds. The bio-oil was quenched with a cooling column at a temperature of 25-30°C, followed by an ESP separator and a series of 1 water condenser and 2 dry ice condensers at -70°C. The ash content on a dry basis was 5.75% for the biomass harvested in September which was comparable to the ash content of the untreated *Phragmites australis* (5.7 wt% d.b.), and 7.36 wt% for the feedstock harvested in early June. Their results indicated that the bio-oil yield was 59.1 wt% d.b., 16.3 wt% of biochar and 15.1 wt% of gases for the biomass with the lowest ash content and 50.9 wt% bio-oil yield and 26.1 wt% biochar yield and 15.3 wt% of gases, which was more in line with the results of this study. Fahmi et al. [229] studied the fast pyrolysis of different feedstocks in a 150 g/h pyrolysis reactor at 500°C with a vapor residence time of 0.4-1.5 s. The condensation train consisted in a water condenser maintained at 30-40°C followed by an ESP were the first fraction of the oil was collected, then a dry ice condenser for the collection of the second fraction. Based on their feedstock analysis, straw (ash content 6.3%) and Reed canary grass (ash = 5.1%) were the biomass with the closest properties as the untreated *Phragmites australis*. Reed canary grass was the only one with the most similar amount of total alkali metals (K, Na, Mg, Ca) of 4911 ppm, however it had a slight less amount of K (1456 ppm vs 1803 ppm untreated Phragmites) and less amount of Na (74 vs. 537 ppm of untreated Phragmites and these two AAEMs were found to have the most impact in the bio-oil quality. They found that the total bio-oil yield was 60.2 mf wt%, with 22 % of biochar yield and 11.1% of gases. Straw, instead, had more similar yield to the one of this research study, with

50.5% of total liquid yield, 31.9 % of char and 15.6 % of gases. The water content in the bio-oil fraction of reed canary grass was 23.2 wt% and 47.4 wt% for the bio-oil produced from straw. The results from *Phragmites australis* oil produced with the reaction at 30 and 40 °C are similar to the straw bio-oil with 37 and 36 wt%, respectively.

Boateng et al. [281] studied the fast pyrolysis of Switchgrass in a 2.2 kg/h bench-scale fluidized bed reactor at 500°C with a impinger-type condensation unit comprising of 4 canisters in series in a water bath chilled with dry ice, followed by a ESP. The Switchgrass ash content 2.61 wt% dry basis. The bio-oil yield was 60.7 wt%, the biochar yield 12.9 wt% and non-condensable gases 11.3 wt%. They also reported the volatile content of the char remaining after the pyrolysis experiment which was 29.48 wt% dry basis, which is higher than the one produced at 500°C and collected in the char collector (24.3 wt%).

Table 5.4 – Product yields of untreated *Phragmites australis* (wt% d.b.). Gas yield was calculated by difference.

Reactor T (°C)	C_1 T (°C)	C_1 yield	C_2 yield	C_3 yield	Connecting lines + Cotton filter yield	Total Bio-oil yield	Biochar yield	Gas yield
450	40	20%	5%	11%	2%	37%	29%	34%
450	40	20%	7%	3%	5%	35%	31%	33%
500	40	31%	7%	5%	7%	49%	25%	26%
500	40	30%	10%	6%	4%	50%	26%	23%
550	40	26%	8%	3%	11%	47%	22%	31%
550	40	24%	7%	11%	3%	45%	23%	31%
450	80	15%	17%	8%	6%	45%	27%	27%
450	80	11%	14%	13%	3%	42%	31%	28%
500	80	9%	21%	7%	6%	43%	25%	32%
500	80	13%	15%	12%	5%	44%	26%	30%

550	80	7%	14%	5%	9%	36%	22%	42%
550	80	9%	16%	9%	3%	37%	23%	40%
500	60	18%	17%	12%	4%	51%	24%	25%
500	60	12%	16%	11%	10%	50%	26%	24%
500	30	21%	3%	10%	6%	40%	25%	35%
500	30	30%	4%	10%	0%	44%	24%	32%

To further investigate the influence of the reactor and condenser temperature on the bio-oil water content and relative higher heating value, all the bio-oil fractions were analyzed by Karl Fischer titration and the C_1 fractions by bomb calorimeter (Table 5.6). Typically, bio-oil water content ranges from 5-30 wt%, which is difficult to remove and can lead to phase separation above certain values. The HHV of bio-oil is usually below 26 MJ/kg (lower than 42–45 MJ/kg of conventional fuel oils) [282,283].

The moisture content of the bio-oil decreased with increasing condenser (C_1) temperature. When the condenser temperature was set at 40°C, the water content was stable at around 35% with HHV between 11 and 17 MJ/kg. Increasing the C_1 temperature to 80°C further decrease the moisture to 8% at 450°C and 0% above 500°C.

Table 5.5 – Water content (%) and HHV (MJ/kg) of the untreated bio-oil fractions

Reactor temperature (°C)	Condenser temperature (°C)		Water content (%)	HHV (MJ/kg)
	C_1	40	34.66±2.05	17.42±1.19
450	C_2	25	43.00±2.76	
	C_3	0	59.14±1.97	
	C_1	40	35.52±0.43	15.02±1.40
500	C_2	25	42.67±6.46	
	C_3	0	73.35±5.36	
	C_1	40	34.59±3.78	10.90±0.22
550	C_2	25	72.60±2.69	
	C_3	0	69.84±9.25	
	C_1	80	8.37±4.18	23.69±1.23
450	C_2	25	49.02±0.91	
	C_3	0	60.41±1.49	

500	C_1	80	0.57±0.29	24.04±0.20
	C_2	25	56.88±1.19	
	C_3	0	59.52±6.00	
550	C_1	80	0.00±0.00	N/A
	C_2	25	52.14±1.67	
	C_3	0	72.34±0.06	
500	C_1	30	37.13±0.20	12.59±0.98
	C_2	25	48.99±2.76	
	C_3	0	22.16±3.35	
500	C_1	60	12.73±1.93	19.93±0.74
	C_2	25	36.76±0.14	
	C_3	0	39.23±2.20	

5.2.4.2   Product yields of pre-treated biomass

According to the results obtained by HPLC analysis, the highest levoglucosan content in the first condenser (C_1) was achieved when the reactor temperature was 500°C and the first condenser at 60°C (Figure 5.8 and Figure 5.11). The data consisted of two independent variables (reactor and condenser (C_1) temperature) and one dependent variable (the total levoglucosan yield (sum of the yields in C_1, C_2, C_3)). To have a better visualization of the levoglucosan yield, a surface was fitted to the data adopting a quadratic polynomial model (poly22), using the Curve Fitting Toolbox implemented in MATLAB R2019b (Figure 5.8). The Toolbox provides the SSE (Sum of squares due to error), R-Square (R^2), the Adjusted R-square (R_{adj}^2) to evaluate the fit of the model. The results of the model are reported in Appendix C.
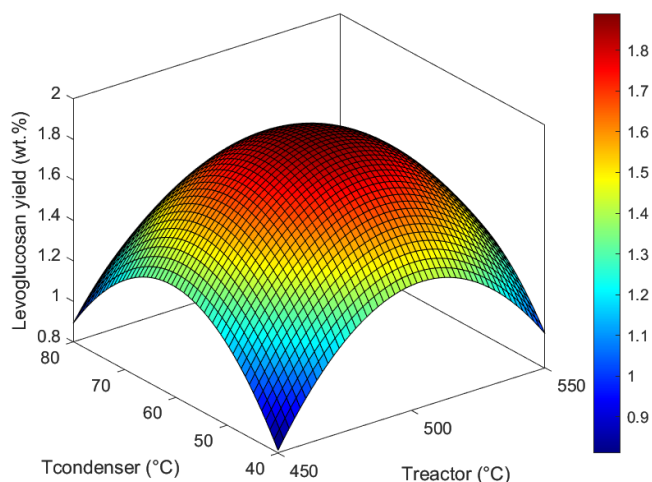
Figure 5.8 – Curve fitting of total levoglucosan yield (wt%)

Therefore 500°C and 60°C were chosen as optimal operating conditions for the levoglucosan production.

Compared to the experiments performed at the same operating conditions with the untreated biomass, the total bio-oil yield of the pre-treated biomass increased from 50% to 57-58%, the only exceptions were the biomass pretreated with 90°C 24 h - acetic acid and the Soxhlet extractor, in those cases the bio-oil yield achieved was lower at 55% and 51% respectively. The biochar decreased from 24-26% to 18-21%.
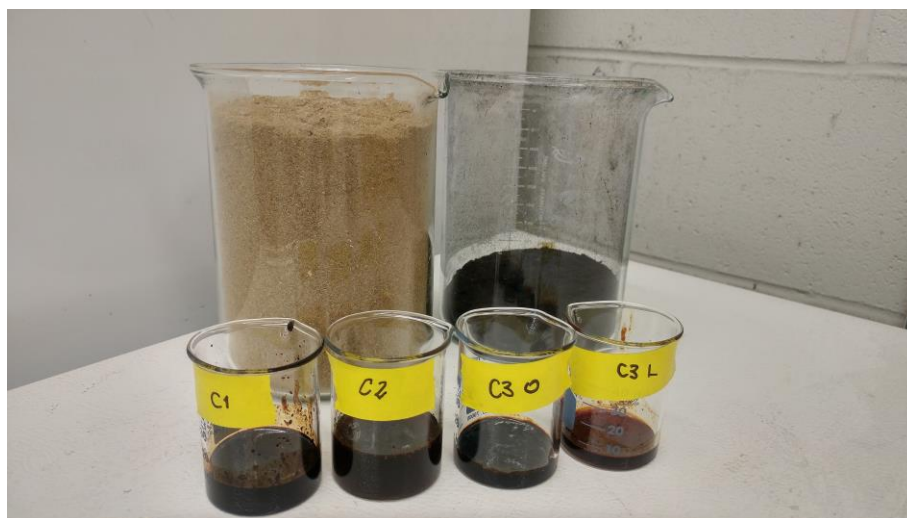
Figure 5.9 – Biomass and pyrolysis products of the run at 500°C, C_1=60°C

Table 5.6 – Product yields (wt% d.b.) of pretreated *Phragmites australis* (pyrolysis conditions $T_{reactor}$=500°C, T_{C1}=60°C); Gas yield calculated by difference.

Pre-treatment	C_1 yield	C_2 yield	C_3 yield	Connecting lines + Cotton filter yield	Total bio-oil yield	Biochar yield	Gas yield
30°C 1h H_2O	23%	15%	11%	8%	57%	21%	22%
90°C 1h H_2O	20%	15%	13%	10%	58%	20%	22%
90°C 24h H_2O	20%	12%	17%	9%	58%	21%	21%
30°C 24h H_2O	19%	12%	15%	13%	58%	18%	24%
30°C 24h ac. acid	19%	10%	19%	8%	57%	18%	25%
90°C 24h ac. acid	25%	13%	9%	8%	55%	22%	24%
Soxhlet H_2O 48h	25%	10%	14%	3%	51%	18%	30%

5.2.5 Bio-oil characteristics

All the bio-oil fractions were analyzed by HPLC. The levoglucosan yield was reported in in % g/g of initial biomass d.b. (Figure 5.10 and Figure 5.11) and g/L_{oil} and Figure 5.11). The levoglucosan yield had a maximum at 500°C when the temperature of the first condenser was 40°C. When the temperature of the first condenser was raised to 80°C, a drop of the levoglucosan of almost half in the first condenser and a subsequent increase in the second and third condenser (Figure 5.10) can be observed.
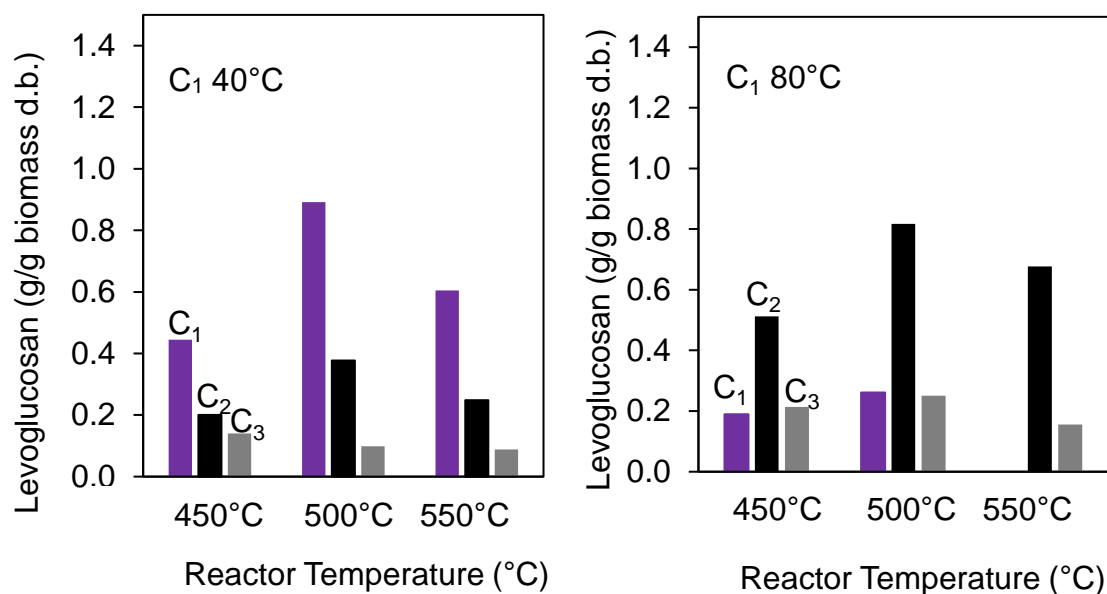
Figure 5.10 – Levoglucosan wt% untreated *Phragmites australis*

Overall the highest levoglucosan yield was obtained at 500°C, therefore for the next set of experiments, the reactor temperature was kept constant at 500°C and the temperature of the first condenser was varied from 30°C and 80°C (Figure 5.11 c), d)). The levoglucosan content in the first condenser varied slightly from 30 to 60°C and increased in the second condenser with the increased C_1 temperature. Then, the levoglucosan concentration (g/L) for all the experiments at 500°C (Figure 5.11) was evaluated.
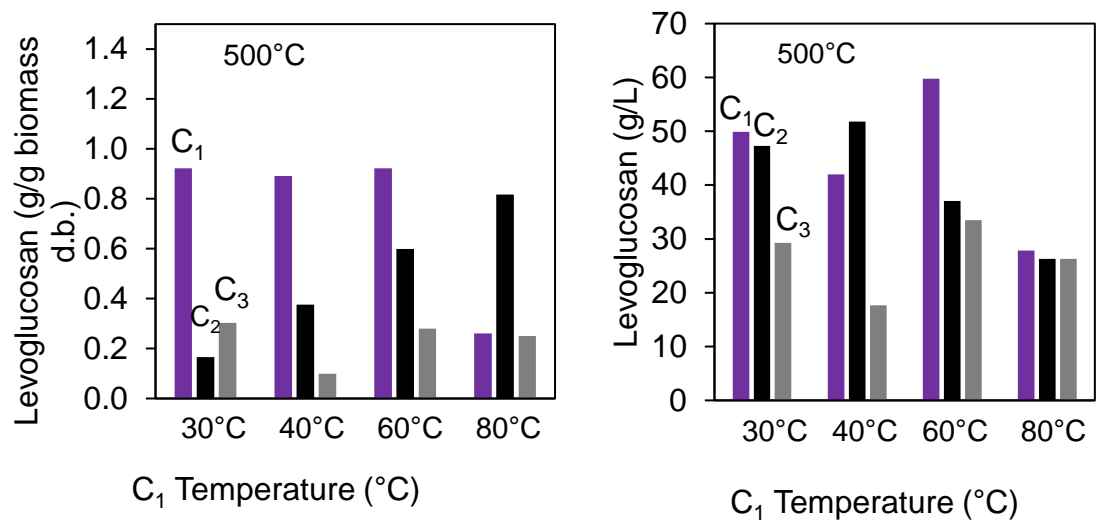
Figure 5.11 – Levoglucosan wt% and g/L in bio-oil fractions produced during pyrolysis at 500°C
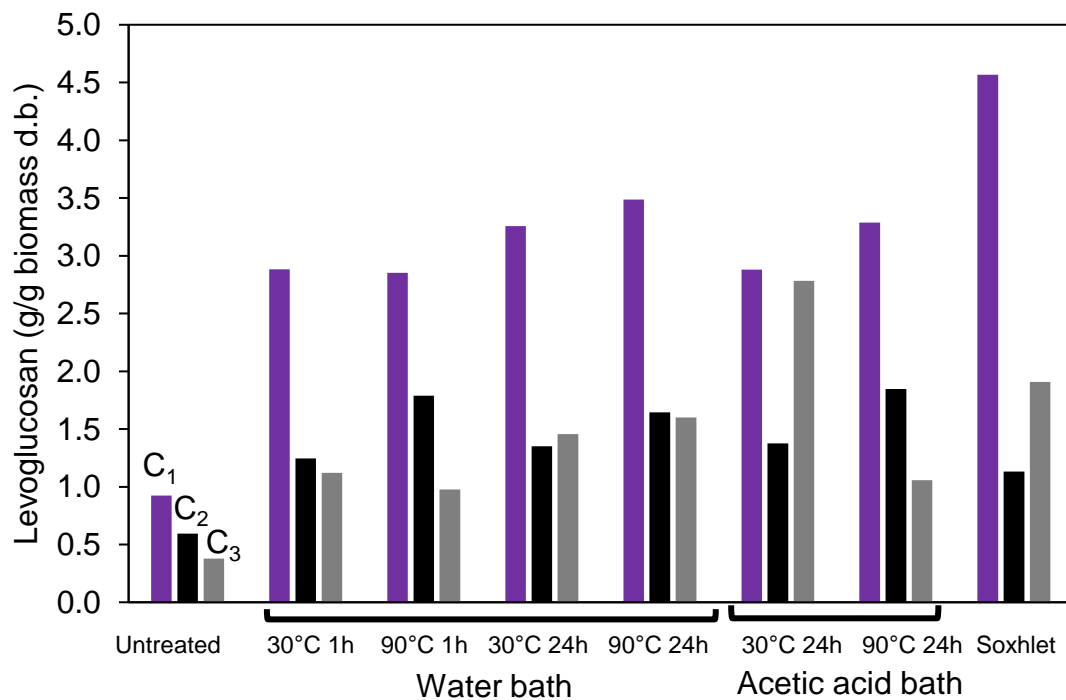
Figure 5.12 – Levoglucosan yield wt% on initial biomass basis
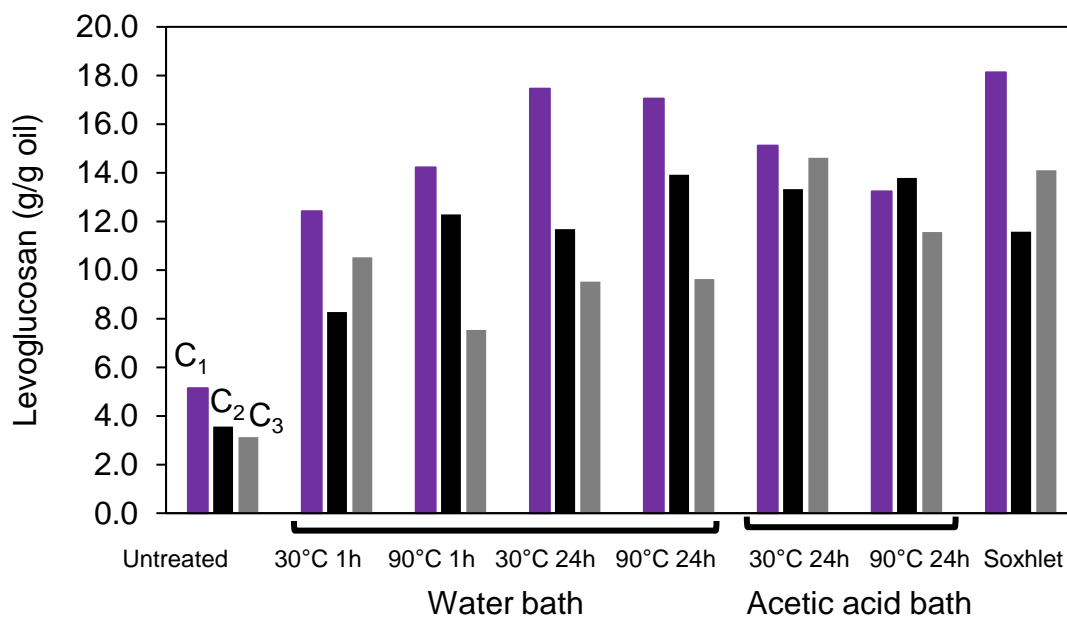
Figure 5.13 – Levoglucosan yield wt% in oil fraction

The levoglucosan content increased for all pretreatments (Figure 5.12, 5.13).

Patwardhan et al. [111] investigated the catalytic effects of inorganic salts on the primary cellulose pyrolysis reactions observing that the cations had the following trend relative to the decrease in levoglucosan yield such as, $K^+ > Na^+ > Ca^{2+} > Mg^{2+}$. A similar trend was observed in this work (Figure 5.14), with K and Na having the highest influence on the total levoglucosan yield. Mg didn't seem to affect the levoglucosan yield.
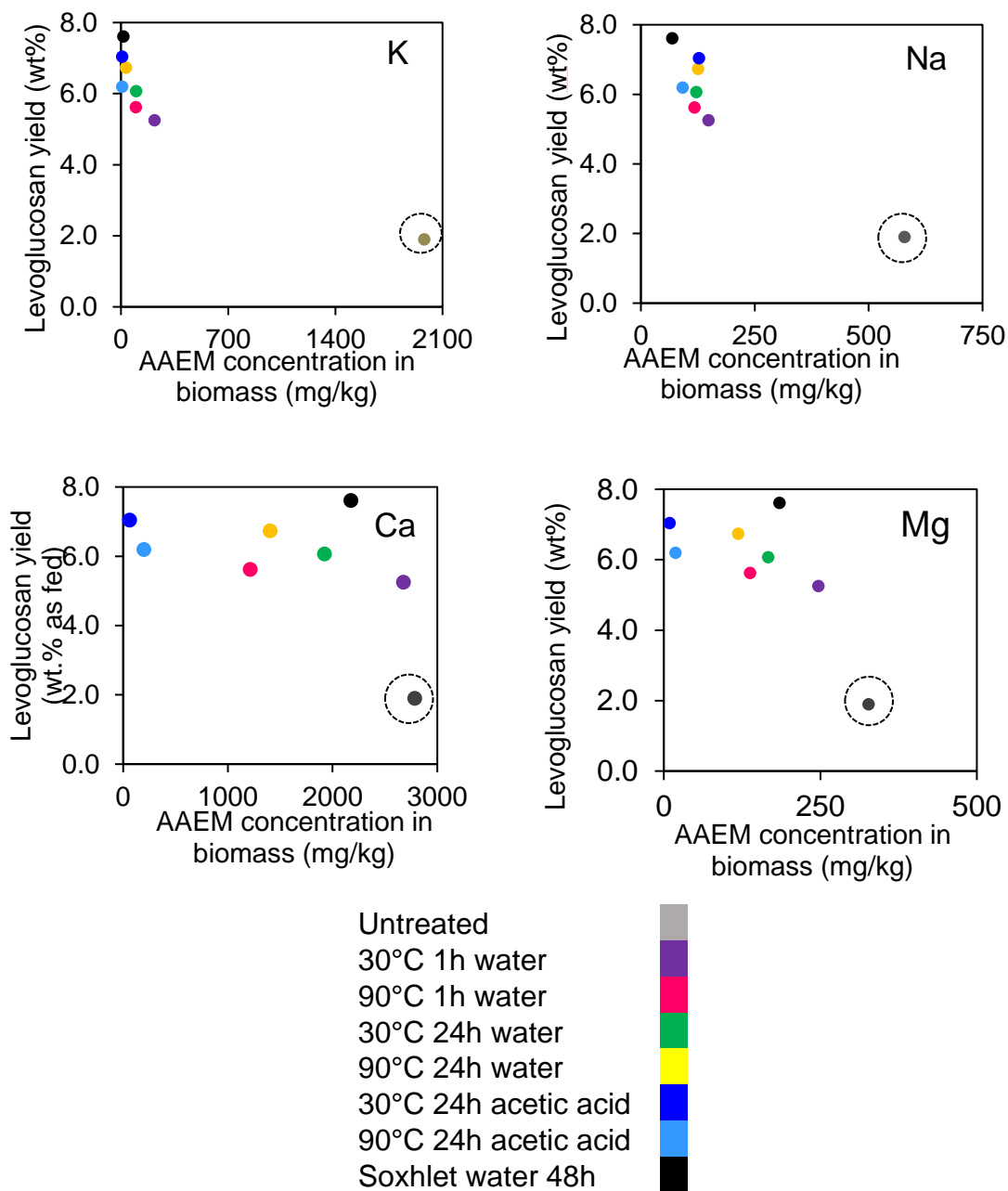
Figure 5.14 – Total levoglucosan yield (=sum of the yield in the three bio-oil fractions) as a function of the inorganic components in the biomass. The values with a dotted circle are the untreated biomass

The second chemical of interest was acetic acid; however, the objective wasn't to maximize it but instead gather a better understanding of its distribution in the different fractions. Increasing C_1 temperature changed the fractionation of acetic acid (Figure 5.15). At $C_1=40°C$, the highest yield was recorded in the first condenser, while increasing C_1 to 80°C decreased the yield from 1 wt% to 0.45 wt% at 450°C and from 1.65 wt% to 0.6 wt% at 500°C. It was observed that increasing the reactor temperature to 500°C increased the acetic acid yield to a maximum, and then, the yield decreased again when the reactor temperature was raised to 550°C. Another detail worth noting, is that when the first condenser was at 80°C, the yield of acetic acid doubled in the second condenser, from 0.51 wt% to 1.17 wt% at 450°C, 0.61 wt% to 1.65 wt% at 500°C and 0.47 wt% to 1.05 wt% at 550°C. A similar trend was seen for the third condenser. This could be further improved by studying different combinations of reactor/condenser temperatures to collect the most acetic acid in only one fraction.
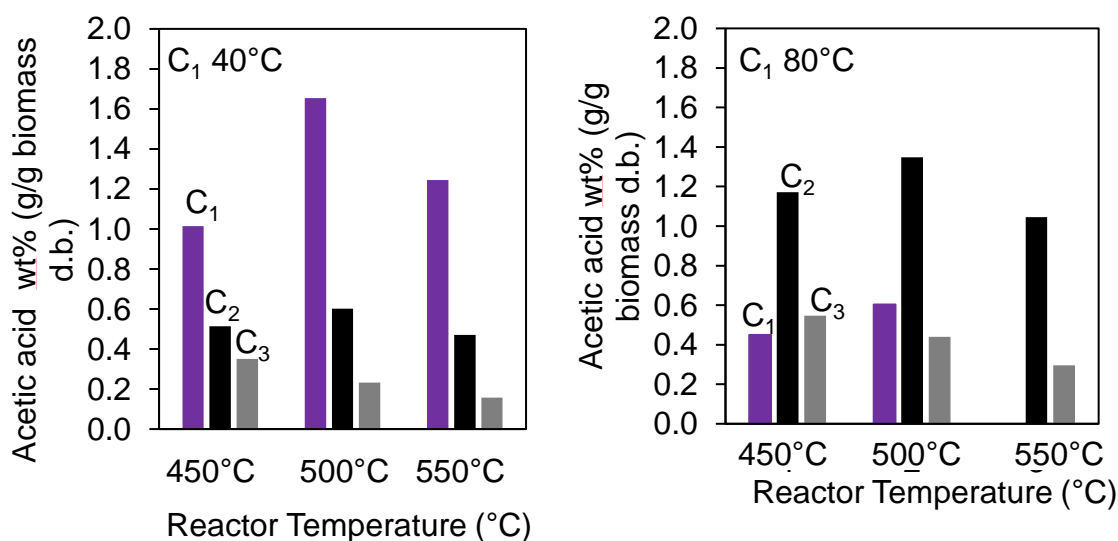
Figure 5.15 – Effect of reactor temperature and C1 temperature on the acetic acid yield

The effect of C_1 temperature on the acetic acid yield and concentration can be seen in Figure 5.16 a) and b). As was inferred before (Figure 5.16 a) and b)), the acetic acid yield decreased in the bio-oil collected in C_1 when the temperature of C_1 was increased above

40°C, while it increased steadily in C_2. However, the concentration of acetic acid in the oil fractions reached its maximum when the condenser temperature was 60°C. This is particularly important for the extraction of acetic acid.
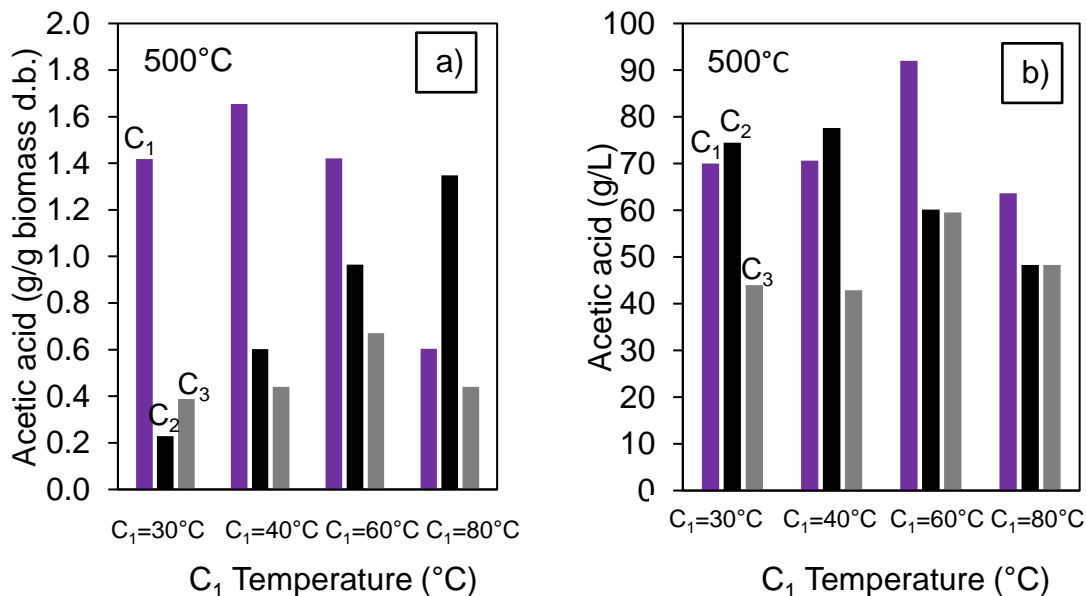
Figure 5.16 – Effect of C_1 temperature on the acetic acid yield and concentration.

The effect of the different pre-treatments on the acetic acid can be seen in Figure 5.17. For comparison purposes, the scale of the graphs was kept the same as levoglucosan. When the biomass was washed with water at 30°C for 1 hour, the acetic acid yield remained unchanged, a slightly decrease was noted in the first condenser when the pretreatment temperature was raised to 90°C. Instead, when the washing time was increased to 24 hours, the acetic acid yield decreased from 1.42 wt% (untreated) to 0.60 wt% (30°C 24h) and 0.77 wt% (90°C 24h). Washing the biomass with acetic acid, decreased the acetic acid yield from 1.42 to 0.67 wt% (30°C 24h), however when the pretreatment temperature was increased to 90°C, the acetic acid yield increased slightly compared to the untreated biomass to 1.47 wt%. The treatment performed with the

Soxhlet extractor increased the yield to 1.73 wt% in C_1. Only minor changes where observed in C_2 and C_3 from the untreated biomass.
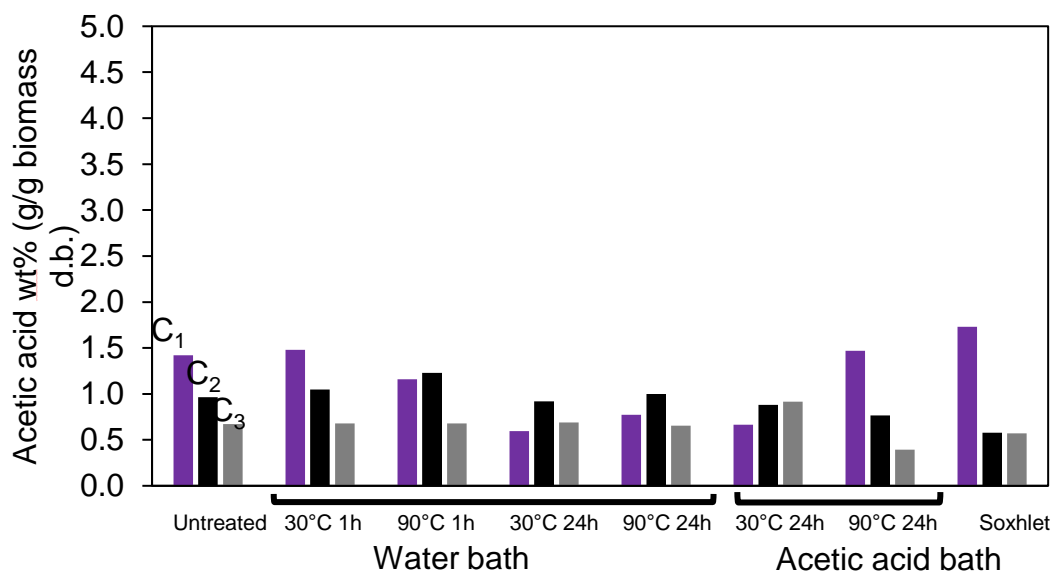
Figure 5.17 – Effect of pretreatment on the acetic acid yield on biomass basis

The acetic acid yield on oil basis when the biomass was washed with water for 1 hour slightly decreased the yield in C_1 from 7.9 wt% (untreated) to 6.4 and 5.77 wt% for 30°C and 90°C, respectively. The yield slightly increased in C_2 from 5.79 wt% (untreated) to 6.97 and 8.44 wt% for 30°C and 90°C, respectively. When the washing time was 24 hours, the yield increased to 7.95 wt% for 30°C and 8.5 wt% for 90°C. The acetic acid yield was the same whether the biomass was treated with water at 30°C and 24 h or acetic acid at the same conditions. However, when the biomass was treated at 90°C and 24 hours with acetic acid and with the Soxhlet extractor, only a minor difference was noted compared to the untreated biomass.

Furthermore, to understand the impact of the pretreatment on the GC detectable compounds all the bio-oil fractions were analyzed by GC-MS. As mentioned before the GC-MS relative area only gives an indication of the relative content of the compound

within the fraction (Figure 5.19). It can be observed that the most abundant component were carboxylic acids followed by carbohydrates, phenols and furans.

The detail list of all the chemicals detected with the GC-MS is provided in Table C.6 and Table C.7 Appendix C. It can be noted that the relative content of carboxylic acids (only acetic acid) decreases and the content of carbohydrate in the same fraction increases.
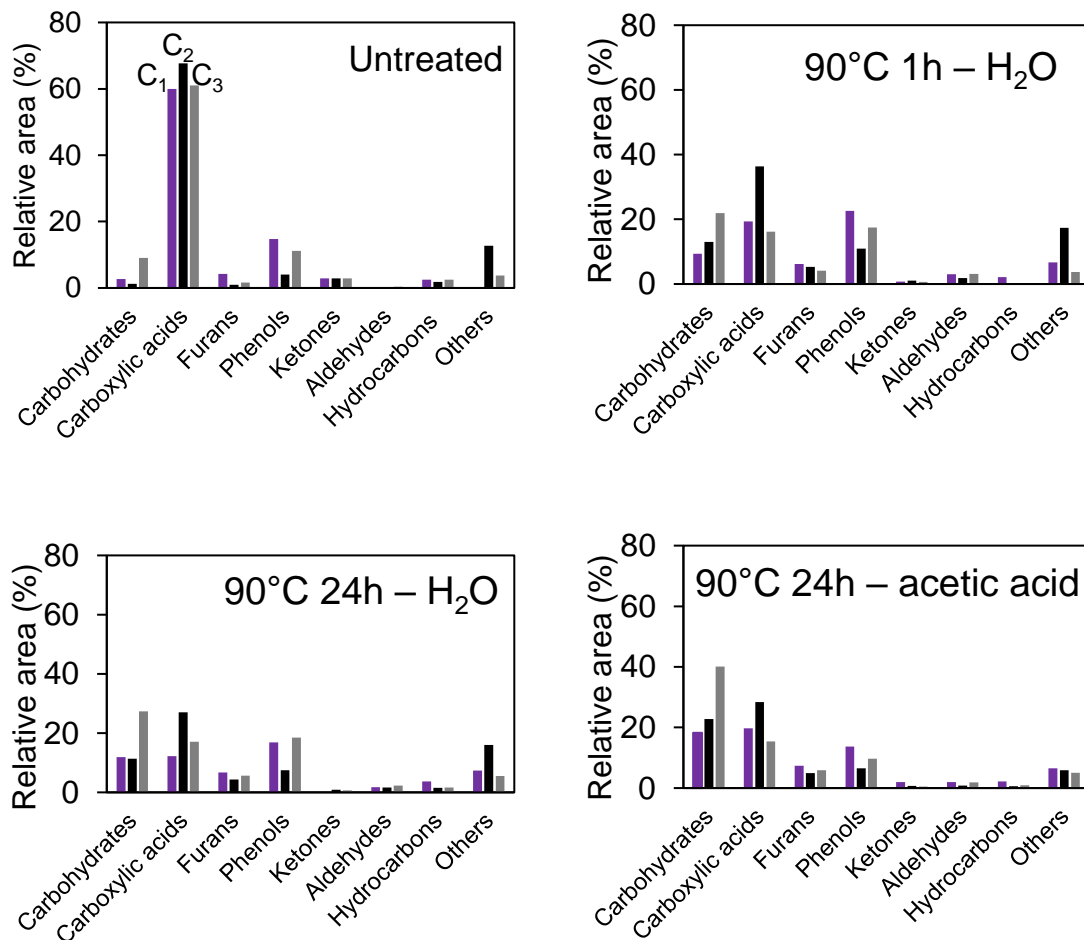
Figure 5.18 – GC-MS of the untreated bio-oil fractions and pretreated at 90°C

Then, to study whether the pre-treatment influenced the water content, HHV and elemental content of the bio-oil fractions produced at 500°C, the first condenser was kept at 60°C. The bio-oil obtained from the untreated biomass had the highest water content at 13%. All the pre-treatments showed to decrease the moisture below 10%, in particular

when the biomass was washed with water and acetic acid for 24 hours at 30 and 90°C the water content decreased to 5%. It is well documented that higher ash content would promote dehydration reactions, resulting in a bio-oil with lower organic content and higher water content [115,284]. The ultimate analysis was performed on the untreated bio-oil samples and the pre-treated samples (Table 5.8). Overall, the carbon content of the bio-oils obtained with the pre-treated biomass increased for all the fractions. It was noted that the oil collected from the ice bath from the untreated biomass was less viscous than the oil sample collected after pyrolyzing the pre-treated feedstock. This was also confirmed by the water content of the C_3 fraction of the oil that decreased from 40% to 20% after the pre-treatment. Hydrogen, nitrogen and Sulphur had only minor differences compared to the untreated one.

Table 5.7 – Water content (%) and HHV of the bio-oils produced at 500°C from untreated and pretreated biomass (C_1=60°C, C_2=25°C, C_3=0°C)

Pre-treatment	Condenser	Water content (%)	HHV (MJ/kg)
Untreated	C_1	12.73±1.93	19.93
	C_2	36.76±0.14	
	C_3	39.23±2.20	
30°C 1h H_2O	C_1	9.33±0.26	20.60
	C_2	47.19±0.40	
	C_3	23.26±0.18	
90°C 1h H_2O	C_1	8.71±0.08	19.33
	C_2	41.57±0.16	
	C_3	30.45±0.21	
30°C 24h H_2O	C_1	5.14±0.01	20.80
	C_2	33.74±0.33	
	C_3	22.46±0.95	
90°C 24h H_2O	C_1	5.68±0.12	19.63
	C_2	35.78±1.10	
	C_3	20.12±0.12	
30°C 24h ac. acid	C_1	4.74±0.27	19.97
	C_2	35.89±1.17	
	C_3	18.14±0.96	
90°C 24h ac. acid	C_1	7.81±0.20	19.26
	C_2	30.85±5.07	
	C_3	22.17±1.22	

	C_1	6.52±2.07	19.55
Soxhlet	C_2	33.39±4.53	
	C_3	15.97±2.13	

Table 5.8 – Ultimate analysis of the bio-oils produced at 500°C from untreated and pretreated biomass (C_1=60°C, C_2=25°C, C_3=0°C). Oxygen calculated by difference.

Pre-treatment	Condenser	Ultimate analysis (wt%)				
		C	**H**	**O**	**N**	**S**
Untreated	C_1	34.51±0.24	7.76±0.29	56.37±0.07	1.36±0.05	0.00±0.00
	C_2	12.76±0.16	7.18±0.13	79.60±0.15	0.46±0.07	0.00±0.00
	C_3	19.44±0.10	8.02±0.16	71.82±0.07	0.72±0.07	0.00±0.00
30°C 1h H_2O	C_1	50.87±0.03	6.97±0.09	40.70±0.42	1.46±0.30	0.00±0.00
	C_2	26.39±0.27	7.93±0.06	64.70±0.28	0.98±0.07	0.00±0.00
	C_3	42.75±0.22	7.52±0.26	48.64±0.75	1.09±0.30	0.00±0.00
90°C 1h H_2O	C_1	47.35±0.45	6.49±0.08	45.62±0.60	0.54±0.07	0.00±0.00
	C_2	28.67±0.40	7.46±0.13	63.32±0.72	0.55±0.23	0.00±0.00
	C_3	41.91±1.91	7.92±0.30	48.34±1.95	1.84±0.04	0.00±0.00
30°C 24h H_2O	C_1	50.60±1.06	6.64±0.10	41.48±1.32	1.15±0.17	0.13±0.03
	C_2	28.54±0.66	6.94±0.49	63.81±0.66	0.53±0.10	0.19±0.04
	C_3	42.11±0.94	7.26±0.27	49.16±1.22	1.33±0.16	0.15±0.04
90°C 24h H_2O	C_1	48.89±2.14	6.52±0.25	43.58±2.30	1.02±0.09	0.00±0.00
	C_2	31.16±0.66	6.80±0.14	61.70±0.54	0.35±0.09	0.00±0.00
	C_3	43.47±0.82	6.80±0.24	49.222±1.05	0.51±0.01	0.00±0.00
30°C 24h ac. acid	C_1	50.04±0.12	5.88±0.05	43.23±0.23	0.85±0.06	0.00±0.00
	C_2	27.90±0.79	6.30±0.41	65.48±0.40	0.32±0.04	0.00±0.00
	C_3	43.38±0.57	7.00±0.27	48.21±0.68	1.37±0.16	0.03±0.05
90°C 24h ac. acid	C_1	46.97±0.53	6.08±0.26	46.09±0.85	0.85±0.08	0.00±0.00
	C_2	37.15±0.44	6.85±0.34	54.67±0.49	1.33±0.20	0.00±0.00
	C_3	42.74±0.53	6.58±0.26	49.17±0.77	1.50±0.11	0.00±0.00
Soxhlet	C_1	46.51±0.50	6.15±0.28	46.84±0.83	0.50±0.06	0.00±0.00
	C_2	32.35±0.36	6.94±0.23	60.46±0.55	0.25±0.06	0.00±0.00
	C_3	44.30±0.90	6.54±0.15	48.20±1.14	0.97±0.17	0.00±0.00

5.2.6 Biomass and biochar characteristics

The proximate and ultimate analysis of the biomass and biochars obtained after the pyrolysis experiments were investigated (Table 5.9). The characteristics of the biochar retrieved in the collector (considered as the real product) with the biochar that was left in the reactor were also discussed. If we compared the results from the char samples

collected in the char collector, increasing the reactor temperature from 450°C to 550°C slightly increased the fixed carbon, the volatile content decreased from 27.9 wt% at 450°C to 19.3 wt% at 550°C, and the ash content increased from 20.2 wt% to 27.7 wt% at 550°C. Increasing the temperature also increased the pH, which became more alkaline, and increased the HHV from 22 MJ/kg at 450°C to 23 MJ/kg at 550°C. The char that was left in the reactor after the pyrolysis experiments had differences from the biochar extracted only in terms of fixed carbon and volatiles. The ultimate analysis of the samples showed that increasing the temperature increased the carbon content and decreased the oxygen and hydrogen.

Table 5.9 – Proximate and ultimate analysis of the biochar from untreated biomass (Oxygen calculated by difference)

	char 450 (collector)	char 450 (reactor)	char 500 (collector)	char 500 (reactor)	char 550 (collector)	char 550 (reactor)
Proximate analysis (wt%)						
Fixed C	48.20±0.80	51.00±1.06	47.17±0.80	51.80±1.27	50.28±0.19	58.10±0.86
Volatiles	27.91±0.29	21.02±0.39	24.34±0.23	19.10±0.79	19.33±0.31	13.4±0.31
Ash	20.21±0.22	22.97±0.88	23.90±0.69	25.77±0.52	27.73±0.35	26.09±0.59
Moisture (%)	3.65±0.12	4.43±0.21	4.41±0.048	3.87±0.21	2.77±0.15	2.20±0.11
pH (H$_2$O)	8.57±0.03	10.73±0.11	9.67±0.01	10.26±0.00	10.12±0.01	10.61±0.02
HHV (MJ/kg)	22.0	22.7	22.6	22.5	23.0	24.5
Ultimate analysis (wt%)						
C	57.34±0.51	60.89±0.99	57.92±1.13	59.25±0.70	55.46±1.58	57.64±0.61
H	3.44±0.11	2.67±0.04	2.71±0.11	2.46±0.18	2.26±0.05	2.22±0.02
O	16.77±0.50	11.23±0.96	13.17±1.00	10.19±0.81	12.17±1.55	11.56±0.58
N	1.78±0.08	1.74±0.03	1.58±0.08	1.58±0.15	1.56±0.06	1.66±0.03
S	0.45±0.05	0.49±0.04	0.71±0.03	0.76±0.03	0.81±0.04	0.84±0.02
H/C	0.7	0.5	0.6	0.5	0.5	0.5
O/C	0.4	0.3	0.3	0.3	0.3	0.3

The FTIR spectra of the biochar produced at 550 °C and retrieved in the collector was compared to the spectra of the biochar produced at 550°C under slow pyrolysis condition,

with 1 L/min N_2 flow rate and 60 minutes holding time (Figure 5.19). The two spectra were similar, with difference manly due to the intensity of the peaks. The band between 1800-1650 cm^{-1} was assigned to the C=O stretching vibration in carbonyl groups (hemicelluloses) and was more pronounced in the slow pyrolysis char than the fast char. The band at 1650-1500 cm^{-1} was assigned to C=C stretching vibration in aromatic rings and was more intense in the fast pyrolysis char. Then, the peak at 1367 cm^{-1} due to the C–O stretching vibrations in carboxylate groups was broader in the fast pyrolysis char and almost not detected in the slow pyrolysis sample. The broad and intense peak at 1033 cm^{-1} was assigned to the C–O stretching vibration in alcohols, phenols, ether or ester groups recorded in both samples, however the intensity was higher in the fast pyrolysis sample. The C–H out-of-plane bending in benzene derivative vibrations were assigned to the band at 875 cm^{-1}. For the chars the intensities of aromatic C=C rings and aromatic C–H out-of-plane bending vibrations become stronger, indicating increased aromatization compared to the raw feedstock.
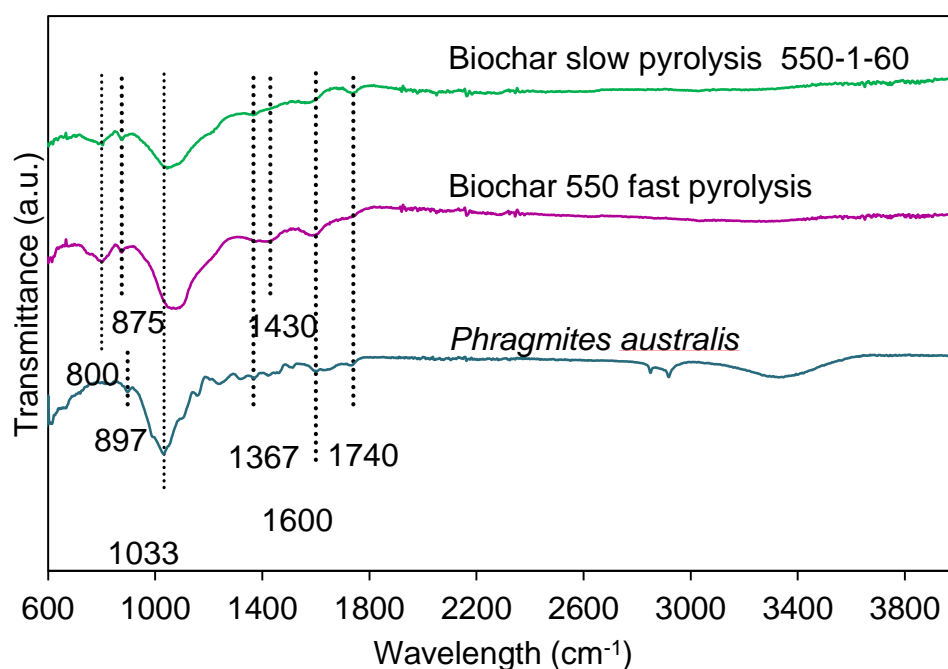
Figure 5.19 – FTIR spectra of the feedstock and biochar produced at 500°C with slow and fast pyrolysis

The characteristics of the biochars produced from the pre-treated biomass were compared to the char obtained from the char collector from the pyrolysis of the untreated biomass (Table 5.10).

The ash content increased compared to the biochar from untreated biomass for the samples washed at 30°C with water and decreased for the samples washed at 90°C and for the Soxhlet. The biochar samples from the acetic acid washing increased the ash content slightly at 90°C.

An important difference relative to the pH was observed. All the biochars exhibited a neutral pH compared to the untreated one, with only the sample washed with acetic acid at 90°C and 24 hours being on the acidic side. The biochar from untreated biomass had a pH of 9.7; as stated in previous chapters, from the literature the alkalinity is credited to the carbonates ($CaCO_3$ and $MgCO_3$) and AAEMs (such as K, Na, Ca and Mg).

The ultimate analysis showed only minor differences between samples.

Table 5.10 – Proximate and ultimate analysis of the biochars obtained from the pyrolysis of untreated and pre-treated biomass (Oxygen calculated by difference)

| | Untreated | Water bath | | | | Acetic acid | | Soxhlet |
		30°C 1h	90°C 1h	30°C 24h	90°C 24h	30°C 24h	90°C 24h	
Proximate analysis (wt%)								
Fixed C	47.17± 0.80	55.91± 0.03	59.51± 0.03	47.66± 0.64	44.71± 0.75	55.91± 0.28	55.79± 0.40	58.81± 0.50
Volatile	24.34± 0.23	16.96± 0.12	18.76± 0.20	21.04± 0.55	20.71 ±0.23	15.70± 0.41	17.50± 0.50	17.61± 0.42
Ash	23.90± 0.69	25.93± 0.02	20.21± 0.18	29.21± 0.46	21.55± 0.71	27.00± 0.29	24.79± 0.52	21.80± 0.33
Moisture (%)	4.41± 0.04	1.18± 0.06	1.54± 0.03	2.07± 0.20	1.86± 0.27	1.38± 0.11	1.91± 0.33	1.78± 0.02
pH (H₂O)	9.7	7.7	7.5	6.7	6.0	6.6	4.5	6.8
HHV (MJ/kg)	22.6	23.80± 0.10	25.07± 0.34	21.93± 0.40	22.56± 0.30	22.50± 0.33	23.51± 0.26	24.26± 0.30

Ultimate analysis (wt%)							
C	57.92± 1.13	62.46± 3.82	60.82± 1.03	57.58± 2.26	59.15± 0.97	62.77± 2.31	64.00± 1.18	66.95± 1.61
H	2.71± 0.11	2.43± 0.21	2.53± 0.11	2.37± 0.04	2.17± 0.38	2.53± 0.09	2.64± 0.02	2.62± 0.15
O	13.17± 1.00	8.18± 4.69	15.23± 1.24	9.74± 2.25	15.81± 1.08	6.63± 2.39	7.64± 1.16	7.63± 1.15
N	1.58± 0.08	0.99± 0.07	1.21± 0.14	1.10± 0.03	1.30± 0.03	1.07± 0.11	0.93± 0.08	0.91± 0.02
S	0.71± 0.03	0.00± 0.00	0.00± 0.00	0.00± 0.00	0.00± 0.00	0.00± 0.00	0.00± 0.00	0.00± 0.01
H/C	0.6	0.5	0.5	0.5	0.4	0.5	0.5	0.5
O/C	0.3	0.2	0.4	0.3	0.4	0.2	0.2	0.2

The X-ray diffraction patters of the biochar of the untreated and pre-treated biomass (90°C 24 h water, 90°C 24 acetic acid and Soxhlet extractor (Figure 5.20), showed the intensity of the diffracted beam as a function of the Bragg angle (2θ). There are two major drawback to consider when using the XRD technique: it only detects concentrations higher than 1% and the diffraction patterns of the compounds and the amorphous carbon usually cause a high background scattering (23°) [285,286]. The biochar from untreated biomass had multiple sharp peaks, which indicated the presence of inorganic matter [227]. A common peak in all biochars was observed at 26.5°, most likely due to quartz (SiO_2), which was the only peak observed in the biochar produced with biomass pre-treated at 90°C 24h with acetic acid. The peak at 29.4° was the second peak detected in the biochar from the sample washed with 90°C 24h, in the untreated sample, and in the Soxhlet which was assigned to calcite ($CaCO_3$). The presence of calcium in the relative biomass samples was also confirmed by ICP. In fact, it was noted that the Soxhlet had the highest calcium content. The only biochar sample without the calcite peak was the one washed with acetic acid, which was the only treatment that lowered consistently the calcium in the biomass (Table 5.3). The intensity of this peak was particularly high in the biochar from Soxhlet. A peak at 30.8° was observed in the Soxhlet and it was assigned to dolomite ($CaMg(CO_3)_2$) [287,288].
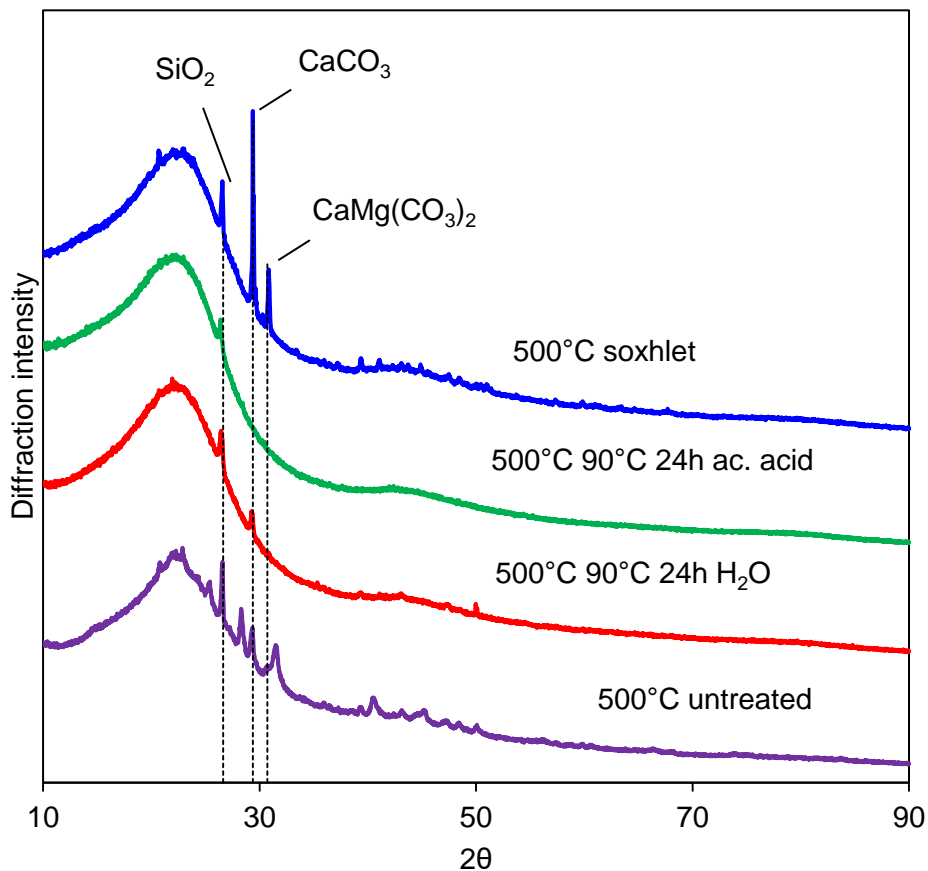
Figure 5.20 – X-ray diffraction patters of the biochar from untreated and pre-treated biomass

The morphology structure of the biomass pre-treated at 90°C 24h with water, 90°C 24 h with acetic acid and with the Soxhlet and the relative biochars was investigated by SEM-EDX analysis (Figures 5.22-5.27). Some porosity can be observed in the biomass sample washed at 90°C 24h with water.

An important observation could be done with the Soxhlet biomass sample. The EDX detected high Si concentration, which are not uncommon in herbaceous feedstocks.

The surface area (BET) was evaluated for biochars produced at 500°C and 550°C from untreated Phragmites. The surface area at 500°C was below 2 m^2/g, and increasing the temperature to 550°C increased the surface area to 102 m^2/g. The pore size distribution

(Figure 5.21) is different between the two biochars, with total pore volume considerably higher for the sample pre-treated at 550°C, however the average pore size diameter is similar. The BET surface area was evaluated for the biochar samples from feedstock that underwent 90°C 24h water, 90°C 24h acetic acid and Soxhlet treatment. Compared to the untreated biochar there is an increase of surface area for all the samples between 12 to 17 m^2/g and an increased total pore volume. The average pore size diameter was higher (6.83 nm) for the acetic acid treatment and lower (4.78 nm) for the Soxhlet extractor.

Table 5.11 – BET surface area, total pore volume and pore size diameter of biochars from untreated and treated feedstocks

Sample I.D.	BET surface area (m^2/g)	Total pore volume (cm^3/g)	Average pore size diameter (nm)
500°C biochar untreated	1.835	0.0027	5.87
550°C biochar untreated	102.295	0.1480	5.79
500°C 90°C24h water	13.096	0.0183	5.59
500°C 90°C24h acetic acid	17.408	0.0297	6.83
500°C Soxhlet extractor	12.410	0.0148	4.78
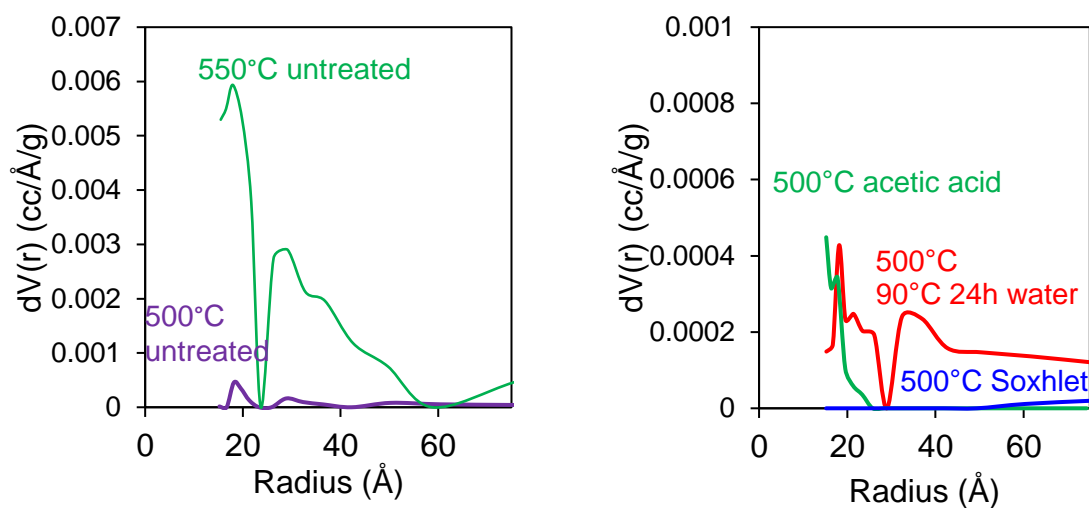
Figure 5.21 – Pore size distribution of biochars
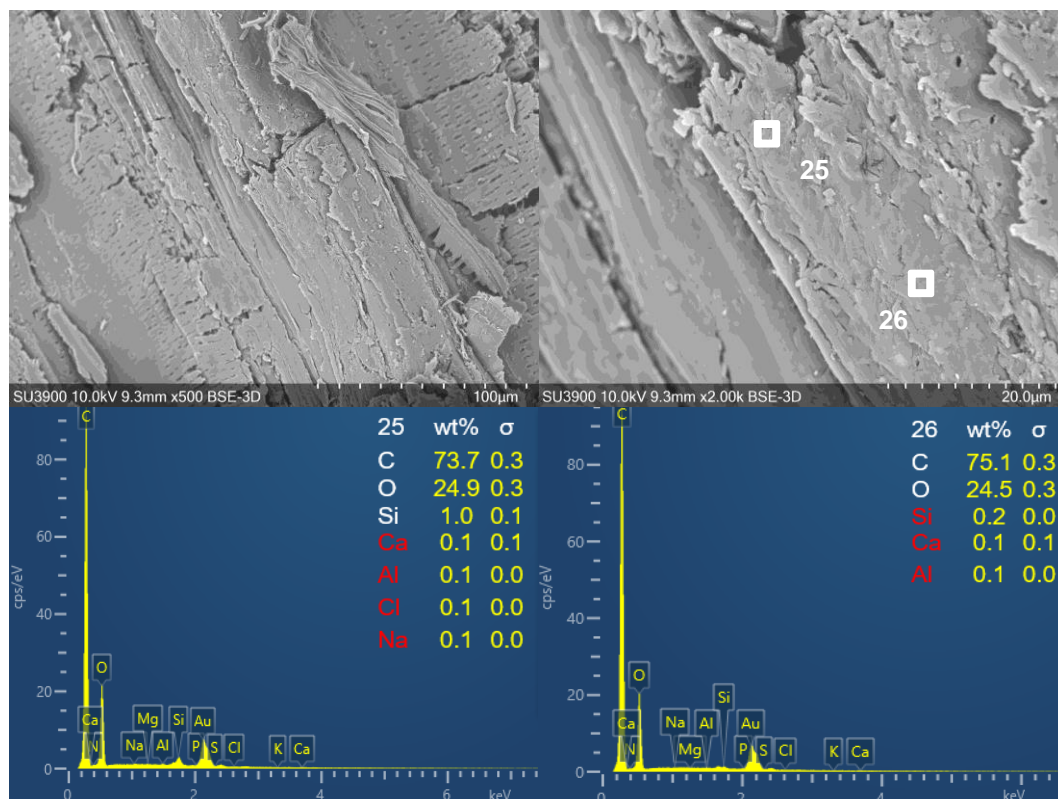
Figure 5.22 – SEM-EDX of 90°C 24h water washed biomass
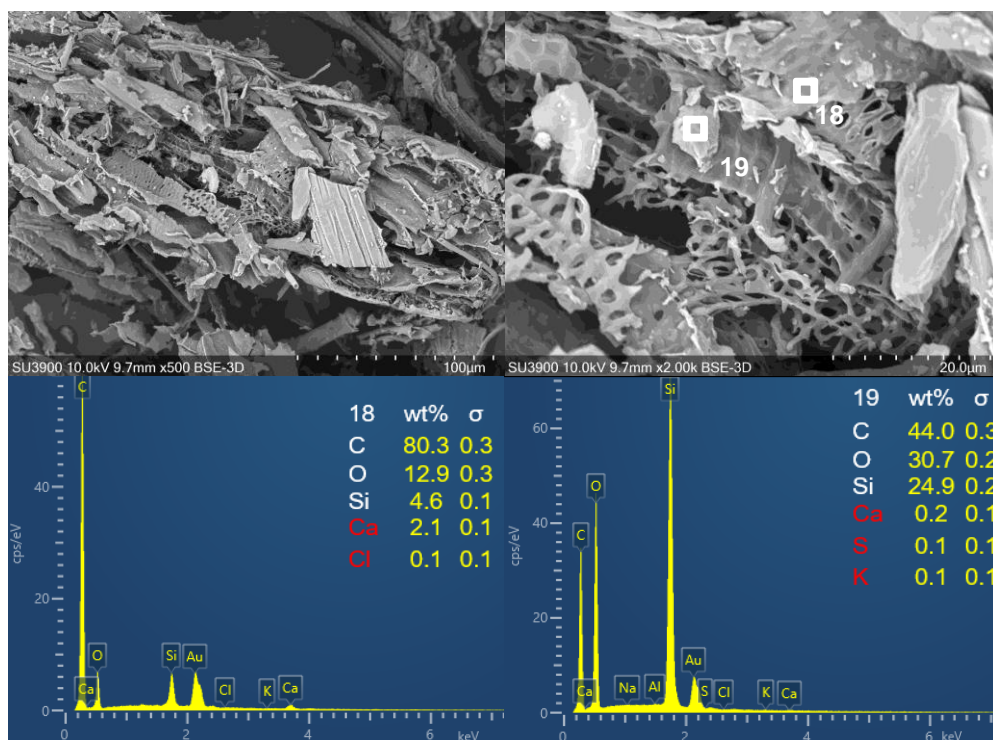
Figure 5.23 – SEM-EDX of 90°C 24h H₂O biochar
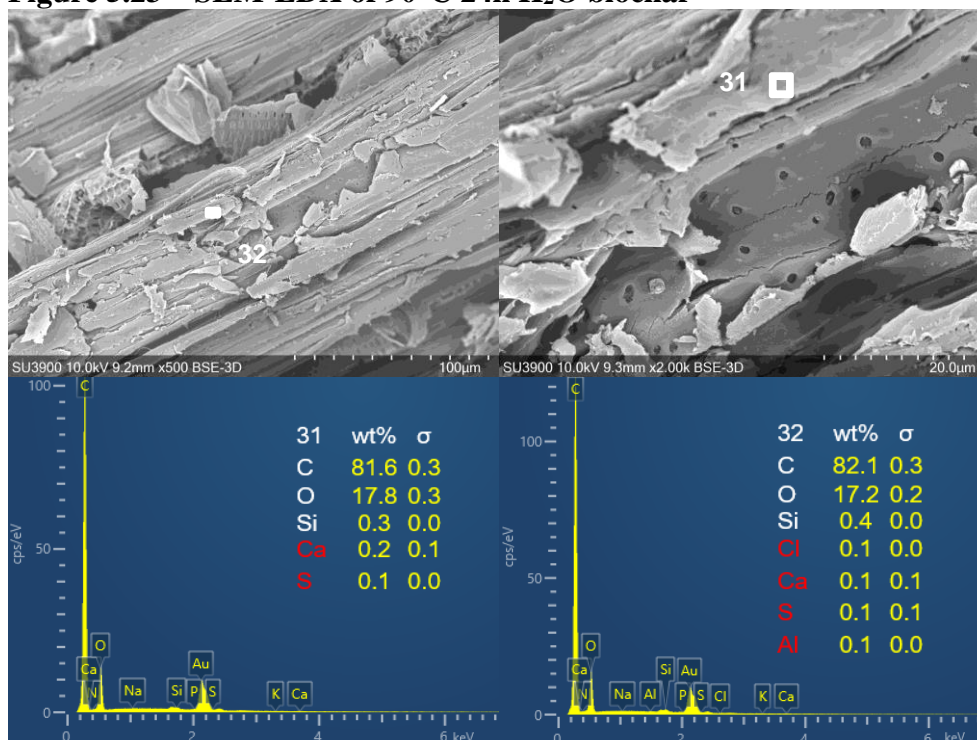
Figure 5.24 – SEM-EDX of biomass 90°C 24h with acetic acid
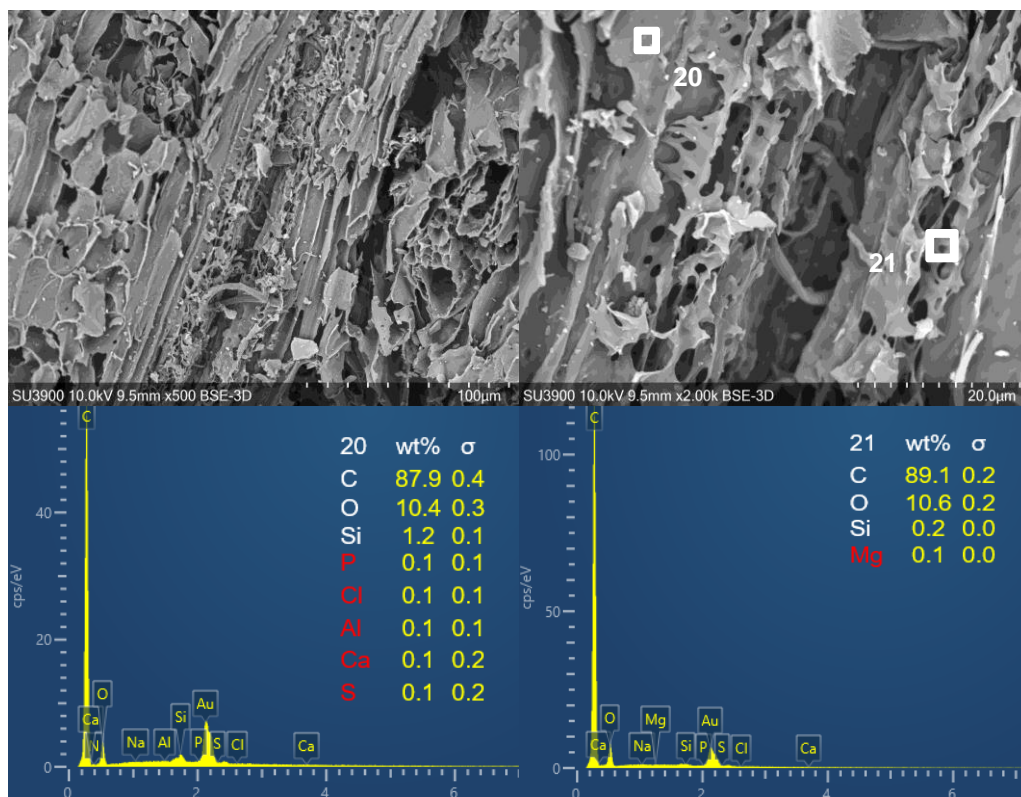
Figure 5.25 – SEM of biochar 90°C 24h with acetic acid
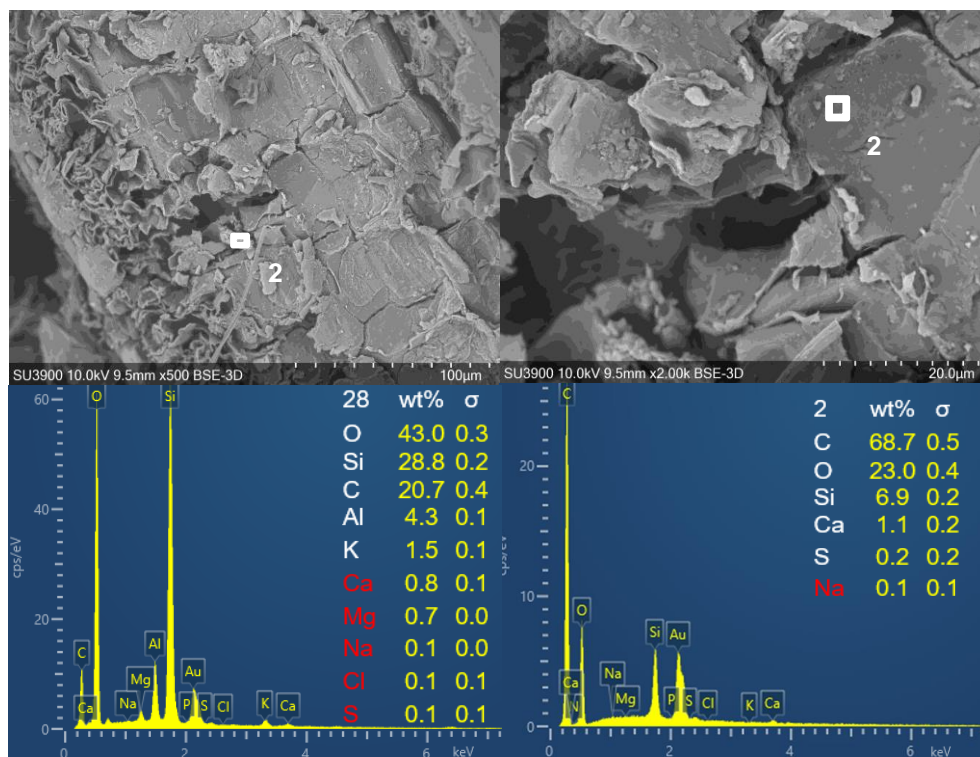
Figure 5.26 – SEM-EDX of biomass treated with Soxhlet
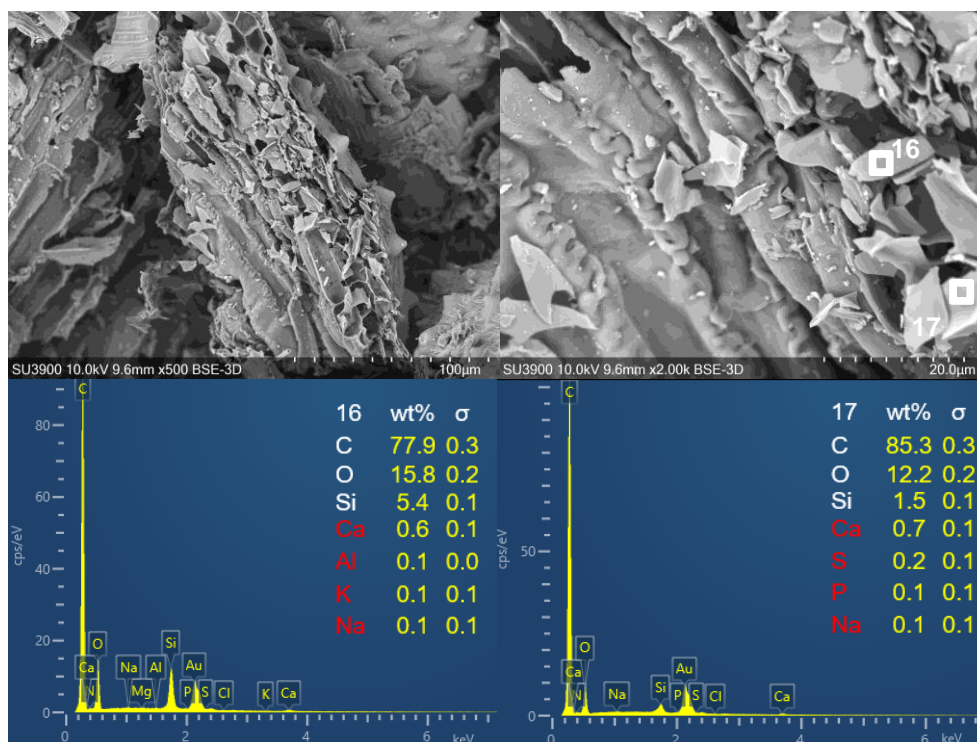
Figure 5.27 – SEM-EDX biochar from Soxhlet

5.2.7   Gas characterization

The gases produced in the pyrolysis experiments were collected two times during each run with gas bags and analyzed by Micro-GC analysis. The effect of the first condenser temperature on the gas yield can be observed in Table 5.12. CO_2, C_3H_8 and C_4H_{10} were detected at each reactor and condenser temperature. CO was detected at 4 wt% in the sample pyrolyzed at 550°C when C_1 was kept at 80°C and C_2H_6 at 550°C for both condenser temperatures.

Table 5.12 – Gas composition. Yields (wt%) are reported as g_{gas} $g^{-1}_{biomass}$

	450°C	**500°C**	**550°C**
C_1=40°C			
H_2	0.01±0.00	0.02±0.00	0.05±0.01
CH_4	0.00±0.00	0.00±0.00	0.00±0.00
CO	0.00±0.00	0.00±0.00	0.00±0.00
CO_2	19.84±3.14	14.75±0.57	17.06±2.82
C_2H_4	0.00±0.00	0.00±0.00	0.00±0.00

C_2H_6	0.00±0.00	0.00±0.00	4.85±0.77
C_3H_6	0.00±0.00	0.00±0.00	0.00±0.00
C_3H_8	11.42±0.40	5.75±0.73	5.01±0.97
C_4H_{10}	2.74±2.74	2.89±0.16	4.35±1.08
$C_1=80°C$			
H_2	0.00±0.00	0.02±0.00	0.04±0.01
CH_4	0.00±0.00	0.00±0.00	0.00±0.00
CO	0.00±0.00	0.00±0.00	4.47±4.47
CO_2	17.11±1.44	15.67±0.18	15.33±0.93
C_2H_4	0.00±0.00	0.00±0.00	0.72±0.04
C_2H_6	0.00±0.00	0.00±0.01	3.73±0.62
C_3H_6	0.00±0.00	0.00±0.00	0.00±0.00
C_3H_8	7.04±1.14	9.93±0.92	9.62±4.98
C_4H_{10}	3.35±0.17	4.83±0.74	6.28±1.15

A similar trend was observed when C_1 was maintained at 60°C with the reactor temperature at 500°C (Table 5.13). All gas samples from the pyrolysis of pre-treated biomass showed an increase in CO_2 yield from 6% to 9-16%.

Table 5.13 – Gas composition. Yields (wt%) are reported as g_{gas} $g^{-1}_{biomass}$

	Untreated	Water				Acetic acid		Soxhlet
		30°C 1h	90°C 1h	30°C 24h	90°C 24h	30°C 24h	90°C 24h	
H_2	0.00± 0.00	0.03± 0.01	0.18± 0.16	0.07± 0.00	0.01± 0.00	0.00± 0.00	0.00± 0.00	0.01± 0.00
CH_4	0.00± 0.00	0.00± 0.00	0.00± 0.00	0.00± 0.00	0.00± 0.00	0.00± 0.00	0.00± 0.00	0.00± 0.00
CO	0.00± 0.00	0.00± 0.00	0.00± 0.00	0.00± 0.00	0.00± 0.00	0.00± 0.00	0.00± 0.00	0.00± 0.00
CO_2	6.01± 1.35	9.17± 0.00	8.59± 0.26	9.95± 0.16	10.12± 0.80	9.46± 0.95	9.39± 0.53	15.55± 0.17
C_2H_4	0.00± 0.00	0.60± 0.02	0.54± 0.05	0.72± 0.01	0.62± 0.00	0.74± 0.04	0.71± 0.04	0.87± 0.04
C_2H_6	12.96± 3.29	3.68± 0.05	3.43± 0.41	2.66± 0.20	2.71± 0.44	3.72± 0.30	4.48± 0.40	4.01± 0.19

C_3H_6	0.00± 0.00	0.00± 0.00	0.00± 0.00	0.00± 0.00	0.00± 0.00	0.00± 0.00	0.00± 0.00	0.00± 0.00
C_3H_8	4.02± 1.27	4.94± 0.08	4.50± 0.12	5.15± 0.42	3.67± 0.16	5.86± 0.38	4.95± 0.39	4.01± 0.01
C_4H_{10}	2.39± 0.66	3.62± 0.13	4.43± 0.68	5.75± 0.06	4.28± 0.19	5.23± 0.90	4.00± 0.27	5.99± 0.04

5.3   Conclusions

Preprocessing the biomass with water and acid washing decreased the AAEMs content, K was reduced below 100 mg/kg for all the treatments with the exception of 30°C 1h. Na decreased by 75-88% in all treatments. Mg and Ca were the AAEMs more difficult to remove with water, in particular only around 60% of Mg was removed when the water was kept at 90°C and only 25-50% removal was achieved when the temperature was kept at 30°C for 1h and 24, respectively. However, when the biomass was washed with acetic acid at either temperature the removal was above 90%. Ca was only removed with acetic acid.

The impact of the pyrolysis conditions on the bio-oil yield were studied by varying reactor and C_1 temperatures. The total bio-oil yield was the highest (49-51%) at 500°C and C_1 40 and 60°C. Increasing C_1 temperature decreased the yield in C_1 and increased the yield in C_2 from 3-4% at 30°C ($T_{reactor}$=500°C), 7-10% at 40°C ($T_{reactor}$=500°C), 16-17% at 60°C ($T_{reactor}$=500°C) and 15-21% at 80°C ($T_{reactor}$=500°C). Only minor differences were observed in C_3.

The biochar yield decreased from 30% at 450°C to 23% at 550°C.

After inorganic leaching the oil yield increased from 50% to 57-58%, the only exceptions were the biomass pretreated with acetic acid at 90°C 24 h and with the Soxhlet extractor, in those cases the bio-oil yield achieved was lower at 55% and 51% respectively. The biochar decreased from 24-26% to 18-21%. The levoglucosan yield increased from 0.92 wt% to above 2.9 wt% when the AAEMs were leached out. In particular, washing with

water at either 30°C or 90°C for 1 hour led to a levoglucosan yield of 2.9 wt%, washing for 24 hour the biomass increased the levoglucosan content to 3.3 and 3.5 wt% at 30°C and 90°C respectively. Washing the biomass with acetic acid at 30°C for 24h led to a levoglucosan yield similar to the pretreatment 30°C 1 h with water and washing at 90°C with acetic acid led to a result similar when the biomass was washed with water at 30°C 24 h. The best results in terms of levoglucosan yield were achieved with the Soxhlet extractor (4.6 wt%) and 90°C 24h. Overall, the AAEMs that impacted the most the total levoglucosan yield were K and Na.

The pyrolysis conditions showed an effect also on the acetic acid distribution, increasing C_1 temperature decreased the acetic acid yield in the first condenser and increased in the second condenser. The pre-treatments influenced the acetic acid content by decreasing it in the first fraction for most of the washing techniques with the exception of 30°C 1h water, 90°C 24h acetic acid and Soxhlet.

Chapter 6

6 High temperature slow pyrolysis for biochar production

6.1 Introduction

Slow pyrolysis is a relatively simple process where the biomass components are converted at a certain temperature and in the absence of oxygen to make biochar and bio-oil. When high pyrolysis temperature and long solid residence time are employed the bio-oil contains a relative high amount of aqueous phase compared to the organic tarry phase. Aqueous phase characteristics are high water and acetic acid content. In this study, the biochar was produced in the new pyrolysis unit in batch condition to study the effect of different temperatures, holding times and nitrogen flow rate on the pyrolysis products. Then, an in-depth investigation of the physicochemical characteristic of the biochars was carried out to advance the knowledge on the use of *Phragmites australis* as a low-cost feedstock for the production of high value products.

6.2 Materials and methods

The pyrolysis reactor used for this chapter is the batch version of the continuous pyrolysis unit described in Chapter 5 Section 5.1.1.5.

Experiments were planned to study the effect of temperature, holding time and nitrogen flow rate on the pyrolysis product yields and characteristics, in particular the acetic acid content and the biochar properties.

The temperatures selected for the experiments were 500, 550, 600, 650 and 700 °C. The heating rate was kept constant for each expeiment to 10 °C min^{-1}, while the N_2 flow rate was varied at 0.5 and 1 L min^{-1} and the holding time (time after the temperature set point was reached) was varied to 30 and 60 minutes.

Phragmites australis samples of about 100 g were heated to the set point temperature with the selected N_2 flow rate and then kept for 30 or 60 minutes to complete the pyrolysis reaction.

6.3   Results and discussion

6.3.1   Product yields

The effect of holding time at can be seen in Figure 6.1 a) and b). The biomass was pyrolyzed at the same holding time and N_2 flow rate of 0.5 L min^{-1}, the bio-oil yield was stable between 40 to 43%, while the biochar yield dropped from 33% at 500°C to 29-30 above 650°C. When the holding time was increased to 1 hour, the bio-oil decreased from 42% to around 37-38% at temperatures above 600°C, while the biochar decreased from 31 to 28% from 500 to 700°C.

Then the same temperatures at 1 L min^{-1} with 30 and 60 minutes of holding time were studied and the same trend as the one performed with 0.5 L min^{-1} was observed. In general, the gas yield increased with increasing temperatures for all the experiments. This is because high temperatures favor cracking reactions of the volatiles and some gasification reactions were promoted, thus increasing the gas yield [21].
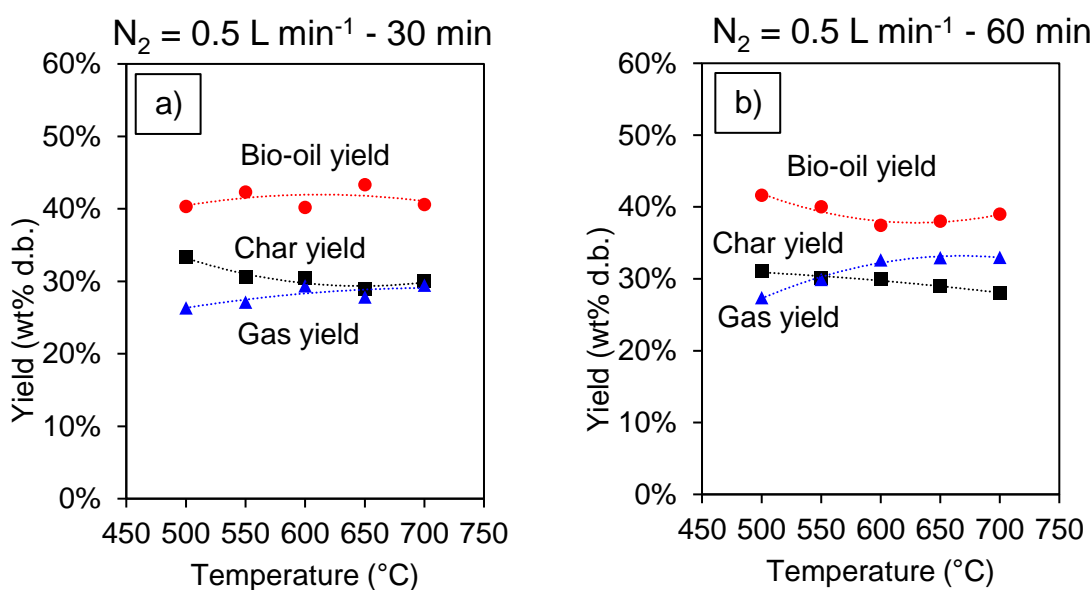
Figure 6.1 – Yields of pyrolysis products at 30 and 60 minutes holding times where 0.5 L min^{-1} of nitrogen were used at sweeping gas
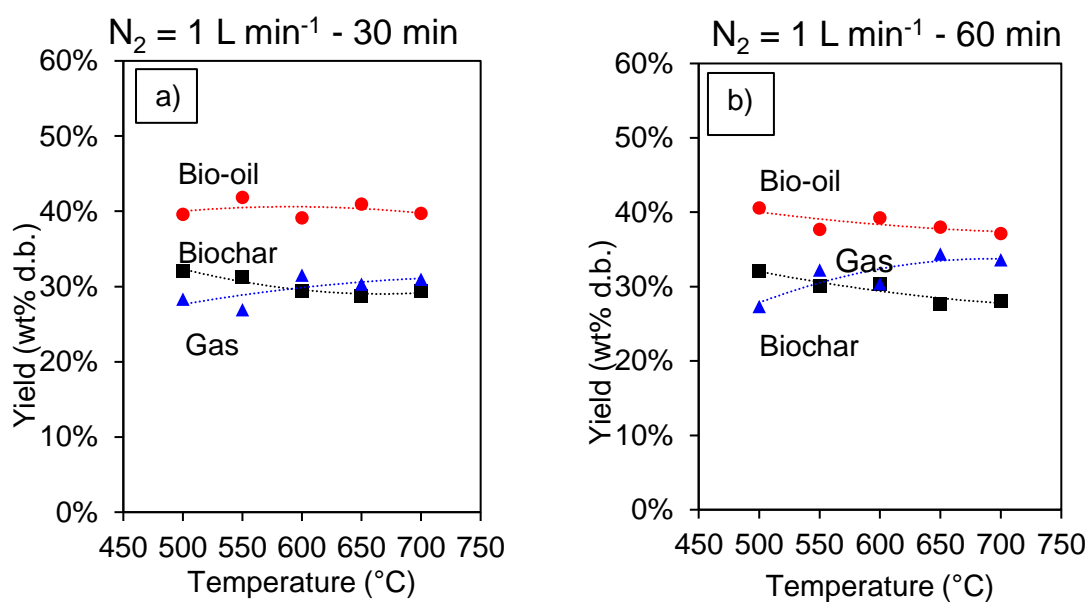
Figure 6.2 – Yields of pyrolysis products at 30 and 60 minutes holding times where 1 L min⁻¹ of nitrogen where used at sweeping gas

The ratio of the biomass and the pyrolysis products can be observed in Figure 6.3.
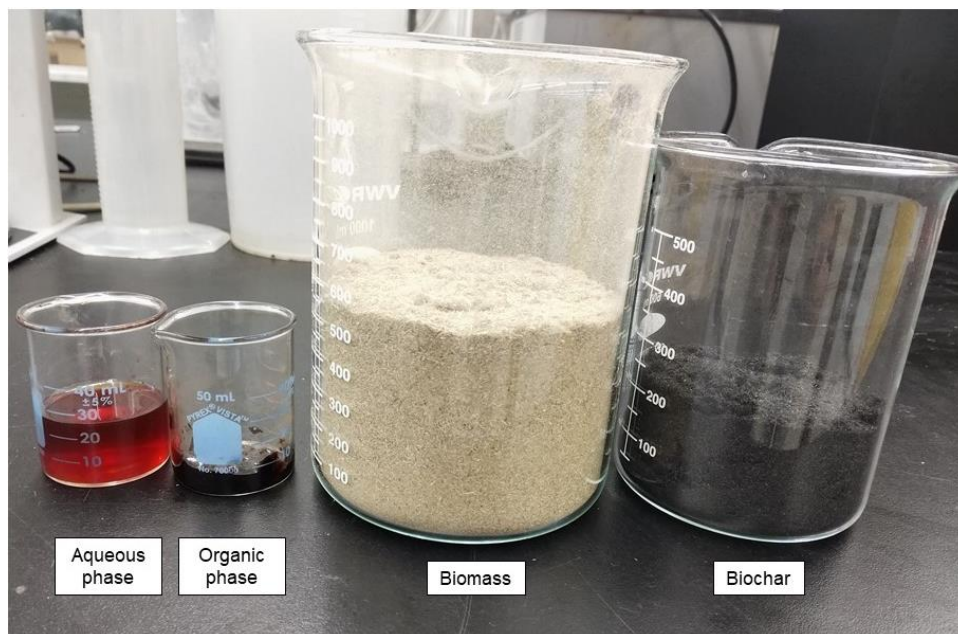
Figure 6.3 – Biomass and pyrolysis products of the run at 500°C, 0.5 L min⁻¹ of nitrogen and 60 minutes holding time

6.3.2   Biomass and biochar characterizations

Proximate analysis was performed to measure moisture, volatile matter, fixed carbon and ash content of the biomass and all the biochars (Table 6.1). The ash content of all the biochar samples was stable between 19-21%. The volatile matter decreased with increasing temperature and with increasing holding time at 500°C. Above 500°C, the effect of holding time and nitrogen flow rate for each temperature was minimal, probably indicating the high degree of carbonization reached at higher temperatures. The higher pyrolysis temperature increased the fixed carbon amount in the biochar. The carbon content increased with an increase in pyrolysis temperature, whereas the O and H content were reduced by the release of functional groups containing them. The comparison between the relative contribution of hydrogen and carbon and oxygen and carbon can be used as an indication of the chemical structure of the biochars (Table 6.2). The H/C and O/C ratio can be used as an indication of the aromaticity and degree of condensation of the biochars, although it should be kept in mind that the high mineral content which contain H and O can interfere with the quantification [289]. The values of O/C ratios can

give an indication of the biochar stability [212]. Low O/C ratio (as low as 0.10 at 700°C for the biochar 700-0.5-30) and low H/C ratio (0.16-0.18 at 700°C for all the samples) are observed for all the biochars, which supported the increased aromaticity due to the loss of carbon compounds [290] and the hydrophobic tendency [291]. The nitrogen content slightly increased with the pyrolysis temperature and it decreased from 30 minutes holding time to 60 minutes for almost all the biochars prepared at the same temperatures and nitrogen flow rates with few exceptions (550-1-30 and 550-1-60; 700-1-30 and 700-1-60).

The pH of biochar in solution slightly increased with the pyrolysis temperature from 10 to 11. According to Ronsse et al. [208], the pH of the biochar and its ash content is probably correlated with the oxygen functional groups, since at higher temperature the amount of carboxyl groups is lower and/or the acidic groups have become deprotonated to the conjugate bases resulting in more alkaline pH. Moreover, several studies reported how the alkalinity is also influenced by carbonates ($MgCO_3$ and $CaCO_3$) and AAEM (Na and K) [205,287,292,293], that were not analyzed in the biochars, however, the AAEM were identified in the SEM-EDX point analysis.

Table 6.1 – Properties of biomass and biochars (Proximate analysis, pH and HHV)

Reactor T (°C)-N₂ flow rate (LPM)-HT (min)	Proximate analysis (wt%, d.b.)			Moisture (wt%)	pH (H₂O)	HHV (MJ/kg)
	Fixed C	Volatiles	Ash			
Phragmites australis	8.35± 1.41	76.19± 1.91	6.97± 0.38	8.50± 0.10		18.64± 0.09
500-0.5-30	63.67± 0.64	12.52± 0.23	20.32± 0.65	3.48± 0.13	10.36	25.49± 0.14
500-0.5-60	63.54± 0.75	11.92± 0.52	20.01± 0.25	4.53± 0.04	10.28	25.31± 0.09
500-1-30	61.68± 0.97	13.25± 0.54	20.81± 0.57	4.26± 0.17	10.14	25.33± 0.16
500-1-60	63.44± 0.39	12.83± 0.22	19.20± 0.18	4.53± 0.03	10.27	25.50± 0.10

550-0.5-30	64.91± 0.30	10.76± 0.30	20.50± 0.29	3.84± 0.01	10.69	24.94± 0.11
550-0.5-60	64.66± 0.25	11.19± 0.36	19.51± 0.14	4.65± 0.00	10.62	24.64± 0.04
550-1-30	65.22± 0.17	10.83± 0.04	20.03± 0.27	3.92± 0.12	10.78	25.39± 0.15
550-1-60	64.17± 0.44	10.84± 0.35	20.31± 0.09	4.69± 0.16	10.63	25.33± 0.10
600-0.5-30	70.76± 0.41	7.35± 0.35	20.00± 0.42	1.90± 0.44	11.28	24.41± 0.05
600-0.5-60	69.50± 0.25	7.29± 0.11	20.83± 0.19	2.38± 0.12	11.17	23.98± 0.17
600-1-30	67.74± 0.11	7.68± 0.24	21.88± 0.43	2.69± 0.20	11.04	24.26± 0.10
600-1-60	67.58± 0.25	8.45± 0.34	21.46± 0.26	2.51± 0.11	11.12	25.29± 0.00
650-0.5-30	67.23± 0.86	8.07± 0.51	19.93± 0.31	4.77± 0.10	11.30	24.24± 0.14
650-0.5-60	66.46± 0.08	7.85± 0.80	20.73± 0.01	4.96± 0.01	11.20	24.12± 0.13
650-1-30	65.02± 0.31	8.51± 0.35	21.39± 0.11	5.08± 0.09	11.30	24.55± 0.05
650-1-60	66.48± 0.42	7.86± 0.23	19.31± 0.11	6.34± 0.14	11.50	24.42± 0.00
700-0.5-30	67.98± 1.13	7.44± 0.93	20.71± 0.26	4.52± 0.12	11.10	24.97± 0.00
700-0.5-60	69.04± 0.01	6.41± 0.22	20.05± 0.32	4.50± 0.07	11.10	25.11± 0.19
700-1-30	68.49± 1.09	6.99± 0.34	20.32± 1.82	4.20± 0.22	11.20	24.89± 0.01
700-1-60	68.93± 1.62	6.47± 0.47	20.28± 0.77	4.33± 1.11	11.00	25.27± 0.00

Table 6.2 – Ultimate analysis of biomass and biochars (Oxygen calculated by difference)

Reactor T (°C)-N$_2$ flow rate (LPM)-HT (min)	Ultimate analysis (wt%)				
	C	**H**	**O**	**N**	**S**
Phragmites australis	46.31±0.31	6.37±0.39	38.79±0.61	1.32±0.14	0.25±0.02
500-0.5-30	65.51±1.21	2.13±0.03	9.83±1.18	1.83±0.04	0.36±0.02
500-0.5-60	66.67±1.33	1.89±0.12	9.37±1.20	1.71±0.08	0.35±0.04
500-1-30	65.83±0.93	2.15±0.11	9.12±0.43	1.72±0.11	0.37±0.01
500-1-60	67.36±2.67	1.46±0.08	9.96±1.29	1.670.37	0.35±0.02
550-0.5-30	66.46±2.01	1.68±0.07	9.62±2.14	1.51±0.08	0.24±0.00
550-0.5-60	66.75±0.80	1.60±0.07	10.06±0.90	1.56±0.08	0.52±0.06
550-1-30	66.17±0.59	1.43±0.20	10.35±0.84	1.54±0.11	0.48±0.04
550-1-60	66.85±1.08	1.63±0.03	9.09±1.12	1.64±0.08	0.49±0.03
600-0.5-30	68.24±0.53	1.36±0.08	8.31±0.49	1.54±0.06	0.55±0.17
600-0.5-60	67.21±0.52	1.27±0.07	8.79±0.56	1.39±0.03	0.51±0.03
600-1-30	67.43±1.02	1.38±0.07	7.39±1.16	1.49±0.09	0.42±0.08
600-1-60	67.24±0.53	1.32±0.09	8.00±0.50	1.57±0.08	0.41±0.03
650-0.5-30	70.50±0.77	1.17±0.01	6.47±0.73	1.48±0.02	0.46±0.02
650-0.5-60	68.76±0.73	1.08±0.05	7.43±0.68	1.33±0.09	0.67±0.02
650-1-30	69.27±0.46	1.25±0.01	6.11±0.52	1.52±0.04	0.46±0.04
650-1-60	69.97±0.85	1.05±0.12	7.59±0.90	1.42±0.14	0.65±0.04
700-0.5-30	71.35±0.59	1.01±0.04	4.98±0.54	1.46±0.01	0.49±0.01
700-0.5-60	70.10±0.45	1.02±0.02	6.79±0.41	1.36±0.03	0.68±0.04
700-1-30	69.38±0.36	1.07±0.06	7.22±0.46	1.50±0.02	0.51±0.02
700-1-60	68.98±1.03	0.94±0.10	7.52±1.17	1.54±0.07	0.74±0.06

The FTIR spectra of the *Phragmites australis* and the biochars 500-1-60 and 700-1-60 were analyzed and compared (Figure 6.4). As mentioned in previous chapters, the broad band between 3200-3400 cm^{-1}, which is attributed to -OH from alcohols, phenols and water and the peaks at 2920 and 2851 cm^{-1} assigned to C-H aliphatic functional groups disappeared with the pyrolysis treatment indicating a decrease of non-polar group components [225]. The removal of OH and aliphatic groups at high pyrolysis temperature

occurs with the development of fused-ring structures and it is also confirmed by the decrease of O and H from the ultimate analysis (Table 6.2).

Compared to the biomass, both biochars exhibited a slight increased intensity in the peak at 1746 cm^{-1} attributed to carbonyl C=O groups in hemicellulose.

The reduced aliphatic groups content is accompanied by an increased presence of aromatic structures at 1600 cm^{-1}, 1440 cm^{-1}, 875 cm^{-1}.

The peak at around 1600 cm^{-1} due to aromatic C=C stretching (due to the phenolic groups in lignin [294,295]) is present in the biochar at 500°C and disappeared with increasing pyrolysis temperature, while the band at 1440 cm^{-1} could be due either to C-O stretch of carbonates due to the increased inorganic content [296] or aromatic skeletal vibration combined with C-H in plane deformation [297].

The peak at 1370 cm^{-1} is assigned to phenolic OH region and aliphatic CH stretch due to lignin (syringyl ring and guaiacyl ring condensed [298]). The broad peak at 1050 cm^{-1} due to the C-O stretching gradually decreased from 500°C to 700°C, which represented the oxygenated functional groups of cellulose. The peak at 875 cm^{-1} likely resulted from the presence of Si (Si-O-Si) [299] or carbonates. Otherwise, this peak could also be assigned to aromatic C-H or C-O from carbonates. The peak at 815 cm^{-1} is assigned to the aromatic C-H out of plane deformation which are again present in the sample prepared at 500°C and disappeared at 700°C. To conclude, the FTIR spectra confirms the presence of aromatic C and lignocellulosic-derived products at 500°C and an increased degree of condensation at 700°C, with a more graphitic-like spectra.
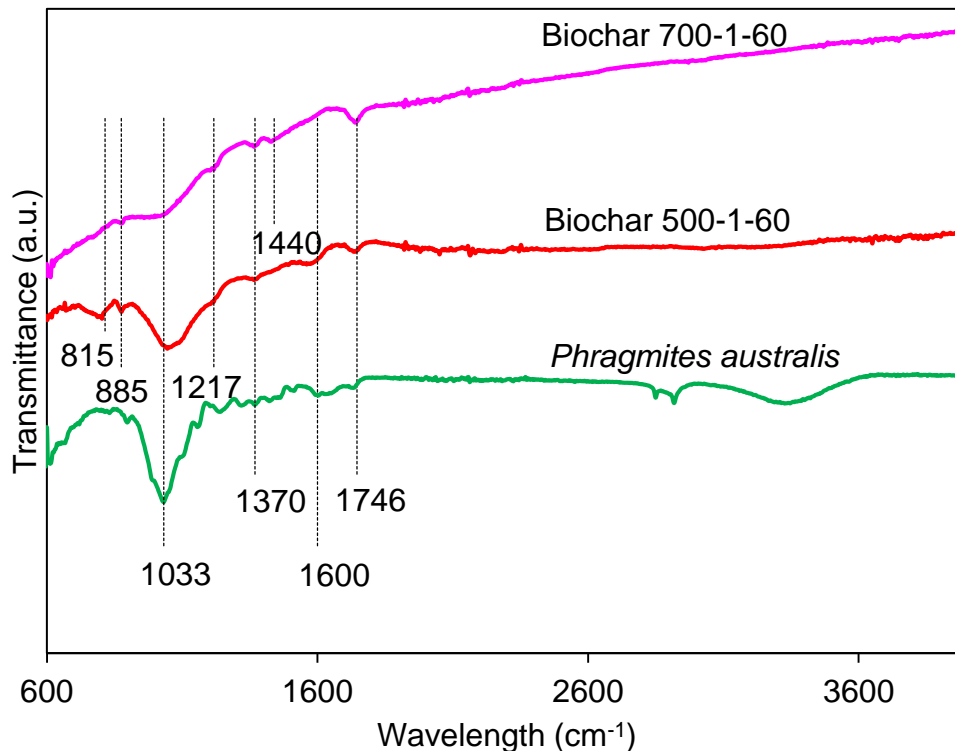
Figure 6.4 – FTIR spectra of *Phragmites australis* biomass and biochars

The morphological characteristics of the biochar produced at 700-1-60 were evaluated with the SEM-EDX (Figure 6.6). The biochar seemed composed of different particles of various sizes, which confirmed the dehydration and fragmentation of the biomass components during pyrolysis, showing the disintegration of the structure [300]. The EDX analysis was carried out on the same sample to detect the elements on the biochar surface (Figure 6.6). Although the EDX doesn't provide the total element content in the biochar, it can give a rapid and qualitative analysis of the presence or absence of some elements on the surface. The sample pyrolyzed at 700°C with 1 L min^{-1} of nitrogen flow rate and 60 minutes holding time presented considerable amounts of Ca, S, K, Cl and Na and of P, Si, and Mg. The BET surface areas of different biochars pyrolyzed at 550, 650 and 700°C at 1 L min^{-1} N$_2$ flow rate and 60 minutes holding time is reported in Table 6.3. The surface area decreased with increasing temperature, this behavior could be explained by

the cracking of tar on the biochar surface which might decrease the porosity [205] as well as pore collapsing at higher temperature.

Table 6.3 – BET surface area, total pore volume and average pore size diameter of biochars

Sample I.D.	BET surface area (m²/g)	Total pore volume (cm³/g)	Average pore size (nm)
550-1-60	91.421	0.076	3.33
650-1-60	18.794	0.027	5.74
700-1-60	6.329	0.01	6.77
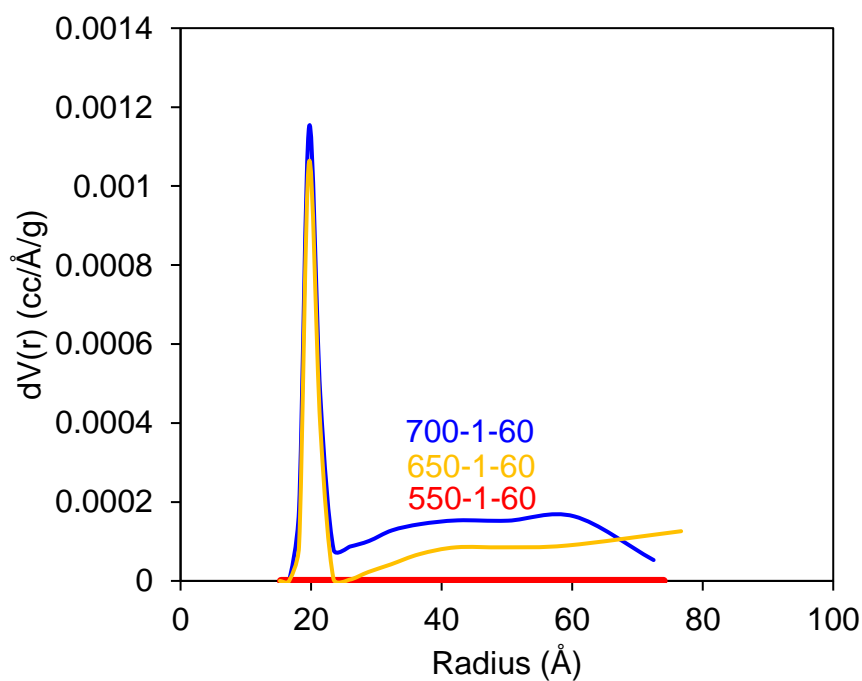
Figure 6.5 – Pore size distribution of the slow pyrolysis biochars
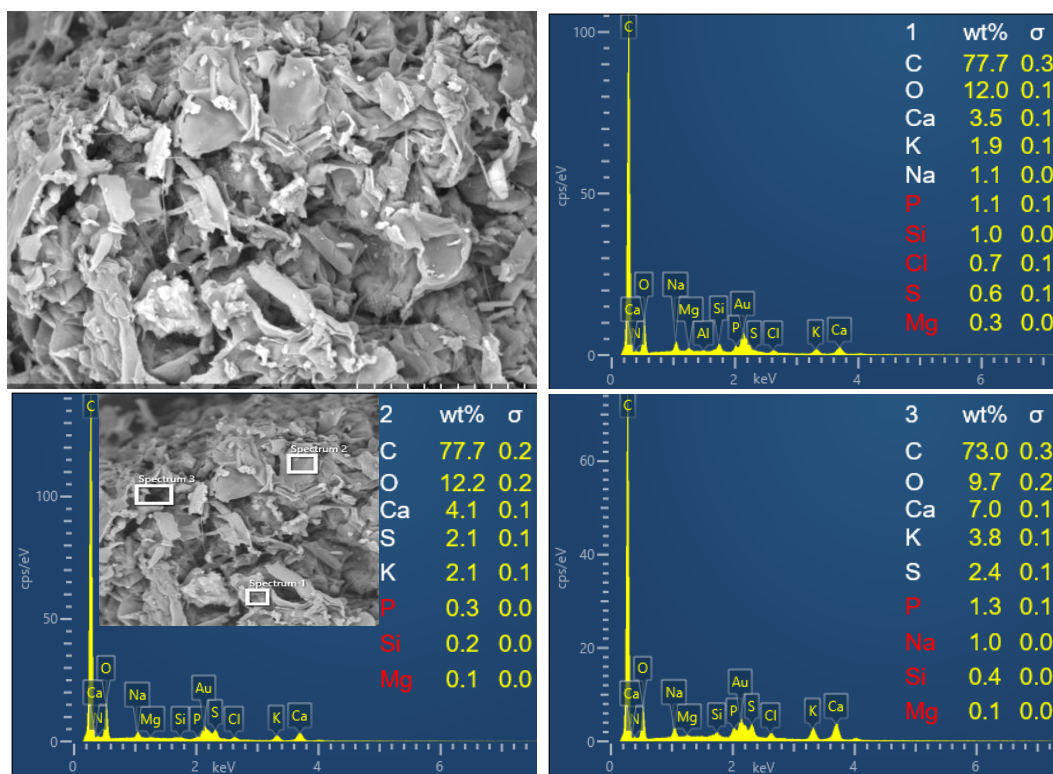
Figure 6.6 – SEM-EDX of the sample 700-1-60

6.3.2.1 Micro-CT and optical macroscope images of *Phragmites australis* (Cav.) Trin. Ex Steud. and biochar

The *Phragmites australis* stem was investigated by Micro-CT scanning to visualize how the pyrolysis treatment would affect the integrity and structure of the stem. The stem was cut in a section that comprised the node, which is the point where a leaf or bud will grow [301]. No other pre-treatments have been done before the optical microscope and Micro-CT scanning of the reed. The stem was then pyrolyzed in the new pyrolysis unit. It was placed on top of two thermocouples (one controlling the heater and the other one connected to the temperature recorder – profile showed on Figure 6.7). The final temperature was 481.5°C, heating rate 14.5 °C min^{-1}, no holding time and no nitrogen was used during the run. After the run the charred stem yield was 35 wt%.
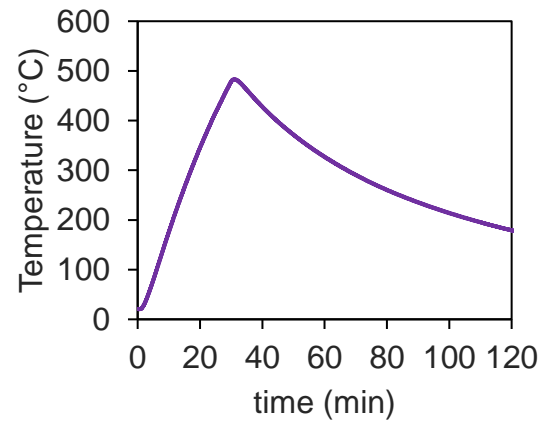
Figure 6.7 – Pyrolysis conditions for the stem used for the Micro-CT scan

The stem 'density' was estimated as the pixel intensities of a region. The methodology used is explained in Chapter 2, Section 2.3.9.

Okorn et al. [302] used the Micro-CT scanning technique to visualize internodal region structures such as the septum and the vascular bundles which are important for the assessment of mechanical properties of the plant tissue. The pictures from the optical macroscope were performed before (Figure 6.8 a) and b) and after the pyrolysis experiment (Figure 6.8 c)). The typical feature of the *Phragmites australis* is the tall hollow stem, with a layer of stellate parenchyma Figure 6.8 a), a form of aeration tissue typical of aquatic and wetland plants. The vascular and support tissues can be seen in the longitudinal and cross section images (Figures 6.9 and 6.10). After pyrolysis, all the parts kept their shape.
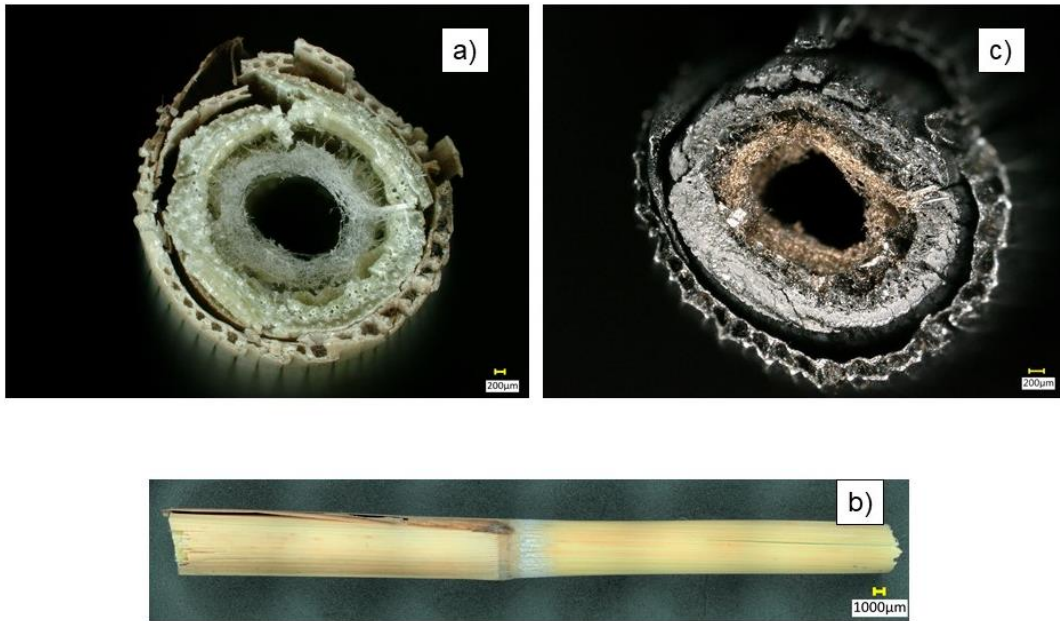
Figure 6.8 – **Optical microscopy of the *Phragmites australis* before pyrolysis cross section a); longitudinal section b); and cross section after pyrolysis c)**

The material "density" before and after pyrolysis was investigated with the Micro-CT scanner. The plant organs vary in tissue density, so we carefully selected the same slices for comparison. Since the nodal region was easy to recognize and maintained its integrity, it was selected as a reference. As explained in Chapter 2 Section 2.3.9, we selected the blue, green and red module to display the stem and to investigate the density development before and after pyrolysis. The warmer colors (yellow towards red) showed the part of the plants where the density was higher. The vascular bundles on top of the septum, circular bundles and the swelling of the inner part of the stem were also observed in another study [302]. After the pyrolysis treatment, the warmer color along the stem almost disappeared, as well as along the cross-sectional area in Figure 6.9 e) and f). This change in structure is probably due to the degradation of the lignocellulosic components in the plant that have different temperature stability. *Phragmites australis* composition comprised 37.2% cellulose, 24.8% hemicellulose and 21% of lignin. At 480°C, cellulose and hemicellulose are mostly all degraded, which is confirmed by the TGA analysis in Chapter 3 Figure 3.1, whereas lignin decomposed over a wider range of temperature and

it is the most recalcitrant component of the three.
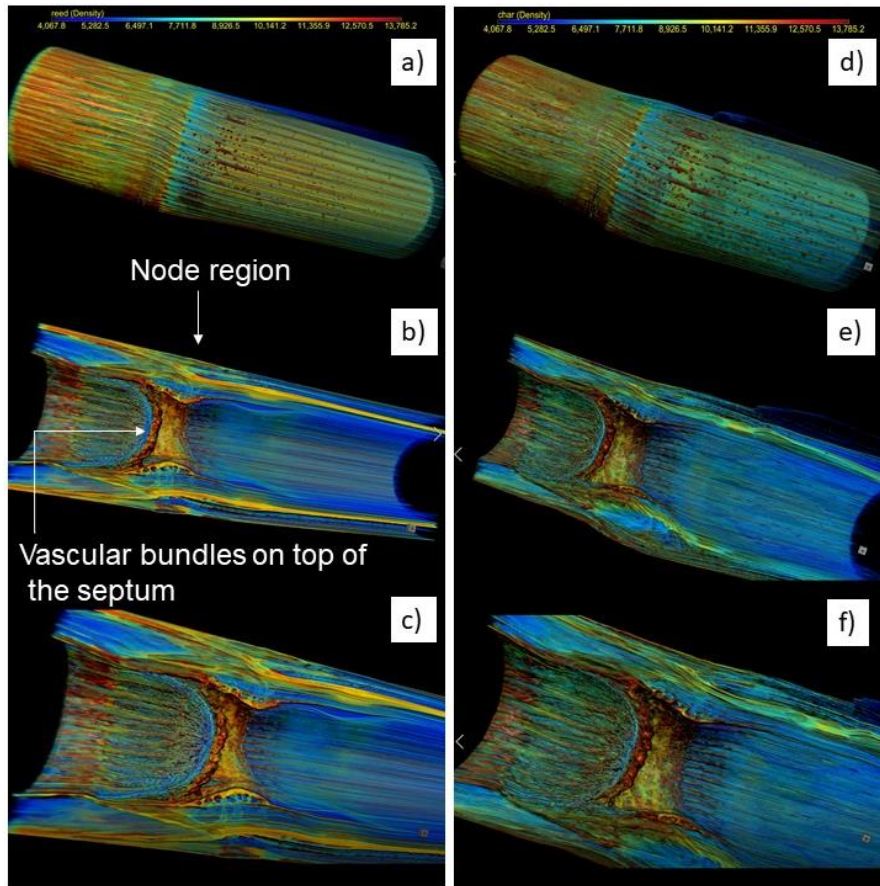
Figure 6.9 – **Micro-CT scan of longitudinal section of the *Phragmites austalis* before a),b),c) and after pyrolysis d),e),f)**
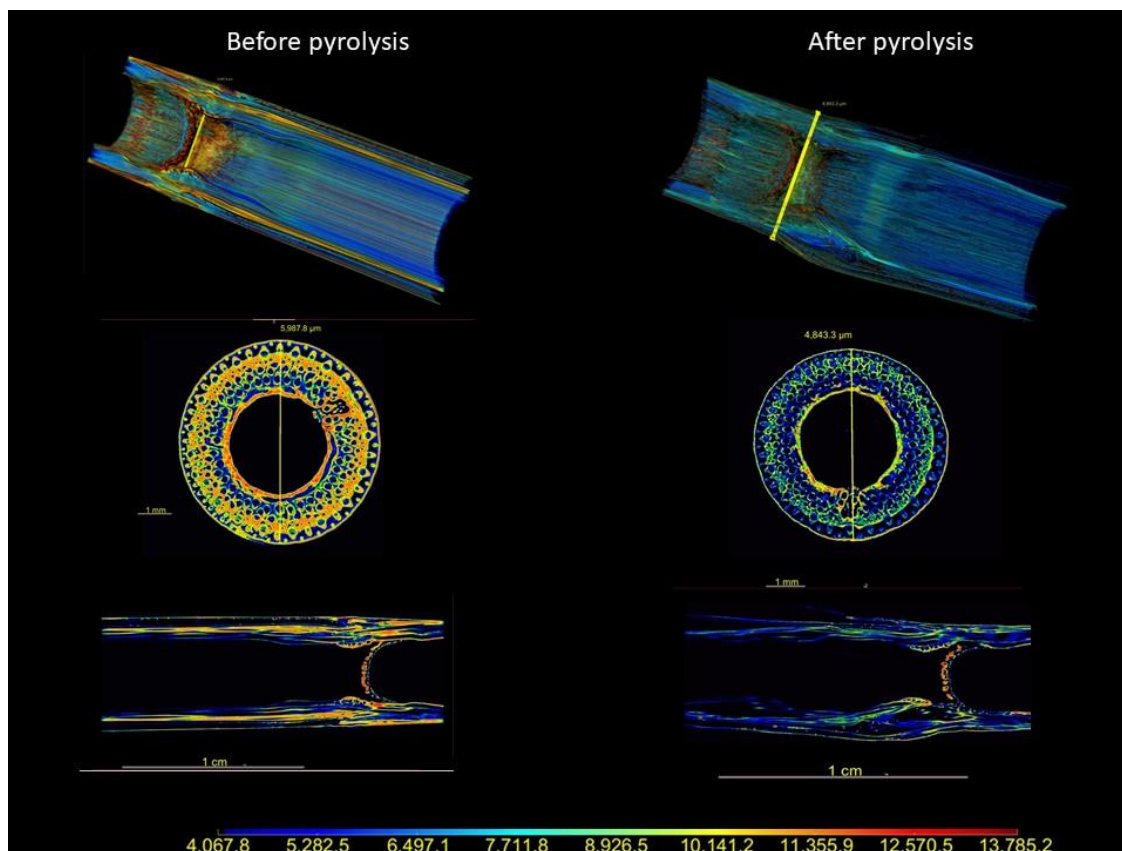
Figure 6.10 – **Cross section of the stem, slice indicated by the yellow line.**

6.3.3   Bio-oil characterizations

The bio-oil aqueous phase was characterized by HPLC to determine the organic acids and sugar concentration, in particular acetic acid and levoglucosan (Table 6.4 and Table 6.5). Beside water, acetic acid had the highest concentration (79-94 g/L) followed by acetol (13-19 g/L) and lactic acid (7-12 g/L). Acetic acid is derived from the decomposition of cellulose, hemicellulose [158,303]. In fact, during pyrolysis, the acetyl groups from the hemicellulose portion of the biomass, which were linked to the xylose units are eliminated and acetic acid is formed. The main products from the degradation of hemicellulose, in particular from the xylan units are water, methanol, formic acid and propionic acid. Levoglucosan also decomposes to acetic acid. Formic acid is derived from carboxylic groups during the degradation of xylan [283].

As expected, the levoglucosan content in the aqueous fraction is very low compared to the fast pyrolysis oils (all fractions), confirming that the bed of char, low heating rate and low vapor residence time affect the sugar content.

Table 6.4 – Water content and acetic acid, levoglucosan, xylose and acetol identified by HPLC

Reactor T (°C)-N$_2$ flow rate (L min^{-1}) -HT (min)	Water content (%)	Acetic acid (g/L)	Levoglucosan (g/L)	Xylose (g/L)	Acetol (g/L)
500-0.5-30	72.61	79.62	3.3	0	14.76
550-0.5-30	75.05	85.17	2.97	0.57	14.55
600-0.5-30	68.48	82.44	2.34	0	13.98
650-0.5-30	77.95	91.41	2.49	0	14.49
700-0.5-30	76.48	88.32	1.92	0	13.74
500-0.5-60	72.27	85.74	2.76	0	14.7
550-0.5-60	77.38	87.39	2.76	0	14.73
600-0.5-60	72.88	83.1	2.76	0	14.46
650-0.5-60	70.39	92.94	3.15	0.6	16.17
700-0.5-60	66.5	84.45	2.37	0.57	12.54
500-1-30	68.86	83.22	3.18	0	15.42
550-1-30	73.76	81.6	2.97	0.6	14.22
600-1-30	71.61	82.92	2.82	0	15.18
650-1-30	72.64	94.11	2.73	0.57	18.12
700-1-30	74.47	83.4	3.06	0.63	16.71
500-1-60	75.18	86.64	3.18	0	15.58
550-1-60	74.53	83.7	2.64	0	14.22
600-1-60	78.75	78.83	2.82	0	14.34
650-1-60	62.19	90.18	2.49	0.6	18.69
700-1-60	76.05	87.18	2.61	0	14.85

Table 6.5 – Compounds identified by HPLC analysis

Reactor T (°C)-N₂ flow rate (L min⁻¹) - HT (min)	Lactic acid (g/L)	Formic acid (g/L)	Propionic acid (g/L)	Iso-butyric acid (g/L)	Butyric acid (g/L)	Iso-Valeric acid (g/L)	Catechol (g/L)
500-0.5-30	9.3	2.1	5.4	5.04	1.02	n.d.	0.78
550-0.5-30	10.32	1.56	6.72	5.76	0.24	n.d.	2.67
600-0.5-30	8.88	2.16	5.94	4.74	2.4	n.d.	0.54
650-0.5-30	8.4	2.04	7.47	6.93	2.16	0.36	1.77
700-0.5-30	7.08	1.89	6.57	5.94	0.27	n.d.	1.47
500-0.5-60	9	2.4	6.24	5.52	2.22	n.d.	0.54
550-0.5-60	11.85	1.77	6.03	6.42	0.9	n.d.	2.79
600-0.5-60	8.4	2.04	5.64	4.86	0.96	n.d.	n.d.
650-0.5-60	11.52	2.25	7.08	7.05	1.86	0.6	2.55
700-0.5-60	8.31	1.38	6.96	5.25	1.38	n.d.	2.28
500-1-30	10.56	2.34	5.22	4.74	0.72	n.d.	n.d.
550-1-30	9.93	1.71	5.94	5.22	1.02	0.48	2.4
600-1-30	9.9	2.22	5.34	4.86	n.d.	n.d.	0.84
650-1-30	9.21	2.64	10.11	5.73	0.33	0.33	1.65
700-1-30	10.17	2.01	8.94	5.37	0.3	n.d.	1.32
500-1-60	9.48	2.58	5.64	4.98	n.d.	n.d.	0.36
550-1-60	8.88	2.4	5.64	4.68	n.d.	n.d.	0.48
600-1-60	8.76	2.34	5.22	4.44	n.d.	n.d.	0.42
650-1-60	8.16	2.4	9.9	7.74	0.21	0.69	0.81
700-1-60	8.49	2.28	6.27	5.37	0.27	0.54	1.62

The bio-oil aqueous phase of samples 650-1-30 and 650-0.5-60 were also analyzed by GC-MS (Table 6.6). These two samples were chosen for an additional characterization since they had the highest acetic acid content. The compounds were ordered from the highest % area to the lowest.

The first part of the table contains the chemicals that were common for both samples. Only 25 compounds were detected. Different groups were observed, such as carboxylic acid (acetic acid), furans comprising 2-furanmethanol, tetrahydro-2-furanmethanol, phenols with phenol, 2,6-dimethoxyphenol, 2-methoxyphenol and hydroquinone, benzenediols such as catechol, 1,2-benzenediol, 3-methoxy-, ketones such as 2-

propanone, 1-(acetyloxy)-, 1-hydroxy-2-butanone and hydrocarbons such as 3-methylcyclopentane-1,2-dione. The degradation of lignin produced predominantly phenolic compounds (e.g. methoxy phenols and alkyl phenols are produced during primary pyrolysis of lignin while from the secondary pyrolysis of lignin derives phenols and phenol derivatives. From the degradation of xylan some products are formed such as 1-hydroxy-2-butanone.

Table 6.6 – Chemicals identified by GC-MS

Chemicals	650-1-30	650-0.5-60
Acetic acid	76.16	73.12
2-Furanmethanol	2.48	2.45
2-Propanone, 1-(acetyloxy)-	1.78	1.72
1-Hydroxy-2-butanone	1.73	1.63
3-Methylcyclopentane-1,2-dione	1.56	1.67
Butyrolactone	1.53	1.59
Phenol, 2-methoxy-	1.47	1.61
2-Furanmethanol, tetrahydro-	2.57	3.03
1,2-Benzenediol	1.36	1.55
Phenol	1.16	1.36
Cyclopropyl carbinol	1.03	1.29
Phenol, 2,6-dimethoxy-	1	1.22
1,4:3,6-Dianhydro-.alpha.-d-glucopyranose	0.76	1.09
1,2-Benzenediol, 3-methoxy-	0.72	1.03
Phenol,3-methyl-	0.68	0.97
D-Allose	0.64	0.93
Phenol, 4-ethyl-2-methoxy-	0.54	0.65
2-Cyclopenten-1-one, 3-ethyl-2-hydroxy-	0.46	0.47
Phenol, 4-ethyl-	0.45	0.52
2-Cyclopenten-1-one	0.92	
2-Cyclopenten-1-one, 2-methyl-	0.37	
4-Hydroxy-2-butanone	0.32	
Acetic acid, 4-methylphenyl ester	0.31	
2-Butanone, 3-hydroxy-		0.58
1,2-Benzenediol, 4-methyl-		0.52
Hydroquinone		0.49

6.3.4   Gas characterization

The gas composition was analyzed by Micro-GC at 350, 450, 550 and final temperature 600 °C (Figure 6.11). The data is presented on weight percent of each gas evolved on a nitrogen free basis. The gas comprised CO_2, CO, CH_4, H_2 and some light hydrocarbons C_2-C_4. The experiments performed at 0.5 and 1 L min^{-1} of nitrogen flow rate showed the same trend in terms of gas released. CO_2 and CO were the dominant gas species at 350°C, mainly from the primary devolatilization of cellulose and hemicellulose, also confirmed by the TGA-FTIR analysis in Chapter 3. At temperatures above 500°C, the CO_2 released was mainly a contribution from the degradation of lignin [103]. CH_4 had a peak at 550 °C and then decreased gradually to zero at 600°C, while H_2 started evolving at temperature above 450°C from the decomposition of lignin and from secondary cracking of hydrocarbons. The release of light hydrocarbons were most likely after the secondary cracking of the bio-oil as well as reforming reactions of the vapors [304]. The release was generally low except for C_2H_6 which had a peak between 450 and 550°C and C_3H_8 and C_2H_4 increased at temperatures above 550 °C.
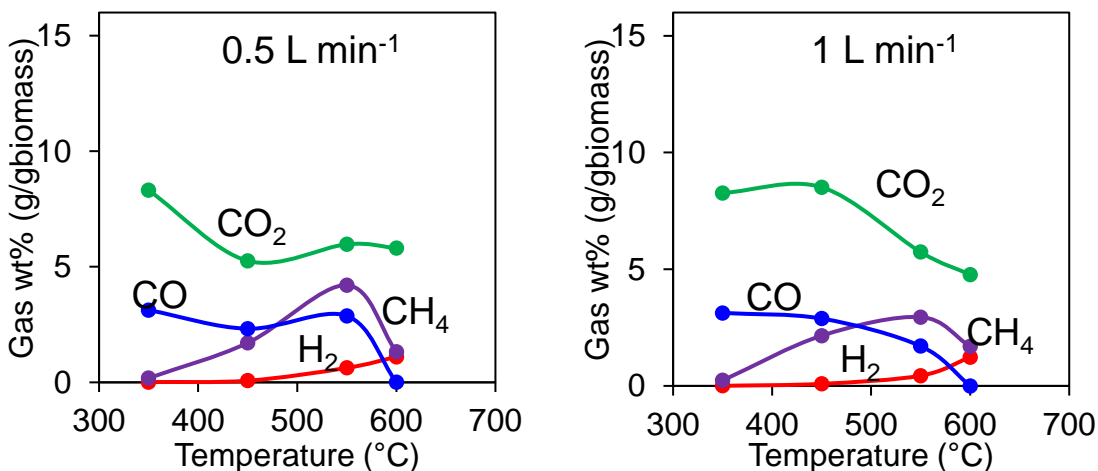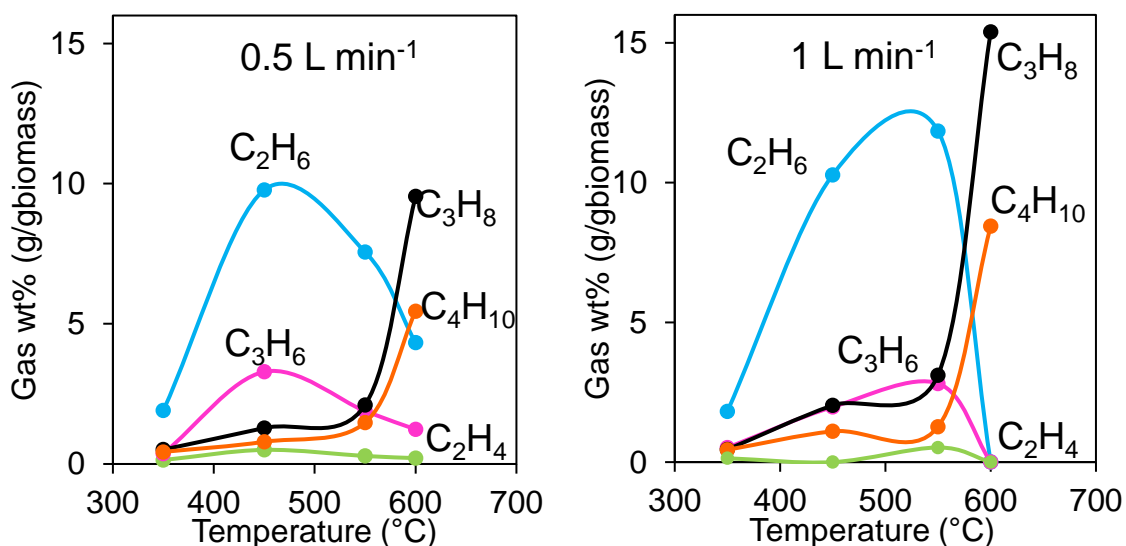
Figure 6.11 – Gas composition (wt%)

6.4   Conclusion

In this study, the biochar and aqueous phase of bio-oil produced by slow pyrolysis under several operating conditions were investigated. At the selected temperatures ($\geq 500°C$) the biochars had a high degree of carbonization, confirmed by the high fixed carbon and low volatile content. The aromatic structure of the char was also confirmed by the high alkalinity of the biochars in solution. These results are supported by the FTIR spectra and the O/C ratio (from 0.15 at 500°C to 0.1 at 700°C). The biochars exhibited a decrease in surface area with increasing temperature, probably due to the cracking of the tar on the biochar surface. The biochar produced at 550°C, 1 L/min of N_2 and 60 minutes holding time exhibited the highest surface area (91 m^2/g).

The aqueous phase bio-oil water content ranged from 62 to 79%. The highest acetic acid content of 94 g/L was observed for the sample 650-1-30. Overall, the aqueous phase oil exhibit similar water and acetic acid content over the selected temperature range with minor differences.

Chapter 7

7 Activation of biochar produced from *Phragmites australis* and adsorption of ibuprofen on biochar and activated biochar

7.1 Introduction

Pharmaceutically active components in wastewater, surface water and drinking water are an emerging concern. Their removal is challenging since these compounds are not biodegradable and frequently not completely removed from wastewater. The non-steroidal anti-inflammatory drugs (NSAIDs) belong to a specific class of emerging pollutants, which are biologically active and have strong impacts on the environment even in small concentrations. Although there are different wastewater treatment methods, which decrease the contaminates to acceptable levels, in reality there isn't an effective method for the NSAIDs removal, since wastewater and drinking water treatments are not designed specifically for this purpose. Therefore, the removal of ibuprofen with biochar and activated biochar was investigated. Ibuprofen is an NSAID used to treat minor pain, fever and inflammation by inhibiting the synthesis of prostaglandins, which are body chemicals that sensitize nerve endings [305]. Ibuprofen is one of the most used drugs worldwide and the occurrence in aquatic environments is mainly due to therapeutic use, in particular in Canada approximately 780,000 prescriptions of ibuprofen 600 mg have been issued each year between 2010 and 2015 [306]. In the body, drug-metabolizing enzymes play an important role to convert totally or partially ibuprofen in conjugated forms, that are then execrated in the urine [307]. A recent study analyzed the occurrence of different pharmaceutical in receiving water bodies of five pharmaceutical facilities in Ontario, Canada. The manufacturing facilities had no on-site treatment of the pharmaceutical prior to discharge to sewers. Ibuprofen detected during production measured in the direct effluent had a maximum concentration of 340,000 ng/L (average 227,400 ng/L) at one of the facilities. They stated that, based on the weekly production of ibuprofen, up to 200 g/d could be discharged in the receiving sewers.

Previous studies showed the biochars and activated carbon could be successfully used to remove ibuprofen and other NSAID drugs. Essandoh et al. [308] demonstrated the adsorption of ibuprofen on biochar produced from pinewood with fast pyrolysis conditions achieving the best adsorption capacity (10.74 mg/g) at low pH (2) at 308 K. Salem and Yakoot [170] used rice straw biochar produced with steam pyrolysis, stating that temperature had a significant effect on the physicochemical properties of the biochars. The highest adsorption removal of 56 mg/g was achieved with the biochar produced at 500°C. The aim of this study was to investigate if the biochars and activated biochars from *Phragmites australis* could be used as adsorbents for ibuprofen removal in water. Different temperatures, adsorbent dose, pH and time were investigated.

7.2 Activation of biochar produced from *Phragmites australis*

7.2.1 Materials and methods

The biochars were produced with the methodology described in Chapter 6. The activated biochar was produced with the equipment described in Chapter 2 Section 2.1.3.

7.2.2 Results and discussion

The activation experiments were carried out with 4 g of 650-1-60 biochar and 200 mL/min of CO_2. These conditions were selected based on another study on activation [309]. The burn off was calculated as the difference between the weight of the biochar used as a feedstock and the activated biochar produced, divided by the weight of biochar.

Table 7.1 – **Activation conditions and burn off (%)**

Sample I.D.	Temperature (°C)	Activation time (min)	Burn off %
AB850°C – 60 minutes	850	60	40.34
AB900°C – 60 minutes	900	60	69.11
AB900°C – 90 minutes	900	90	73.07

The amorphous nature of the biochar was confirmed by the XRD spectra analysis (Figure 7.1). The peak at 2θ 28° and 43° of the biochar were due to amorphous carbon [286]. The peak at 29.4° was assigned to calcite ($CaCO_3$). The peaks at 31.46° in the biochar and at 31.32 and 35.9° on the activated biochar were assigned to dolomite ($CaMg(CO_3)_2$). The sharp peak at 21.8° in the activated biochar's sample indicated the presence of crystalline silica in the form of cristobalite SiO_2 [310–312]. The presence of Ca and Si is also confirmed by SEM-EDX analysis (Figure 7.9) where Ca and Si were identified by the EDX as the second and third element with the highest concentration in the points selected on the activated biochar surface.
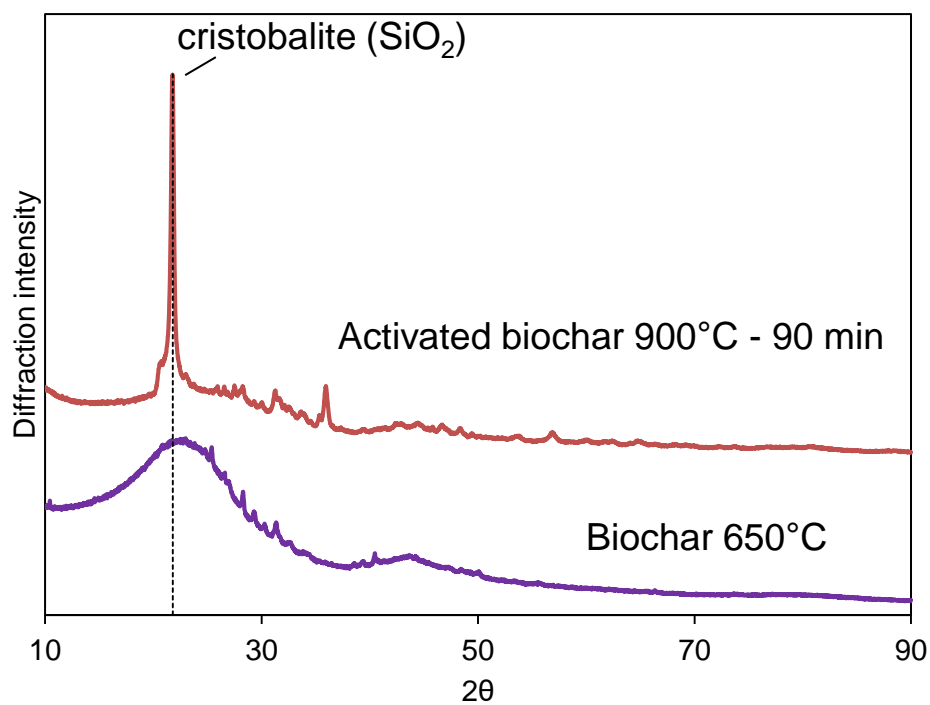
Figure 7.1 – XRD spectra of the biochar and activated biochar produced at 900°C - 90 minutes holding time

The biochar used as a precursor for the activation (650-1-60) and the activated biochar produced at 900°C for 90 minutes and 850°C for 60 minutes were evaluated through SEM-EDX analysis. The activation conditions had the effect of increasing BET surface area from 18.8 m^2/g (biochar 650-1-60) to 522 m^2/g and 576 m^2/g for AC850°C-60

minutes and AC900°C-90 minutes, respectively (Table 7.13). The porous structure and a honeycomb-like surface can be seen in Figure 7.3 and Figure 7.4.
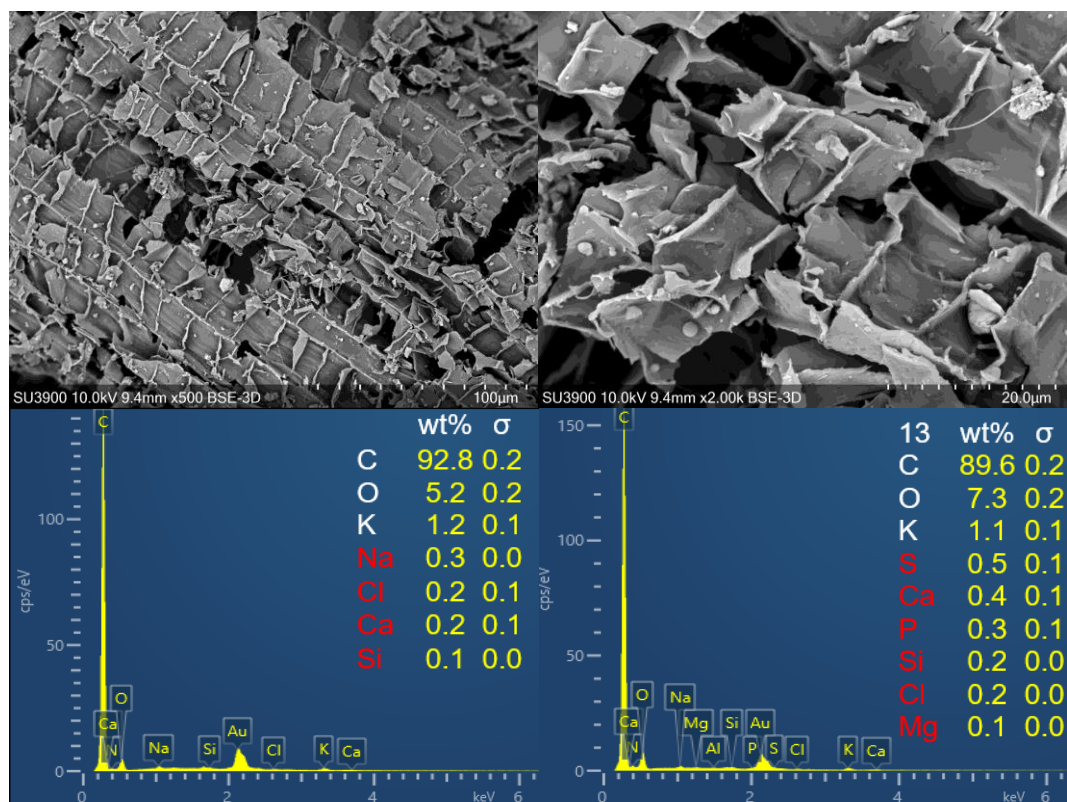
Figure 7.2 – SEM-EDX of biochar 650-1-60
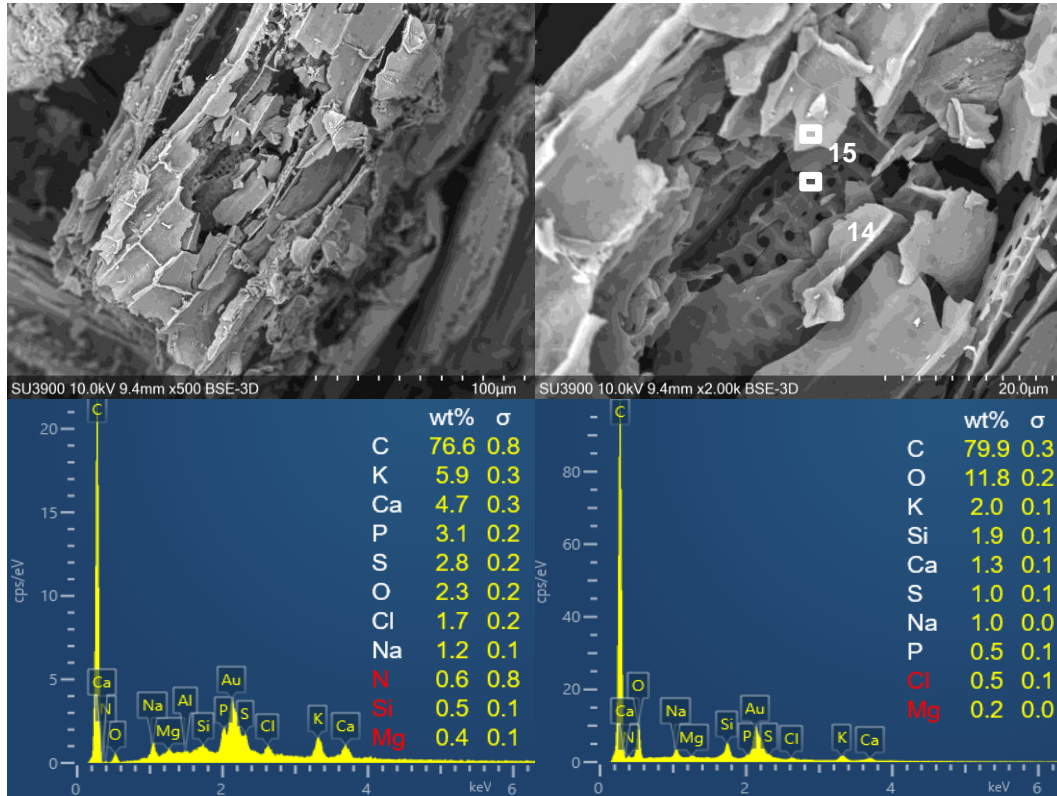
Figure 7.3 – SEM-EDX of activated biochar 850°C-60 minutes
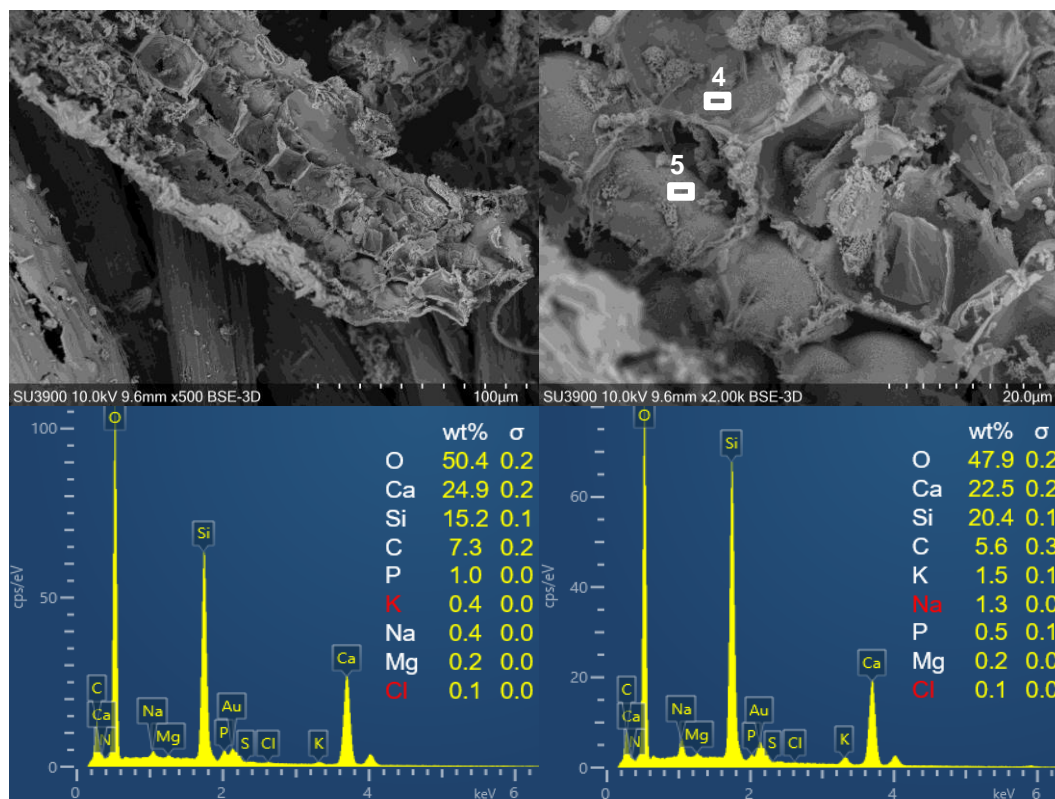
Figure 7.4 – SEM-EDX of activated biochar 900°C-90 minutes

7.3 Adsorption of ibuprofen on biochar and activated biochar

7.3.1 Materials and methods

For the adsorption experiments, the biochars 550-1-60, 700-1-60 and 550°C fast were selected and tested. The proximate and ultimate analysis were presented in Chapter 5 Table 5.9 and Chapter 6 Table 6.2.

Ibuprofen sodium salt ($C_{13}H_{17}NaO_2$, CAS number 31121-93-4, 98 %) was purchased from Sigma Aldrich (Canada). For the adsorption experiments, an initial stock solution of ibuprofen sodium salt was prepared with a concentration of 25 and 50 mg/L. These concentrations were chosen based on the range of concentrations reported in the

literature. The pH was modified with a solution of hydrochloric acid (1N, Fisher Scientific).

Commercially available activated charcoal Norit® SX2 (CAS number 7440-44-0) was purchased from Sigma Aldrich (Canada). As reported by the Sigma Aldrich website [313], peat was steam activated and acid washed. Another study [314] reported the BET surface area for the Norit® SX2 as 660 m^2/g.

7.3.1.1   Adsorption studies

The adsorption studies were reported in Chapter 2 Section 2.4.2.

7.3.2   Results and discussion

7.3.2.1   Adsorption studies of biochar

The point of zero charge (pH$_{pzc}$) was determined using acid-base titration according to the method described in Chapter 2. The pH$_{pzc}$ is the pH at which the net charge on the surface is zero [172,308]. For the biochar sample 550-1-60, the pzc was equal to 10, while for the biochar sample 700-1-60 was equal to 11 and 550°C fast pyrolysis 9 (Figure 7.5 and Table 7.14).
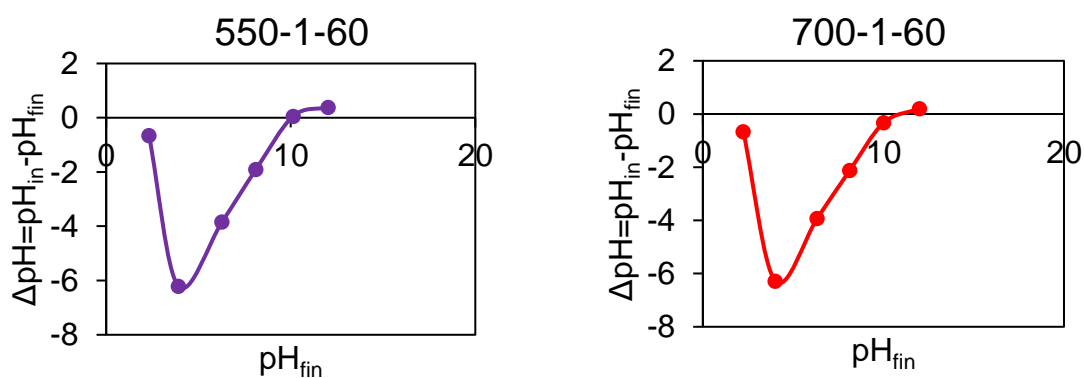
Figure 7.5 – Point of zero charge of the biochar produced at 500 and 700

The ibuprofen molecule contains two functional groups: aryl group (the benzene ring) joined to a carboxylic acid group [315]. The ibuprofen is a weak acidic compound, the

dissociation of ibuprofen in aqueous solution consists of the dissociation of hydrogen ions and its carboxylate conjugate base. Due to the low pKa (4.9 [316]), the equilibrium position is on the left, which implies that the ibuprofen molecules in aqueous solutions are mostly undissociated. An increase of the solution pH corresponds to an increase of the percentage of the ionic species. At pH=pKa, half of the initial concentration of weak acid is dissociated and the rest is still in the molecular form, so ibuprofen is in molecular form before dissociation and is negatively charged after. Since the adsorption depends on the pH of the solution as well as the pKa of the adsorbate and biochar surface, at pH greater than the pKa, the ibuprofen exists in the carboxylate anion R-COO$^-$, while the biochar surface becomes negatively charged, this causes electrostatic repulsion and decrease the adsorption capacity [308,317].

Therefore, the experiments were carried out at pH 2, to study the biochar adsorption capacity and the final pH of the solution (Figure 7.6). The biochars exhibited a similar removal efficiency at each holding time with the biochar 550-1-60 performing slightly better than the 700-1-60. For the biochar produced at 550°C, the % removal increases from 31% after 30 minutes to 41% after 48 h. The % removal for the biochar produced at 700 °C remains stable between 25-27%.
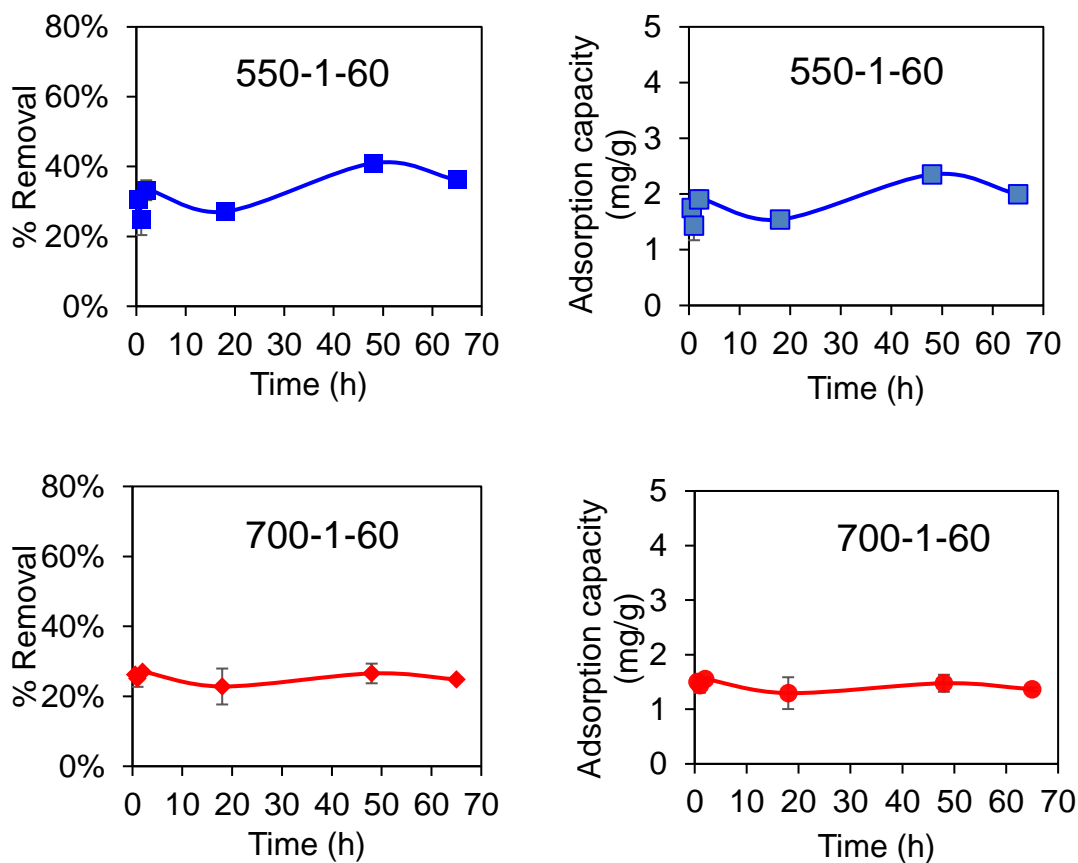
Figure 7.6 – Adsorption of ibuprofen at pH 2 onto biochars (initial concentration 25 mg/L). The error bars represent the standard deviation of triplicate experiments.

The amount of biochar was doubled (160 mg) and the adsorption experiments were repeated for a holding time of 65 h.

Table 7.2 – Effect of adsorbent dose on ibuprofen concentration at pH 2, contact time 65 h

Sample I.D.	80 mg		160 mg	
	% Removal	Adsorption capacity (mg/g)	% Removal	Adsorption capacity (mg/g)
550-1-60	36±1.59	1.99±0.07	62±1.02	1.17±0.018
700-1-60	25±0.07	1.37±0.02	32±0.70	0.67±0.01

The FTIR spectra of the biochar before and after adsorption is presented in Figure 7.7. Almost no difference was noted with the respect of biochar after the adsorption of ibuprofen probably because of the low amount of ibuprofen adsorbed.
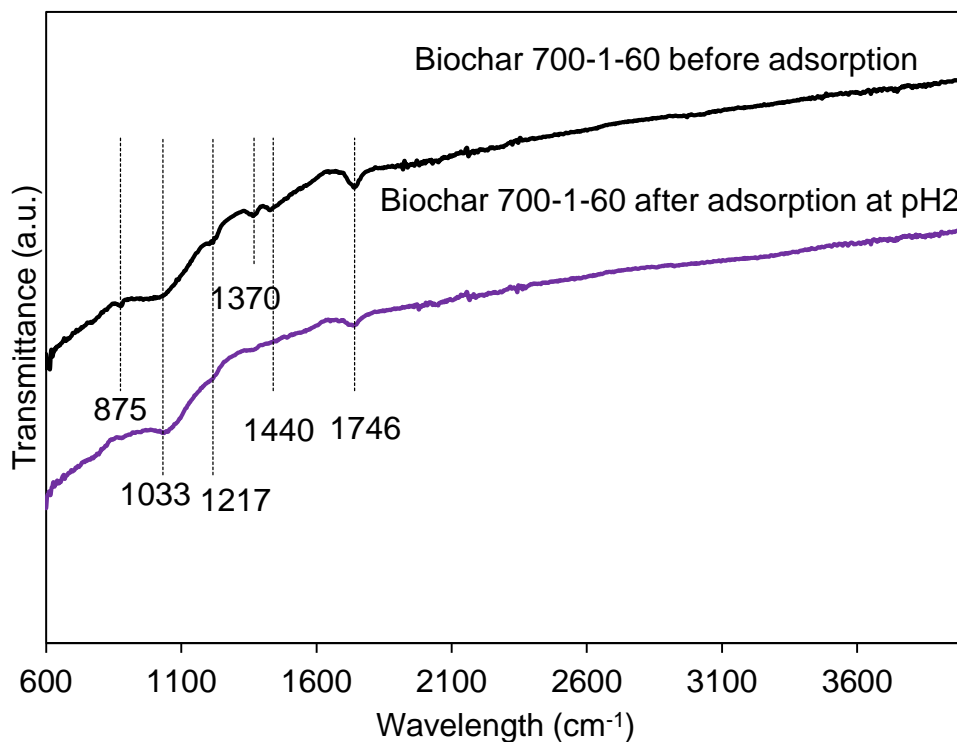
Figure 7.7 – FTIR spectra of biochar 700-1-60 before and after adsorption

The effect of initial pH on the adsorption of ibuprofen was studied for the biochar 550-1-60 for 48 h (Table 7.3). As expected, the pH played an important role in the adsorption process. Even though the initial pH studied was below the pKa of the ibuprofen, approaching the pKa value resulted in a decrease of the removal of ibuprofen and, therefore a decrease on the adsorption capacity. The experimental results showed that the pH of the solution after 48 h of adsorption is above the pKa of the ibuprofen. This might be explained by the acid-neutralization capacity of the biochar. This is a well-known property of the biochar, which has already been studied extensively for soil amendment to decrease soil acidity [318,319]. The alkalinity was linked to the presence of $CaCO_3$ and $MgCO_3$ formed during pyrolysis. In particular, the inorganic carbonates were the

161

major alkaline components produced at high temperatures (500 and 700°C) while the organic anions alkalinity contribution was mostly for the biochar produced at lower temperatures (300°C) [287,318]. The organic functional groups (–COO–and –O–) on the surface of biochars are conjugate bases of weak acids, which accept protons when the biochar is in contact with an acidic solution.

Table 7.3 – Effect of initial pH on ibuprofen adsorption at 48 h

		550-1-60		
pH	% Removal	Adsorption capacity (mg/g)	pH_i	pH_f
2	46±0.72	2.90±0.18	2.0	2.16
3	33±0.86	2.03±0.21	2.9	9.01
4	4±1.71	0.26±0.65	4.1	9.92

The adsorption of ibuprofen was then tested on a biochar produced at 550°C under fast pyrolysis conditions (described in Chapter 5). 80 mg of adsorbent dose at pH 2 and different adsorption times (10 minutes to 65 hours) were tested with an ibuprofen solution of 25 mg/L.
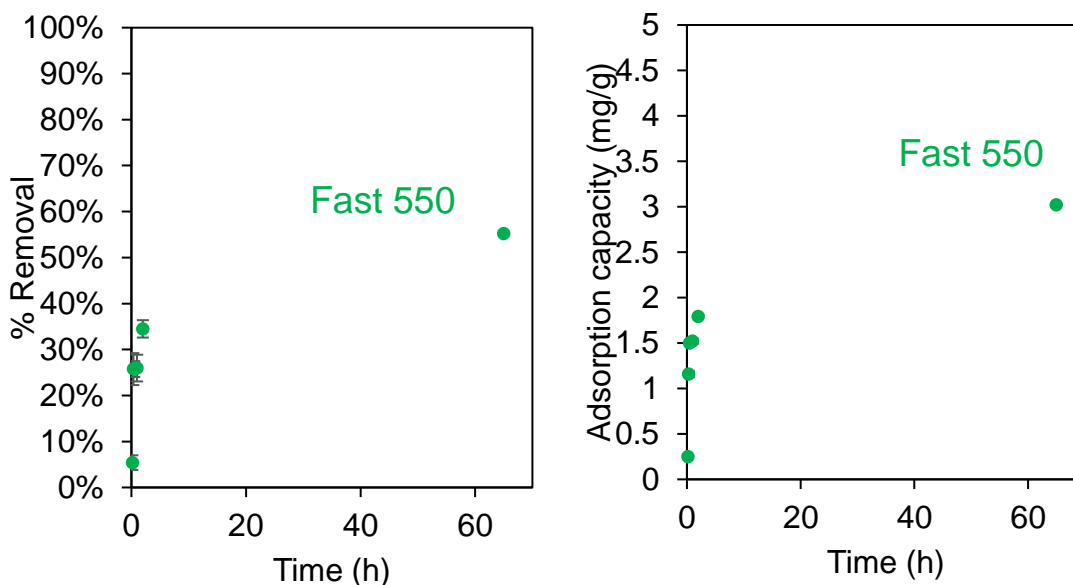
Figure 7.8 – Adsorption of ibuprofen at pH 2 onto biochar produced at 550 under fast pyrolysis conditions (initial concentration 25 mg/L). The error bars represent the standard deviation of triplicate experiments.

The biochar produced under fast pyrolysis condition removed 55% of ibuprofen after 65 hours, compared to 36% and 25% of the biochar 550 and 700 produced under slow pyrolysis conditions, respectively.

7.3.2.2 Adsorption studies on activated biochar produced from *Phragmites australis*

7.3.2.3 Methodology

The biochar produced at 650-1-60 was used for the CO_2 activation (200 mL/min). The activation conditions are reported in Table 7.4.

Table 7.4 – Activation conditions

Activation temperature (°C) – Holding time (min)
AB850°C – 60 minutes
AB900°C – 60 minutes
AB900°C – 90 minutes

The adsorption experiments were performed according to the Box-Behnken design and response surface methodology for the activated biochar 900°C – 90 minutes to study the effect of temperature, adsorbent dose and holding time. After evaluating the operating conditions during adsorption, the activated biochar produced at 850°C and 900°C were used to evaluate the performance of activated biochars prepared at different temperatures and holding time.

Then, the adsorption of ibuprofen was carried out with a commercially available activated carbon Norit® SX2 (CAC).

To conclude the experimental study, the best performing activated biochar produced from *Phragmites australis* was further post-treated with a 1 wt% HCl solution at 30°C for 1 h. After the holding time, the biochar was filtered with Whatman qualitative filter paper, grade 1 and then dried at 105°C. This was done to evaluate if the percentage removal and adsorption capacity could be further increased by an acidic wash, and also to compare the performance with the CAC which was acid washed.

7.3.2.3.1   Box-Behnken design with Response Surface Methodology (RSM)

The experiments for the adsorption of ibuprofen on the activated biochar 900°C – 90 minutes were carried out according to Box-Behnken design coupled with Response Surface methodology (RSM) [320] to determine the combined effects of different variables on the pollutant removal. The Box-Behnken design included three factors, adsorption time (min), adsorbent dose (mg) and temperature (°C) in three levels, three

center points and 15 runs. The actual and predicted response was γ for % removal of ibuprofen from the solution. The pollutant concentration was kept as a constant parameter (25 mg/L). The design of experiment matrix in coded variables (-1, 0, 1) and natural variables is reported in Table 7.5. The optimal value of the three factors was predicted with the second-order polynomial equation 7.1.

$$\gamma = \beta_0 + \sum \beta_i X_i + \sum \beta_{ij} X_i^2 + \sum \sum \beta_{ij} X_i X_j + \varepsilon \qquad (7.1)$$

Where γ is the predicted response (ibuprofen removal %) used as a dependent variable, i = 1, 2, 3 and j = 1, 2, 3; β_0, β_i, β_{ii} and β_{ij} are the model regression coefficients for the intercept, linear, quadratic and interactions and ε, the residual; Xi are the coded variables. Statistical Analysis System (SAS) and Design Expert were used for the regression and the analysis of variances (ANOVA) to obtain the interaction between the parameters and their responses.

Table 7.5 – Natural and coded variables for RSM

Variable	Symbols Natural	Coded	Range and levels -1	0	1
Time (min)	x_1	X_1	10	20	30
Adsorbent dose (mg)	x_2	X_2	10	45	80
Temperature (°C)	x_3	X_3	22	33.5-35	45

To make sure that the polynomial model represented a good fit, the square of the correlation coefficient R^2 was also reported.

Moreover, the statistical significance was evaluated using Fisher F-test. The analysis of variance includes source (the source of the variation); DF (the degree of freedom); SS (the sums of squares of the dependent variables); MS (the mean squares) which are the sums of squares divided by the degree of freedom; Fisher F values; and probability p values.

The probability (p-value) of the given statistical model determines the significance of the model to be accepted or rejected. Generally, based on the p-value the model is accepted

with 95% confidence level. The response surface fitting was performed with MATLAB R2019b software by relating a dependent variable to two inputs. These three-dimensional (3-D) plots show the simultaneous interaction of two variables on the response while keeping the third variable constant in the polynomial equation. Furthermore, based on the main variables in the 3-D surface and contour plots, the optimum region is determined.

7.3.2.3.1.1 Results and discussion

The results from the design of experiments is presented in Table 7.6.

Table 7.6 – Results from the Design of Experiments

Run	Order	Coded variable			Natural variable			Response		
		X_1	X_2	X_3	Time (min)	AC (mg)	Temp (°C)	% Removal	pH_i	pH_f
1	3	-1	-1	0	10	10	35	46%	6.59	8.38
2	13	-1	1	0	10	80	35	100%	6.80	9.62
3	12	1	-1	0	30	10	35	50%	6.59	8.01
4	8	1	1	0	30	80	35	100%	6.80	9.62
5	1	-1	0	-1	10	45	22	94%	6.59	8.76
6	10	-1	0	1	10	45	45	89%	6.59	10.13
7	6	1	0	-1	30	45	22	100%	6.59	9.66
8	5	1	0	1	30	45	45	97%	6.59	9.80
9	7	0	-1	-1	20	10	22	49%	6.59	8.00
10	15	0	-1	1	20	10	45	58%	6.59	7.80
11	4	0	1	-1	20	80	22	100%	6.59	9.95
12	14	0	1	1	20	80	45	98%	6.59	10.13
13	9	0	0	0	20	45	35	100%	6.80	8.01
14	2	0	0	0	20	45	35	99%	6.80	8.61
15	11	0	0	0	20	45	35	96%	6.80	9.11

Table 7.7 – Fit summary and ANOVA for the response

ANOVA for γ_1

Source		Master Model			
	DF	Sum of squares (SS)	Mean of squares (MS)	F values	Pr > F
Time (t)	1	0.0039	0.0039	2.9476	0.1467
AC	1	0.4712	0.4712	350.38	< 0.0001
Temperature (T)	1	0.0000	0.0000	0.0079	0.9327
t*t	1	0.0030	0.0030	2.2669	0.1925
t*AC	1	0.0005	0.0005	0.3368	0.5868
t*T	1	0.0000	0.0000	0.0166	0.9026

AC*AC	1	0.1688	0.1688	125.53	< 0.0001
AC*T	1	0.0030	0.0030	2.2553	0.1935
T*T	1	0.0001	0.0001	0.0753	0.7948
Model	9	0.6486	0.0721	53.59	0.0002
(Linear)	3	0.4752	0.1584	117.78	< 0.0001
(Quadratic)	3	0.1699	0.0567	42.12	0.0006
(Cross Product)	3	0.0035	0.0012	0.8696	0.5152
Error	5	0.0067	0.0013		
(Lack of fit)	3	0.0061	0.0020	6.1202	0.1437
(Pure Error)	2	0.0007	0.0003		
Total	14	0.6554			

Fit Statistics for γ_1

Mean	0.8508
R^2	98.97%
Adj. R^2	97.13%
Predicted R^2	84.97%
Std. Dev	0.0367
C.V. %	4.31

The analysis of variance (ANOVA) was performed to check the adequacy of the model in predicting the ibuprofen removal, which returns the statistical parameters such as the coefficient of determination (R^2). An adjusted R^2=0.9713, predicted R^2=0.8497, and R^2=0.9897 indicated that the model was a good fit of the ibuprofen removal. The fit summary indicated that the quadratic model is statistically significant with F-value of 53.59. Therefore, at least one of the terms in the regression model has a significant effect. Cubic model was aliased and therefore not considered in the discussion (not showed in SAS).

The second-order model is given by equation 7.2 in coded variables:

$$\gamma = 98.3 + 0.022X_1 + 0.24X_2 - 0.00115X_3 - 0.029X_1^2 - 0.01X_1X_2 + 0.00236X_1X_3 - 0.21X_2^2 - 0.028X_2X_3 - 0.0052X_3^2 \tag{7.2}$$

Only the adsorbent dose was found to be significant (p-value<0.0001). The adequate precision (ratio between signal and noise) was 19.052 (>4) which indicated an adequate

signal. Moreover, the Lack of Fit F-value of 6.12 is a good indication of the fitting of the model. The Table 7.8 lists the experimental results and the theoretical results according to the predictive model and the experimental results were plotted versus the results generated by the predictive model (Figure 7.9).

Table 7.8 – Experimental results (%) vs. Predictive model results (%)

% Removal (experimental)	% Removal (predicted)
46%	46%
100%	97%
50%	53%
100%	99%
94%	93%
89%	92%
100%	97%
97%	97%
49%	49%
58%	55%
100%	104%
98%	98%
100%	98%
99%	98%
96%	98%
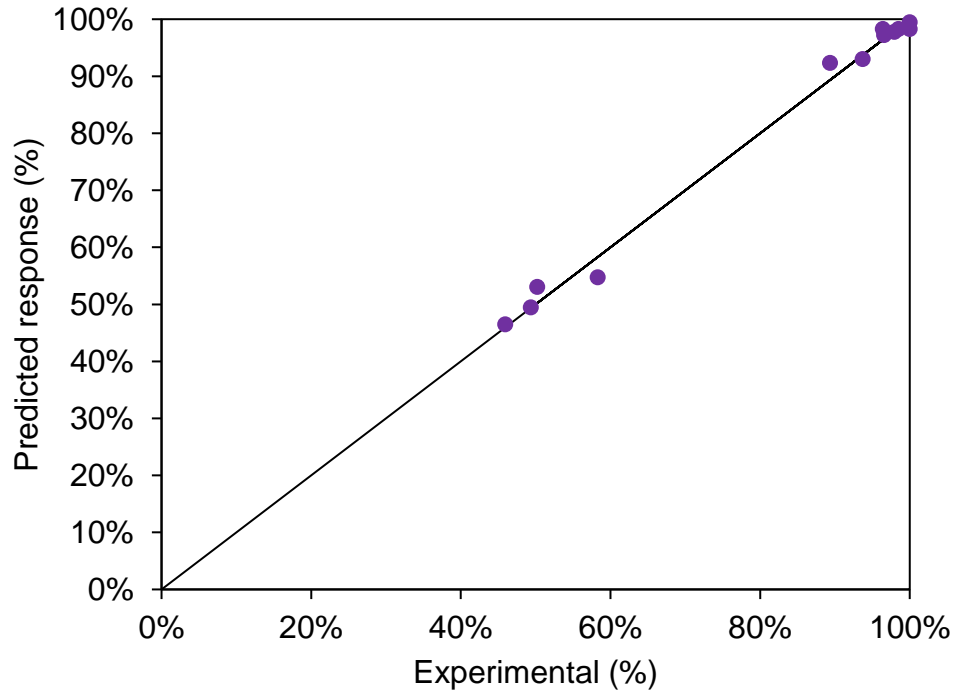
Figure 7.9 – Design plot for predicted model vs. experimental results

MATLAB was used to plot the 3-D response surface model. Increasing the adsorbent dose increases the adsorption with no significant effect of temperature and time. These results agree with those of other studies involving ibuprofen adsorption of activated carbons [174,317].
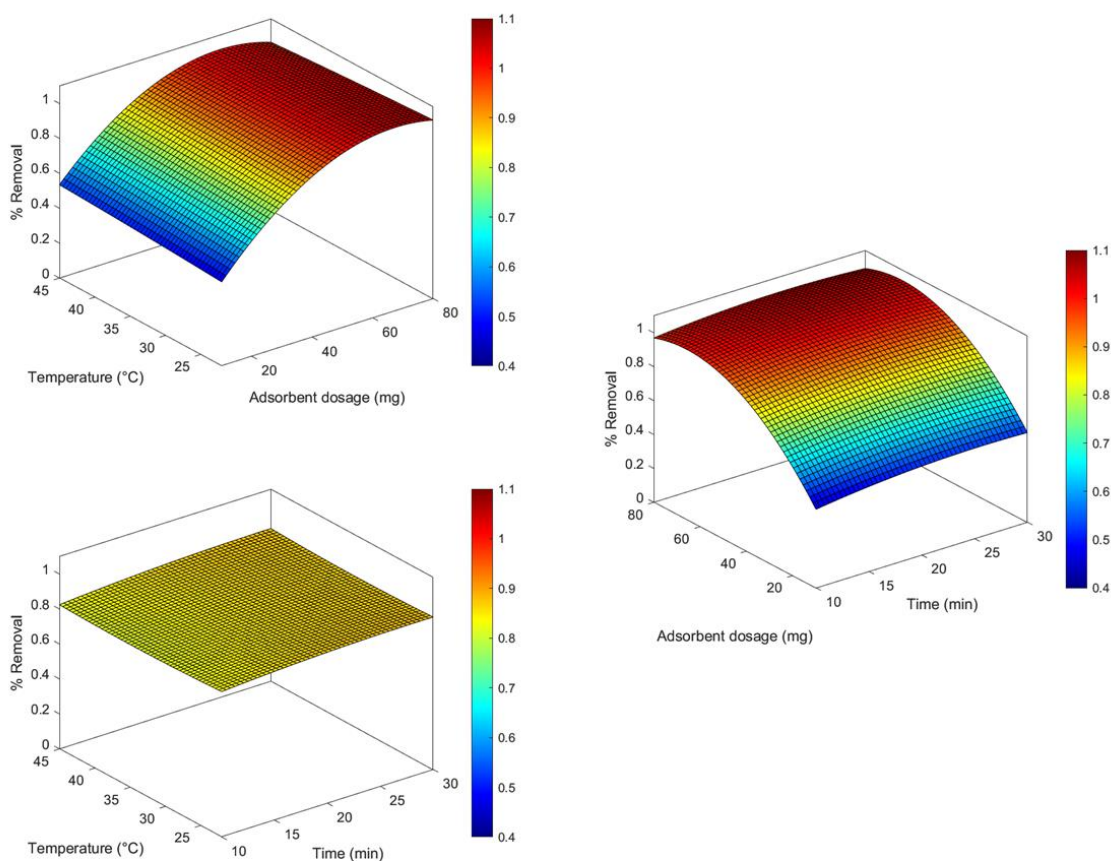
Figure 7.10 – Response surface model graphs with MATLAB

In order to get the value of adsorption capacity for the samples that reached 100% of adsorption removal, the experiments were repeated with an increased concentration of the stock solution (50 mg/L) (Table 7.9).

Table 7.9 – Adsorption of ibuprofen C_0=50 mg/L for AC900-90minutes

				50mg/L		
Time (min)	AC (mg)	Temp (°C)	% Removal	Adsorption capacity (mg/g)	pH$_i$	pH$_f$
10	80	35	88%	10.92	6.80	9.83
30	80	35	97%	12.22	6.80	9.91
30	45	22	85%	21.09	6.59	9.66
20	80	22	96%	11.93	6.59	9.89
20	45	35	81%	21.10	6.80	9.74

7.3.2.3.2   Comparisons of different activated biochars

Two more activated carbon from biochar from *Phragmites australis* were studied at 22°C. Increasing the activation temperature from 850°C to 900°C increased the ibuprofen removal and adsorption capacity from 16% removal (7.98 mg/g) to 49% (21.26 mg/g) using 10 mg of adsorbent prepared at 850°C and 900°C, respectively, and 10 minutes adsorption time. However, increasing the adsorption time to 20 minutes, only slightly increased the removal of ibuprofen. Moreover, for the sample prepared at 900°C, increasing the activation holding time, increased slightly the ibuprofen removal for both adsorption times.

Table 7.10 – Adsorption of ibuprofen on different activated biochars from *Phragmites australis* C$_0$=25mg/L

	10 min					20 min			
	AB850°C – 60 minutes					AB850°C – 60 minutes			
mg	% Removal	mg/g	pH$_i$	pH$_f$	mg	% Removal	mg/g	pH$_i$	pH$_f$
10	16%	7.98	6.59	7.00	10	13%	6.41	6.59	7.09
20	28%	6.66	6.59	7.52	20	34%	9.17	6.59	7.55
40	37%	4.57	6.59	7.24	40	47%	5.78	6.59	8.28
80	52%	3.23	6.59	8.72	80	69%	4.31	6.59	6.62
	AB900°C – 60 minutes					AB900°C – 60 minutes			
mg	% Removal	mg/g	pH$_i$	pH$_f$	mg	% Removal	mg/g	pH$_i$	pH$_f$
10	49%	21.26	6.59	8.82	10	48%	22.37	6.59	8.11
20	60%	14.17	6.59	8.8	20	62%	14.56	6.59	8.80
40	87%	11.71	6.59	9.13	40	87%	12.03	6.59	8.97
80	87%	6.01	6.59	9.34	80	100%	7.00	6.59	9.9
	AB900°C – 90 minutes					AB900°C – 90 minutes			
mg	% Removal	mg/g	pH$_i$	pH$_f$	mg	% Removal	mg/g	pH$_i$	pH$_f$
10	43%	26.16	6.59	8.32	10	49%	25.39	6.59	8.00
20	75%	18.43	6.59	8.51	20	82%	19.45	6.59	8.80
40	94%	12.85	6.59	8.76	40	99%	13.72	6.59	8.71
80	100%	7.03	6.59	9.42	80	100%	6.80	6.59	9.95

The experiments performed with 80 mg of activated biochar were tested at 2.5 and 5 minutes of adsorption time (Figure 7.11). The activated biochars produced at 900°C achieved removal above 50% in the first 2.5 minutes of adsorption.
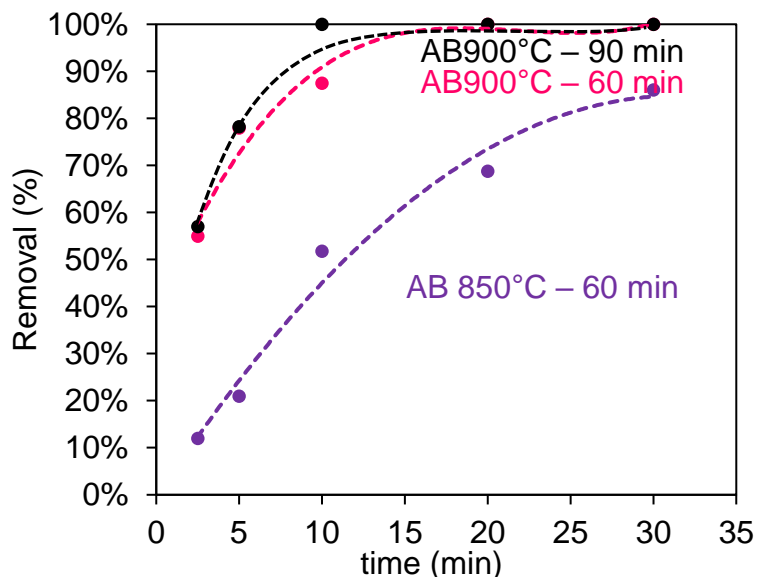
Figure 7.11 – Adsorption of ibuprofen (C_0=25 mg/L), adsorbent dose 80 mg, temperature=22°C

Then, the adsorption experiments were repeated for the activated biochar prepared at 900°C. 10 and 80 mg of activated biochar were used to study the effect of pH=2 (Table 7.11). As expected, the decrease in pH had a beneficial effect on the adsorption, where almost all ibuprofen was removed from the solution in 10 minutes and with the lowest adsorbent dose considered in this study (10 mg). Again, if the adsorption capacity was reported on the base of 100% adsorption, it does not represent the total adsorption capacity of the adsorbent.

Table 7.11 – Adsorption on 900°C activated biochar (ibuprofen C_0=25mg/L and pH=2)

| | **10 min** | | | | | **10 min** | | | |
| | AB900°C – 60 minutes | | | | | AB900°C – 90 minutes | | | |
mg	% Removal	mg/g	pH_i	pH_f	mg	% Removal	mg/g	pH_i	pH_f
10	95%	38.9	2.11	2.14	10	100%	35.7	2.11	2.19
80	100%	6.4	2.11	5.08	80	100%	7.9	2.11	3.82

FTIR spectra of activated biochar AB900°C – 90 minutes holding time before and after adsorption (Figure 7.12) showed that the characteristic peaks present on the activated biochar before adsorption were still present after the ibuprofen was adsorbed. The peak at 1033 cm^{-1} due to the C–O stretching increased after ibuprofen adsorption, having the lowest intensity when the pH was 2. The peak at 1744 cm^{-1} attributed to carboxyl C=O was present only for the sample after adsorption with no pH adjustment, as well as for the peak at 1372 cm^{-1} due to the C–O stretching. The peak at 791 cm^{-1} can be assigned to either aromatic C–H out of plane deformation or Si–O–Si symmetrical stretching vibration [312] for cristobalite. There is a small peak at around 1200 cm^{-1} which is attributed sp^2 C–O single bond stretching of ibuprofen [308]. Compared to the biochar (Figure 7.4), the amount of ibuprofen adsorbed was higher.
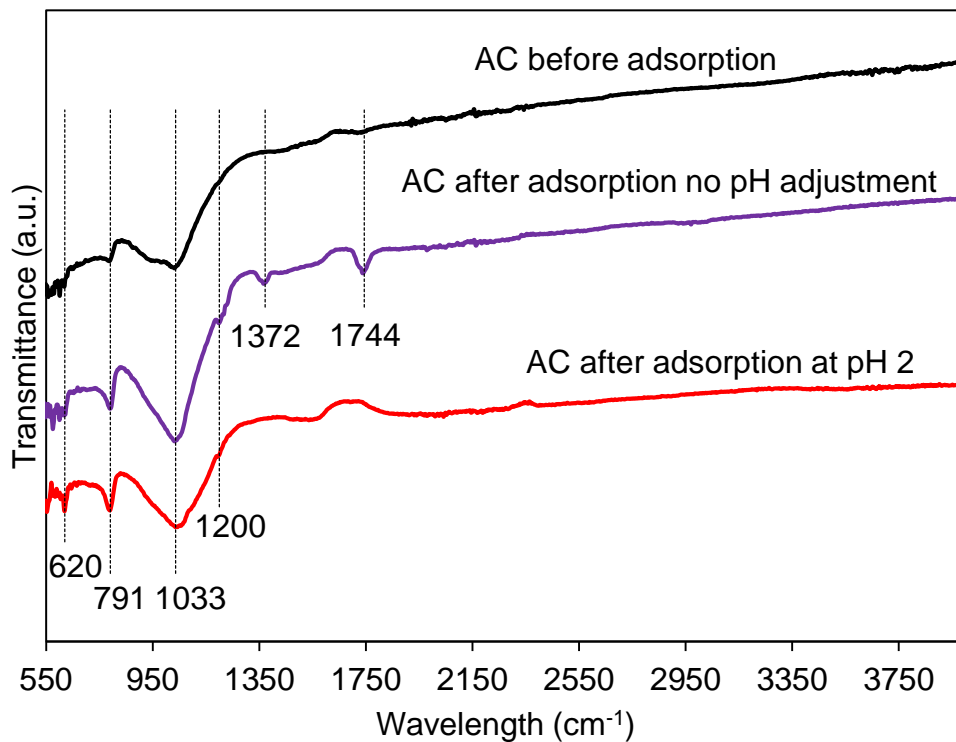
Figure 7.12 – FTIR spectra of activated biochar (AB900°C – 90 minutes) before and after adsorption

7.3.2.4   Comparison between CAC and AB900°C-90minutes

The adsorption of ibuprofen was evaluated on a commercially available activated carbon Norit® SX2 (CAC) with the characteristics described in the Materials and Methods section of this Chapter. Compared to the activated biochar produced at 900°C and 90 minutes, overall, the CAC performed better at the lowest adsorbent dose used (10 mg). The difference observed is the final pH of the solution, which remained below 6 for the CAC and above 9 for the activated biochar.

Table 7.12 – Adsorption on commercial activated carbon with C₀=25 mg/L

Time (min)	AC (mg)	Temp (°C)	% Removal	Adsorption capacity (mg/g)	pH$_i$	pH$_f$
10	10	35	85%	38.61	6.59	5.19
10	80	35	100%	6.53	6.59	5.22
30	10	35	82%	42.42	6.59	5.28
30	80	35	100%	6.32	6.59	5.36
30	45	22	100%	12.85	6.59	5.28
20	10	22	61%	29.44	6.59	5.27
20	10	45	70%	33.98	6.59	5.53
20	80	22	100%	6.37	6.59	5.17
20	45	35	93%	11.73	6.59	5.37

The AB900°C-90minutes was then washed with 1 wt% HCl to test the effect of an acidic wash on the adsorption performance with the lowest carbon dose evaluated in this study (10 mg). The adsorption was performed at 10, 20 and 30 minutes with 10 mg of activated biochar at 35°C.

Table 7.13 – Adsorption of ibuprofen C₀=25 mg/L with AB 900°C-90minutes washed with HCl

Time (min)	AC (mg)	Temp (°C)	% Removal	Adsorption capacity (mg/g)	pH$_i$	pH$_f$
10	10	35	62%	32.64	6.24	6.15
20	10	35	69%	33.98	6.24	6.34
30	10	35	88%	45.05	6.24	6.32

The adsorption capacity after 10 minutes is comparable with the adsorption capacity of CAC. Moreover, after 30 minutes the % removal and adsorption capacity are higher for AB900°C-90minutes washed.

7.3.3 Surface properties comparison between biochars and activated biochars

The activated biochar and the biochars used for the adsorption experiments were characterized for BET surface area, porosity, surface functionalities and morphological

structure to gather a better understanding of all the factors involved for the ibuprofen adsorption.

The BET surface area of the different biochars and activated biochars used as adsorbent is reported in Table 7.14. As stated, the surface area of the biochars gradually decreases with increasing temperature.

Table 7.14 – BET surface area, total pore volume and average pore size diameter of biochars and activated biochars

Sample I.D.	BET surface area (m^2/g)	Total pore volume (cm^3/g)	Average pore size diameter (nm)
BC550°C Fast pyrolysis	102.3	0.148	5.79
BC550°C Slow pyrolysis	91.4	0.076	5.05
BC650°C Slow pyrolysis	18.8	0.027	5.74
BC700°C Slow pyrolysis	6.3	0.017	6.77
AB850°C – 60minutes	522.1	0.400	3.06
AB900°C – 60minutes	588.5	0.425	2.89
AB900°C – 90minutes	576.3	0.389	2.78
AB900°C – 90minutes 1wt% HCl wash	660.4	0.414	2.50

The pore size distribution for the activated biochar and biochars are reported in Figure 7.13. The pore size distribution curves of the biochar 650-1-60 and 700-1-60 overlapped therefore only the 700-1-60 is reported for clarity. All the samples contained average pore size diameters between 2.50 to 5.79 nm which correspond to mesopores. Micro porosity could not be performed; however, it would be of interest to understand the pyrolysis and

activation conditions influence on micropores and how the adsorption relate to the micropores [173,317,321].
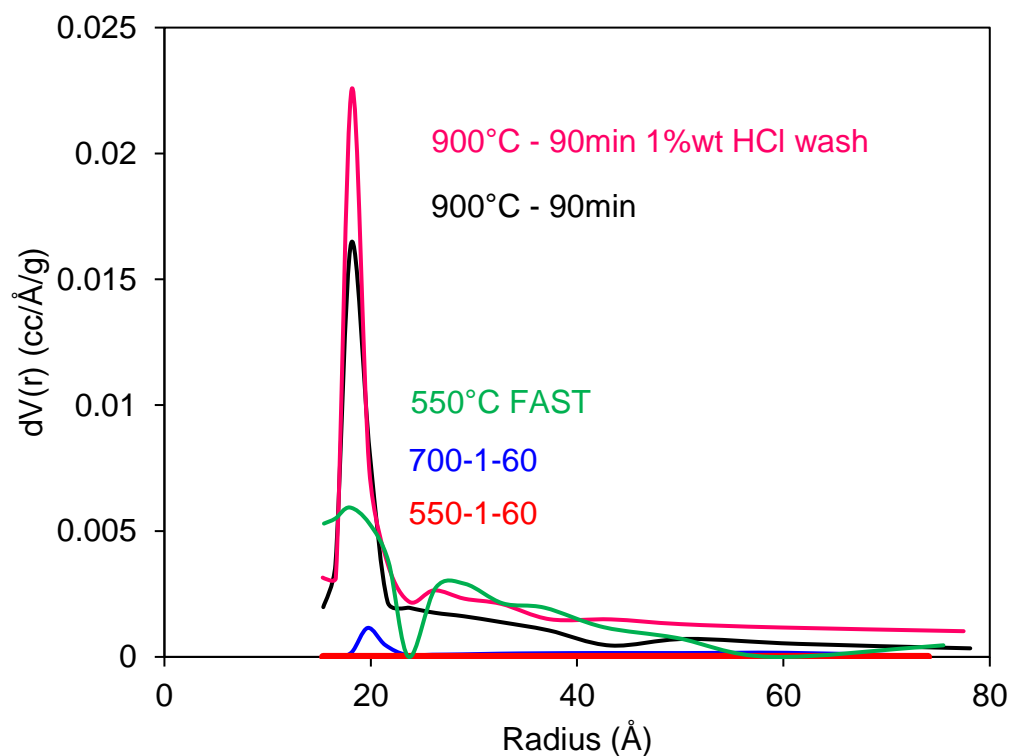
Figure 7.13 – Pore size distribution

The nitrogen adsorption-desorption isotherms of the activated biochar are reported in the Appendix.

Since the presence of oxygen containing functional groups on the adsorbent may affect the adsorption of ibuprofen, Boehm titration was used to evaluate the acidic and basic functional groups on the biochars and activated biochars (Table 7.15). The biochars present similar total acidic groups, with the biochar produced at 550°C under slow pyrolysis conditions having the highest total acidic content. Increasing the temperature to 700°C decreased the acidic groups and increased the basic groups. This trend is also confirmed by the oxygen content which decreases from 9.0% to 7.52% for 550-1-60 and 700-1-60, respectively (Table 6.2). Whereas the biochar produced at 550°C under fast

pyrolysis conditions contains 12.2% of oxygen (Table 5.8). However, the activated biochars had lower values of total acidic and basic groups compared to biochars, with the exception of the sample washed with HCl. The lower thermal stability of the oxygen functional groups is also reported in other studies [322–324].

The pH_{pzc} is above 9 for all the adsorbents except for the activated biochar washed with HCl (pH_{pzc} 2.4). The sample's surface area on the removal of ibuprofen seems to indicate that higher surface areas correspond to higher adsorption, particularly for the activated biochars (Figure 7.14 and Figure 7.15). However, no clear trend could be established for acidic and basic groups.

Table 7.15 – Surface properties of the adsorbents

Sample I.D.	pH_{pzc}	Total acidic groups (mmol/g)	Total basic groups (mmol/g)
BC550°C Fast pyrolysis	9.0	1.30	0.74
BC550°C Slow pyrolysis	10.1	1.61	1.14
BC700°C Slow pyrolysis	11.2	1.02	1.34
AB850°C – 60 minutes	9.7	0.15	0.68
AB900°C – 60 minutes	9.7	0.38	0.91
AB900°C – 90 minutes	10.3	0.52	0.59
AB900°C – 90 minutes – HCl washed	2.4	1.88	0.49
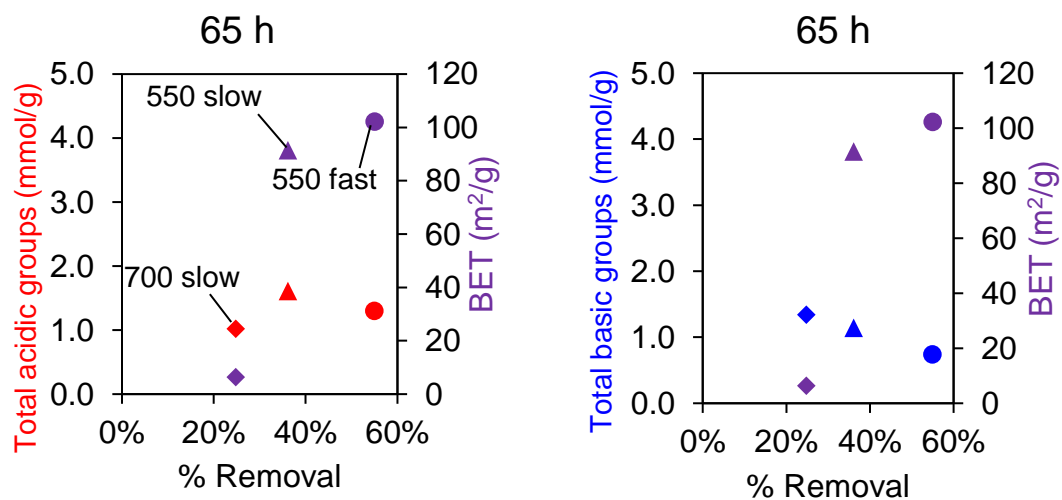
Figure 7.14 – Total acidic and total basic groups vs. BET area in biochars
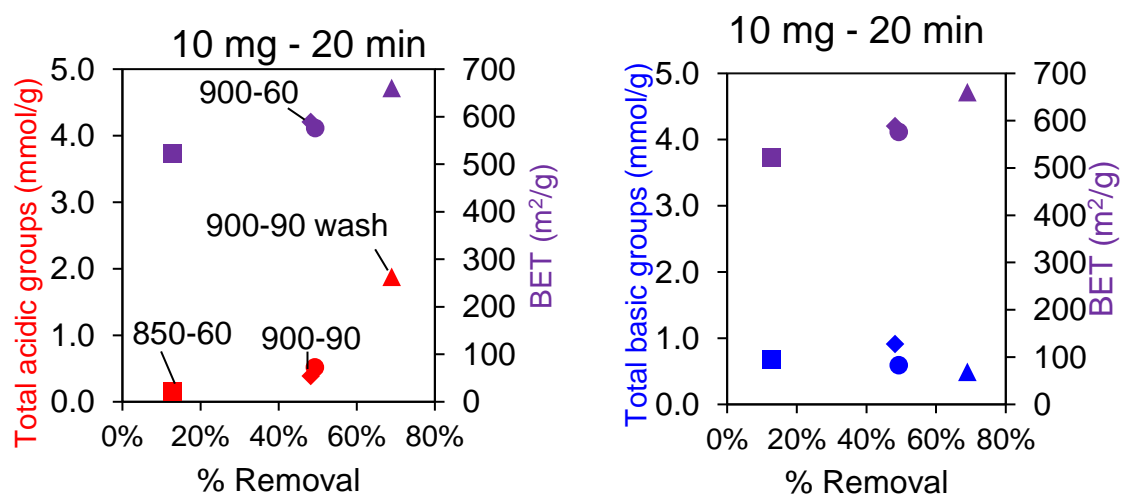
Figure 7.15 – Total acidic and total basic groups vs. BET area in activated biochars

The activated biochar AB900°C-90min was also evaluated after ibuprofen adsorption through SEM-EDX analysis (Figure 7.16). The sample after adsorption seemed to have lost part of its 3D shape due to either flattening of the surface because of the shaking or filled pores.
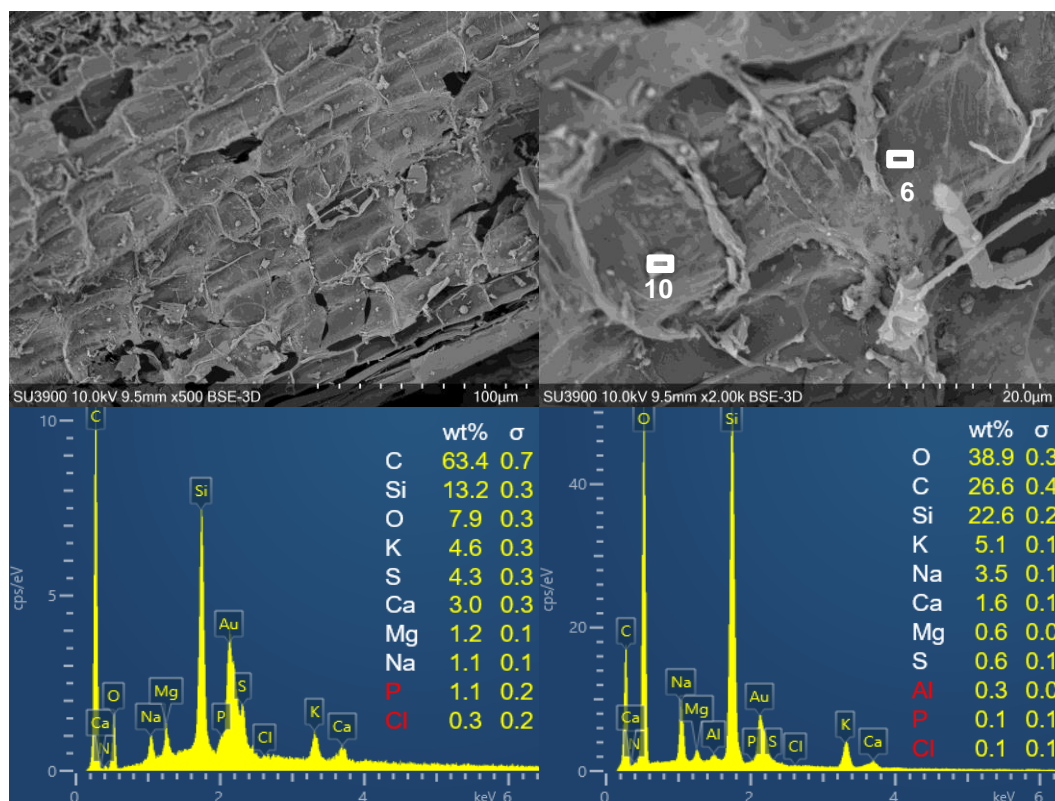
Figure 7.16 – SEM-EDX of activated biochar 900°C - 90 minutes after adsorption

Overall, the best performing adsorbents were found to be AB900°C-90min and AB900°C-90min-HCl washed. The optimal conditions of the activated biochar produced at 900°C and 90 minutes were found to be 45 mg and 20 minutes of adsorption time without any pH adjustment, with % removal and ibuprofen uptake (mg/g) comparable to the CAC. Surface area and surface acidic and basic functional groups could be both involved in the adsorption of ibuprofen. In fact, the biochars with a surface area considerably lower than the activated biochars didn't perform as good as the activated biochars. This study showed that the effect of pH is important when biochars were used as adsorbents, whereas activated biochars performed excellently without any pH adjustment. Previous studies have suggested different mechanisms of adsorption for carbonaceous materials: van der Waals dispersion forces, permanent dipole–dipole attractions, $\pi - \pi$ interactions and hydrogen bond formation. At basic pH, the repulsion

between the carbon surface (negatively charged) and the ibuprofen is the dominant mechanism [308]. However at pH lower that the pKa of the ibuprofen, the presence of oxygen and aromatic groups could promote hydrogen bonding interactions with the carboxyl group of ibuprofen [172], due to the fact the ibuprofen would be present in either anionic or neutral form. Further investigation is required to gather a better understanding on the specific interactions between surface functionalities, including carbonyl, carboxyl, phenolic, lactonic groups with the ibuprofen molecule at pH above the pKa of ibuprofen to further improve the adsorption on activated biochars and to better tailor the biochar characteristics for ibuprofen removal.

7.4   Conclusion

The biochars and activated biochars prepared from *Phragmites australis* were tested for the adsorption of ibuprofen at different pH. Biochars prepared at 550°C and 700°C, adsorbed 36% and 25% of the ibuprofen solution at pH 2 after 65 hours, with the 550-biochar performing slightly better. The low pH favored the adsorption of ibuprofen. The adsorption capacities went from 1.75 mg/g after 30 minutes to 2.35 mg/g after 48 hours for the 550°C biochar and from 1.5 mg/g after 30 minutes to 1.48 mg/g after 48 h for the 700°C biochar. The biochar produced at 550°C under fast pyrolysis conditions showed the same trend of the biochar produced under slow pyrolysis condition for the first 2 hours of adsorption time, however the adsorption removal continued to increase to 55% at 65 hours. These results are promising, considering that biochar could be employed as a low-cost wastewater treatment. The activated biochar produced from *Phragmites australis* biochar at AB900°C-90minutes was tested for different conditions of dose, adsorption time and temperatures. From the ANOVA, only the dose was found to be significant. The highest adsorption capacity of 29.36 mg/g was achieved in 10 minutes, with 40 mg of activated biochar and 45°C. Then, three activated biochars produced from *Phragmites australis* at different temperatures and holding times were tested. Increasing the activation temperature from 850°C to 900°C and 60 minutes activation time increased the adsorption removal from 13% to 48% when 10 mg of activated biochar were used in 20 minutes and from 69% to 100% with 80 mg of adsorbent dose in 20 minutes. The tests

performed with 10 mg of AB900°C-60minutes at pH 2 in 10 minutes showed a faster removal with 95% ibuprofen adsorbed, 39 mg/g of adsorption capacity compared to the activated biochar used with the same conditions but without any pH adjustment (49% removal with 21 mg/g adsorption capacity). The AB900°C-90 min performed better with 100% removal and above 35 mg/g of adsorption capacity at pH 2 compared to the condition without any pH adjustment (43% removal and 25 mg/g adsorption capacity). The commercially activated carbon was found to perform slightly better than the AB900°C-90 min, although the acid washing could have further improved the adsorption. Therefore, the AB900°C-90 min was washed with an acidic solution and a further increase in the adsorption removal was observed with the same and better values than CAC after 10 and 30 minutes, respectively. This study showed that the activated biochar produced from *Phragmites australis* have excellent ibuprofen adsorption removal.

8   Conclusions and Recommendations

This chapter provides a summary of the main conclusions from the studies carried out in this thesis.

8.1   Conclusions

This thesis investigated the use of *Phragmites australis* as a negative-value feedstock for the production of valuable chemicals through slow and fast pyrolysis. The main objectives listed in Chapter 1 and findings are summarized as follows:

1. This research confirmed the suitability of *Phragmites australis* as an inexpensive lignocellulosic biomass to produce bio-based products.

2. Effect of pre-processing, reactor technology and post-processing:

    a. The impact of different washing pre-treatments on the removal of AAEMs and their effect on the composition of fast pyrolysis products, in particular levoglucosan concentration in bio-oil was carried out in the new unit. Results showed the importance of considering a pre-processing treatment for the *Phragmites australis*.

    b. Study slow and fast pyrolysis with two different reactor technologies:

        i. The slow pyrolysis of cellulose, xylose and lignin in different ratios was carried out in a previously design MFR reactor to investigate the similarities and differences in comparison to the real biomass. In general, the bio-oil yield was higher for the model compounds (47-50%) compared to 40-43% for the actual biomass. While the char yield was higher from Phragmites biomass (37% compared to 31-32% yield for the model compounds). GC-MS analysis showed a different distribution of the bio-oil chemical compounds, with increased furfural in the bio-oil from the synthetic biomass. The different trends and products obtained from

the real biomass and the model compounds highlight that the structure of the lignocellulosic components in the biomass plays a significant role in the pyrolysis product distribution.

ii. The results of the pyrolysis in the MFR reactor show that there is a marginal effect on bio-oil and biochar yields at the heating rates investigated in this study. Temperature had the highest impact on the product yields. It was observed that the sweeping gas flow rate did not have a consistent effect on the biochar products, although some minor differences were noted. The results from bio-oil tested via GC-MS show a prevalence of phenolic compounds in the organic fraction while acetic acid was the predominant component in the aqueous phase. Therefore, this study shows the possibility to transform negative-value invasive common reed species into high-value energy and chemical products, such as acetic acid and phenols in bio-oil, and a biochar residue with increased aromaticity and polarity.

The biochar and aqueous phase of bio-oil produced by slow pyrolysis in the new unit under several operating conditions were investigated. At the selected temperatures ($\geq 500°C$) the biochars had a high degree of carbonization, confirmed by the high fixed carbon and low volatile content. The aromatic structure of the char was also confirmed by the high alkalinity of the biochars in solution. The biochars exhibited a decrease in surface area with increasing temperature, probably due to the cracking of the tar on the biochar surface. The biochar produced at 550°C, 1 L/min of N_2 and 60 minutes holding time exhibited the highest surface area (91 m^2/g). The aqueous phase bio-oil water content ranged from 62 to 79%. The highest acetic acid content of 94 g/L was observed for the sample produced at 650°C. Overall, the aqueous phase oil

exhibit similar water and acetic acid content over the selected temperature range with minor differences.

iii.   Design and develop a continuous pyrolysis unit to perform fast pyrolysis. The results from the pyrolysis runs showed good comparison with the data published in the literature. The pyrolysis unit allowed experiments to be performed with reliable and consistent results. It is necessary to pre-treat *Phragmites australis* to lower its ash content, when levoglucosan is the product of interest. In fact, compared to the untreated biomass, the treatments showed an increased levoglucosan yield of almost 5-fold. A concentration of around 200 g/L of levoglucosan was achieved in C_1 compared to 50 g/L when the biomass processed without any pretreatment. Based on these results, the important factor to consider when processing a biomass with high ash content are K and Na concentrations, since they had the highest impact on the total levoglucosan yield. After inorganic leaching the bio-oil yield increased from 50% to 57-58%, the only exceptions were the biomass pretreated with acetic acid at 90°C 24 h and with the Soxhlet extractor, in those cases the bio-oil yield achieved was lower at 55% and 51% respectively. The biochar decreased from 24-26% to 18-21%.

c.   The slow pyrolysis biochar produced in the new unit was activated to compare the performance of biochar and activated biochar on the adsorption of ibuprofen. Results showed that biochar produced under slow pyrolysis conditions at 550°C achieved 36% removal of 25 mg/L of ibuprofen when the pH was adjusted at 2, and biochar produced at 550°C under fast pyrolysis condition removed 55% of the ibuprofen in the solution at the same conditions (80 mg adsorbent dose, 22°C and 65 h). Whereas the activated biochar from *Phragmites australis* achieved total

removal without any pH adjustment. In particular, activated biochar from *Phragmites australis* showed adsorption capacity higher or similar to the ones obtained with a commercial activated carbon. This study showed that the activated biochar produced from *Phragmites australis* have excellent ibuprofen adsorption removal, this is promising for wastewater treatment applications.

8.2   Recommendations

The design and optimization of the pyrolysis conditions of the new unit showed that very good results in terms of products yields could be achieved.

Moreover, the experiments performed with the biomass with lower mineral content showed an increased bio-oil yield reaching almost 60 wt%. It is recommended to consider these results when designing the condensation unit based on low ash biomasses, which would likely require additional condensers.

It would be of interest to study the extraction of levoglucosan, acetic acid and phenolic compounds with the use of biochar and activated biochar to maximize the use of the pyrolysis products while minimizing the waste streams.

Moreover, the study of adsorption of contaminants from the water should be extended to different NSAIDs and pollutants of concerns as individual molecules and mixes to resemble real cases in water treatment plants. It would be interesting to evaluate the micro porosity of the biochars and activated biochar to complete the surface properties and to further investigate the possible mechanisms involved in the adsorption.

References

[1]   R. Vaičekonytė, E. Kiviat, F. Nsenga, A. Ostfeld, An exploration of common reed
        (*Phragmites australis*) bioenergy potential in North America, 2013.
        http://www.mires-and-peat.net/, (accessed March 21, 2019).

[2]   K. Saltonstall, D.P. Hauber, Notes on *Phragmites australis* (Poaceae:
        Arundinoideae) in North America, J. Bot. Res. Inst. Texas. 1 (2007) 385–388.
        doi:10.2307/41971424.

[3]   R.M. Chambers, L.A. Meyerson, K. Saltonstall, Expansion of *Phragmites australis*
        into tidal wetlands of North America, Aquat. Bot. 64 (1999) 261–273.
        doi:10.1016/S0304-3770(99)00055-8.

[4]   K. Saltonstall, Cryptic invasion by a non-native genotype of the common reed,
        Phragmites australis, into North America, Proc. Natl. Acad. Sci. 99 (2002) 2445–
        2449. doi:10.1073/pnas.032477999.

[5]   M. and A.S. Ontario. Ministry of Natural Resources. Science and Information
        Branch. Inventory, *Phragmites* in Ontario, (2010).

[6]   A. and P. Marinch, Best Management Practices in Ontario, (2016).
        https://www.ontarioinvasiveplants.ca/wp-content/uploads/2016/07/2016-
        Phragmites-Webinar_-Feb-3-2016_ALWL.pdf (accessed March 23, 2018).

[7]   M. Komulainen, P. Simi, E. Hagelberg, I. Ikonen, S. Lyytinen, Reed Energy:
        Possibilities of Using the Common Reed for Energy Generation in Southern
        Finland, 2008. http://julkaisut.turkuamk.fi (accessed April 16, 2020).

[8]   J. Li, Y. Qiao, P. Zong, S. Qin, C. Wang, Y. Tian, Fast pyrolysis characteristics of
        two typical coastal zone biomass fuels by thermal gravimetric analyzer and down
        tube reactor, Bioresour. Technol. 283 (2019) 96–105.

doi:10.1016/J.BIORTECH.2019.02.097.

[9] Y.-K.K. Park, M.L. Yoo, H.S. Heo, H.W. Lee, S.H.S.-S.S. Park, S.-C.C. Jung, S.H.S.-S.S. Park, S.-G.G. Seo, Wild reed of Suncheon Bay: Potential bio-energy source, Renew. Energy. 42 (2012) 168–172. doi:10.1016/j.renene.2011.08.025.

[10] N. Szijártó, Z. Kádár, E.E. Varga, A.B. Thomsen, M. Costa-Ferreira, K. Réczey, Pretreatment of reed by wet oxidation and subsequent utilization of the pretreated fibers for ethanol production, Appl. Biochem. Biotechnol. 155 (2009) 386–396. doi:10.1007/s12010-009-8549-4.

[11] N. Sathitsuksanoh, Z. Zhu, N. Templeton, J.A. Rollin, S.P. Harvey, Y.-H.H.P. Zhang, Saccharification of a potential bioenergy crop, *phragmites australis* (Common Reed), by lignocellulose fractionation followed by enzymatic hydrolysis at decreased cellulase loadings, Ind. Eng. Chem. Res. 48 (2009) 6441–6447. doi:10.1021/ie900291s.

[12] F. Cotana, G. Cavalaglio, A. Pisello, M. Gelosia, D. Ingles, E. Pompili, Sustainable Ethanol Production from Common Reed (*Phragmites australis*) through Simultaneuos Saccharification and Fermentation, Sustainability. 7 (2015) 12149–12163. doi:10.3390/su70912149.

[13] H. Zhao, H. Yan, C. Zhang, X. Liu, Y. Xue, Y. Qiao, Y. Tian, S. Qin, Pyrolytic characteristics and kinetics of *Phragmites australis*, Evidence-Based Complement. Altern. Med. 2011 (2011). doi:10.1155/2011/408973.

[14] K. Gao, S. Boiano, A. Marzocchella, L. Rehmann, Cellulosic butanol production from alkali-pretreated switchgrass (Panicum virgatum) and phragmites (*Phragmites australis*), Bioresour. Technol. 174 (2014) 176–181. doi:10.1016/j.biortech.2014.09.152.

[15] G. Trebbi, Power-production options from biomass: The vision of a southern European utility, Bioresour. Technol. 46 (1993) 23–29. doi:10.1016/0960-

8524(93)90050-L.

[16]   F.A. Agblevor, B. Rejai, R.J. Evans, K.D. Johnson, Pyrolytic analysis and catalytic
       upgrading of lignocellulosic materials by molecular beam mass spectrometry.,
       Energy from Biomass Wastes. 16 (1993) 767–795.

[17]   M.A. Delucchi, Impacts of biofuels on climate change, water use, and land use,
       Ann. N. Y. Acad. Sci. 1195 (2010) 28–45. doi:10.1111/j.1749-6632.2010.05457.x.

[18]   Perennial Grasses for Bioenergy and Bioproducts, Elsevier, 2018.
       doi:10.1016/c2016-0-03729-4.

[19]   A. V. Bridgwater, Review of fast pyrolysis of biomass and product upgrading,
       Biomass and Bioenergy. 38 (2012) 68–94. doi:10.1016/j.biombioe.2011.01.048.

[20]   D. Mohan, C.U. Pittman, P.H. Steele, Pyrolysis of Wood / Biomass for Bio-oil : A
       Critical Review, Energy & Fuesl. 20 (2006) 848–889. doi:10.1021/ef0502397.

[21]   A. V. Bridgwater, D. Meier, D. Radlein, An overview of fast pyrolysis of biomass,
       Org. Geochem. 30 (1999) 1479–1493. doi:10.1016/S0146-6380(99)00120-5.

[22]   S. Wang, Y. Wang, Q. Cai, X. Wang, H. Jin, Z. Luo, Multi-step separation of
       monophenols and pyrolytic lignins from the water-insoluble phase of bio-oil, Sep.
       Purif. Technol. 122 (2014) 248–255. doi:10.1016/j.seppur.2013.11.017.

[23]   L. Fele Žilnik, A. Jazbinšek, Recovery of renewable phenolic fraction from
       pyrolysis oil, Sep. Purif. Technol. 86 (2012) 157–170.
       doi:10.1016/j.seppur.2011.10.040.

[24]   D. Fu, S. Farag, J. Chaouki, P.G. Jessop, Extraction of phenols from lignin
       microwave-pyrolysis oil using a switchable hydrophilicity solvent, Bioresour.
       Technol. 154 (2014) 101–108. doi:10.1016/j.biortech.2013.11.091.

[25]   M.R. Rover, A. Aui, M.M. Wright, R.G. Smith, R.C. Brown, Production and
       purification of crystallized levoglucosan from pyrolysis of lignocellulosic biomass,

Green Chem. 21 (2019). doi:10.1039/c9gc02461a.

[26]   M.R. Rover, P.A. Johnston, T. Jin, R.G. Smith, R.C. Brown, L. Jarboe, Production of clean pyrolytic sugars for fermentation, ChemSusChem. 7 (2014) 1662–1668. doi:10.1002/cssc.201301259.

[27]   S.M. Haslam, Phragmites Communis Trin. (Arundo Phragmites L.,? Phragmites Australis (Cav.) Trin. ex Steudel), J. Ecol. 60 (1972) 585. doi:10.2307/2258363.

[28]   W.D. Clayton, The Correct Name of the Common Reed, Taxon. 17 (1968) 168–169. doi:10.2307/1216507.

[29]   K. Saltonstall, P.M. Peterson, R.J. Soreng, Recognition of Phragmites australis subsp. americanus (Poaceae: Arundinoideae) in North America: Evidence from morphological and genetic analyses, SIDA, Contrib. to Bot. 21 (2004) 683–692. https://repository.si.edu/bitstream/handle/10088/3352/Final_Saltonstall-etal_Phragmites_683-692.pdf (accessed March 18, 2019).

[30]   O.A. Clevering, J. Lissner, Taxonomy, chromosome numbers, clonal diversity and population dynamics of Phragmites australis, Aquat. Bot. 64 (1999) 185–208. doi:10.1016/S0304-3770(99)00059-5.

[31]   C. Lambertini, B.K. Sorrell, T. Riis, B. Olesen, H. Brix, Exploring the borders of European Phragmites within a cosmopolitan genus., AoB Plants. 2012 (2012) pls020. doi:10.1093/aobpla/pls020.

[32]   C. Lambertini, I.A. Mendelssohn, M.H.G. Gustafsson, B. Olesen, T. Riis, B.K. Sorrell, H. Brix, Tracing the origin of Gulf Coast Phragmites (Poaceae): A story of long-distance dispersal and hybridization, Source Am. J. Bot. 99 (2012) 538–551. doi:10.3732/ajb.

[33]   J. Swearingen, Phragmites field guide: distinguishing native and exotic forms of common reed (P*hragmites australis*) in the united states, 2012. http://www.nps.gov/plants/alien/pubs/index.htm (accessed March 18, 2019).

[34]   W.A. Niering, Our dynamic tidal marshes, vegetation changes as revealed by peat analysis: Connecticut Arboretum, Connecticut College, Bulletin no. 22, New London, Connecticut, 13 p., (1977). http://digitalcommons.conncoll.edu/arbbulletinshttp://digitalcommons.conncoll.edu/arbbulletins/21 (accessed March 18, 2019).

[35]   A. Richard, R.A. Orson, R.S. Warren, W.A. Niering, Development of a tidal marsh in a New England river valley, Estuaries and Coasts. 10 (1987) 20–27. https://link.springer.com/content/pdf/10.2307%2F1352021.pdf (accessed March 18, 2019).

[36]   P.M. Catling, G. Mitrow, The Recent Spread and Potential Distribution of *Phragmites australis* subsp. *australis* in Canada, Can. Field-Naturalist. 125 (2011) 95. doi:10.22621/cfn.v125i2.1187.

[37]   J. Suda, L.A. Meyerson, I.J. Leitch, P. Pyšek, The hidden side of plant invasions: the role of genome size, New Phytol. 205 (2015) 994–1007. doi:10.1111/nph.13107.

[38]   P. Pyšek, J. Čuda, P. Šmilauer, H. Skálová, Z. Chumová, C. Lambertini, M. Lučanová, H. Ryšavá, P. Trávníček, K. Šemberová, L.A. Meyerson, Competition among native and invasive *Phragmites australis* populations: An experimental test of the effects of invasion status, genome size, and ploidy level, Ecol. Evol. 10 (2020) 1106–1118. doi:10.1002/ece3.5907.

[39]   P. Pyšek, H. Skálová, J. Čuda, W.-Y. Guo, J. Suda, J. Doležal, O. Kauzál, C. Lambertini, M. Lučanová, T. Mandáková, L. Moravcová, K. Pyšková, H. Brix, L.A. Meyerson, Small genome separates native and invasive populations in an ecologically important cosmopolitan grass, Ecology. 99 (2018) 79–90. doi:10.1002/ecy.2068.

[40]   T.K. Mal, L. Narine, The biology of Canadian weeds. 129. *Phragmites australis* (Cav.) Trin. ex Steud., Can. J. Plant Sci. 84 365–396. www.nrcresearchpress.com

(accessed March 18, 2019).

[41] J.S. Caplan, C. Wheaton, T.J. Mozdzer, SPECIAL ISSUE : *Phragmites australis* in
      North America and Europe OPEN ACCESS -RESEARCH ARTICLE
      Belowground advantages in construction cost facilitate a cryptic plant, (2014).

[42] C. Deakin, R. Ferguson, B. Hope, D. Featherstone, Mapping and Removal of
      Phragmites australis along Western Collingwood Shoreline through Community
      Action and Local Partnerships, 2016. https://www.nvca.on.ca/Shared
      Documents/Phragmites Management in Collingwood 2015 2016 Summary
      Report.pdf (accessed October 30, 2018).

[43] E.L.G. Hazelton, T.J. Mozdzer, D.M. Burdick, K.M. Kettenring, D.F. Whigham,
      Phragmites australis management in the United States: 40 years of methods and
      outcomes, AoB Plants. 6 (2014). doi:10.1093/aobpla/plu001.

[44] R. Ferguson, B. Hope, D. Featherstone, Mapping and Removal of *Phragmites
      australis* along Western Collingwood Shoreline through Community Action and
      Local Partnerships, 2015. https://www.nvca.on.ca/Shared
      Documents/Phragmites_Management_in_Collingwood_Ontario_Report_2015.pdf
      (accessed October 30, 2018).

[45] M.S. Ailstock, C.M. Norman, P.J. Bushmann, Common Reed *Phragmites
      australis*: Control and Effects Upon Biodiversity in Freshwater Nontidal Wetlands,
      Restor. Ecol. 9 (2001) 49–59. doi:10.1046/j.1526-100x.2001.009001049.x.

[46] N.R. Cowie, W.J. Sutherland, M.K.M. Ditlhogo, R. James, The Effects of
      Conservation Management of Reed Beds. II. The Flora and Litter Disappearance,
      J. Appl. Ecol. 29 (1992) 277. doi:10.2307/2404496.

[47] S.E. Hellings, J.L. Gallagher, The Effects of Salinity and Flooding on *Phragmites
      australis*, J. Appl. Ecol. 29 (2006) 41. doi:10.2307/2404345.

[48] Sara Finnimore and Sarah Campbell, Mapping and Removal of *Phragmites*

australis along Western Collingwood Shoreline through Community Action and Local Partnerships, 2017. https://www.nvca.on.ca/Shared Documents/2017_Phrag_Report_NVCA.pdf (accessed March 21, 2019).

[49]   Ü. Kask, L. Kask, S. Link, Combustion characteristics of reed and its suitability as a boiler fuel, Mires Peat. 13 (2013) 1–10. http://www.mires-and-peat.net/, (accessed May 4, 2020).

[50]   K. Baute, L.L. Van Eerd, D.E. Robinson, P.H. Sikkema, M. Mushtaq, B.H. Gilroyed, K. Baute, L.L. Van Eerd, D.E. Robinson, P.H. Sikkema, M. Mushtaq, B.H. Gilroyed, Comparing the Biomass Yield and Biogas Potential of Phragmites australis with Miscanthus x giganteus and Panicum virgatum Grown in Canada, Energies. 11 (2018) 2198. doi:10.3390/en11092198.

[51]   K.A. Baute, D.E. Robinson, L.L. Van Eerd, M. Edson, P.H. Sikkema, B.H. Gilroyed, Survival of seeds from perennial biomass species during commercial-scale anaerobic digestion, Weed Res. 56 (2016) 258–266. doi:10.1111/wre.12202.

[52]   H. Sutcu, Pyrolysis of *Phragmites australis* and characterization of liquid and solid products, J. Ind. Eng. Chem. 14 (2008) 573–577. doi:10.1016/j.jiec.2008.04.012.

[53]   H. Zhao, H. Yan, C. Zhang, B. Sun, Y. Zhang, S. Dong, Y. Xue, S. Qin, Thermogravimetry study of pyrolytic characteristics and kinetics of the giant wetland plant *Phragmites australis*, J. Therm. Anal. Calorim. 110 (2012) 611–617. doi:10.1007/s10973-011-2018-3.

[54]   F. Patuzzi, T. Mimmo, S. Cesco, A. Gasparella, M. Baratieri, Common reeds (*Phragmites australis*) as sustainable energy source: Experimental and modelling analysis of torrefaction and pyrolysis processes, GCB Bioenergy. 5 (2013) 367–374. doi:10.1111/gcbb.12000.

[55]   M. Baratieri, F. Patuzzi, N. Thevs, S. Zerbe, Assessment of suitable energy conversion scenarios of common reeds, *Phragmites australis*, 19th Eur. Biomass

Conf. Exhib. (2011) 1501–1514. doi:10.5071/19thEUBCE2011-VP2.3.38.

[56]   R. Garrido, J. Reckamp, J. Satrio, Effects of Pretreatments on Yields, Selectivity and Properties of Products from Pyrolysis of *Phragmites australis* (Common Reeds), Environments. 4 (2017) 96. doi:10.3390/environments4040096.

[57]   P. Liu, M. Yue, H. Zhang, Adsorptive performance of Ni(II) from aqueous solutions using biochar made of *Phragmites australis* by adding ammonium polyphosphate as flame retardant, J. Chem. 2016 (2016). doi:10.1155/2016/1797396.

[58]   World of Plants, n.d. https://www.bookdepository.com/Usborne-World-Plants-L-Howell/9780746046166 (accessed April 16, 2020).

[59]   P. Basu, Biomass Gasification, Pyrolysis and Torrefaction: Practical Design and Theory, Elsevier Inc., 2013. doi:10.1016/C2011-0-07564-6.

[60]   S. Wang, Z. Luo, Pyrolysis of biomass, De Gruyter, Berlin, Boston, 2017. doi:10.1201/b18314-17.

[61]   A. Heredia, A. Jim6nez, R. Guill6n, Composition of plant cell walls, 1995.

[62]   V.B. Agbor, N. Cicek, R. Sparling, A. Berlin, D.B. Levin, Biomass pretreatment: Fundamentals toward application, Biotechnol. Adv. 29 (2011) 675–685. doi:10.1016/j.biotechadv.2011.05.005.

[63]   J. Pérez, J. Muñoz-Dorado, T. De La Rubia, J. Martínez, Biodegradation and biological treatments of cellulose, hemicellulose and lignin: An overview, Int. Microbiol. 5 (2002) 53–63. doi:10.1007/s10123-002-0062-3.

[64]   B. Pecha, M. Garcia-Perez, Pyrolysis of Lignocellulosic Biomass, in: A. Dahiya (Ed.), Bioenergy, Elsevier, 2015: pp. 413–442. doi:10.1016/b978-0-12-407909-0.00026-2.

[65]   S. Vorwerk, S. Somerville, C. Somerville, The role of plant cell wall

polysaccharide composition in disease resistance, Trends Plant Sci. 9 (2004) 203–209. doi:10.1016/j.tplants.2004.02.005.

[66] V. Dhyani, T. Bhaskar, Pyrolysis of Biomass, in: S.R. Ashok Pandey, Christian Larroche, Claude-Gilles Dussap, Edgard Gnansounou, Samir Kumar Khanal (Ed.), Biofuels Altern. Feed. Convers. Process. Prod. Liq. Gaseous Biofuels, Academic Press, 2019: pp. 217–244. doi:10.1016/B978-0-12-816856-1.00009-9.

[67] A.P. Karmanov, O.Y. Derkacheva, Application of fourier transform infrared spectroscopy for the study of lignins of herbaceous plants, Russ. J. Bioorganic Chem. 39 (2013) 677–685. doi:10.1134/S1068162013070066.

[68] R. Schmid, L. Graham, J. Graham, L. Wilcox, K. Stern, J. Bidlack, S. Jansky, G. Uno, Plant Biology, Taxon. 54 (2005) 573. doi:10.2307/25065406.

[69] Z. Jin, K.S. Katsumata, T.B.T. Lam, K. Iiyama, Covalent linkages between cellulose and lignin in cell walls of coniferous and nonconiferous woods, Biopolymers. 83 (2006) 103–110. doi:10.1002/bip.20533.

[70] A. Ephraim, P. Arlabosse, A. Nzihou, D. Pham Minh, P. Sharrock, Biomass Categories, in: Handb. Charact. Biomass, Biowaste Relat. By-Products, Springer International Publishing, Cham, 2020: pp. 1–29. doi:10.1007/978-3-030-35020-8_1.

[71] T. Tscharntke, H.-J. Greiler, Insect communities, grasses, and grasslands, 1995. www.annualreviews.org (accessed April 22, 2020).

[72] M. Hoekstra, E. , Westerhof, R. J., Brilman, W. , Van Swaaij, W. P., Kersten, S. R., Hogendoorn, K. J. and Windt, Heterogeneous and homogeneous reactions of pyrolysis vapors from pine wood., AIChE J. 58 (2012) 2830-2842. doi:10.1002/aic.

[73] P. Thy, B.M. Jenkins, S. Grundvig, R. Shiraki, C.E. Lesher, High temperature elemental losses and mineralogical changes in common biomass ashes, Fuel. 85

(2006) 783–795. doi:10.1016/j.fuel.2005.08.020.

[74]   T.R. Miles, L.L. Baxter, R.W. Bryers, B.M. Jenkins, L.L. Oden, Alkali deposits found in biomass power plants, Vol 1, NREL Rep. I (1995) 1–122. doi:10.1017/CBO9781107415324.004.

[75]   K. Raveendran, A. Ganesh, K.C. Khilar, Influence of mineral matter on biomass pyrolysis characteristics, Fuel. 74 (1995) 1812–1822. doi:10.1016/0016-2361(95)80013-8.

[76]   A.G.W. Bradbury, Y. Sakai, F. Shafizadeh, A kinetic model for pyrolysis of cellulose, J. Appl. Polym. Sci. 23 (1979) 3271–3280. doi:10.1002/app.1979.070231112.

[77]   J. Piskorz, D.S.A.G. Radlein, D.S. Scott, S. Czernik, Pretreatment of wood and cellulose for production of sugars by fast pyrolysis, J. Anal. Appl. Pyrolysis. 16 (1989) 127–142. doi:10.1016/0165-2370(89)85012-0.

[78]   M.J. Antal, G. Varhegyi, Cellulose Pyrolysis Kinetic: The Current State of Knowledge, Ind. Eng. Chem. Res. 34 (1995) 703–717. doi:10.1021/ie00042a001.

[79]   F. Shafizadeh, R.H. Furneaux, T.G. Cochran, J.P. Scholl, Y. Sakai, Production of levoglucosan and glucose from pyrolysis of cellulosic materials, J. Appl. Polym. Sci. 23 (1979) 3525–3539. doi:10.1002/app.1979.070231209.

[80]   O. Boutin, M. Ferrer, J. Lédé, Radiant flash pyrolysis of cellulose - Evidence for the formation of short life time intermediate liquid species, J. Anal. Appl. Pyrolysis. 47 (1998) 13–31. doi:10.1016/S0165-2370(98)00088-6.

[81]   T. Fisher, M. Hajaligol, B. Waymack, D. Kellogg, Pyrolysis behavior and kinetics of biomass derived materials, J. Anal. Appl. Pyrolysis. 62 (2002) 331–349. doi:10.1016/S0165-2370(01)00129-2.

[82]   Z. Wang, A.G. McDonald, R.J.M. Westerhof, S.R.A. Kersten, C.M. Cuba-Torres,

S. Ha, B. Pecha, M. Garcia-Perez, Effect of cellulose crystallinity on the formation of a liquid intermediate and on product distribution during pyrolysis, J. Anal. Appl. Pyrolysis. 100 (2013) 56–66. doi:10.1016/j.jaap.2012.11.017.

[83] F. Shafizadeh, Introduction to pyrolysis of biomass, J. Anal. Appl. Pyrolysis. 3 (1982) 283–305. doi:10.1016/0165-2370(82)80017-X.

[84] F. Shafizadeh, Pyrolysis and Combustion of Cellulosic Materials, Adv. Carbohydr. Chem. 23 (1968) 419–474. doi:10.1016/S0096-5332(08)60173-3.

[85] M.J. Antal, Biomass Pyrolysis: A Review of the Literature Part 1—Carbohydrate Pyrolysis, in: Adv. Sol. Energy, Springer New York, 1983: pp. 61–111. doi:10.1007/978-1-4684-8992-7_3.

[86] Kilzer, FJ, A. Broido, Speculations on the nature of cellulose pyrolysis, in: Pyrodynamics, 1965: p. 151—163.

[87] E.M. Essig, M. G.; Richards, G. N.; Schenck, Mechanism of Formation of the Major Volatile Products from Pyrolysis of Cellulose, Schuerch, J. Wiley & Sons:, 1989.

[88] J. Scheirs, G. Camino, W. Tumiatti, Overview of water evolution during the thermal degradation of cellulose, Eur. Polym. J. 37 (2001) 933–942. doi:10.1016/S0014-3057(00)00211-1.

[89] D.K. Shen, S. Gu, The mechanism for thermal decomposition of cellulose and its main products, Bioresour. Technol. 100 (2009) 6496–6504. doi:10.1016/j.biortech.2009.06.095.

[90] G.N. Richards, Glycolaldehyde from pyrolysis of cellulose, J. Anal. Appl. Pyrolysis. 10 (1987) 251–255. doi:10.1016/0165-2370(87)80006-2.

[91] X. Zhou, W. Li, R. Mabon, L.J. Broadbelt, A Critical Review on Hemicellulose Pyrolysis, Energy Technol. 5 (2017) 52–79. doi:10.1002/ente.201600327.

[92]   F. Shafizadeh, G.D. McGinnis, C.W. Philpot, Thermal degradation of xylan and related model compounds, Carbohydr. Res. 25 (1972) 23–33. doi:10.1016/S0008-6215(00)82742-1.

[93]   Y. Peng, S. Wu, The structural and thermal characteristics of wheat straw hemicellulose, J. Anal. Appl. Pyrolysis. 88 (2010) 134–139. doi:10.1016/j.jaap.2010.03.006.

[94]   P.R. Patwardhan, R.C. Brown, B.H. Shanks, Product distribution from the fast pyrolysis of hemicellulose, ChemSusChem. 4 (2011) 636–643. doi:10.1002/cssc.201000425.

[95]   X. Zhou, W. Li, R. Mabon, L.J. Broadbelt, Energy & Environmental Science A mechanistic model of fast pyrolysis of hemicellulose A mechanistic model of fast pyrolysis of hemicellulose †, Energy Environ. Sci. 11 (2018) 1240. doi:10.1039/c7ee03208k.

[96]   D. Ferdous, A.K. Dalai, S.K. Bej, R.W. Thring, Pyrolysis of Lignins: Experimental and Kinetics Studies, (2002). doi:10.1021/ef0200323.

[97]   M.G.D.M. Nassar, Mamdouh M., Mechanism of Thermal Decomposition of Lignin, Wood Fiber Sci. 16 (1984) 441–453. https://wfs.swst.org/index.php/wfs/article/view/262/262 (accessed April 17, 2020).

[98]   R.J. Evans, T.A. Milne, M.N. Soltys, Direct mass-spectrometric studies of the pyrolysis of carbonaceous fuels. III. Primary pyrolysis of lignin, J. Anal. Appl. Pyrolysis. 9 (1986) 207–236. doi:10.1016/0165-2370(86)80012-2.

[99]   M. Asmadi, H. Kawamoto, S. Saka, Thermal reactions of guaiacol and syringol as lignin model aromatic nuclei, J. Anal. Appl. Pyrolysis. 92 (2011) 88–98. doi:10.1016/j.jaap.2011.04.011.

[100] M. Asmadi, H. Kawamoto, S. Saka, Gas- and solid/liquid-phase reactions during pyrolysis of softwood and hardwood lignins, J. Anal. Appl. Pyrolysis. 92 (2011)

417–425. doi:10.1016/j.jaap.2011.08.003.

[101] R.J. Evans, T. a Milne, Molecular characterization of pyrolysis of biomass. 1. Fundamentals, Energy & Fuels. 1 (1987) 123–138. doi:0887-0624/87/2501-0123.

[102] C. Saiz-Jimenez, J.W. De Leeuw, Lignin pyrolysis products: Their structures and their significance as biomarkers, Org. Geochem. 10 (1986) 869–876. doi:10.1016/S0146-6380(86)80024-9.

[103] H. Yang, R. Yan, H. Chen, D.H. Lee, C. Zheng, Characteristics of hemicellulose, cellulose and lignin pyrolysis, Fuel. 86 (2007) 1781–1788. doi:10.1016/J.FUEL.2006.12.013.

[104] Y.-C. Qu, Z. Wang, Q. Lu, Y. Zhang, Selective Production of 4-Vinylphenol by Fast Pyrolysis of Herbaceous Biomass, (2013). doi:10.1021/ie401626d.

[105] T.R. Nunn, J.B. Howard, J.P. Longwell, W.A. Peters, Product Compositions and Kinetics in the Rapid Pyrolysis of Sweet Gum Hardwood, Ind. Eng. Chem. Process Des. Dev. 24 (1985) 836–844. doi:10.1021/i200030a053.

[106] M. V. Ramiah, Thermogravimetric and differential thermal analysis of cellulose, hemicellulose, and lignin, J. Appl. Polym. Sci. 14 (1970) 1323–1337. doi:10.1002/app.1970.070140518.

[107] P. Murugan, N. Mahinpey, K.E. Johnson, M. Wilson, Kinetics of the Pyrolysis of Lignin Using Thermogravimetric and Differential Scanning Calorimetry Methods, (n.d.). doi:10.1021/ef700730u.

[108] A. Oasmaa, I. Fonts, M.R. Pelaez-Samaniego, M.E. Garcia-Perez, M. Garcia-Perez, Pyrolysis Oil Multiphase Behavior and Phase Stability: A Review, Energy and Fuels. 30 (2016) 6179–6200. doi:10.1021/acs.energyfuels.6b01287.

[109] S. Turn, C. Kinoshita, D. Ishimura, B. Jenkins, J. Zhou, Leaching of Alkalis in Biomass Using Banagrass as a Prototype Herbaceous Species, 2003.

http://www.osti.gov/bridge (accessed April 18, 2020).

[110] B.M. Jenkins, R.R. Bakker, J.B. Wei, On the properties of washed straw, Biomass and Bioenergy. 10 (1996) 177–200. doi:10.1016/0961-9534(95)00058-5.

[111] P.R. Patwardhan, J.A. Satrio, R.C. Brown, B.H. Shanks, Influence of inorganic salts on the primary pyrolysis products of cellulose, Bioresour. Technol. 101 (2010) 4646–4655. doi:10.1016/j.biortech.2010.01.112.

[112] J. Piskorz, D. Radlein, D.S. Scott, On the mechanism of the rapid pyrolysis of cellulose, J. Anal. Appl. Pyrolysis. 9 (1986) 121–137. doi:10.1016/0165-2370(86)85003-3.

[113] P.M. Molton, Reaction Mechanisms in Cellulose Pyrolysis, (1977) 178.

[114] J. Piskorz, P. Majerski, D. Radlein, A. Vladars-Usas, D.S. Scott, Flash pyrolysis of cellulose for production of anhydro-oligomers, J. Anal. Appl. Pyrolysis. 56 (2000) 145–166. doi:10.1016/S0165-2370(00)00089-9.

[115] P. Das, A. Ganesh, P. Wangikar, Influence of pretreatment for deashing of sugarcane bagasse on pyrolysis products, Biomass and Bioenergy. 27 (2004) 445–457. doi:10.1016/j.biombioe.2004.04.002.

[116] L. Jiang, S. Hu, L. shi Sun, S. Su, K. Xu, L. mo He, J. Xiang, Influence of different demineralization treatments on physicochemical structure and thermal degradation of biomass, Bioresour. Technol. 146 (2013) 254–260. doi:10.1016/j.biortech.2013.07.063.

[117] X. Liu, X.T. Bi, Removal of inorganic constituents from pine barks and switchgrass, Fuel Process. Technol. 92 (2011) 1273–1279. doi:10.1016/j.fuproc.2011.01.016.

[118] D. Carpenter, T.L. Westover, S. Czernik, W. Jablonski, Biomass feedstocks for renewable fuel production: a review of the impacts of feedstock and pretreatment

on the yield and product distribution of fast pyrolysis bio-oils and vapors, Green Chem. 16 (2014) 384–406. doi:10.1039/C3GC41631C.

[119] D.S.A.G. Radlein, J. Piskorz, A. Grinshpun, D.S. Scott, FAST PYROLYSIS OF PRE-TREATED WOOD AND CELLULOSE., in: ACS Div. Fuel Chem. Prepr., 1987: pp. 29–35. https://web.anl.gov/PCS/acsfuel/preprint archive/Files/32_2_DENVER_04-87_0029.pdf (accessed April 24, 2018).

[120] R. Fahmi, A. V. Bridgwater, L.I. Darvell, J.M. Jones, N. Yates, S. Thain, I.S. Donnison, The effect of alkali metals on combustion and pyrolysis of Lolium and Festuca grasses, switchgrass and willow, Fuel. 86 (2007) 1560–1569. doi:10.1016/j.fuel.2006.11.030.

[121] N. Kuzhiyil, D. Dalluge, X. Bai, K.H. Kim, R.C. Brown, Pyrolytic sugars from cellulosic biomass, 2012. doi:10.1002/cssc.201200341.

[122] S.R.G. Oudenhoven, R.J.M. Westerhof, N. Aldenkamp, D.W.F. Brilman, S.R.A. Kersten, Demineralization of wood using wood-derived acid: Towards a selective pyrolysis process for fuel and chemicals production, in: J. Anal. Appl. Pyrolysis, Elsevier B.V., 2013: pp. 112–118. doi:10.1016/j.jaap.2012.10.002.

[123] S.R.G. Oudenhoven, R.J.M. Westerhof, S.R.A. Kersten, Fast pyrolysis of organic acid leached wood, straw, hay and bagasse: Improved oil and sugar yields, J. Anal. Appl. Pyrolysis. 116 (2015) 253–262. doi:10.1016/j.jaap.2015.09.003.

[124] S.R.G. Oudenhoven, Improving the selectivity of pyrolysis by pyrolytic acid leaching of biomass : the role of AAEMs, anhydrosugar production and process design & evaluation, University of Twente, 2016. doi:10.3990/1.9789036541381.

[125] S.R.G. Oudenhoven, A.G.J. van der Ham, H. van den Berg, R.J.M. Westerhof, S.R.A. Kersten, Using pyrolytic acid leaching as a pretreatment step in a biomass fast pyrolysis plant: Process design and economic evaluation, Biomass and

Bioenergy. 95 (2016) 388–404. doi:10.1016/j.biombioe.2016.07.003.

[126] A. V. Bridgwater, Principles and practice of biomass fast pyrolysis, J. Anal. Appl. Pyrolysis. 51 (1999) 3–22. doi:https://doi.org/10.1016/S0165-2370(99)00005-4.

[127] A. V. Bridgwater, G.V.C. Peacocke, Fast pyrolysis processes for biomass, Renew. Sustain. Energy Rev. 4 (2000) 1–73. doi:10.1016/S1364-0321(99)00007-6.

[128] P.W. Venderbosch RH, Fast pyrolysis technology development, Biofuels, Bioprod. Biorefining. (2010) 178–208. doi:10.1002/bbb.

[129] K. Maniatis, J. Baeyens, H. Peeters, G. Roggeman, The EGEMIN Flash Pyrolysis Process: Commissioning and Initial Results, in: Adv. Thermochem. Biomass Convers., Springer Netherlands, 1993: pp. 1257–1264. doi:10.1007/978-94-011-1336-6_98.

[130] J. Lédé, H.Z. Li, J. Villermaux, H. Martin, Fusion-like behaviour of wood pyrolysis, J. Anal. Appl. Pyrolysis. 10 (1987) 291–308. doi:10.1016/0165-2370(87)80019-0.

[131] J. Lede, J. Panagopoulos, H.Z. Li, J. Villermaux, Fast pyrolysis of wood: direct measurement and study of ablation rate, Fuel. 64 (1985) 1514–1520. doi:10.1016/0016-2361(85)90365-5.

[132] G.V.C. Peacocke, A. V. Bridgwater, Design of a Novel Ablative Pyrolysis Reactor, in: Adv. Thermochem. Biomass Convers., Springer Netherlands, 1993: pp. 1134–1150. doi:10.1007/978-94-011-1336-6_88.

[133] A. V. Bridgwater, Challenges and Opportunities in Fast Pyrolysis of Biomass: Part I, Johnson Matthey Technol. Rev. 62 (2018) 118–130. doi:10.1595/205651318X696693.

[134] B.M. Wagenaar, W. Prins, W.P.M. van Swaaij, Pyrolysis of biomass in the rotating cone reactor: modelling and experimental justification, Chem. Eng. Sci. 49

(1994) 5109–5126. doi:10.1016/0009-2509(94)00392-0.

[135] BTL pyrolysis technology - BTG Bioliquids BV, (n.d.). https://www.btg-btl.com/en/technology (accessed June 11, 2020).

[136] D. Meier, O. Faix, State of the art of applied fast pyrolysis of lignocellulosic materials — a review, Bioresour. Technol. 68 (1999) 71–77. doi:10.1016/S0960-8524(98)00086-8.

[137] E. Technologies, RTP GREEN FUEL: AN OVERVIEW FOR RENEWABLE HEAT AND POWER, n.d.

[138] RTP Biomass Conversion, (n.d.). https://uop.honeywell.com/en/industry-solutions/renewable-fuels/rtp-biomass-conversion (accessed June 11, 2020).

[139] A. Oasmaa, Y. Solantausta, V. Arpiainen, E. Kuoppala, K. Sipilä, Fast pyrolysis bio-oils from wood and agricultural residues, Energy and Fuels. 24 (2010) 1380–1388. doi:10.1021/ef901107f.

[140] C. Pfitzer, N. Dahmen, N. Tröger, F. Weirich, J. Sauer, A. Günther, M. Müller-Hagedorn, Fast Pyrolysis of Wheat Straw in the Bioliq Pilot Plant, Energy and Fuels. 30 (2016) 8047–8054. doi:10.1021/acs.energyfuels.6b01412.

[141] E. Henrich, N. Dahmen, F. Weirich, R. Reimert, C. Kornmayer, Fast pyrolysis of lignocellulosics in a twin screw mixer reactor, Fuel Process. Technol. 143 (2016) 151–161. doi:10.1016/j.fuproc.2015.11.003.

[142] A. Demirbas, G. Arin, An Overview of Biomass Pyrolysis, Energy Sources. 24 (2002) 471–482. doi:10.1080/00908310252889979.

[143] J.A. Garcia-Nunez, M.R. Pelaez-Samaniego, M.E. Garcia-Perez, I. Fonts, J. Abrego, R.J.M. Westerhof, M. Garcia-Perez, Historical Developments of Pyrolysis Reactors: A Review, Energy and Fuels. 31 (2017) 5751–5775. doi:10.1021/acs.energyfuels.7b00641.

[144] Y.-H. Kiang, Other and emerging alternative energy technology, in: Fuel Prop. Estim. Combust. Process Charact., Elsevier, 2018: pp. 363–401. doi:10.1016/b978-0-12-813473-3.00010-6.

[145] Y. Mei, R. Liu, Q. Yang, H. Yang, J. Shao, C. Draper, S. Zhang, H. Chen, Torrefaction of cedarwood in a pilot scale rotary kiln and the influence of industrial flue gas, Bioresour. Technol. 177 (2015) 355–360. doi:10.1016/j.biortech.2014.10.113.

[146] W. Klose, W. Wiest, Experiments and mathematical modeling of maize pyrolysis in a rotary kiln, Fuel. 78 (1999) 65–72. doi:10.1016/S0016-2361(98)00124-0.

[147] W.R. Tsai, C.I. Lin, On the mixing of granular materials in a screw feeder, Powder Technol. 80 (1994) 119–126. doi:10.1016/0032-5910(94)02839-7.

[148] C.M. Belcher, Fire Phenomena and the Earth System, John Wiley & Sons, Oxford, 2013. doi:10.1002/9781118529539.

[149] R.J.M. Westerhof, D.W.F. Brilman, M. Garcia-Perez, Z. Wang, S.R.G. Oudenhoven, W.P.M. Van Swaaij, S.R.A. Kersten, Fractional condensation of biomass pyrolysis vapors, Energy and Fuels. 25 (2011) 1817–1829. doi:10.1021/ef2000322.

[150] A. Tumbalam Gooty, D. Li, C. Briens, F. Berruti, Fractional condensation of bio-oil vapors produced from birch bark pyrolysis, Sep. Purif. Technol. 124 (2014) 81–88. doi:10.1016/j.seppur.2014.01.003.

[151] A.-C.C. Johansson, K. Iisa, L. Sandström, H. Ben, H. Pilath, S. Deutch, H. Wiinikka, O.G.W. Öhrman, Fractional condensation of pyrolysis vapors produced from Nordic feedstocks in cyclone pyrolysis, J. Anal. Appl. Pyrolysis. 123 (2017) 244–254. doi:10.1016/J.JAAP.2016.11.020.

[152] A.S. Pollard, M.R. Rover, R.C. Brown, Characterization of bio-oil recovered as stage fractions with unique chemical and physical properties, J. Anal. Appl.

Pyrolysis. 93 (2012) 129–138. doi:10.1016/j.jaap.2011.10.007.

[153] M.R. Rover, P.A. Johnston, L.E. Whitmer, R.G. Smith, R.C. Brown, The effect of pyrolysis temperature on recovery of bio-oil as distinctive stage fractions, J. Anal. Appl. Pyrolysis. 105 (2014) 262–268. doi:10.1016/J.JAAP.2013.11.012.

[154] E. de Jong, H. Stichnothe, G. Bell, M. Henning Jørgensen, I. de Bari, E. Jacco van Haveren, J. Lindorfer, E. an der Johannes Kepler, Bio-Based Chemicals A 2020 Update Bio-Based Chemicals With input from: (pdf version) Published by IEA Bioenergy, 2020.

[155] B. Sukhbaatar, P.H. Steele, M.G. Kim, Use of lignin separated from bio-oil in oriented strand board binder phenol-formaldehyde resins, BioResources. 4 (2009) 789–804. doi:10.15376/biores.4.2.789-804.

[156] A. Effendi, H. Gerhauser, A. V. Bridgwater, Production of renewable phenolic resins by thermochemical conversion of biomass: A review, Renew. Sustain. Energy Rev. 12 (2008) 2092–2116. doi:10.1016/j.rser.2007.04.008.

[157] J.S. Kim, Production, separation and applications of phenolic-rich bio-oil - A review, Bioresour. Technol. 178 (2015) 90–98. doi:10.1016/j.biortech.2014.08.121.

[158] C.M. Lakshmanan, B. Gal-Or, H.E. Hoelscher, Production of Levoglucosan by Pyrolysis of Carbohydrates, Starch - Stärke. 22 (1970) 221–227. doi:10.1002/star.19700220703.

[159] P.J. Hodges, G. Procter, 1,6-Anhydroglucose in organic synthesis; preparation of fragments suitable for natural product synthesis, Tetrahedron Lett. 26 (1985) 4111–4114. doi:10.1016/S0040-4039(00)89306-5.

[160] V. Bailliez, A. Olesker, J. Cleophax, Synthesis of polynitrogenated analogues of glucopyranoses from levoglucosan, Tetrahedron. 60 (2004) 1079–1085. doi:10.1016/j.tet.2003.11.080.

[161] S. Czernik, A. V. Bridgwater, Overview of Applications of Biomass Fast Pyrolysis Oil, Energy & Fuels. 18 (2004) 590–598. doi:10.1021/ef034067u.

[162] Acetic Acid Prices, Markets & Analysis | ICIS, (n.d.). https://www.icis.com/explore/commodities/chemicals/acetic-acid/ (accessed April 26, 2020).

[163] C.H. Associates, G.W.S. Cole, H. Associates, S. Andrews Lane, BIO-OIL COMMERCIALIZATION PLAN Bio-Oil Commercialization Plan BIO-OIL COMMERCIALIZATION PLAN, 2004.

[164] T. Tobin, R. Gustafson, R. Bura, H.L. Gough, Integration of wastewater treatment into process design of lignocellulosic biorefineries for improved economic viability, Biotechnol. Biofuels. 13 (2020) 24. doi:10.1186/s13068-020-1657-7.

[165] B.M. Jenkins, J.D. Mannapperuma, R.R. Bakker, Biomass leachate treatment by reverse osmosis, Fuel Process. Technol. 81 (2003) 223–246. doi:10.1016/S0378-3820(03)00010-9.

[166] A.R. Rajabzadeh, N. Ruzich, S. Zendehboudi, M. Rahbari, Biomass leachate treatment and nutrient recovery using reverse osmosis: Experimental study and hybrid artificial neural network modeling, Energy and Fuels. 26 (2012) 7155–7163. doi:10.1021/ef301452s.

[167] R. Teoh, E. Caro, D.B. Holman, S. Joseph, S.J. Meale, A. V. Chaves, Effects of Hardwood Biochar on Methane Production, Fermentation Characteristics, and the Rumen Microbiota Using Rumen Simulation, Front. Microbiol. 10 (2019) 1534. doi:10.3389/fmicb.2019.01534.

[168] S.A. Terry, G.O. Ribeiro, R.J. Gruninger, A. V. Chaves, K.A. Beauchemin, E. Okine, T.A. McAllister, A Pine Enhanced Biochar Does Not Decrease Enteric CH4 Emissions, but Alters the Rumen Microbiota, Front. Vet. Sci. 6 (2019) 308. doi:10.3389/fvets.2019.00308.

[169] H.P. Schmidt, N. Hagemann, K. Draper, C. Kammann, The use of biochar in animal feeding, PeerJ. 2019 (2019). doi:10.7717/peerj.7373.

[170] N.A. Salem, S.M. Yakoot, Non-steroidal anti-inflammatory drug, ibuprofen adsorption using rice straw based biochar, Int. J. Pharmacol. 12 (2016) 729–736. doi:10.3923/ijp.2016.729.736.

[171] J. Rivera-Utrilla, I. Bautista-Toledo, M.A. Ferro-García, C. Moreno-Castilla, Activated carbon surface modifications by adsorption of bacteria and their effect on aqueous lead adsorption, J. Chem. Technol. Biotechnol. 76 (2001) 1209–1215. doi:10.1002/jctb.506.

[172] P. Chakraborty, S. Show, S. Banerjee, G. Halder, Mechanistic insight into sorptive elimination of ibuprofen employing bi-directional activated biochar from sugarcane bagasse: Performance evaluation and cost estimation, J. Environ. Chem. Eng. 6 (2018) 5287–5300. doi:10.1016/J.JECE.2018.08.017.

[173] A.S. Mestre, J. Pires, J.M.F. Nogueira, J.B. Parra, A.P. Carvalho, C.O. Ania, Waste-derived activated carbons for removal of ibuprofen from solution: Role of surface chemistry and pore structure, Bioresour. Technol. 100 (2009) 1720–1726. doi:10.1016/j.biortech.2008.09.039.

[174] R. Baccar, M. Sarrà, J. Bouzid, M. Feki, P. Blánquez, Removal of pharmaceutical compounds by activated carbon prepared from agricultural by-product, Chem. Eng. J. 211–212 (2012) 310–317. doi:10.1016/j.cej.2012.09.099.

[175] O. Adam, Removal of Resorcinol from Aqueous Solution by Activated Carbon: Isotherms, Thermodynamics and Kinetics, Am. Chem. Sci. J. 16 (2016) 1–13. doi:10.9734/acsj/2016/27637.

[176] C.-A. Lin, T.-C. An, Y.-H. Hsu, Study on the Far Infrared Ray Emission Property and Adsorption Performance of Bamboo Charcoal/Polyvinyl Alcohol Fiber, Polym. Plast. Technol. Eng. 46 (2007) 1073–1078.

doi:10.1080/03602550701522518.

[177] A. Çay, J. Yanık, Ç. Akduman, G. Duman, H. Ertaş, Application of textile waste derived biochars onto cotton fabric for improved performance and functional properties, J. Clean. Prod. 251 (2020) 119664. doi:10.1016/j.jclepro.2019.119664.

[178] K. Wang, J. Zhang, B.H. Shanks, R.C. Brown, The deleterious effect of inorganic salts on hydrocarbon yields from catalytic pyrolysis of lignocellulosic biomass and its mitigation, Appl. Energy. 148 (2015) 115–120. doi:10.1016/J.APENERGY.2015.03.034.

[179] D. Mourant, Z. Wang, M. He, X.S. Wang, M. Garcia-Perez, K. Ling, C.Z. Li, Mallee wood fast pyrolysis: Effects of alkali and alkaline earth metallic species on the yield and composition of bio-oil, Fuel. 90 (2011) 2915–2922. doi:10.1016/j.fuel.2011.04.033.

[180] D.S. Scott, L. Paterson, J. Piskorz, D. Radlein, Pretreatment of poplar wood for fast pyrolysis: Rate of cation removal, J. Anal. Appl. Pyrolysis. 57 (2001) 169–176. doi:10.1016/S0165-2370(00)00108-X.

[181] K.O. Davidsson, J.G. Korsgren, J.B.C. Pettersson, U. Jäglid, The effects of fuel washing techniques on alkali release from biomass, Fuel. 81 (2002) 137–142. doi:10.1016/S0016-2361(01)00132-6.

[182] A. Sluiter, B. Hames, R. Ruiz, C. Scarlata, J. Sluiter, D. Templeton, D. Crocker, Determination of Structural Carbohydrates and Lignin in Biomass: Laboratory Analytical Procedure (LAP) (Revised July 2011), 2008. http://www.nrel.gov/biomass/analytical_procedures.html (accessed April 28, 2019).

[183] A.S. for T. ASTM, Materials, Standard Test Method for Volatile Matter in the Analysis of Particulate Wood Fuels E872 - 82, ASTM Int. 82 (2011) 14–16. doi:10.1520/E0872-82R06.2.

[184] ASTM International, ASTM E1755-01(2015), Standard Test Method for Ash in Biomass, ASTM International, West Conshohocken, PA, 2015, 2015. doi:10.1520/E1755-01R15.

[185] ASTM D 1762-84, Standard Test Method for Chemical Analysis of Wood Charcoal., ASTM Int. 84 (2011) 1–2. doi:10.1520/D1762-84R07.2.

[186] W. Bleam, Natural Organic Matter, in: Soil Environ. Chem., Elsevier, 2017: pp. 333–384. doi:10.1016/b978-0-12-804178-9.00007-0.

[187] Astm, Standard Test Method for Heat of Combustion of Liquid Hydrocarbon Fuels by Bomb Calorimeter, ASTM D 240-92 (Reapproved 1997). (1997) 144–151. doi:10.1520/D0240-09.2.

[188] S. Rajkovich, A. Enders, K. Hanley, C. Hyland, A.R. Zimmerman, J. Lehmann, Corn growth and nitrogen nutrition after additions of biochars with varying properties to a temperate soil, Biol. Fertil. Soils. 48 (2012) 271–284. doi:10.1007/s00374-011-0624-7.

[189] Carl Zeiss Microscope GmbH, ZEISS Xradia Versa Family Your 3D X-ray Microscope for Advanced Discovery, Prod. Fly. (n.d.). https://applications.zeiss.com/C125792900358A3F/0/529386581C2991E8C1257F5E005253D2/$FILE/EN_44_012_024_Versa_Flyer.pdf.

[190] E203 − 16 Standard Test Method for Water Using Volumetric Karl Fischer Titration, n.d. doi:10.1520/E0203-16.

[191] M. Nageeb, Adsorption Technique for the Removal of Organic Pollutants from Water and Wastewater, in: Org. Pollut. - Monit. Risk Treat., InTech, 2013. doi:10.5772/54048.

[192] J.A. Menéndez, M.J. Illán-Gómez, C.A.L. y León, L.R. Radovic, On the difference between the isoelectric point and the point of zero charge of carbons, Carbon N. Y. 33 (1995) 1655–1657. doi:10.1016/0008-6223(95)96817-R.

[193] H.P. Boehm, Some aspects of the surface chemistry of carbon blacks and other carbons, Carbon N. Y. 32 (1994) 759–769. doi:10.1016/0008-6223(94)90031-0.

[194] S.L. Goertzen, K.D. Thériault, A.M. Oickle, A.C. Tarasuk, H.A. Andreas, Standardization of the Boehm titration. Part I. CO2 expulsion and endpoint determination, Carbon N. Y. 48 (2010) 1252–1261. doi:10.1016/j.carbon.2009.11.050.

[195] P.T. Williams, S. Besler, The Influence of Temperature and Heating Rate on the Slow Pyrolysis of Biomass, Renew. Energy. 7 (1996) 233–250. doi:10.1016/0960-1481(96)00006-7.

[196] J.S.J. Lehmann, Biochar for environmental management: science and technology., Earthscan, London, 2009.

[197] Y.P. Gong, Z.Y. Ni, Z.Z. Xiong, L.H. Cheng, X.H. Xu, Phosphate and ammonium adsorption of the modified biochar based on *Phragmites australis* after phytoremediation, Environ. Sci. Pollut. Res. 24 (2017) 8326–8335. doi:10.1007/s11356-017-8499-2.

[198] H. Yang, R. Yan, H. Chen, C. Zheng, D.H. Lee, D.T. Liang, In-depth investigation of biomass pyrolysis based on three major components: Hemicellulose, cellulose and lignin, Energy and Fuels. 20 (2006) 388–393. doi:10.1021/ef0580117.

[199] S. Wu, D. Shen, J. Hu, H. Zhang, R. Xiao, Cellulose-hemicellulose interactions during fast pyrolysis with different temperatures and mixing methods, Biomass and Bioenergy. 95 (2016) 55–63. doi:10.1016/J.BIOMBIOE.2016.09.015.

[200] X. Gu, X. Ma, L. Li, C. Liu, K. Cheng, Z. Li, Pyrolysis of poplar wood sawdust by TG-FTIR and Py–GC/MS, J. Anal. Appl. Pyrolysis. 102 (2013) 16–23. doi:10.1016/J.JAAP.2013.04.009.

[201] Z. Ma, D. Chen, J. Gu, B. Bao, Q. Zhang, Determination of pyrolysis characteristics and kinetics of palm kernel shell using TGA-FTIR and model-free

integral methods, Energy Convers. Manag. 89 (2015) 251–259.
doi:10.1016/j.enconman.2014.09.074.

[202] O. Onay, Influence of pyrolysis temperature and heating rate on the production of bio-oil and char from safflower seed by pyrolysis, using a well-swept fixed-bed reactor, Fuel Process. Technol. 88 (2007) 523–531.
doi:10.1016/j.fuproc.2007.01.001.

[203] P.T. Williams, N. Nugranad, Comparison of products from the pyrolysis and catalytic pyrolysis of rice husks, Energy. 25 (2000) 493–513. doi:10.1016/S0360-5442(00)00009-8.

[204] P.A. Horne, P.T. Williams, Influence of temperature on the products from the flash pyrolysis of biomass, Fuel. 75 (1996) 1051–1059. doi:10.1016/0016-2361(96)00081-6.

[205] J. Park, Y. Lee, C. Ryu, Y.-K.K. Park, Slow pyrolysis of rice straw: Analysis of products properties, carbon and energy yields, Bioresour. Technol. 155 (2014) 63–70. doi:10.1016/J.BIORTECH.2013.12.084.

[206] F. Karaosmanoğlu, A. Işigigür-Ergüdenler, A. Sever, Biochar from the straw-stalk of rapeseed plant, Energy and Fuels. 14 (2000) 336–339. doi:10.1021/ef9901138.

[207] I. Demiral, E.A. Ayan, Pyrolysis of grape bagasse: Effect of pyrolysis conditions on the product yields and characterization of the liquid product, Bioresour. Technol. 102 (2011) 3946–3951. doi:10.1016/j.biortech.2010.11.077.

[208] F. Ronsse, S. van Hecke, D. Dickinson, W. Prins, Production and characterization of slow pyrolysis biochar: Influence of feedstock type and pyrolysis conditions, GCB Bioenergy. 5 (2013) 104–115. doi:10.1111/gcbb.12018.

[209] A. Enders, K. Hanley, T. Whitman, S. Joseph, J. Lehmann, Characterization of biochars to evaluate recalcitrance and agronomic performance, Bioresour. Technol. 114 (2012) 644–653. doi:10.1016/j.biortech.2012.03.022.

[210] P.A. Della Rocca, G.I. Horowitz, P. Bonelli, M.C. Cassanello, A.L. Cukierman, Olive Stones Pyrolysis: Chemical, Textural and Kinetics Characterization, in: Dev. Thermochem. Biomass Convers., Springer Netherlands, 1997: pp. 176–190. doi:10.1007/978-94-009-1559-6_13.

[211] M.J. Wornat, R.H. Hurt, N.Y.C. Yang, T.J. Headley, Structural and compositional transformations of biomass chars during combustion, Combust. Flame. 100 (1995) 131–143. doi:10.1016/0010-2180(94)00055-W.

[212] K.A. Spokas, Review of the stability of biochar in soils: predictability of O:C molar ratios, Carbon Manag. 1 (2010) 289–303. doi:10.4155/cmt.10.32.

[213] A. Budai, A.R. Zimmerman, A.L. Cowie, J.B.W. Webber, B.P. Singh, B. Glaser, C.A. Masiello, D. Andersson, F. Shields, J. Lehmann, M. Camps Arbestain, M. Williams, S. Sohi, S. Joseph, Biochar Carbon Stability Test Method : An assessment of methods to determine biochar carbon stability, Int. Biochar Initiat. 10 (2013) 1–10. www.biochar-international.org/sites/default/files/IBI_Report_Biochar_Stability_Test_Method_Final.pdf (accessed May 15, 2020).

[214] EBC (2012), European Biochar Certificate - Guidelines for a Sustainable Production of Biochar', Eur. Biochar Found. (EBC), Arbaz, Switzerland. Version 6.1 19th June,. (2015) 1–22. doi:10.13140/RG.2.1.4658.7043.

[215] B. Zhao, D. O'Connor, J. Zhang, T. Peng, Z. Shen, D.C.W. Tsang, D. Hou, Effect of pyrolysis temperature, heating rate, and residence time on rapeseed stem derived biochar, J. Clean. Prod. 174 (2018) 977–987. doi:10.1016/j.jclepro.2017.11.013.

[216] K. Weber, P. Quicker, Properties of biochar, Fuel. 217 (2018) 240–261. doi:10.1016/j.fuel.2017.12.054.

[217] R.L. Burwell Jr., Manual of Symbols and Terminology for Physicochemical

Quantities and Units - Appendix II. Definitions, Terminology and Symbols in Colloid and Surface Chemistry. Part II: Heterogeneous Catalysis, Pure Appl. Chem. 46 (1976) 71–90. doi:10.1351/pac197646010071.

[218] C.-M. Popescu, M.-C. Popescu, C. Vasile, Characterization of fungal degraded lime wood by FT-IR and 2D IR correlation spectroscopy, Microchem. J. 95 (2010) 377–387. doi:10.1016/j.microc.2010.02.021.

[219] G.E. Acquah, B.K. Via, O.O. Fasina, L.G. Eckhardt, Rapid Quantitative Analysis of Forest Biomass Using Fourier Transform Infrared Spectroscopy and Partial Least Squares Regression., J. Anal. Methods Chem. 2016 (2016) 1839598. doi:10.1155/2016/1839598.

[220] J. Shi, J. Li, Metabolites and chemical group changes in the wood-forming tissue of pinus koraiensis under inclined conditions, BioResources. 7 (2012) 3463–3475. doi:10.15376/biores.7.3.3463-3475.

[221] B. Chen, E.J. Johnson, B. Chefetz, L. Zhu, B. Xing, Sorption of polar and nonpolar aromatic organic contaminants by plant cuticular materials: Role of polarity and accessibility, Environ. Sci. Technol. 39 (2005) 6138–6146. doi:10.1021/es050622q.

[222] E. Lau, M. Goldoftas, V.D. Baldwin, P. Dayanandan, J. Srinivasan, P.B. Kaufman, Structure and localization of silica in the leaf and internodal epidermal system of the marsh grass *Phragmites australis*, Can. J. Bot. 56 (1978) 1696–1701. doi:10.1139/b78-199.

[223] A. Macherius, P. Kuschk, C. Haertig, M. Moeder, N.I. Shtemenko, A.H. Bayona, J.A.H. Guerrero, M. Gey, Composition changes in the cuticular surface lipids of the helophytes *Phragmites australis* and Juncus effusus as result of pollutant exposure, Environ. Sci. Pollut. Res. 18 (2011) 727–733. doi:10.1007/s11356-010-0416-x.

[224] Y. Chen, H. Yang, X. Wang, S. Zhang, H. Chen, Biomass-based pyrolytic polygeneration system on cotton stalk pyrolysis: Influence of temperature, Bioresour. Technol. 107 (2012) 411–418. doi:10.1016/J.BIORTECH.2011.10.074.

[225] B. Chen, D. Zhou, L. Zhu, Transitional adsorption and partition of nonpolar and polar aromatic contaminants by biochars of pine needles with different pyrolytic temperatures, Environ. Sci. Technol. 42 (2008) 5137–5143. doi:10.1021/es8002684.

[226] Y. Chun, G. Sheng, G.T. Chiou, B. Xing, Compositions and sorptive properties of crop residue-derived chars, Environ. Sci. Technol. 38 (2004) 4649–4655. doi:10.1021/es035034w.

[227] M. Keiluweit, P.S. Nico, M. Johnson, M. Kleber, Dynamic molecular structure of plant biomass-derived black carbon (biochar), Environ. Sci. Technol. 44 (2010) 1247–1253. doi:10.1021/es9031419.

[228] H. Zhang, C. Chen, E.M. Gray, S.E. Boyd, Effect of feedstock and pyrolysis temperature on properties of biochar governing end use efficacy, Biomass and Bioenergy. 105 (2017) 136–146. doi:10.1016/j.biombioe.2017.06.024.

[229] R. Fahmi, A. V. Bridgwater, I. Donnison, N. Yates, J.M. Jones, The effect of lignin and inorganic species in biomass on pyrolysis oil yields, quality and stability, Fuel. 87 (2008) 1230–1240. doi:10.1016/j.fuel.2007.07.026.

[230] E. Epstein, SILICON, Annu. Rev. Plant Physiol. Plant Mol. Biol. 50 (1999) 641–664. doi:10.1146/annurev.arplant.50.1.641.

[231] S.H. Beis, Ö. Onay, Ö.M. Koçkar, Fixed-bed pyrolysis of safflower seed: Influence of pyrolysis parameters on product yields and compositions, Renew. Energy. 26 (2002) 21–32. doi:10.1016/S0960-1481(01)00109-4.

[232] S. Yorgun, Y.E. Şimşek, Catalytic pyrolysis of Miscanthus × giganteus over activated alumina, Bioresour. Technol. 99 (2008) 8095–8100.

doi:10.1016/J.BIORTECH.2008.03.036.

[233] M. Nurul Islam, M. Nurul Islam, M. Rafiqul Alam Beg, M. Rofiqul Islam, Pyrolytic oil from fixed bed pyrolysis of municipal solid waste and its characterization, Renew. Energy. 30 (2005) 413–420. doi:10.1016/J.RENENE.2004.05.002.

[234] A.E. Pütün, A. Özean, E. Pütün, Pyrolysis of hazelnut shells in a fixed-bed tubular reactor: Yields and structural analysis of bio-oil, J. Anal. Appl. Pyrolysis. 52 (1999) 33–49. doi:10.1016/S0165-2370(99)00044-3.

[235] L. Jiang, N. Wu, A. Zheng, X. Wang, M. Liu, Z. Zhao, F. He, H. Li, X. Feng, Effect of glycerol pretreatment on levoglucosan production from corncobs by fast pyrolysis, Polymers (Basel). 9 (2017). doi:10.3390/polym9110599.

[236] S. Uçar, S. Karagöz, The slow pyrolysis of pomegranate seeds: The effect of temperature on the product yields and bio-oil properties, J. Anal. Appl. Pyrolysis. 84 (2009) 151–156. doi:10.1016/j.jaap.2009.01.005.

[237] G. Lv, S. Wu, G. Yang, J. Chen, Y. Liu, F. Kong, Comparative study of pyrolysis behaviors of corn stalk and its three components, J. Anal. Appl. Pyrolysis. 104 (2013) 185–193. doi:10.1016/j.jaap.2013.08.005.

[238] Q. Liu, Z. Zhong, S. Wang, Z. Luo, Interactions of biomass components during pyrolysis: A TG-FTIR study, J. Anal. Appl. Pyrolysis. 90 (2011) 213–218. doi:10.1016/J.JAAP.2010.12.009.

[239] J. Yu, N. Paterson, J. Blamey, M. Millan, Cellulose, xylan and lignin interactions during pyrolysis of lignocellulosic biomass, Fuel. 191 (2017) 140–149. doi:10.1016/j.fuel.2016.11.057.

[240] J. Zhang, Y.S. Choi, C.G. Yoo, T.H. Kim, R.C. Brown, B.H. Shanks, Cellulose-hemicellulose and cellulose-lignin interactions during fast pyrolysis, ACS Sustain. Chem. Eng. 3 (2015) 293–301. doi:10.1021/sc500664h.

[241] T. Hosoya, H. Kawamoto, S. Saka, Cellulose-hemicellulose and cellulose-lignin interactions in wood pyrolysis at gasification temperature, J. Anal. Appl. Pyrolysis. 80 (2007) 118–125. doi:10.1016/j.jaap.2007.01.006.

[242] T.P. Schultz, M.C. Templeton, G.D. McGinnis, Rapid Determination of Lignocellulose by Diffuse Reflectance Fourier Transform Infrared Spectrometry, Anal. Chem. 57 (1985) 2867–2869. doi:10.1021/ac00291a027.

[243] Damayanti, H.S. Wu, Pyrolysis kinetic of alkaline and dealkaline lignin using catalyst, J. Polym. Res. 25 (2018). doi:10.1007/s10965-017-1401-6.

[244] H. Zhou, Y. Long, A. Meng, Q. Li, Y. Zhang, The pyrolysis simulation of five biomass species by hemi-cellulose, cellulose and lignin based on thermogravimetric curves, Thermochim. Acta. 566 (2013) 36–43. doi:10.1016/j.tca.2013.04.040.

[245] X. Wu, Y. Ba, X. Wang, M. Niu, K. Fang, Evolved gas analysis and slow pyrolysis mechanism of bamboo by thermogravimetric analysis, Fourier transform infrared spectroscopy and gas chromatography-mass spectrometry, Bioresour. Technol. 266 (2018) 407–412. doi:10.1016/j.biortech.2018.07.005.

[246] X. Yang, Y. Zhao, R. Li, Y. Wu, M. Yang, A modified kinetic analysis method of cellulose pyrolysis based on TG–FTIR technique, Thermochim. Acta. 665 (2018) 20–27. doi:10.1016/j.tca.2018.05.008.

[247] Q. Liu, S. Wang, Y. Zheng, Z. Luo, K. Cen, Mechanism study of wood lignin pyrolysis by using TG–FTIR analysis, J. Anal. Appl. Pyrolysis. 82 (2008) 170–177. doi:10.1016/J.JAAP.2008.03.007.

[248] C. Zhao, E. Jiang, A. Chen, Volatile production from pyrolysis of cellulose, hemicellulose and lignin, J. Energy Inst. 90 (2017) 902–913. doi:10.1016/j.joei.2016.08.004.

[249] I. Kurnia, A. Yoshida, Y.A. Situmorang, Y. Kasai, A. Abudula, G. Guan,

Utilization of Dealkaline Lignin as a Source of Sodium-Promoted MoS 2 /Mo 2 C Hybrid Catalysts for Hydrogen Production from Formic Acid, 2019. doi:10.1021/acssuschemeng.9b00488.

[250] C.E. Efika, J.A. Onwudili, P.T. Williams, Influence of heating rates on the products of high-temperature pyrolysis of waste wood pellets and biomass model compounds, Waste Manag. 76 (2018) 497–506. doi:10.1016/j.wasman.2018.03.021.

[251] D. Angin, Effect of pyrolysis temperature and heating rate on biochar obtained from pyrolysis of safflower seed press cake, Bioresour. Technol. 128 (2013) 593–597. doi:10.1016/j.biortech.2012.10.150.

[252] D. Chen, J. Zhou, Q. Zhang, Effects of heating rate on slow pyrolysis behavior, kinetic parameters and products properties of moso bamboo, Bioresour. Technol. 169 (2014) 313–319. doi:10.1016/j.biortech.2014.07.009.

[253] K. Crombie, O. Mašek, S.P. Sohi, P. Brownsort, A. Cross, The effect of pyrolysis conditions on biochar stability as determined by three methods, GCB Bioenergy. 5 (2013) 122–131. doi:10.1111/gcbb.12030.

[254] A. Dufour, M. Castro-Diaz, N. Brosse, M. Bouroukba, C. Snape, The origin of molecular mobility during biomass pyrolysis as revealed by in situ 1H NMR spectroscopy, ChemSusChem. 5 (2012) 1258–1265. doi:10.1002/cssc.201100442.

[255] J. Montoya, B. Pecha, F.C. Janna, M. Garcia-Perez, Micro-explosion of liquid intermediates during the fast pyrolysis of sucrose and organosolv lignin, J. Anal. Appl. Pyrolysis. 122 (2016) 106–121. doi:10.1016/j.jaap.2016.10.010.

[256] S. Zhou, B. Pecha, M. van Kuppevelt, A.G. McDonald, M. Garcia-Perez, Slow and fast pyrolysis of Douglas-fir lignin: Importance of liquid-intermediate formation on the distribution of products, Biomass and Bioenergy. (2014). doi:10.1016/j.biombioe.2014.03.064.

[257] B. Shrestha, Y. Le Brech, T. Ghislain, S. Leclerc, V. Carré, F. Aubriet, S. Hoppe, P. Marchal, S. Pontvianne, N. Brosse, A. Dufour, A Multitechnique Characterization of Lignin Softening and Pyrolysis, ACS Sustain. Chem. Eng. 5 (2017) 6940–6949. doi:10.1021/acssuschemeng.7b01130.

[258] A. Dufour, M. Castro-Ďaz, P. Marchal, N. Brosse, R. Olcese, M. Bouroukba, C. Snape, In situ analysis of biomass pyrolysis by high temperature rheology in relations with 1H NMR, Energy and Fuels. 26 (2012) 6432–6441. doi:10.1021/ef301310x.

[259] N. Toloue Farrokh, H. Suopajärvi, O. Mattila, K. Umeki, A. Phounglamcheik, H. Romar, P. Sulasalmi, T. Fabritius, Slow pyrolysis of by-product lignin from wood-based ethanol production– A detailed analysis of the produced chars, Energy. 164 (2018) 112–123. doi:10.1016/j.energy.2018.08.161.

[260] C.P. (Chandra P. Sharma, Plant micronutrients, Science Publishers, 2006.

[261] Y. Huang, L. Wang, Y. Chao, D.S. Nawawi, T. Akiyama, T. Yokoyama, Y. Matsumoto, Analysis of lignin aromatic structure in wood based on the IR spectrum, J. Wood Chem. Technol. 32 (2012) 294–303. doi:10.1080/02773813.2012.666316.

[262] K.K. Pandey, A study of chemical structure of soft and hardwood and wood polymers by FTIR spectroscopy, J. Appl. Polym. Sci. 71 (1999) 1969–1975. doi:10.1002/(SICI)1097-4628(19990321)71:12<1969::AID-APP6>3.0.CO;2-D.

[263] S. Kang, X. Li, J. Fan, J. Chang, Characterization of hydrochars produced by hydrothermal carbonization of lignin, cellulose, d-xylose, and wood meal, in: Ind. Eng. Chem. Res., 2012: pp. 9023–9031. doi:10.1021/ie300565d.

[264] L. Pachuau, D.C. Vanlalfakawma, S.K. Tripathi, H. Lalhlenmawia, Muli bamboo (Melocanna baccifera) as a new source of microcrystalline cellulose, J. Appl. Pharm. Sci. 4 (2014) 87–94. doi:10.7324/JAPS.2014.41115.

[265] H. Yang, R. Yan, H. Chen, D.H. Lee, D.T. Liang, C. Zheng, Mechanism of Palm Oil Waste Pyrolysis in a Packed Bed, (2006). doi:10.1021/ef0600311.

[266] I. Demiral, N.G. Atilgan, S. Şensöz, Production of biofuel from soft shell of pistachio (Pistacia vera L.), in: Chem. Eng. Commun., 2009: pp. 104–115. doi:10.1080/00986440802300984.

[267] F. Dughiero, Induction Heating : fundamentals Induction heating fundamentals, Control Power Electron. Convert. Syst. (2018) 1–29. doi:10.1016/B978-0-12-816136-4.00022-1.

[268] A. V. Bridgwater, Biomass Pyrolysis, Task 34 Overview, IEA Bioenergy T34200701. (2007) 1–20. http://www.ieabioenergy.com/wp-content/uploads/2013/10/Task-34-Booklet.pdf.

[269] Y.B. Ho, Mineral composition of *Phragmites australis* in Scottish lochs as related to eutrophication. I. Seasonal changes in organs, Hydrobiologia. 85 (1981) 227–237. doi:10.1007/BF00017612.

[270] F.C. Lanning, B.W.X. Ponnaiya, C.F. Crumpton, The Chemical Nature of Silica in Plants., Plant Physiol. 33 (1958) 339–343. doi:10.1104/pp.33.5.339.

[271] E. Epstein, The anomaly of silicon in plant biology, Proc. Natl. Acad. Sci. U. S. A. 91 (1994) 11–17. doi:10.1073/pnas.91.1.11.

[272] J. Schaller, C. Brackhage, M.O. Gessner, E. Bäuker, E. Gert Dudel, Silicon supply modifies C:N:P stoichiometry and growth of *Phragmites australis*, Plant Biol. 14 (2012) 392–396. doi:10.1111/j.1438-8677.2011.00537.x.

[273] S. V. Vassilev, D. Baxter, L.K. Andersen, C.G. Vassileva, An overview of the chemical composition of biomass, Fuel. 89 (2010) 913–933. doi:10.1016/j.fuel.2009.10.022.

[274] S. V Vassilev, C.G. Vassileva, Water-Soluble Fractions of Biomass and Biomass

Ash and Their Significance for Biofuel Application, Energy and Fuels. 33 (2019) 2763–2777. doi:10.1021/acs.energyfuels.9b00081.

[275] L. Deng, T. Zhang, D. Che, Effect of water washing on fuel properties, pyrolysis and combustion characteristics, and ash fusibility of biomass, Fuel Process. Technol. 106 (2013) 712–720. doi:10.1016/j.fuproc.2012.10.006.

[276] H. Wu, K. Yip, Z. Kong, C.Z. Li, D. Liu, Y. Yu, X. Gao, Removal and recycling of inherent inorganic nutrient species in mallee biomass and derived biochars by water leaching, Ind. Eng. Chem. Res. 50 (2011) 12143–12151. doi:10.1021/ie200679n.

[277] S.B. Liaw, H. Wu, Leaching characteristics of organic and inorganic matter from biomass by water: Differences between batch and semi-continuous operations, Ind. Eng. Chem. Res. 52 (2013) 4280–4289. doi:10.1021/ie3031168.

[278] K. Raveendran, A. Ganesh, K.C. Khilar, Pyrolysis characteristics of biomass and biomass components, Fuel. 75 (1996) 987–998. doi:10.1016/0016-2361(96)00030-0.

[279] I.Y. Eom, K.H. Kim, J.Y. Kim, S.M. Lee, H.M. Yeo, I.G. Choi, J.W. Choi, Characterization of primary thermal degradation features of lignocellulosic biomass after removal of inorganic metals by diverse solvents, Bioresour. Technol. 102 (2011) 3437–3444. doi:10.1016/j.biortech.2010.10.056.

[280] M. Mos, S.W. Banks, D.J. Nowakowski, P.R.H. Robson, A. V. Bridgwater, I.S. Donnison, Impact of Miscanthus x giganteus senescence times on fast pyrolysis bio-oil quality, Bioresour. Technol. 129 (2013) 335–342. doi:10.1016/j.biortech.2012.11.069.

[281] A.A. Boateng, D.E. Daugaard, N.M. Goldberg, K.B. Hicks, Bench-scale fluidized-bed pyrolysis of switchgrass for bio-oil production, Ind. Eng. Chem. Res. 46 (2007) 1891–1897. doi:10.1021/ie0614529.

[282] A. Oasmaa, S. Czernik, Fuel oil quality of biomass pyrolysis oils - state of the art for the end users, Energy and Fuels. 13 (1999) 914–921. doi:10.1021/ef980272b.

[283] A. Demirbas, The influence of temperature on the yields of compounds existing in bio-oils obtained from biomass samples via pyrolysis, Fuel Process. Technol. 88 (2007) 591–597. doi:10.1016/j.fuproc.2007.01.010.

[284] M.R. Gray, W.H. Corcoran, G.R. Gavalas, Pyrolysis of a Wood-Derived Material. Effects of Moisture and Ash Content, Ind. Eng. Chem. Process Des. Dev. 24 (1985) 646–651. doi:10.1021/i200030a020.

[285] B. Singh, B.P. Singh, A.L. Cowie, Characterisation and evaluation of biochars for their application as a soil amendment, in: Aust. J. Soil Res., CSIRO Publishing, 2010: pp. 516–525. doi:10.1071/SR10058.

[286] T. Limwikran, I. Kheoruenromne, A. Suddhiprakarn, N. Prakongkep, R.J. Gilkes, Dissolution of K, Ca, and P from biochar grains in tropical soils, Geoderma. 312 (2018) 139–150. doi:10.1016/j.geoderma.2017.10.022.

[287] J.-H. Yuan, R.-K. Xu, H. Zhang, The forms of alkalis in the biochar produced from crop residues at different temperatures, Bioresour. Technol. 102 (2011) 3488–3497. doi:10.1016/J.BIORTECH.2010.11.018.

[288] S. Ramola, T. Mishra, G. Rana, R.K. Srivastava, Characterization and pollutant removal efficiency of biochar derived from baggase, bamboo and tyre, Environ. Monit. Assess. 186 (2014) 9023–9039. doi:10.1007/s10661-014-4062-5.

[289] K. Hammes, R.J. Smernik, J.O. Skjemstad, M.W.I. Schmidt, Characterisation and evaluation of reference materials for black carbon analysis using elemental composition, colour, BET surface area and 13C NMR spectroscopy, Appl. Geochemistry. 23 (2008) 2113–2122. doi:10.1016/j.apgeochem.2008.04.023.

[290] K. Jindo, H. Mizumoto, Y. Sawada, M.A. Sanchez-Monedero, T. Sonoki, Physical and chemical characterization of biochars derived from different agricultural

residues, Biogeosciences. 11 (2014) 6613–6621. doi:10.5194/bg-11-6613-2014.

[291] J. Lehmann, S. Joseph, Biochar for environmental management: An introduction, in: S.J. Johannes Lehmann (Ed.), Biochar Environ. Manag. Sci. Technol., 2nd, revised ed., Routledge, 2015, 2012: pp. 1–12. doi:10.4324/9781849770552.

[292] R. Fidel, Evaluation and implementation of methods for quantifying organic and inorganic components of biochar alkalinity, 2012. https://lib.dr.iastate.edu/etd (accessed April 25, 2020).

[293] Y. Lee, J. Park, C. Ryu, K.S. Gang, W. Yang, Y.K. Park, J. Jung, S. Hyun, Comparison of biochar properties from biomass residues produced by slow pyrolysis at 500°C, Bioresour. Technol. 148 (2013) 196–201. doi:10.1016/j.biortech.2013.08.135.

[294] C. Morterra, M.J.D. Low, IR studies of carbons-II. The vacuum pyrolysis of cellulose, Carbon N. Y. 21 (1983) 283–288. doi:10.1016/0008-6223(83)90092-1.

[295] M.K. Bahng, B.S. Donohoe, M.R. Nimlos, Application of an fourier transform-infrared imaging tool for measuring temperature or reaction profiles in pyrolyzed wood, Energy and Fuels. 25 (2011) 370–378. doi:10.1021/ef101312a.

[296] E. Smidt, M. Schwanninger, Characterization of waste materials using FTIR spectroscopy: Process monitoring and quality assessment, Spectrosc. Lett. 38 (2005) 247–270. doi:10.1081/SL-200042310.

[297] S. Kloss, F. Zehetner, A. Dellantonio, R. Hamid, F. Ottner, V. Liedtke, M. Schwanninger, M.H. Gerzabek, G. Soja, Characterization of Slow Pyrolysis Biochars: Effects of Feedstocks and Pyrolysis Temperature on Biochar Properties, J. Environ. Qual. 41 (2012) 990–1000. doi:10.2134/jeq2011.0070.

[298] C.G. Boeriu, D. Bravo, R.J.A. Gosselink, J.E.G. Van Dam, Characterisation of structure-dependent functional properties of lignin with infrared spectroscopy, in: Ind. Crops Prod., Elsevier, 2004: pp. 205–218. doi:10.1016/j.indcrop.2004.04.022.

[299] B. Gámiz, K. Hall, K.A. Spokas, L. Cox, Understanding Activation Effects on Low-Temperature Biochar for Optimization of Herbicide Sorption, Agronomy. 9 (2019) 588. doi:10.3390/agronomy9100588.

[300] D. Pattnaik, S. Kumar, S.K. Bhuyan, S.C. Mishra, Effect of carbonization temperatures on biochar formation of bamboo leaves, in: IOP Conf. Ser. Mater. Sci. Eng., 2018. doi:10.1088/1757-899X/338/1/012054.

[301] K.R. Adams, prehistoric reedgrass (*Phragmites*) "Cigarettes" with tobacco (nicotiana) contents: a case sludy from red bow cliff dwelling, Arizona, 1990. https://ethnobiology.org/sites/default/files/pdfs/JoE/10-2/Adams.pdf (accessed June 7, 2019).

[302] G. Okorn, B. Metscher, G. Draxler, G.A. Janauer, Value-adding application of micro-CT to highly rigid plant tissues: *Phragmites australis* (Cav.) Trin. Ex Steud. knot sections, Verh. Zool.-Bot. Ges. Österreich. 147 (2010) 93–98. www.biologiezentrum.at.

[303] W.P. Pan, G.N. Richards, Influence of metal ions on volatile products of pyrolysis of wood, J. Anal. Appl. Pyrolysis. 16 (1989) 117–126. doi:10.1016/0165-2370(89)85011-9.

[304] V. Strezov, T.J. Evans, C. Hayman, Thermal conversion of elephant grass (Pennisetum Purpureum Schum) to bio-gas, bio-oil and charcoal, Bioresour. Technol. 99 (2008) 8394–8399. doi:10.1016/j.biortech.2008.02.039.

[305] ibuprofen -- Britannica Academic, (n.d.). https://academic-eb-com.proxy1.lib.uwo.ca/levels/collegiate/article/ibuprofen/41948 (accessed March 28, 2020).

[306] Summary Safety Review - Oral Ibuprofen (Non-steroidal Anti-inflammatory Drug; NSAID) - Health Canada, (n.d.). https://hpr-rps.hres.ca/reg-content/summary-safety-review-detail.php?linkID=SSR00031 (accessed March 28, 2020).

[307] K.D. Rainsford, Ibuprofen: pharmacology, efficacy and safety, (n.d.). doi:10.1007/s10787-009-0016-x.

[308] M. Essandoh, B. Kunwar, C.U. Pittman, D. Mohan, T. Mlsna, Sorptive removal of salicylic acid and ibuprofen from aqueous solutions using pine wood fast pyrolysis biochar, Chem. Eng. J. 265 (2015) 219–227. doi:10.1016/J.CEJ.2014.12.006.

[309] A. Colomba, Production of Activated Carbons from Pyrolytic Char for Environmental Applications, 2015.

[310] S. V. Vassilev, D. Baxter, L.K. Andersen, C.G. Vassileva, T.J. Morgan, An overview of the organic and inorganic phase composition of biomass, Fuel. 94 (2012) 1–33. doi:10.1016/j.fuel.2011.09.030.

[311] H. Namkung, Y.J. Lee, J.H. Park, G.S. Song, J.W. Choi, J.G. Kim, S.J. Park, J.C. Park, H.T. Kim, Y.C. Choi, Influence of herbaceous biomass ash pre-treated by alkali metal leaching on the agglomeration/sintering and corrosion behaviors, Energy. 187 (2019) 115950. doi:10.1016/j.energy.2019.115950.

[312] C. Tang, J. Zhu, Z. Li, R. Zhu, Q. Zhou, J. Wei, H. He, Q. Tao, Surface chemistry and reactivity of SiO_2 polymorphs: A comparative study on α-quartz and α-cristobalite, Appl. Surf. Sci. 355 (2015) 1161–1167. doi:10.1016/j.apsusc.2015.07.214.

[313] Activated Charcoal Norit®, from peat, multi-purpose activated charcoal, steam activated and acid washed, powder | C | Sigma-Aldrich, (n.d.). https://www.sigmaaldrich.com/catalog/product/sigald/93067?lang=en&region=CA (accessed April 24, 2020).

[314] N.A. Rashidi, S. Yusup, A. Borhan, Isotherm and Thermodynamic Analysis of Carbon Dioxide on Activated Carbon, in: Procedia Eng., Elsevier Ltd, 2016: pp. 630–637. doi:10.1016/j.proeng.2016.06.527.

[315] L.D. Nghiem, T. Fujioka, Removal of Emerging Contaminants for Water Reuse by

Membrane Technology, in: Emerg. Membr. Technol. Sustain. Water Treat., Elsevier B.V., 2016: pp. 217–247. doi:10.1016/B978-0-444-63312-5.00009-7.

[316] National Center for Biotechnology Information, (2019) 1723–1723. doi:10.1007/978-3-662-48986-4_301184.

[317] A.S. Mestre, J. Pires, J.M.F. Nogueira, A.P. Carvalho, Activated carbons for the adsorption of ibuprofen, Carbon N. Y. 45 (2007) 1979–1988. doi:10.1016/J.CARBON.2007.06.005.

[318] J.H. Yuan, R.K. Xu, N. Wang, J.Y. Li, Amendment of Acid Soils with Crop Residues and Biochars, Pedosphere. 21 (2011) 302–308. doi:10.1016/S1002-0160(11)60130-6.

[319] R. yong SHI, J. yu LI, N. NI, R. kou XU, Understanding the biochar's role in ameliorating soil acidity, J. Integr. Agric. 18 (2019) 1508–1517. doi:10.1016/S2095-3119(18)62148-3.

[320] M.A. Bezerra, R.E. Santelli, E.P. Oliveira, L.S. Villar, L.A. Escaleira, Response surface methodology (RSM) as a tool for optimization in analytical chemistry, Talanta. 76 (2008) 965–977. doi:10.1016/j.talanta.2008.05.019.

[321] H. Guedidi, L. Reinert, Y. Soneda, N. Bellakhal, L. Duclaux, Adsorption of ibuprofen from aqueous solution on chemically surface-modified activated carbon cloths, Arab. J. Chem. 10 (2017) S3584–S3594. doi:10.1016/j.arabjc.2014.03.007.

[322] P. Chingombe, B. Saha, R.J. Wakeman, Sorption of atrazine on conventional and surface modified activated carbons, J. Colloid Interface Sci. 302 (2006) 408–416. doi:10.1016/j.jcis.2006.06.065.

[323] A. Witkowski, H. Grajek, M. Pakula, S. Biniak, Z. Witkiewicz, Voltammetric studies of the gradual thermal decomposition of activated carbon surface oxygen complexes, in: Colloids Surfaces A Physicochem. Eng. Asp., Elsevier, 2002: pp. 313–320. doi:10.1016/S0927-7757(02)00158-9.

[324] C. Peiris, O. Nayanathara, C.M. Navarathna, Y. Jayawardhana, S. Nawalage, G. Burk, A.G. Karunanayake, S.B. Madduri, M. Vithanage, M.N. Kaumal, T.E. Mlsna, E.B. Hassan, S. Abeysundara, F. Ferez, S.R. Gunatilake, The influence of three acid modifications on the physicochemical characteristics of tea-waste biochar pyrolyzed at different temperatures: A comparative study, RSC Adv. 9 (2019) 17612–17622. doi:10.1039/c9ra02729g.

Appendices

A. Chapter 3

This Appendix contains the GC-MS results of all the fractions analyzed in Chapter 3.

Table A.1 – Slow pyrolysis organic fraction 5°C min⁻¹ (% area) by GC-MS

Chemical compounds detected in bio-oil fractions using GC-MS (% area)	350°C	400°C	450°C	500°C	550°C
Carbohydrates					
Levoglucosan		0.84	0.68		0.49
Carboxylic acids					
Acetic acid	7.9	10.43	6.81	6.09	8.07
Furans					
2-Furan methanol	2.05	2	1.85	1.82	2.21
2, 3-Dihydrobenzofuran	4.08	3.34	3.46	2.85	3.65
Tetrahydro-2-furanmethanol	1.48	1.05	1.32	1.38	1.26
Phenolic compounds					
2,6-Dimethoxyphenol	2.99	2.43	2.36	2.12	2.35
2-Methoxyphenol	3.2	2.6	2.91	2.46	3.27
2-Methoxy-4-vinylphenol	3.04	2.27	2.45	2.21	2.63
Phenol, 2-methoxy-4-(1-propenyl)-	1.2	0.89	1.05	0.92	1
Phenol	2.22	2.71	2.6	3.43	3.58
2-Methylphenol	0.49	0.74	0.71	1.32	1.14
3-Methylphenol	2.44		2.66	2.61	3.42
4-Methylphenol		3.56			
4-Ethylphenol	4.22	3.84	3.8	3.66	4.11
4-ethyl-2-methoxy-Phenol	3.21	2.21	2.53	1.98	2.53
1,2-Benzenediol	2.2	3.83	2.71	2.73	2.9
1,2-Benzenediol, 3-methoxy-	1.62	2.5	1.97	1.99	1.98
4-Ethyl-1, 2-benzenediol	1.32	2.04	1.83	1.5	1.66

Ketones

1-Hydroxy-2-propanone	0.93				
3-Hydroxy-2-butanone	0.25			0.3	0.27
2-Methyl-2-cyclopenten-1-one	0.26	0.35	0.35	0.42	0.49
2-Propanone, 1-(acetyloxy)-	0.6	0.56	0.58	0.49	0.69

Others

Methoxy Benzenes

Benzene, 1,2,3-trimethoxy-5-methyl-	1.4	1.23		0.99	0.84
Phenol, 2-methoxy-4-methyl-	1.56	1.23	1.47	1.27	1.61

Table A.2 – Slow pyrolysis aqueous phase 5°C min^{-1} (% area) by GC-MS

Chemical compounds detected in bio-oil fractions using GC-MS (%area)	350°C	400°C	450°C	500°C	550°C
Carbohydrates					
Levoglucosan	0.67	1.8	2	1.7	1.33
Carboxylic acid					
Acetic acid	47.82	40.31	39.02	41.65	44.92
Furans					
2-Furan methanol	3.37	2.97	3.08	3.31	3.7
2, 3-Dihydrobenzofuran					
Tetrahydro-2-furanmethanol	1.76	1.46	1.35	1.44	1.35
Furaldehyde (Furfural)	2.17	1.94	1.7	1.46	0.87
2(5H)-Furanone	1	0.91	1.07		
Phenolic compounds					
2,6-Dimethoxyphenol	1.59	2.59	2.54	2.86	1.09
2-Methoxyphenol	1.21	1.35	1.29	2.86	3.13
2-Methoxy-4-vinylphenol	0.37	0.25	1.39	1.31	
Phenol	0.92	0.96	0.86	0.99	0.99
3-Methylphenol		1.71		1.13	1.38
Hydroquinone	0.49	2.26	1.58	1.66	3.56
1,2-Benzenediol	3.65	4.6	3.67	4.91	
1,2-Benzenediol, 3-methoxy-	1.06	1.54	1.54	1.23	1.03
Ketones					
1-Hydroxy-2-butanone	1.19	1.12	1.06	1.01	1.01
2-Propanone, 1-(acetyloxy)-	1.75	1.63	1.53	1.67	1.72

Aldehydes

Pentanal	3.44	3.28	3.62	3.71	4.22

Others

Pyridines

4-Pyridinol	3.21	3.12	3.95		

Hydrocarbons (Cyclopentanes)

2-Cyclopenten-1-one, 2-hydroxy-3-methyl-	1.55		1.44	1.4	1.54

Table A.3 – Slow pyrolysis organic fraction 15°C min⁻¹ (%area) by GC-MS

Chemical compounds detected in bio-oil fractions using GC-MS (%area)	350°C	400°C	450°C	500°C	550°C
Carbohydrates					
Levoglucosan					
Carboxylic acids					
Acetic acid	6.63	7.99	5.44	5.99	7.17
Furans					
2-Furan methanol	1.88	1.67	1.27	1.4	1.85
2, 3-Dihydrobenzofuran	3.88	3.6	3.88	4.43	5.28
Tetrahydro-2-furanmethanol	1.56	0.85	0.6	0.69	0.45
2(5H)-Furanone		1.04	0.83		1.12
Furaldehyde (Furfural)	1.41				
Phenolic compounds					
2,6-Dimethoxyphenol	2.71	2.16	4.1	5.44	5.31
2-Methoxyphenol	3.15	2.85	1.14	0.91	1.48
2-Methoxy-4-vinylphenol	3	2.34			
Phenol, 2-methoxy-4-(1-propenyl)- (Isoeugenol)	3.23	3	3.03	1.45	1.8
Phenol	2.43	3.05	4.1	5.44	5.31
2-Methylphenol	0.6	0.8	1.72	2.18	1.86
3-Methylphenol	2.41	2.76	3.06	4.34	3.85
4-Ethylphenol	4.4	5.48	6.03	6.99	6.36
4-ethyl-2-methoxy-Phenol	3.23	3.03	3.03	1.45	1.8
1,2-Benzenediol	1.79	3.41	4.34	4.02	3.55
1,2-Benzenediol, 3-methoxy-	1.61	2.7			
4-Ethyl-1, 2-benzenediol	0.99	2.37	2.66	2.7	2.33
1,2-Benzenediol, 4-methyl-	1.07	1.94	2.63	2.46	1.9

Ketones

3-Methyl-1,2-cyclopentanedione	1.21	1.47	0.85	1.01	1.09
2-Propanone, 1-(acetyloxy)-	0.66	0.53	0.33	0.31	0.47

Others

Methoxy Benzenes					
Phenol, 2-methoxy-4-methyl-			1.36	1.62	0.56

Table A.4 – Slow pyrolysis aqueous fraction 15°C min⁻¹ (% area) by GC-MS

Chemical compounds detected in bio-oil fractions using GC-MS (%area)	350°C	400°C	450°C	500°C	550°C
Carbohydrates					
Levoglucosan	1.63	0.83	0.99	0.97	1.13
Carboxylic acid					
Acetic acid	38.83	51.51	51.39	47.71	49.46
Furans					
2-Furan methanol	3.04	3.04	2.88	2.89	3.18
Tetrahydro-2-furanmethanol	1.41	1.03	1.09	1.23	0.81
Furaldehyde (Furfural)	2.22	2.46	1.63	0.93	0.83
2(5H)-Furanone		1.04	0.83		1.12
Phenolic compounds					
2,6-Dimethoxyphenol	2.32	1.25	0.79	0.91	0.55
2-Methoxyphenol		1.25	0.82	0.83	1.07
2-Methoxy-4-vinylphenol		0.36	0.53	0.52	0.44
Phenol	0.83	1.02	1.17	1.34	1.43
Hydroquinone		0.66	0.62	0.84	0.76
1,2-Benzenediol	3.78	3.41	3.74	4.18	4.04
1,2-Benzenediol, 3-methoxy-	1.68	1.2	0.82	0.89	0.98
Ketones					
1-Hydroxy-2-propanone	5.89		5.29	5.11	4.63
1-Hydroxy-2-butanone	1.12	1.15	0.97	0.92	0.84
2-Propanone, 1-(acetyloxy)-	1.47	1.47	1.47	1.47	1.47
Aldehydes					
Pentanal	3.41	2.53	1.86	2.33	2.42
Others					
Pyridines					
3-Pyridinol	4.45	2.43	2.7	2.38	2.55

Hydrocarbons (Cyclopentanes)					
2-Cyclopenten-1-one, 2-hydroxy-3-methyl-	1.41	1.82	1.3	1.38	1.4

B. Chapter 4

Table B.1 – Slow pyrolysis bio-oil chemical compounds distribution produced at 450°C with model compounds

	Chemical compounds detected in bio-oil	5°C min^{-1}	15°C min^{-1}
Carbohydrates			
	Levoglucosan	2.42	12.28
Carboxylic acids			
	Acetic acid	27.73	23.89
Furans			
	2(5H)-Furanone	2.28	
	Furaldehyde (Furfural)	25.23	21.63
	Tetrahydro-2-furanmethanol		1
Phenolic compounds			
	2,6-Dimethoxyphenol	0.62	
	Phenol, 2-methoxy-4-methyl-	0.62	
	2-Methoxyphenol		1.16
	2-Methoxy-4-vinylphenol		
	4-ethyl-2-methoxy-Phenol		
	Phenol, 2-methoxy-4-(1-propenyl)- (Isoeugenol)		
	Phenol	0.53	0.79
	2-Methylphenol		0.68
	3-Methylphenol		0.68
	1,2-Benzenediol	2.04	3.17
	1,2-Benzenediol, 3-methoxy-		
	4-Ethyl-1, 2-benzenediol		
Ketones			
	1-Hydroxy-2-butanone	0.51	0.54
Aldehydes			
	Vanillin	1.68	1.93

Others		
Pyrans		
	Maltol	1.72
Hydrocarbons (Cyclopentanes)		
	2-Cyclopenten-1-one, 2-hydroxy-	2	1.73
Alcohols		
	Ethanol, 2-(1-methylethoxy)-	0.43	3.82

C. Chapter 5

This Appendix contains the calibration of the different moving parts of the reactor used in

Chapter 5, as well as ICP data, the model used in MATLAB for the optimization and the

GC-MS data of the bio-oil fractions.

Table C.1 – Feed rate calibration. P=% of power of the motors. Values are reported as average of duplicates.

	P (%)	rpm	P (%)	rpm	P (%)	rpm	P (%)	rpm	P (%)	rpm
Feeder	70%	100	50%	80	30%	46	10%	20	< 10%	6
Stirrer	50%	50	50%	50	50%	50	50%	50	50%	50
Breaker	10%	22	10%	22	10%	22	10%	22	10%	22
Trench	90%	100	90%	100	90%	100	90%	100	90%	100
Loaded in feeder (g)	195.5		192		189.5		189		186	
Time (min)	5		5		5		5		5	
Char collector (g)	70.5		66.5		64		71		48	
Line extractor-reactor (g)	115		116		99.5		65		1	
Left in the feeder (g)	8		7		25.5		51.5		137	
Total fed (g)	185.5		182.5		163.5		136		49	

Feed rate (g biomass/min)	37.1	36.5	32.7	27.2	9.8
Extraction rate (g biomass/min)	14.1	13.3	12.8	14.2	9.6

The ICP of the biomass are reported in Table 9.7-9.10

Table C.2 – ICP of individual batches pretreated at 30°C 1h in water

Element ID (mg/kg)	Batch 1	Batch 2	Batch 3
Al	31.002	43.957	23.727
Ca	1059.204	2051.148	1566.374
Cd	<0.125	<0.125	<0.125
Co	<0.125	<0.125	<0.125
Cr	0.489	1.354	1.041
Cu	3.294	2.978	4.020
Fe	73.051	126.948	102.342
K	268.524	237.530	156.200
Mg	193.206	232.154	173.510
Mn	25.094	24.497	25.556
Mo	<0.25	<0.25	<0.25
Na	152.586	140.879	117.449
Ni	0.308	0.593	0.437
P	1022.783	974.051	967.261
Pb	<1.25	<1.25	<1.25
Se	<1.25	<1.25	<1.25
Si	806.223	661.450	953.528
Ti	1.353	1.727	0.884
Zn	23.463	21.769	21.066

Table C.3 – ICP of individual batches pretreated at 90°C 24h in water

Element ID (mg/kg)	Batch 1	Batch 2	Batch 3
Al	26.06	28.92	24.52
Ca	1406.06	2448.90	754.00
Cd	<0.125	<0.125	<0.125
Co	<0.125	<0.125	<0.125

Cr	0.97	1.38	0.36
Cu	2.79	2.96	4.81
Fe	124.49	104.25	62.89
K	46.99	34.48	23.37
Mg	148.98	127.12	103.08
Mn	15.47	16.80	14.96
Mo	<0.25	<0.25	<0.25
Na	59.87	119.99	109.56
Ni	0.41	0.55	0.25
P	37.74	379.77	329.64
Pb	<1.25	<1.25	<1.25
Se	<1.25	<1.25	<1.25
Si	524.98	654.92	711.39
Zn	17.27	17.88	26.80

Table C.4 – ICP of mixed batches pretreated

		Mix						
		Water bath				10% acetic acid		
ID	Untreated	30°C 1h	30°C 24h	90°C 1h	90°C 24h	30°C 24h	90°C 24h	Soxhlet 48h
Al	33.30	36.08	32.55	30.64	36.07	10.42	22.60	65.42
Ca	1318.32	2678.90	1922.63	1215.27	1404.53	63.55	200.88	2174.81
Cd	<0.125	<0.125	<0.125	<0.125	<0.125	<0.125	<0.125	<0.125
Co	<0.125	<0.125	<0.125	<0.125	<0.125	<0.125	<0.125	<0.125
Cr	0.50	0.87	0.79	0.81	0.68	0.44	0.43	1.29
Cu	4.98	3.45	4.35	3.61	4.73	5.36	4.09	5.13
Fe	75.32	212.13	167.18	144.15	112.69	26.79	89.53	276.43
K	1981.94	220.27	99.76	97.21	33.55	9.05	8.58	17.37
Mg	327.14	246.99	166.56	137.93	119.32	9.41	18.79	184.61
Mn	32.39	24.87	17.86	19.43	15.59	0.61	1.97	14.16
Mo	<0.25	<0.25	<0.25	<0.25	<0.25	<0.25	<0.25	<0.25
Na	578.70	148.91	122.32	117.88	125.62	128.47	91.74	68.90
Ni	0.41	0.47	0.31	0.36	0.37	0.34	0.20	0.59
P	3376.58	846.37	558.06	508.53	338.13	366.25	766.24	496.27
Pb	<1.25	1.53	<1.25	<1.25	<1.25	<1.25	<1.25	<1.25
Se	<1.25	<1.25	<1.25	<1.25	<1.25	<1.25	<1.25	<1.25
Si	857.51	877.41	654.00	640.82	756.98	931.47	487.20	757.76
Zn	27.63	20.87	19.20	19.83	18.69	1.79	2.08	20.36

Table C.5 - ICP of individual batches

	30°C 1h	30°C 24h	90°C 1h	Soxhlet 48h	Soxhlet 48h

ID	Untreated	Batch 1	Batch 1	Batch 1	Batch 1	Batch 2
Ca	2786.50	1531.35	2090.28	1681.83	4084.95	3937.02
Fe	930.21	80.81	99.55	113.71	312.38	330.17
K	1803.75	136.83	85.58	84.03	22.50	20.74
Mg	447.22	181.99	137.45	184.28	370.73	264.93
Na	537.72	114.28	97.59	106.46	38.00	38.03

The model used for MATLAB simulations is reported below.

Linear model Poly22:

$f(x,y) = p00 + p10*x + p01*y + p20*x^2 + p11*x*y + p02*y^2$

where x is normalized by mean 500 and std 40.82

and where y is normalized by mean 60 and std 20

Coefficients (with 95% confidence bounds):

p00 =   1.89 (1.527, 2.253)

p10 =   0.01531 (-0.08947, 0.1201)

p01 =   -0.02 (-0.1248, 0.08478)

p20 =   -0.3508 (-0.499, -0.2027)

p11 =   -0.04797 (-0.1528, 0.05681)

p02 =   -0.4925 (-0.8983, -0.08669)

Goodness of fit:

SSE: 0.1649

R-square: 0.8966

Adjusted R-square: 0.8227

RMSE: 0.1535

Table C.6 – GC-MS (% area) of bio-oil fractions untreated and pre-treated Phragmites australis

	Untreated			30°C1h water			90°C1h water			30°C24h water		
	C_1	C_2	C_3	C_1	C_2	C_3	C_1	C_2	C_3	C_1	C_2	C_3
Carbohydrates												
Levoglucosan	2.73	1.23	6.59	9.85	9.95	18.44	9.38	13.06	20.01	11.36	11.82	25.66
1,6-Anhydro-.alpha.-d-galactofuranose			2.45			2.45			1.91	1.40		2.52
Sucrose												5.22
Carboxylic acids												
Acetic acid	59.98	67.64	60.98	27.86	36.19	17.33	19.38	36.39	16.14	11.30	34.44	14.03
Furans												
2(5H)-Furanone	1.97	1.00		1.58						1.19	0.95	0.74
2, 3-Dihydrobenzofuran	2.30		1.68	4.38	1.71	3.03	3.93	2.34	2.17	3.61	1.40	2.70
Furaldehyde (Furfural)				2.80	2.61	2.27	2.22	2.99	1.92	1.74	2.34	2.02
Phenolic compounds												
2,6-Dimethoxyphenol	1.17	0.50	1.37	2.28	0.59	2.59	1.84	0.81	1.63	1.97	0.73	2.43
Phenol, 2-methoxy-4-methyl-	0.64	0.24		1.62	2.36	3.79		1.77	0.29			
2-Methoxyphenol	1.97	0.65	1.19	1.95		1.14		0.85	2.56	5.50	1.61	1.15
2-Methoxy-4-vinylphenol	1.48	0.33	0.79	3.81	2.44	3.57	4.03	1.73	2.61	3.54	1.73	3.03
4-ethyl-2-methoxy-Phenol	1.55	0.81	3.03	1.32	1.51			1.58	1.37			
Phenol	1.61	0.49	0.77	4.45	1.79	1.63	4.02	1.27	1.92	3.53	1.37	1.97
2-Methylphenol							1.16	0.37		1.21		0.79
3-Methylphenol	1.51		0.77	1.60	3.78	1.95	5.10	0.94				1.57
4-Methylphenol												
4-Ethylphenol	1.71	0.23	0.52	2.54	0.94	1.74	2.27	1.14	1.15	2.30	1.01	1.40
1,2-Benzenediol	2.16	0.45	1.42	3.14			4.20	0.45	1.76	1.60		
1,2-Benzenediol, 3-methoxy-	0.97	0.39	1.30						3.21	3.80		

4-Ethyl-1, 2-benzenediol						1.33		1.01				1.26
1,2-Benzenediol, 4-methyl-				4.41	1.42	3.57						
Ketones												
1-Hydroxy-2-butanone	1.15	1.41	1.32									
3-Methyl-1,2-cyclopentanedione												
2-Propanone, 1-(acetyloxy)-	1.75	1.46	1.58	1.62	1.13		0.78	1.00	0.69	0.78	1.06	0.64
Aldehydes												
5-Hydroxymethylfurfural				1.64	1.07	1.56	2.13	1.23	1.74	0.81	0.81	1.51
Vanillin	0.29		0.41				1.45	0.92	0.59	1.35	0.97	1.38
Dodecanal							2.19				1.26	3.87
Hydrocarbons (Cyclopentanes)												
3-Methylcyclopentane-1,2-dione	2.53	1.32	1.89			2.11						
2-Cyclopenten-1-one, 2-hydroxy-3-methyl-				1.93	1.56	1.32				1.61	1.39	
2-Cyclopenten-1-one, 2-hydroxy-		0.52	0.60							1.91		0.57
Others												
Maltol								0.48	0.75	5.57	1.20	0.50
Acetic acid, methyl ester				2.42	2.28	1.15	1.72	1.75	0.51	2.90	2.03	0.93
Ethanol, 2-(1-methylethoxy)-		12.68	3.76	2.30	12.09	3.75	4.98	15.13	2.46	5.68	19.10	4.61

Table C.7 – GC-MS (% area) of bio-oil fractions untreated and pre-treated *Phragmites australis* (continue)

	90°C24h water			30°C24h acetic acid			90°C24h acetic acid			Soxhlet 48h		
	C_1	C_2	C_3	C_1	C_2	C_3	C_1	C_2	C_3	C_1	C_2	C_3
Carbohydrates												
Levoglucosan	10.89	11.38	27.35	18.97	14.29	38.67	17.67	24.37	31.28	17.41	21.78	39.05
1,6-Anhydro-.alpha.-d-galactofuranose	0.96			0.80			1.10		1.09	0.83	1.04	1.02
Sucrose												
Carboxylic acids												
Acetic acid	12.19	27.03	17.04	13.21	30.20	16.50	16.29	28.58	16.90	19.74	28.39	15.40
Furans												
2(5H)-Furanone	1.20	0.74	0.63	0.90	0.71	0.44	1.02	0.62	0.64	0.92	0.50	0.44
2, 3-Dihydrobenzofuran	3.51	1.67	2.96	4.04	2.15	2.63	3.37	1.55	2.98	3.47	1.49	2.88
Furaldehyde (Furfural)	2.01	1.92	2.09	2.58	2.71	2.75	3.28	3.43	2.99	2.96	2.93	2.61
Phenolic compounds												
2,6-Dimethoxyphenol	2.03	0.74	1.44	0.67	0.39		0.75	0.48	1.08	0.55	0.37	0.54
Phenol, 2-methoxy-4-methyl-		1.97	2.25	1.37	1.14	2.12	1.47	1.04	2.39	1.12	1.45	2.32
2-Methoxyphenol		2.23	0.94	1.36		0.62	1.46	1.03	1.12	1.32	0.69	0.63
2-Methoxy-4-vinylphenol			1.94	4.38	2.39	1.56	3.52	1.43	1.94	2.09	1.14	1.72
4-ethyl-2-methoxy-Phenol				1.96	1.87	0.42	2.28	0.43		1.70	0.50	0.36
Phenol	4.19	1.44	1.97	6.70	1.69	2.87	6.12	2.37	2.68	4.45	1.77	2.44
2-Methylphenol	1.17		0.65	0.36								
3-Methylphenol	5.65		1.08		2.96							
4-Methylphenol				1.07			0.44					
4-Ethylphenol	2.32	1.13	1.32	1.04	0.95	0.61	0.94	0.65	1.34	1.16	0.62	0.67

| Compound												
1,2-Benzenediol	1.52		1.44									0.96
1,2-Benzenediol, 3-methoxy-			1.94									
4-Ethyl-1, 2-benzenediol			0.53									
1,2-Benzenediol, 4-methyl-			2.99							1.31		
Ketones												
1-Hydroxy-2-butanone												
3-Methyl-1,2-cyclopentanedione					1.17					1.06		
2-Propanone, 1-(acetyloxy)-	0.84	0.66								0.94	0.68	0.53
Aldehydes												
5-Hydroxymethylfurfural	1.73	0.73	1.42	1.31	0.59	1.28	1.61	0.40	1.59	1.35	0.43	1.37
Vanillin		0.89	0.84	0.63	0.61	0.46	0.64	0.43	0.48	0.59	0.34	0.48
Dodecanal												
Hydrocarbons (Cyclopentanes)												
3-Methylcyclopentane-1,2-dione												
2-Cyclopenten-1-one, 2-hydroxy-3-methyl-	1.60	0.92	0.76	0.88								
2-Cyclopenten-1-one, 2-hydroxy-	2.07	0.62	0.90	2.49	0.37	0.80	2.82	0.81	0.88	2.18	0.64	0.90
Others												
Maltol		0.68	0.24									
Acetic acid, methyl ester	3.36	1.73	0.80	1.89	1.62	0.68	1.72	1.97		1.84	1.90	0.54
Ethanol, 2-(1-methylethoxy)-	3.96	14.24	4.07	3.28	14.46	3.10	4.26	9.54	4.57	4.67	4.01	4.51
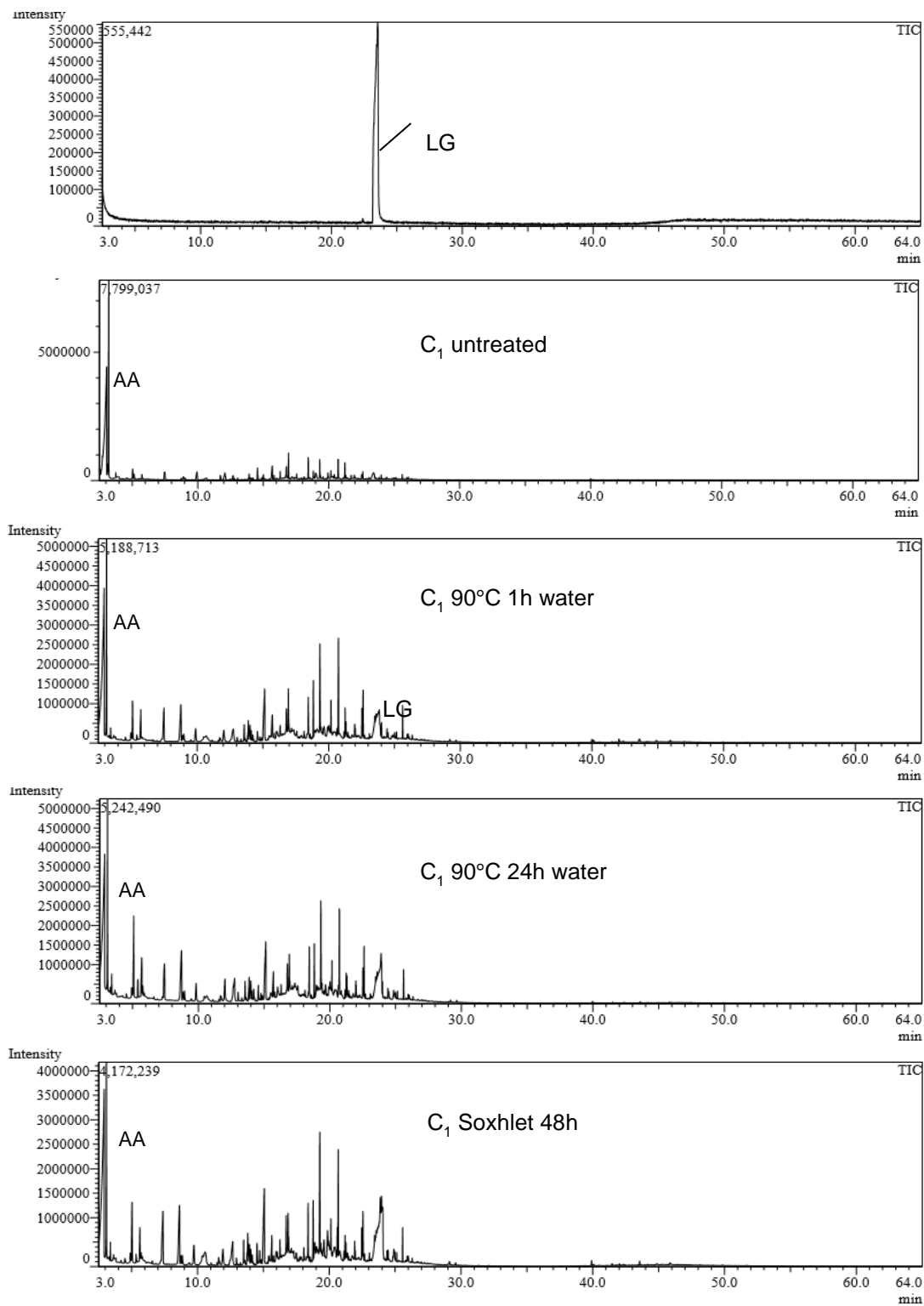
Figure C.1 - GC-MS graphs of the C1 fraction of the bio-oil

D. Chapter 7

The reproducibility of triplicates experiments of ibuprofen adsorption is reported in the following Figures 9.2 and 9.3.
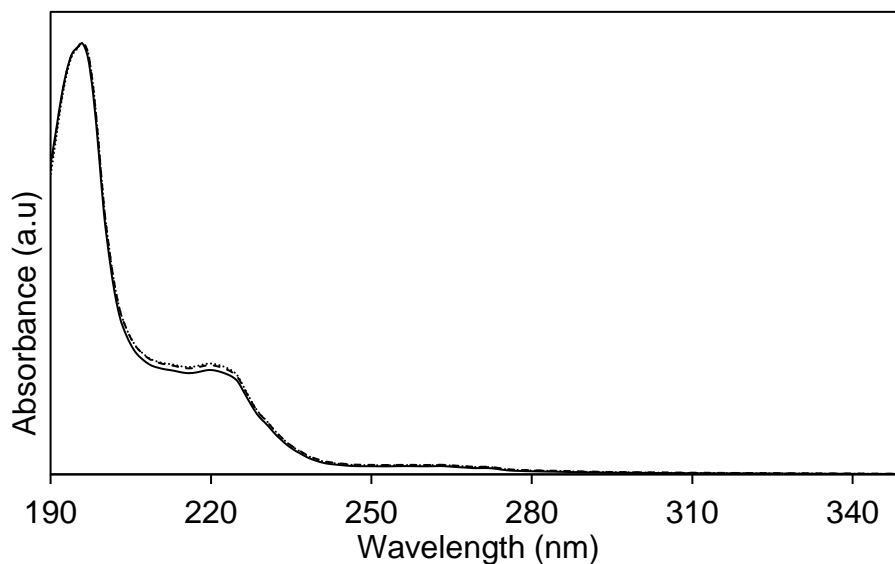

Figure D.1 – Triplicates of biochar 550-1-60, adsorbent dose (80 mg), time (30 min), Temperature 22°C, pH2
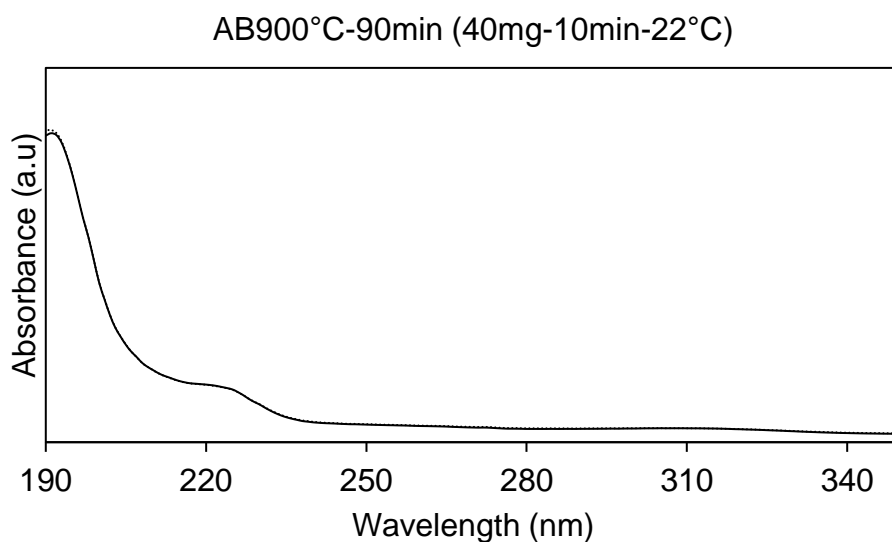

Figure D.2 – Triplicates of activated biochar 900°C-90 minutes, adsorbent dose 40 mg, time 20 min, Temperature 22°C, no pH adjustment
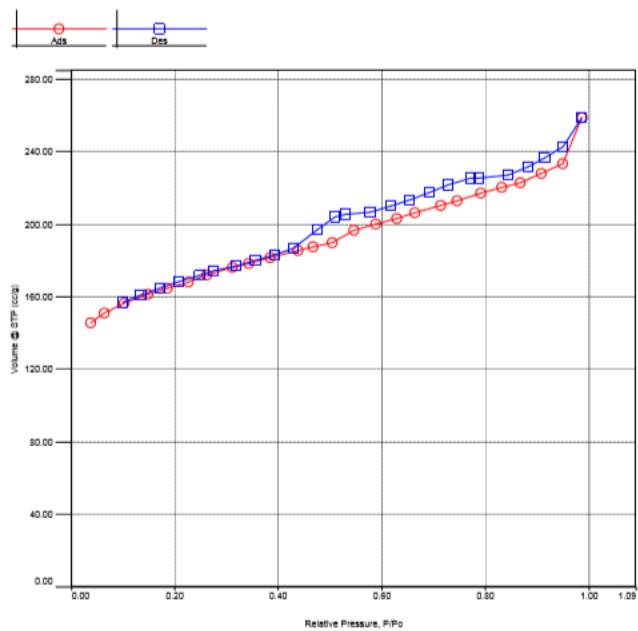
Adsorption and desorption curves of the activated carbons:
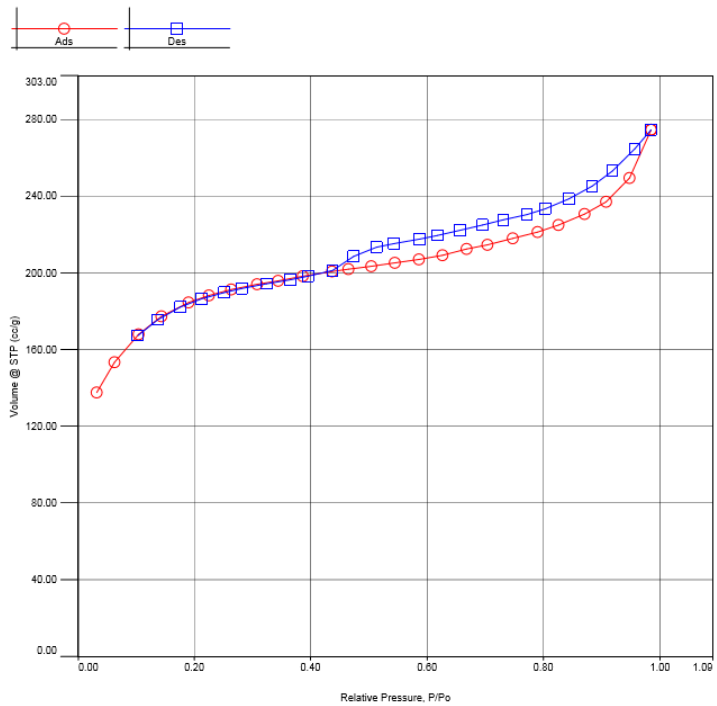

Figure D.3 – Isotherm AB850°C-60minutes

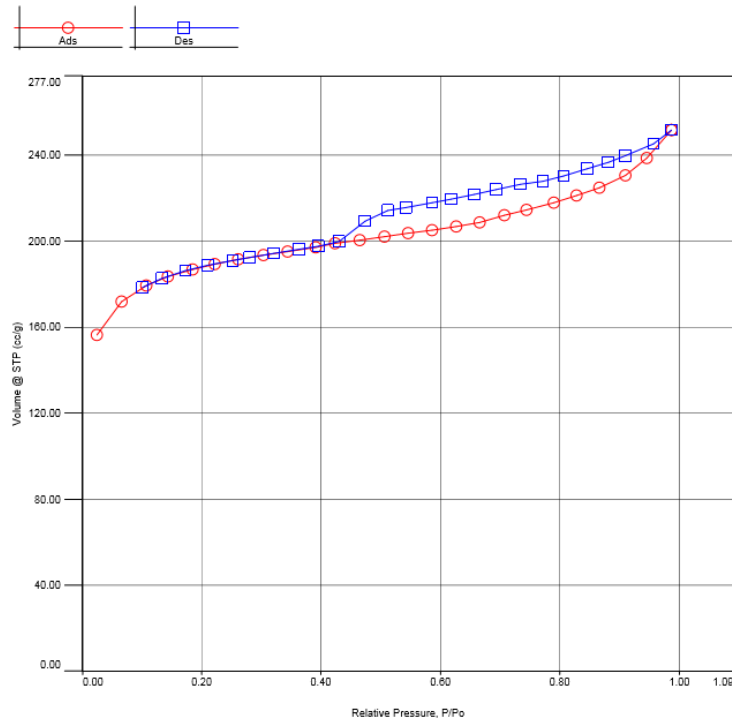**Figure D.4 – Isotherm AB900°C-60minutes**

Figure D.5 – Isotherm AB900°C-90minutes

Curriculum Vitae

Name: Chiara Barbiero

Post-secondary Education and Degrees:

Politecnico di Torino
Torino, Italy
2006-2012 B.E.Sc

Politecnico di Torino
Torino, Italy
2012-2014 M.E.Sc.

The University of Western Ontario
London, Ontario, Canada
2015-2020 Ph.D.

Related Work Experience

Teaching Assistant
The University of Western Ontario
2016